



University
of Glasgow

Gadalla, Kamal Kamal El-Sayed (2012) Virus-mediated delivery of MECP2 as a potential tool for the treatment of Rett syndrome. PhD thesis <http://theses.gla.ac.uk/3501/>

Copyright and moral rights for this thesis are retained by the author

A copy can be downloaded for personal non-commercial research or study, without prior permission or charge

This thesis cannot be reproduced or quoted extensively from without first obtaining permission in writing from the Author

The content must not be changed in any way or sold commercially in any format or medium without the formal permission of the Author

When referring to this work, full bibliographic details including the author, title, awarding institution and date of the thesis must be given.

Virus-mediated delivery of *MECP2* as a potential tool for the treatment of Rett syndrome

**Kamal Kamal El-Sayed Gadalla
MBChB, MSc**

**Thesis submitted in fulfilment of the requirements for the degree of Doctor
of Philosophy
Institute of Neuroscience and Psychology
College of Medical, Veterinary and Life Science
University of Glasgow
Glasgow, G12 8QQ
UK**

April 2012

© KK Gadalla 2012

Abstract

Typical Rett syndrome (RTT) is a paediatric neurological disorder caused in >95 % of cases by loss-of-function mutations in the X-linked gene, methyl-CpG-binding protein 2 (*MECP2*). The gene product, MeCP2, is a widely expressed nuclear protein that is especially abundant in postmitotic neurons of the central nervous system (CNS). Knocking out *Mecp2* function in mice recapitulates many of the overt neurological features seen in RTT patients and provides a very useful model for testing potential therapeutic applications. The absence of a curative therapy together with the monogenicity of the disorder and established reversibility of the phenotype in mice suggest that replacement of the *MECP2* gene is a potential therapeutic option worthy of exploration. In this study I used several viral vectors to test the potential of gene therapy in RTT mice. First, I generated different viral vectors which can express tagged-MeCP2 under the control of ubiquitous and cell-type specific promoters. Secondly, I assessed the ability of these vectors to deliver the *Mecp2* transgene into *Mecp2* knockout mice at both neonatal and adult stages of development. I then aimed to investigate the effect of exogenously delivered *Mecp2* on RTT-like phenotypes.

The results demonstrated that lentiviral vectors were able to effectively deliver an RFP-tagged *Mecp2* minigene into neurons of *Mecp2*-null mice both *in vitro* and *in vivo*. Exogenous *Mecp2* was targeted to the nucleus and displayed heterochromatin localization with no evidence of ectopic expression. Use of the synapsin1 (*syn1*, neuron-specific) promoter resulted in cellular levels of *Mecp2* equal to $85 \pm 0.1\%$ of endogenous protein levels, whereas the phosphoglycerate kinase (PGK) promoter produced cellular levels of exogenous *Mecp2* at a relatively high levels ($210 \pm 0.1\%$ of endogenous levels). Direct brain injection of Lentiviral vector was able to deliver exogenous *Mecp2* into the CA1 region of the hippocampus and to produce high transduction efficiency around the injection sites but with limited spread. The early mortality of the injected mice precluded assessment of the functional consequences of exogenous *Mecp2* expression. However, assessment of the cellular morphology was possible and this analysis revealed delivery of exogenous *Mecp2* to normalise neuronal nuclear volume deficits seen in the *Mecp2*^{stop/y} mice from $86 \pm 0.1\%$ of WT values to $100 \pm 0.04\%$ of WT levels. At the molecular level, I showed that exogenous *Mecp2*

becomes phosphorylated at serine 421 under basal conditions and that the level of phosphorylation of exogenous *Mecp2* is disproportionately higher (5.5 ± 0.4 times) than that seen for endogenous *Mecp2*. I also showed the *Mecp2* overexpression in WT neurons is associated with a reduction in the cellular levels of total histone 4 (78 ± 0.01 % of the endogenous level) and a parallel reduction in cellular levels of acetylated histone 4 (79 ± 0.01 % of the endogenous levels).

In second phase of experiments, I showed that the single stranded Adeno-associated virus (ssAAV)-based vector with chicken beta actin (CBA) promoter and encapsulated with capsid of AAV serotype 9, was able to efficiently deliver exogenous *MECP2* into the brain of *Mecp2*-null as well as WT neonatal mice after intracranial (IC) injection. In contrast to lentiviral vectors, there was widespread transduction of cells throughout the nervous system with transduction efficiency varying between 6.8 ± 2.3 % and 41.5 ± 11.3 % of all cells dependent on the brain region. The transgene was mostly expressed in neurons which represented 67 ± 11.8 % to 98 ± 0.8 % of all transduced cells. ssAAV9 vector expressed exogenous MeCP2 at near-physiological levels (100-125 % of endogenous levels). At the cellular level, exogenous MeCP2 was able to rescue the neuronal nuclear volume of *Mecp2*-null mice (69 ± 0.02 % of WT values) to WT comparable values (97 ± 0.03 % of WT values). At the organismal levels *Mecp2*-null mice treated with ssAAV9/*MECP2* showed extended survival (median survival of 16.7 weeks compared to 9.3 weeks for the *GFP*-treated control) and also displayed a modest, but significant, reduction in the RTT-like phenotype severity score compared to the *GFP*-treated control group. The most robust improvement reported in this study was in the locomotion activity (velocity and total distance moved in the open field test and in performance on a forced motor task). Interestingly, WT mice receiving neonatal injections of ssAAV9/CBA-*MECP2* did not show any significant deficits, suggesting a tolerance for modest MeCP2 overexpression.

In a further experiment, I showed that the self-complementary AAV 9 (scAAV9) vector with an *Mecp2*-endogenous core promoter fragment was able to deliver exogenous *MECP2* into the brain of neonatal mice after intravenous (IV) or (IC) injection. Brain transduction efficiency was 8 - 12 % after IV injection and 48 - 68 % after IC injection in neonatal mice. Cellular levels of exogenous MeCP2 were between 1.4-1.8 times the endogenous levels. At the organismal level,

scAAV9/*MECP2*-injected mice displayed an overt hindlimb motor dysfunction which was observed 3 and 5 weeks post-injection after IV and IC injection respectively. The stereotyped hindlimb dysfunction suggested a toxicity issues with this vector and examination of the lumbar segment of the spinal cord confirmed evidence of axonal degeneration in the dorsal columns. IV injection of scAAV9/*MECP2* into RAG^{-/-} knockout mice (immunocompromised) displayed hindlimb motor dysfunction similar to that observed with *Mecp2*^{stop/y} mice suggesting that the adaptive immune response is not likely to be involved in the pathogenesis of this phenotype. *MECP2*^{stop/y} mice treated with scAAV9/*MECP2* displayed higher RTT-like phenotype severity score than *GFP*-treated controls which is probably due to the effect produced by the hindlimb motor dysfunction on regular RTT-like phenotype (gait, mobility and hindlimb clasping).

In summary, I have demonstrated the successful application of lentiviral and AAV2/9 vectors to deliver exogenous *MECP2* both *in vitro* and *in vivo*. I showed that lentiviral vectors are unlikely to be useful for global brain delivery of *MECP2* due to limited spread of the virus. However the lentiviral vectors I developed are potentially useful where localized brain injection is desirable. The main translational finding is the first, at the proof of concept level, demonstration of therapeutic benefits (including enhanced survival) of exogenously delivered *MECP2* using the ssAAV9/CBA-*MECP2* vector. I also however, identify potential toxicity issues of exogenous *MECP2* delivery whereby a scAAV9 vector was found to produce overt neuromotor deficits. Overall, my data supports the potential of gene therapy in RTT but also emphasises the importance of issues including careful vector design, choice of delivery methods and the timing of treatment in any future clinical translation.

Table of Contents

Abstract	2
List of Tables.....	14
List of Figures.....	15
Acknowledgement.....	19
Author’s Declaration.....	20
Abbreviations	21
Chapter 1	23
Introduction	23
1.1 General introduction	23
1.2 Clinical manifestations of RTT.....	23
1.3 Genetic basis of RTT	25
1.3.1 <i>MECP2</i> and Rett Syndrome	25
1.3.2 <i>MECP2</i> structure	26
1.3.3 Functions of MeCP2.....	28
1.4 Animal models of Rett syndrome.....	29
1.5 Cellular alterations in RTT patients and animal models	32
1.6 Reversibility and treatment strategies for the RTT-like phenotype	33
1.6.1 Reversibility of the RTT-like phenotype in <i>Mecp2</i> knockout mice models	34
1.6.2 Treatment strategies for RTT.....	37
1.6.2.1 Pharmacological approaches in RTT - current challenges	38
1.6.2.2 Neurotransmitter systems - monoamines.....	40
1.6.2.3 Neurotransmitter systems - glutamate	40
1.6.2.4 Neurotransmitter systems - GABA	41
1.6.2.5 Drugs targeting <i>MECP2</i> mutations.....	42
1.6.2.6 Environmental and epigenetic factors	42
1.6.3 RTT therapeutic strategies at the level of the gene	43

1.6.3.1	Reactivation of the normal allele.....	43
1.6.3.2	RTT therapeutic strategies at the level of the gene - gene therapy	45
1.7	Gene therapy	45
1.7.1	Types of gene therapy	45
1.7.1.1	Non-viral methods	46
1.7.1.2	Viral vectors	46
1.7.2	Gene therapy application for RTT	47
1.7.2.1	RTT Propensity to gene therapy	47
1.7.2.2	Challenges for gene therapy application for RTT	47
1.8	Lentiviruses	50
1.8.1	Lentivirus-based vectors.....	50
1.8.1.1	The vector cassette	51
1.8.1.2	The packaging cassette	52
1.8.1.3	The envelope cassette	52
1.8.2	Biosafety of lentivirus-based vectors.....	53
1.8.3	Application of lentivirus-based vectors in neurological disorders and its tractability in RTT.	54
1.9	Adeno-associated virus.....	57
1.9.1	AAV-based vector transduction.....	57
1.9.2	Self-complementary AAV	59
1.9.3	AAV capsids	61
1.9.4	Clinical applications and potentials in RTT	62
Chapter 2	65
Materials and methods	65
2.1	General materials.....	65
2.1.1	Enzymes and reagents	65
2.1.2	Primers.....	66
2.2	General solutions	68

2.2.1	Phosphate buffer (PB) Solution.....	68
2.2.1.1	0.2 M PB	68
2.2.1.2	0.1 M PB	68
2.2.1.3	0.3 M PBS.....	68
2.2.2	1x TBE.....	68
2.2.3	1kb DNA ladder	68
2.2.4	5x DNA loading dye	68
2.2.5	Ethidium Bromide	69
2.2.6	TE buffer	69
2.2.7	Ampicillin solution	69
2.3	Bacterial solutions	69
2.3.1	Luria-Bertani (LB) medium	69
2.3.2	LB agar.....	69
2.3.3	SOB media.....	69
2.3.4	SOC media.....	69
2.4	Solutions for DNA plasmid preparation (Alkaline lysis methods)	69
2.4.1	Solution I (resuspension solution)	69
2.4.2	Solution II (Lysis solution)	70
2.4.3	Solution III (neutralization solution) 3M KAC	70
2.5	Methods.....	70
2.5.1	Restriction endonuclease digestion of plasmid DNA.....	70
2.5.2	Ligation reaction	71
2.5.3	Preparation of chemically competent cell	71
2.5.4	Heat shock transformation of chemically competent <i>E-Coli</i>	72
2.5.5	Plasmid mini-preparation (alkaline lysis)	72
2.5.6	Making glycerol stock	73
2.5.7	Determination of DNA concentration.....	73
2.5.8	Polymerase chain reaction (PCR) for transgene amplification.....	73
2.5.9	Agarose gel electrophoresis.....	74

2.6	Animals	75
2.6.1	Design of the <i>Mecp2</i> -KO mouse models	75
2.6.2	<i>Breeding strategy of Mecp2-KO mice</i>	75
2.6.3	Genotyping	76
2.6.3.1	DNA extraction	76
2.6.3.2	PCR verification of mouse genotypes	76
2.6.4	Phenotype severity score	77
2.7	Hippocampal dissociated cell culture.	79
2.7.1	Animal	79
2.7.2	Materials.....	79
2.7.3	Method.....	80
2.8	Calcium phosphate transfection.....	81
2.8.1	Materials.....	81
2.8.2	Preparation of the transfection mix (for single coverslip)	82
2.8.3	Preparation and transfection of the cell culture.....	82
2.9	Generation of Lentivirus particles	83
2.9.1	Materials.....	83
2.9.2	Preparation of HEK 293T/17 cells.....	84
2.9.2.1	Recovery of HEK 293T cells from liquid nitrogen	84
2.9.2.2	Passage of HEK293T cells.....	84
2.9.3	Lentiviral vector particles preparation	85
2.9.3.1	Preparation of HEK293T cells.....	85
2.9.3.2	Preparation of the transfection solutions	85
2.9.3.3	Transfection of HEK293T cells.....	86
2.9.4	Collection of lentivirus particles	87
2.9.5	Concentration of the Virus particles	87
2.9.6	Titration of lentivirus particles.....	88
2.9.6.1	First method	88
2.9.6.2	Second method.....	88

2.10	Adeno-associated virus production	88
2.11	Stereotaxic brain injection	89
2.12	Neonatal injection	90
2.13	Immunohistochemistry (IHC)	90
2.14	Image analysis.....	92
2.15	Treadmill motor challenge test	92
2.16	Open Field Testing	93
2.17	Whole body plethysmograph	94
2.18	Statistical analysis.....	95
Chapter 3		96
Generation of Lentivirus vector-based approach to deliver exogenous <i>Mecp2</i> <i>in vitro</i> and <i>in vivo</i>		96
3.1	Introduction.....	96
3.2	Study aims.....	97
3.3	Generation of lenti-syn1/PGK- <i>ME1FlagRFP</i> vectors.....	98
3.3.1	Creation of <i>ME1FlagRFP</i> fusion construct	98
3.3.2	Validation of the pCDNAME1 <i>FlagRFP</i> construct.....	100
3.3.3	Cloning of <i>ME1FlagRFP</i> fusion construct into Lentivirus vector backbone.....	104
3.3.4	Confirmation of lenti-PGK/syn1- <i>ME1FlagRFP</i> constructs	106
3.3.5	Delivery of exogenous <i>Mecp2</i> into hippocampal cell culture using Ca ²⁺ phosphate transfection method.....	111
3.3.6	Generation and titration of Lentivirus particles	112
3.3.7	Time course expression analysis of lenti-mediated delivery of <i>Mecp2</i>	114
3.4	Discussion.....	114
Chapter 4		118
Lentivirus-mediated delivery of <i>Mecp2</i> <i>in vitro</i> and <i>in vivo</i> in a mouse model of Rett syndrome		118

4.1	Introduction.....	118
4.2	Study aims.....	120
4.3	Methods.....	120
4.4	Results	122
4.4.1	Lenti-mediated delivery of <i>ME1FlagRFP</i> to cultured neuronal cells	122
4.4.1.1	Neuron-specific expression of <i>Mecp2</i> in the hippocampal dissociated cell culture	122
4.4.1.2	Delivery of exogenous <i>Mecp2</i> in <i>Mecp2</i> ^{+/stop} female mosaic hippocampal cell culture	123
4.4.1.3	Lenti-mediated delivery of <i>Mecp2</i> in neurons and glia under ubiquitous, PGK, promoter in hippocampal dissociated cell culture	124
4.4.1.4	PGK promoter drove expression of high level of exogenous <i>Mecp2</i> in neurons in dissociated hippocampal cell culture.....	125
4.4.2	<i>In vivo</i> injection of lenti- <i>ME1FlagRFP</i> viruses into the mouse brain	127
4.4.2.1	<i>In vivo</i> Neuron-specific delivery of exogenous <i>Mecp2</i> into the mouse brain.....	127
4.4.2.2	Syn1 promoter drove expression of exogenous <i>Mecp2</i> at near- physiological levels <i>in vivo</i>	128
4.4.3	Transgenic expression of <i>ME1FlagRFP</i> in the CA1 region of the hippocampus under the control of the PGK promoter	132
4.4.3.1	Lentiviruses with PGK promoter drove high neuronal expression of the exogenous <i>Mecp2</i>	135
4.4.3.2	Exogenous <i>Mecp2</i> rescued neuronal nuclear volume in <i>Mecp2</i> ^{stop/y} mice	136
4.4.3.3	Exogenous <i>Mecp2</i> produced a modest increase in the nuclear volume of WT mice	137
4.4.3.4	PGK promoter drove high levels of exogenous <i>Mecp2</i> <i>In vivo</i> ..	138
4.4.4	Exogenous <i>Mecp2</i> maintains phosphorylation at serine 421	139
4.4.5	Exogenous <i>Mecp2</i> is highly phosphorylated at S421	141

4.4.6	Neuronal overexpression of exogenous <i>Mecp2</i> alters nuclear levels of histone 4	143
4.4.7	Neonatal brain delivery of lenti-PGK- <i>ME1FlagRFP</i>	145
4.5	DISCUSSION.....	147
Chapter 5		154
Improved Survival and Reduced Phenotypic Severity Following AAV9/ <i>MECP2</i> Gene Transfer to Neonatal Male <i>Mecp2</i> Knockout Mice		154
5.1	Introduction.....	154
5.2	Study aims.....	155
5.3	Methods.....	155
5.4	Results	157
5.4.1	Confirmation of genotypes in <i>Mecp2</i> -null mouse colony by PCR ...	157
5.4.2	Neonatal CNS injection of AAV9/ <i>MECP2</i> resulted in widespread brain expression of MeCP2	158
5.4.3	Neonatal CNS injection of AAV9/ <i>MECP2</i> resulted in spinal cord and liver expression of the exogenous MeCP2	160
5.4.4	Neonatal brain injection of AAV9/ <i>MECP2</i> resulted in MeCP2 expression at near-physiological cellular levels.....	162
5.4.5	AAV9-mediated neonatal delivery of <i>MECP2</i> improved RTT-like phenotypes in <i>Mecp2</i> -null mice	165
5.4.6	AAV9-mediated neonatal delivery of <i>MECP2</i> prolonged life span in <i>Mecp2</i> -null mice	166
5.4.7	Growth deficit persists after AAV9/ <i>MECP2</i> injection however stabilizes	167
5.4.8	AAV9-mediated neonatal delivery of <i>MECP2</i> improved motor phenotypes in <i>Mecp2</i> -null mice	168
5.4.8.1	Tread-mill test	168
5.4.8.2	Open field test	169
5.4.8.3	Improved exploratory behaviours with no effect on the anxiety-related measures	170

5.4.9	AAV9/ <i>MECP2</i> -treated Long-lived mice displayed consistent phenotype improvement.	171
5.5	Overt respiratory phenotypes persist following AAV9-mediated neonatal delivery of <i>MECP2</i> to <i>Mecp2</i> -null mice	173
5.5.1	AAV9-mediated delivery of <i>MECP2</i> rescued the <i>Mecp2</i> -null nuclear volume phenotype.....	174
5.6	Discussion.....	176
Chapter 6	180
	Self-complementary AAV9-mediated delivery of exogenous <i>MECP2</i> into neonatal male <i>Mecp2</i> knockout mice	180
6.1	Introduction.....	180
6.2	Aims	181
6.3	Methods.....	181
6.4	Results	182
6.4.1	Intravenous injection of scAAV9/ <i>MECP2</i> in neonatal mice resulted in widespread expression of exogenous MeCP2	182
6.4.2	IV injection of scAAV9/ <i>MECP2</i> in neonatal mice resulted in MeCP2 expression at near-physiological cellular levels.....	186
6.4.3	CNS injection of scAAV9/ <i>MECP2</i> in neonatal mice produced high transduction efficiency of exogenous MeCP2 throughout the brain	188
6.4.4	IC injection of scAAV9/ <i>MECP2</i> in neonatal mice resulted in high cellular levels of MeCP2 expression	191
6.4.5	scAAV9/ <i>MECP2</i> injection in neonatal mice resulted in hindlimb motor dysfunction.	193
6.4.5.1	Hindlimb motor dysfunction is associated with axonal degeneration of the dorsal column of the lumbar spine in scAAV9/ <i>MECP2</i> -injected mice.....	197
6.4.5.2	CD3 immuno-reactivity in the spinal cord of scAAV9/ <i>MECP2</i> injected mice.....	198
6.4.5.3	Neonatal IV injection of scAAV9/ <i>MECP2</i> produced hindlimb motor dysfunction in RAG knockout mice.	200

6.4.5.4 Neonatal IV injection of scAAV9/ <i>mMecp2</i> led to a similar motor deficit in <i>Mecp2</i> -null mice.	201
6.4.5.5 IC injection of scAAV9/MeP- <i>MECP2</i> produced higher transduction efficiency and cellular protein levels than the ssAAV9/CBA- <i>MECP2</i> in neonatal mice	201
6.5 Discussion.....	203
Chapter 7	209
General discussion	209
7.1 Major findings.....	209
7.1.1 Lenti-mediated <i>Mecp2</i> delivery to <i>Mecp2</i> knockout mice	211
7.1.2 Phenotype rescue and prolonged survival after ssAAV9/CBA- <i>MECP2</i> brain injection in <i>Mecp2</i> -null mice	215
7.1.3 Global and brain-specific delivery of exogenous <i>MECP2</i> using scAAV9/MeP- <i>MECP2</i> vector in neonatal mice.....	217
7.2 Significance of this study	222
7.3 Technical considerations	223
7.4 Future studies	224
7.5 Summary.....	226
References	228

List of Tables

Table 1-1 Mapping the effect of <i>Mecp2</i> deletion or activation in the RTT mice models..	39
Table 1-2 Comparison between lentivirus- and AAV-based vectors as a potential tools for <i>Mecp2</i> delivery	56
Table 2-1 list of enzymes	65
Table 2-2 list of the Kits and their suppliers	65
Table 2-3 Oligonucleotide list	66
Table 2-4 List of Bacterial strains	67
Table 2-5 List of the vectors	67
Table 2-6 Components of the restriction digestion reaction	70
Table 2-7 Components of the ligation reaction	71
Table 2-8 Components of the PCR reactions	74
Table 2-9 Standard PCR condition	74
Table 2-10 Breeding scheme for <i>Mecp2</i> knockout mice	76
Table 2-11 DNA extraction conditions	76
Table 2-12 PCR reaction sets for genotyping of <i>Mecp2</i> -null mice and their WT littermates	77
Table 2-13 PCR conditions for genotype discrimination	77
Table 2-14 Detailed phenotype severity score of <i>Mecp2</i> KO mice	78
Table 2-15 Materials for dissociated hippocampal cell culture	79
Table 2-16 Components of the cell culture buffer	80
Table 2-17 Materials for Ca ²⁺ phosphate transfection	81
Table 2-18 Materials for the generation of lentivirus particles	83
Table 2-19 Vectors concentration for Lentiviruses generation	85
Table 2-20 Primary and secondary antibodies used in IHC	91
Table 4-1 Injection coordinates for the hippocampus stereotaxic brain injection	127
Table 4-2 Injection coordinates for CA1 region of the hippocampus	132
Table 5-1 Identification of mice genotype by PCR reaction	157

List of Figures

Figure 1-1 Clinical manifestations of Rett syndrome	25
Figure 1-2 Composition and splicing pattern of <i>MECP2</i> gene	27
Figure 1-3 MeCP2 protein structure with the most frequent mutation sites,	28
Figure 1-4 Genomic structure of WT lentiviruses.	51
Figure 1-5 Lentivirus-based vector, structure and transduction.....	54
Figure 1-6 Genomic structure of the WT AAV and AAV-based vector.	58
Figure 1-7 AAV-based vector transduction.....	60
Figure 2-1 Hippocampal dissociated cell culture	81
Figure 2-2 Generation of lentivirus particles.....	86
Figure 2-3 DigiGait apparatus	93
Figure 2-4 Open field test	94
Figure 2-5 Whole body plethysmograph apparatus.....	95
Figure 3-1 Cloning strategy of <i>ME1FlagRFP</i> fusion construct	99
Figure 3-2 PCR amplification of <i>ME1Flag</i> fusion construct.	100
Figure 3-3 PCR verification of pCDNARFP vectors for successful cloning of <i>ME1Flag</i> fusion construct.	101
Figure 3-4 Restriction digest validation of pCDNAME1FlagRFP.....	103
Figure 3-5 pCDNA(+)/Zeo <i>ME1FlagRFP</i> vector map.	104
Figure 3-6 Cloning strategy for <i>ME1FlagRFP</i> fusion construct insertion into lentiviral vector backbones.	105
Figure 3-7 PCR validation of lenti-PGK- <i>ME1FlagRFP</i>	107
Figure 3-8 Restriction digest confirmation of plenti-PGK/syn1- <i>ME1FlagRFP</i>	108
Figure 3-9 plenti-PGK/syn1- <i>ME1FlagRFP</i> vector map.	109
Figure 3-10 Sequence alignment of <i>ME1FlagRFP</i> to the mouse <i>Mecp2_e1</i> and <i>RFP</i> encoding sequences.	111
Figure 3-11 Lenti-PGK/syn1- <i>ME1FlagRFP</i> vectors express <i>ME1FlagRFP</i> fusion protein in hippocampal dissociated culture.	112
Figure 3-12 HEK293T cells transduced with lenti-PGK- <i>ME1FlagRFP</i> virus particles.	113
Figure 3-13 Time course expression analysis of exogenous <i>Mecp2</i>	114
Figure 4-1 Lentivirus-based vector constructs	121
Figure 4-2 Synapsin1 promoter drove neuron-specific expression of exogenous <i>Mecp2</i>	123

Figure 4-3 Neuron-specific expression of exogenous <i>Mecp2</i> in <i>Mecp2</i> ^{+/stop} hippocampal cell culture.	124
Figure 4-4 Lentivirus-based vector mediated high neuronal transduction of <i>Mecp2</i> in hippocampal dissociated cell culture.	126
Figure 4-5 Lentivirus-based vector mediated exogenous <i>Mecp2</i> delivery into the hippocampus of <i>Mecp2</i> ^{stop/y} and WT adult mice.	129
Figure 4-6 Syn1 promoter drove near-endogenous levels of exogenous <i>Mecp2</i> <i>in vivo</i>	130
Figure 4-7 Lentivirus-mediated GFP expression showed no effect on the cellular levels of endogenous <i>Mecp2</i>	131
Figure 4-8 Lentivirus-mediated delivery of exogenous <i>Mecp2</i> to CA1 region of the hippocampus of <i>Mecp2</i> ^{stop/y} mouse.	134
Figure 4-9 High neuronal tropism of Lentiviruses	135
Figure 4-10 Exogenous <i>Mecp2</i> rescued nuclear volume in <i>Mecp2</i> ^{stop/y} mice. ...	136
Figure 4-11 Exogenous <i>Mecp2</i> increased pyramidal cells nuclear volume in WT mice.	137
Figure 4-12 PGK promoter drove high levels of exogenous <i>Mecp2</i> <i>in vivo</i>	139
Figure 4-13 Exogenous <i>Mecp2</i> maintains characteristic phosphorylation at S421	140
Figure 4-14 Exogenous <i>Mecp2</i> expression and <i>Mecp2</i> -pS421 in WT mice.	142
Figure 4-15 Exogenous <i>Mecp2</i> expressing cells display high level of <i>Mecp2</i> -pS421 levels	143
Figure 4-16 H4 and Ach4 cellular levels after Lenti-PGK-ME1-FlagRFP transduction.	144
Figure 4-17 Altered cellular levels of H4 and Ach4 in <i>Mecp2</i> overexpressing pyramidal cells.	145
Figure 4-18 Neonatal intracranial injection of lenti-PGK-ME1FlagRFP resulted in limited transgene spread.	146
Figure 5-1 AAV vector-constrcuts and the experimenatal plan	156
Figure 5-2 PCR identification of mice genotype	158
Figure 5-3 Widespread expression of exogenous MeCP2 across the brain following neonatal IC injection of ssAAV9/MECP2.	159
Figure 5-4 IC injection of AAV9/MECP2 in neonatal mice produced high transduction efficiency across the brain.	161

Figure 5-5 IC injection of AAV9/ <i>MECP2</i> into neonatal mice led to widespread spinal cord and liver transduction.	162
Figure 5-6 IC injection of AAV9/ <i>MECP2</i> into neonatal mice produced exogenous MeCP2 levels close to that of the endogenous protein.	164
Figure 5-7 AAV9/ <i>MECP2</i> neonatal injection reduced phenotype severity in <i>Mecp2</i> -null mice.	166
Figure 5-8 Prolonged survival of <i>Mecp2</i> -null mice after neonatal IC injection of AAV9/ <i>MECP2</i>	167
Figure 5-9 Persistent bodyweight deficit in <i>Mecp2</i> -null mice after AAV9/ <i>MECP2</i> injection	168
Figure 5-10 Treadmill motor test of <i>Mecp2</i> -null mice after neonatal injection of AAV9/ <i>MECP2</i>	169
Figure 5-11 Motor-related measures of the open field test	170
Figure 5-12 Exploratory and anxiety related measures of the open field test. .	171
Figure 5-13 Phenotypic analysis of AAV9/ <i>MECP2</i> -treated long-lived <i>Mecp2</i> -null mice.	172
Figure 5-14 Persistent breathing phenotype in <i>Mecp2</i> -null mice after AAV9/ <i>MECP2</i> injection	173
Figure 5-15 Breathing phenotype in <i>Mecp2</i> -null mice after AAV9/ <i>MECP2</i> injection	174
Figure 5-16 Increased nuclear volume in <i>Mecp2</i> ^{-1y} and WT mice after AAV9/ <i>MECP2</i> injection.	175
Figure 6-1 scAAV9 vector-constructs and the experimental plan.	182
Figure 6-2 IV injection of scAAV9/ <i>MECP2</i> in neonatal mice produced widespread expression of exogenous MeCP2 in the peripheral tissues.	183
Figure 6-3 IV injection of scAAV9/ <i>MECP2</i> into neonatal mice resulted in high neuronal transduction in the brain.	184
Figure 6-4 Transduction efficiency of scAAV9/ <i>MECP2</i> in the brain after IV injection in neonatal mice.	185
Figure 6-5 IV injection of scAAV9/ <i>MECP2</i> into neonatal mice produces widespread transgene expression in the spinal cord.	186
Figure 6-6 IV injection of scAAV9/ <i>MECP2</i> produced near-normal cellular levels of MeCP2.	187
Figure 6-7 IC injection of scAAV9/ <i>MECP2</i> produced higher brain transduction than IV injection in neonatal mice.	189

Figure 6-8 IC injection of scAAV9/ <i>GFP</i> in neonatal mice produced a broad GFP expression in the brain.	190
Figure 6-9 IC injection of scAAV9/ <i>MECP2</i> produced high transduction efficiency in neonatal mice.	191
Figure 6-10 scAAV9/ <i>MECP2</i> expressed high cellular levels of exogenous MeCP2 after IC injection in neonatal mice.	192
Figure 6-11 scAAV9/ <i>MECP2</i> injection in neonatal mice resulted in Hindlimb motor dysfunction.	194
Figure 6-12 Phenotype severity and bodyweight measures after IV injection of scAAV9/ <i>MECP2</i> in neonatal mice.	195
Figure 6-13 IC injection of scAAV9/ <i>MECP2</i> results in abnormal phenotypes in WT mice	196
Figure 6-14 Phenotype severity score and bodyweight analysis after IC injection of scAAV9/ <i>MECP2</i> in neonatal mice.	197
Figure 6-15 Axonal degeneration of the dorsal columns of the lumbar spine ...	198
Figure 6-16 Anti-CD3 antibody immunolabelling in the lumbar spine.	199
Figure 6-17 Exogenous MeCP2 expression in RAG ^{-/-} knockout mouse brain	200
Figure 6-18 IV injection of scAAV9/ <i>mMecp2</i> into neonatal <i>Mecp2</i> ^{-/y} mice resulted in hindlimb motor dysfunction.	201
Figure 6-19 scAAV9 mediated higher transduction efficiency and transgene expression after IC injection in neonatal mice.	203

Acknowledgement

All praise and thanks to Allah, the Almighty, on whom I depend for sustenance and guidance.

Firstly I am indebted to my country, Egypt, which has supported my family and me for four years despite on-going economic and political troubles. Without this scholarship, I doubt I would be able to do what I have done.

I owe my deepest gratitude to my supervisors Dr Stuart Cobb and Dr Mark Bailey for giving me this great opportunity to undertake a fascinating and challenging project, and for their continuous guidance, advice and constructive criticism.

I would like to thank Prof. Kumlesh Dev for the help and knowledge he gave me during the first few months of my PhD.

I am also grateful to my assessors Dr Leanne McKay and Prof. Brian Morris for their advice and suggestions during the course of my PhD.

It is a pleasure to thank those whose contributions made this thesis possible especially, Dr Rosemary Spike, Dr Shih-Ming Weng, Paul Turko and Paul Ross.

I am grateful also to Dr Steven Gray and Dr John Riddell for their technical assistance and fruitful collaboration.

I have been fortunate to work with some fantastic people over the past few years. Special thanks go to Faye McLeod, Louise Williams, Katherine Pears, Dr Jian Gan, Dr Sam Booker, and Prof. Imre Vida for their kind help and support during the last four years.

To my mother Farah Zahra, my brothers El Sayed and AbdelRahman, my sisters Fatima, Ehsan and Fayza, love and thanks go to them for their continual belief, prayers and support which has helped me to achieve my goal.

And finally, special thanks and great love goes to my wife Dr Noha Bahey and my sons Hazem and Mostafa. It would have been difficult to achieve this work without you.

Author's Declaration

I declare that the work presented in this thesis is entirely my own with all exceptions being clearly indicated or/and properly cited in the context.

Signature:

Kamal Gadalla

The work has not been presented in part or alone for any other degree programme. Some of the work contained here has been published in part: a list follows.

Gadalla KK, Bailey ME, Cobb SR (2011) MeCP2 and Rett syndrome: reversibility and potential avenues for therapy. The Biochemical journal 439:1-14.

Kamal K. E. Gadalla, Mark E. S. Bailey, Rosemary C. Spike, Paul Ross, Kenton T. Woodard, Jie V. Deng, Anne E. West, R. Jude Samulski, Steven J. Gray and Stuart R. Cobb. Improved Survival and Reduced Phenotypic Severity Following AAV9/MECP2 Gene Transfer to Neonatal and Juvenile Male *Mecp2* Knockout Mice. (Submitted)

Abbreviations

AAV	Adeno-associated virus
ACh4	Acetylate histone 4
Amp	Ampicillin
ANOVA	Analysis of variance
AU	Arbitrary unit
BBB	Blood brain barrier
BDNF	Brain-derived neurotrophic factor
Bp	Base pair
BSA	Bovine serum albumin
Ca ²⁺	Calcium
CBA	Chicken beta actin promoter
ChAT	Choline acetyltransferase
CNS	Central nervous system
CMV	Cytomegalovirus promoter
CpG	Cytosine-guanine dinucleotide
CO ₂	Carbon dioxide
CTD	C-terminal domain
DAPI	4',6-diamidino-2-phenylindole
DNA	Deoxyribonucleic acid
EE	Environmental enrichment
FBS	Fetal bovine serum
GABA	Gamma-aminobutyric acid
GFAP	Glial fibrillary acidic protein
GFP	Green fluorescent protein
H1	Histone 1
H3	Histone 3
H4	Histone 4
HEK	Human embryonic kidney cells
Hp1	Heterochromatin protein 1
IC	Intracranial
IGF	Insulin-like growth factor
IV	Intravenous
IU	Infection unit
ITR	Inverted terminal repeat
KO	Knockout
LB	Luria-bertani medium
LTP	Long term potentiation
LTR	Long terminal repeat
MAP2	Microtubule associated protein
MBD	Methyl-CpG-binding domain

<i>MECP2</i>	Human Methyl-CpG-binding protein 2 gene
<i>Mecp2</i>	Mouse Methyl-CpG-binding protein 2 gene
MeCP2	Human Methyl-CpG-binding protein 2 protein
<i>Mecp2</i>	Mouse Methyl-CpG-binding protein 2 protein
<i>MECP2_e1</i>	Methyl-CpG-binding protein 2 isoform e1
<i>MECP2_e2</i>	Methyl-CpG-binding protein 2 isoform e2
ME1	<i>Mecp2_e1</i>
MeP	<i>Mecp2</i> endogenous core promoter
N	Number
NeuN	Neuron nuclear antigen rbfox3
NLS	Nuclear localisation signal
NTD	N-terminal domain
Orf	Open reading frame
PB	Phosphate buffer
PBS	Phosphate buffer saline
PCR	Polymerase chain reaction
PEI	Polyethylenimine
PGK	Phosphoglycerate kinase
PSC	Premature stop codon
PSD-95	Postsynaptic density protein 95
S421	Serine 421
scAAV	self-complementary Adeno-associated virus
SD	Standard deviation
SDS	Sodium dodecyl sulphate
SEM	Standard error of mean
ssAAV	Single-stranded Adeno-associated virus
Syn1	Synapsin1 promoter
RFP	Red fluorescent protein
RNA	Ribonucleic acid
rpm	round per minute
RTT	Rett syndrome
TF IIB	Transcription factor IIB
TRD	Transcription repression domain
vg	vector genome
WT	Wild-type
XCI	X chromosome inactivation
Yb1	Y box binding protein 1

Chapter 1

Introduction

1.1 General introduction

Rett syndrome (RTT) is a paediatric neurological disorder with a delayed onset of symptoms and is a leading cause of severe mental retardation in girls. First described in the 1960s by Andreas Rett (Rett, 1966) and thereafter by Bengt Hagberg in 1983 (Hagberg et al., 1983), RTT was shown in 1999 to be caused primarily by mutations in the X-linked gene, *MECP2* (Amir et al., 1999). After a number of groups had developed *Mecp2* knockout mouse models (Chen et al., 2001, Guy et al., 2001, Shahbazian et al., 2002a) and shown their utility in modelling aspects of the disorder, a number of attempts to reverse the signs after onset, or to prevent onset, were made. The initial successes reported have demonstrated the tractability of various aspects of the phenotype and highlighted the potential for treatments for Rett patients that address early stages in the pathogenetic pathway and go beyond merely ameliorating the downstream consequences. In this thesis I used *Mecp2* knockout mice to evaluate therapeutic approaches based on virus-mediated delivery of a wild-type copy of *Mecp2* to cells lacking this protein. Delivery of exogenous *Mecp2* to the brain is a challenging approach not just because of the inherent obstacles to delivering substances to the CNS but also because of the difficulties in transducing large number of cells and also to maintain exogenous *Mecp2* levels within physiological limits to prevent overexpression-related toxicity. Evaluation of the outcomes of these experiments should provide information about challenges, benefits, drawbacks and prospect of gene therapy application in the treatment of Rett syndrome.

1.2 Clinical manifestations of RTT

RTT (MIM 312750) is traditionally considered a neurodevelopmental disorder and is a primary cause of severe mental retardation in girls with an incidence of approximately 1 in 10,000 female births (Neul et al., 2010). RTT is characterized

by its almost exclusive occurrence in females and by a constellation of clinical features (Neul et al., 2010). These features, which distinguish RTT from the autism spectrum disorders that they are often co-classified with, include an initial period 6-18 month of apparently normal growth, however low mean birth weight and head circumference were also observed (Leonard and Bower, 1998, Huppke et al., 2003), followed by a highly characteristic developmental regression period during which the patients display loss of hand skills, impaired mobility and speech, development of stereotypic hand movements (continuous repetitive wringing, twisting, clapping hand automatism during wakefulness) and social interaction deficits (with features reminiscent of autism, figure 1-1). This regression phase is usually followed by a recovery or stationary phase for years, with some patients partially regaining skills. Nevertheless, the late motor deterioration phase usually takes place with its characteristic severe motor disabilities (Engerstrom, 1992, Hagberg, 2002).

Epilepsy is a common feature of RTT that occurs most often during the stationary phase (Hagberg, 2002), however the severity tends to decrease after the age of 20 years (Steffenburg et al., 2001). Other features include musculoskeletal abnormalities in the form of scoliosis, which starts at early school age, and lower limb distal deformity (Hagberg, 2002). Autistic features are frequent in RTT and include expressionless face, hypersensitivity to sound, indifference to the surrounding environment, and un-responsiveness to the social cues (Nomura, 2005) and mental retardation (Chahrour and Zoghbi, 2007). Episodic hyperventilation, breath holding and frequent apnoea during wakefulness are among the autonomic features of RTT (Julu et al., 1997, Kerr et al., 1997, Julu et al., 2001). Swallowing dysfunction, gastro oesophageal reflux, constipation and distension are also observed in RTT patients (Hagberg, 2002, Isaacs et al., 2003). Some of the previously mentioned features may be a direct result of the primary CNS deficits, but several may also be influenced by peripheral effects.

Clinical presentation and severity show a wide variation, and patients may exhibit all the essential features necessary for the RTT diagnosis (typical RTT), or they may show differences that enable their assignment to one of a range of atypical RTT diagnoses (Neul et al., 2010).

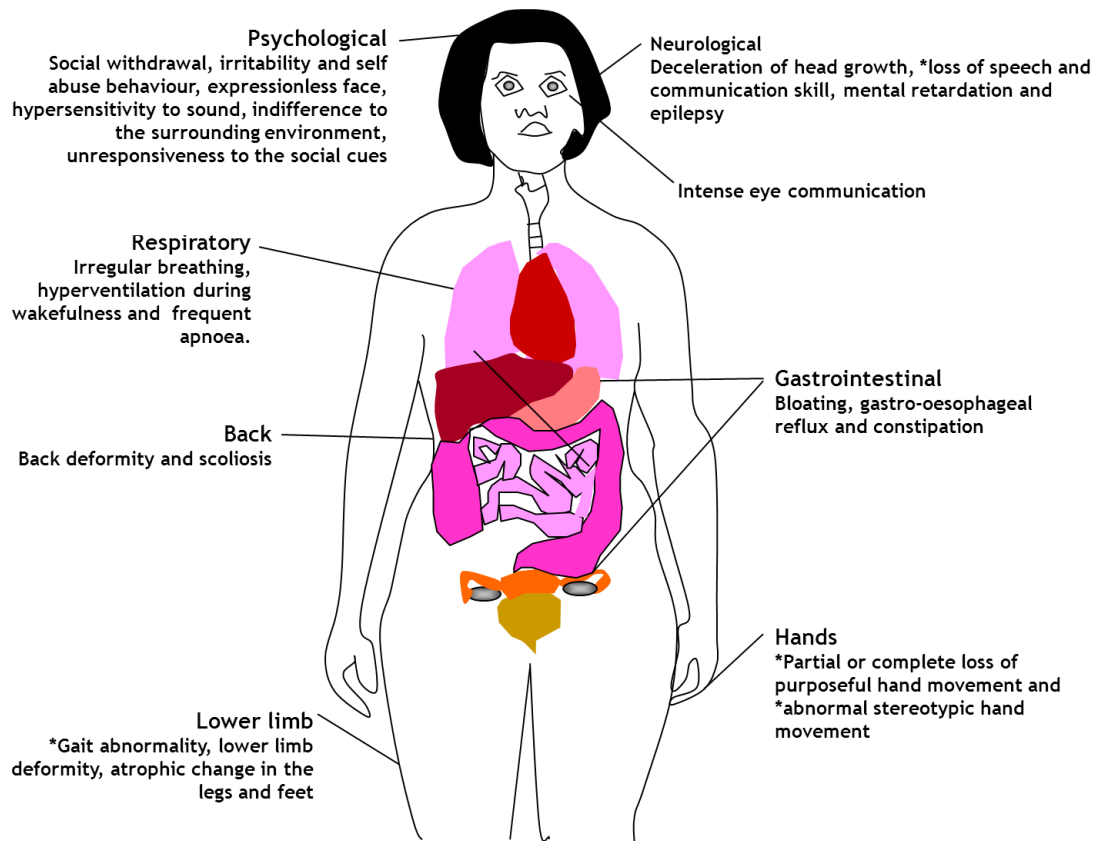


Figure 1-1 Clinical manifestations of Rett syndrome
Representative diagram showing the characteristic RTT clinical presentation.* indicates main criteria essential for typical RTT diagnosis.

1.3 Genetic basis of RTT

1.3.1 *MECP2* and Rett Syndrome

RTT cases are usually the result of dominantly-acting, *de novo* (Girard et al., 2001) mutations in the X-linked gene *MECP2*, which encodes methyl-CpG-binding protein 2 (MeCP2). More than 600 pathogenic *MECP2* mutations have been reported (RettBase: <http://mecp2.chw.edu.au/mecp2/>), including missense, nonsense, frameshift and large deletion mutations. Most pathogenic mutations in *MECP2* cause RTT in heterozygous females (Bienvenu and Chelly, 2006), but a range of *MECP2* mutations associated with other phenotypic outcomes, including milder forms of learning disability and, rarely, autism, are also known (Moretti and Zoghbi, 2006). Boys inheriting a mutant *MECP2* allele that would normally cause typical RTT in a female are much more severely affected, presenting with infantile encephalopathy and usually not surviving infancy. The differences between the observed phenotypes in males and in females are explained in terms of the proportion of cells in the nervous system expressing the mutant allele. Whilst all MeCP2-containing cells will express the mutant allele in males

that have inherited a single mutant X chromosome, the female brain, due to random X-chromosome inactivation, will develop into a mosaic network of cells with some expressing the mutant allele and others expressing the normal allele. In this way the pathology associated with the mutant allele is diluted (at the network level) in the female brain, albeit for direct cell-autonomous actions of the mutation.

1.3.2 *MECP2* structure

MeCP2 is predominantly a nuclear protein that was first discovered through its affinity for DNA sequences containing methylated 5'-CpG-3' dinucleotides (Lewis et al., 1992). It is a member of a small family of methylated DNA binding domain (MBD) proteins some of whose members can act as transcriptional repressors (Klose and Bird, 2006). MeCP2 is expressed quite widely throughout the body, with notably high expression in postnatal neurons (LaSalle et al., 2001, Shahbazian et al., 2002b, Zhou et al., 2006). It is expressed as two major splice variant isoforms, e1 and e2, that encode proteins with different N-termini (Kriaucionis and Bird, 2004, Mnatzakanian et al., 2004)(Figure 1.2). The first identified isoforms, *MECP2_e2* (*MECP2B* or *MECP2a*) uses a translational start site within exon 2, whereas the new isoform, *MECP2_e1* (*MECP2a* or *MECP2b*) derives from mRNA in which exon 2 is excluded and a new in-frame ATG located within exon 1 is used (figure 1-2).

Mecp2_e1 is the most abundant *Mecp2* isoform throughout the brain (Mnatzakanian et al., 2004, Dragich et al., 2007) and is translated more efficiently *in vivo* (Kriaucionis and Bird, 2004). Mutations in exon1 (only translated in *Mecp2_e1*) are sufficient to produce neurological manifestation and affect *MECP2_e2* translation. In contrast, there is no RTT-associated specific exon 2 mutation observed so far (Mnatzakanian et al., 2004, Saxena et al., 2006). A recent report showed that *Mecp2_e2* is up regulated during neuron-induced toxicity and it's forced over expression enhanced apoptosis in healthy neurons. In addition to this knocking down *Mecp2_e2* was found to be neuro-protective (Dastidar et al., 2012). In another study, knocking down *Mecp2_e2* by exon 2-specific deletion produced no RTT-associated symptoms suggesting this isoform is dispensable. However, further analysis showed that mutations of the

Mecp2_e2 allele were associated with placental defects and survival disadvantage.

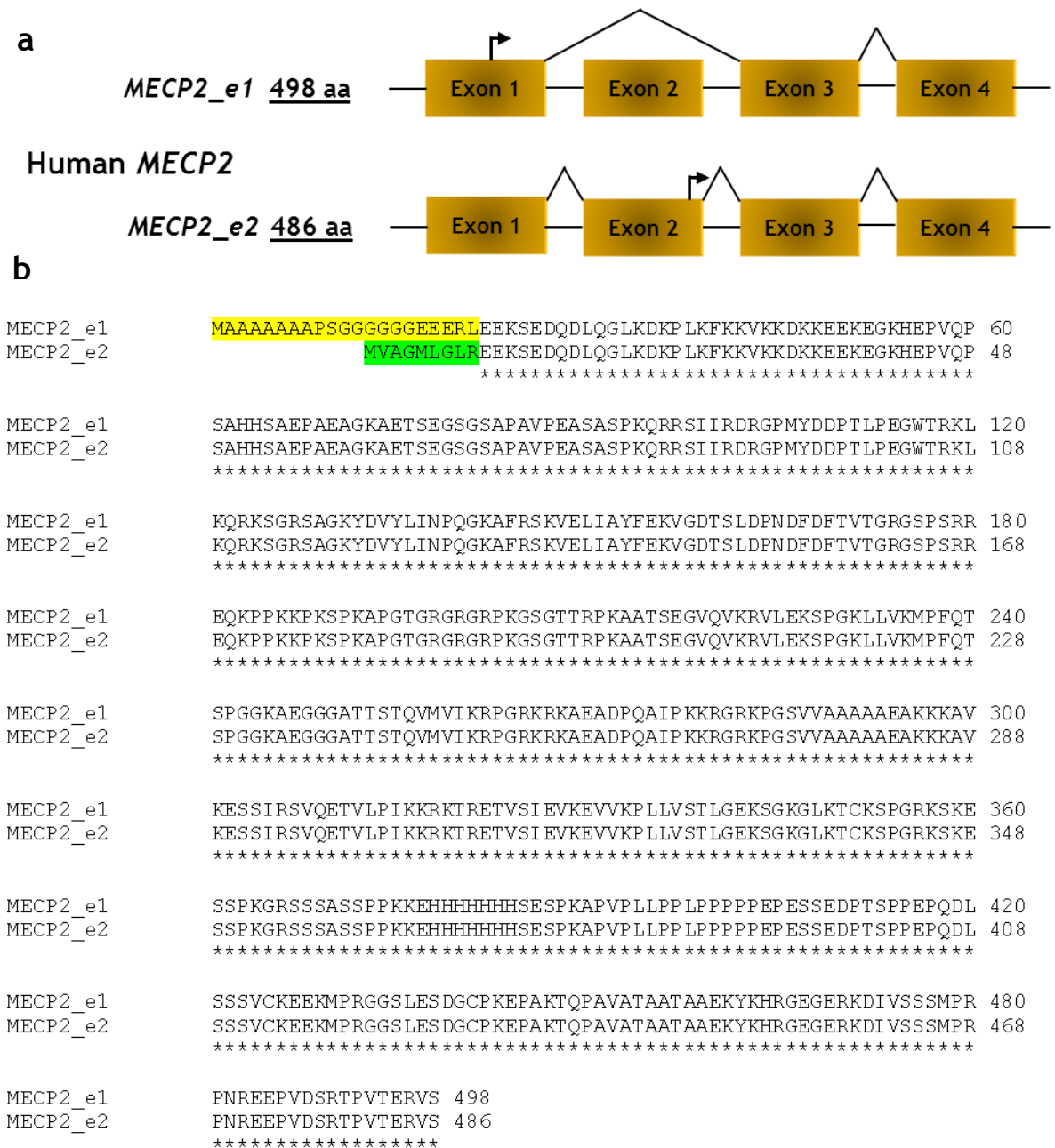


Figure 1-2 Composition and splicing pattern of *MECP2* gene

(a) Representative figure showing the Splicing patterns of *MECP2* gene. Two mRNA isoforms are generated; *MECP2_e1* and *MECP2_e2*. (b) The two isoforms generate two protein isoforms of MeCP2 with differing N-termini due to the use of alternative translation start sites (bent arrows). Yellow and green shadows refer to the amino acid differences in the N-terminal of both MeCP2_e1 (GenBank accession no. NM_001110792.1) and MeCP2_2 (GenBank accession no. NM_004992.3) isoforms respectively.

Both isoforms are thought to have two primary functional domains (figure 1-3), a methyl-CpG binding domain (MBD; 85 amino acids in length and has high affinity binding to 5-methyl cytosine) and a transcriptional repressor domain (TRD; 104 amino acid in length), that interacts with, amongst other things, histone

deacetylase (Nan et al., 1997, Jones et al., 1998) and the Sin3a repressor complex (Nan et al., 1998). MeCP2 protein has two nuclear localization signals (NLS) which are responsible for nucleus targeting of the Mecp2 (Nan et al., 1996) and a C-terminal segment which helps its binding to the nucleosome core (Chandler et al., 1999).

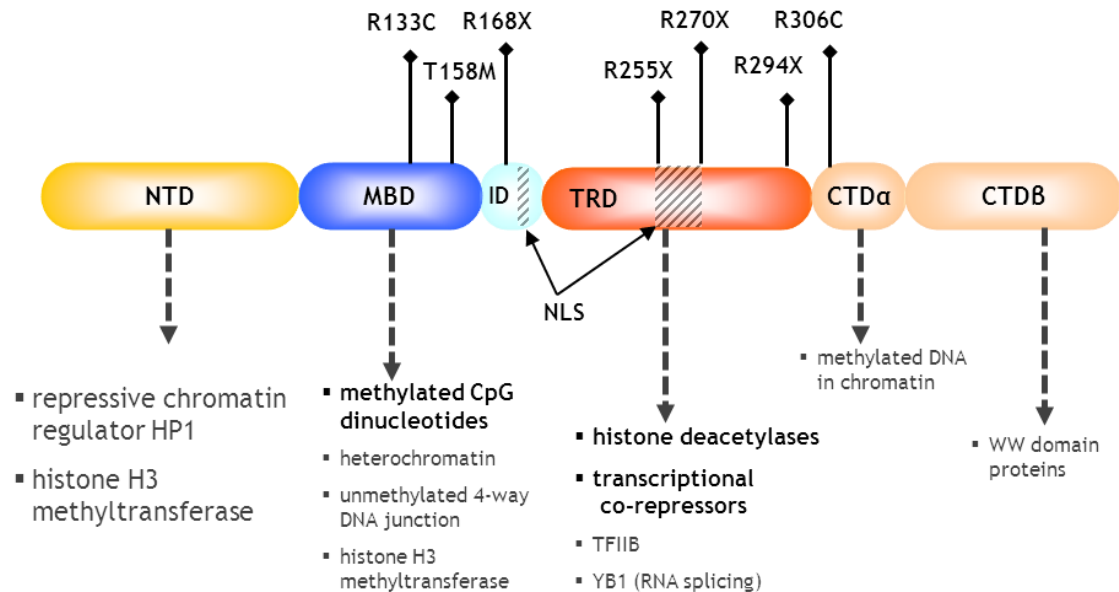


Figure 1-3 MeCP2 protein structure with the most frequent mutation sites, Representative figure showing the distinct functional domains of MeCP2. Apart from the N-terminus, both MeCP2 isoforms are identical and contain several functionally distinct domains: NTD, N-terminal domain; MBD, methyl binding domain; ID, inter domain; TRD, transcription repression domain; CTD, C-terminal domain; NLS; nuclear localisation signals. Locations of 7 of the most common point mutations in RTT are indicated (◆). Below each domain are indicated major (bold) and other (grey) interactors and functions. HP1; heterochromatin protein 1, TFIIB; transcription factor IIB, YB1; Y box binding protein 1. This figure was taken from (Gadalla et al., 2011).

1.3.3 Functions of MeCP2

MeCP2 is expressed in neuronal stem cells (Jung et al., 2003, Namihira et al., 2004) with an observed role in embryonic neurogenesis in *Xenopus* (Stancheva et al., 2003). However, neuronal proliferation and differentiation from neural precursor of *Mecp2* knockout and WT mice were identical indicating that *Mecp2* is not likely to be involved in early cell fate decision or neuron differentiation but rather that it impacts neuronal maturation and maintenance (Kishi and Macklis, 2004, Smrt et al., 2007). During development, *Mecp2* expression is very low or absent in immature neurons and increases during neuronal maturation to reach its highest levels in postmitotic neurons and remains high throughout adult life (Kishi and Macklis, 2004, Matarazzo et al., 2004). Knocking out *Mecp2* in the

adult mice brain resulted in very similar neurological and motor deficits to germ line knockout mice suggesting an essential role of *Mecp2* in the maintenance of neuronal function (McGraw et al., 2011).

Recent biophysical studies have probed the binding specificity of MeCP2 and have reported the interaction (via hydration within the major groove) with methylated DNA and also the interaction with nucleosomes (Ho et al., 2008, Yang et al., 2011). Despite this knowledge, the precise biological function of MeCP2 remains unclear. Proposed additional or alternative functions include selective enhancement/activation of gene expression (Chahrour et al., 2008), chromatin regulation (Nikitina et al., 2007), and RNA processing (Long et al., Young et al., 2005). It has recently been established that MeCP2 is distributed across the genome very much in parallel with methylation density, and to the exclusion, in neurons, of histone H1 (Skene et al., 2010). These data suggest that MeCP2 plays a major role in the suppression of transcription throughout very large scale genome-wide actions; in this way it may be best to describe MeCP2's function in terms of global dampening of transcriptional noise.

1.4 Animal models of Rett syndrome

RTT's status as, relatively common, monogenic disorder has created considerable interest in investigating the underlying pathology. A large part of this interest comes from a desire to develop rational therapies for patients, but it has also emerged that gaining a fuller understanding of the underlying pathology and neuronal dysfunction in RTT may provide insights into the pathophysiology of neurodevelopmental disorders more generally (Neul and Zoghbi, 2004). Since most *MECP2* mutations leading to RTT involve loss of function of the mutant allele, RTT can be modelled using *Mecp2* knockout mice.

Several of the models that have been created recapitulate many of the cardinal features that characterize RTT in humans, although there are important differences. An early animal model of RTT was generated by deletion of exon 3 (encodes 116 amino acids most of it located in the MBD of *Mecp2* protein)(Chen et al., 2001). *Mecp2*^{-y} male mice in which *Mecp2* was knocked out either globally or specifically in the central nervous system were apparently normal in the first few weeks of life. However abnormal behaviours such as nervousness,

body trembling, pila erection and occasionally hard respiration were observable by the age of 5 weeks. With the disease progression, these mice displayed hypoactivity, increased trembling, loss of the bodyweight and premature death around 10 weeks of age. In contrast heterozygous females, *Mecp2*^{-/+} (more accurate model of human RTT) that have mosaic network of cells expressing WT *Mecp2* allele and cells expressing the mutant *Mecp2* allele (lacking *Mecp2*) displayed, similar to RTT patients, initial period (~4 months) of apparently normal growth followed by weight gain, reduced activity and ataxia and gait abnormalities at a later stage. To test the effect of neuron-specific deletion of *Mecp2* on the RTT-like phenotype, another mouse model in which *Mecp2* was knocked out specifically in postnatal neurons was generated by the same authors. Interestingly these mice displayed a phenotype similar, however milder, to that seen in animals carrying a germ line *Mecp2* deletion. The close similarity in the phenotype between these animal models (global, brain- and neuron-specific deletion of *Mecp2*) suggests that a lack of functional *Mecp2* in neurons is the primary cause of the RTT-like phenotype.

Another early model was created by Guy and colleagues in which *Mecp2*-exon 3 and 4 were deleted (Guy et al., 2001). *Mecp2*^{-ly} mice from this line displayed a relatively normal phenotype in the first 3-4 weeks of postnatal life that was followed by the development of uncoordinated gait, reduced spontaneous movement, irregular breathing, hindlimb claspings, uneven wearing of the teeth and un-descended testes. Four weeks later these mice showed rapid loss of bodyweight and died prematurely at approximately 8-10 weeks. On the other hand, brain-specific deletion of *Mecp2* resulted in a phenotype similar to that of the germ line deletion providing further evidence for the importance of the brain in the development of the RTT-like phenotype. Heterozygous female mice (*Mecp2*^{-/+}) recapitulate a similar phenotype trajectory to that observed in female patients (Hagberg, 2002) with initial period of apparently normal development lasting about 3 months followed by development of inertia and hind limb claspings. This is then followed by a period of long term phenotype stability similar to that observed in the stationary phase in human patients. Most of these females develop similar RTT-like phenotype by the age of nine months, however some remain without symptoms even at one year.

Another functional knockout mouse model was generated through silencing the endogenous *Mecp2* gene by the insertion of a lox-Stop cassette (Dragatsis and Zeitlin, 2001) into intron 2 of *Mecp2* gene (Guy et al., 2007). *Mecp2*^{stop/y} male mice were phenotypically comparable to *Mecp2*-null mice and displayed tremor, abnormal breathing, lack of spontaneous mobility, wide-based gait, hind limb clasp and bad general condition. These mice were underweight and died as early as 11 weeks. A modification of this animal model was used in a reactivation study in which Cre recombinase and a modified oestrogen receptor (Cre-ER) were combined with the *Mecp2*^{lox-Stop} allele allowing conditional activation of endogenous *Mecp2* under its own promoter and regulatory elements (Guy et al., 2007).

Most of these *Mecp2* knockout mice display an anxiety phenotype including reduced exploration, increased thigmotaxis and altered plus and zero maze behaviour (Pelka et al., 2006, Stearns et al., 2007). The motor dysfunction that is a characteristic part of the RTT phenotype places severe limits on the range of cognitive tests that can be carried out but impairments in fear conditioning and novel object recognition have been reported.

Mecp2-null (Chen et al., 2001, Guy et al., 2001) or stop (Guy et al., 2007) male mice recapitulate severe neurological diseases comparable to that observed in the human males making them a good model to test efficacy of new therapies. However, the early morbidity and mortality observed in these models prohibits long-term behavioural analysis. Therefore Shahbazian and colleagues have created a mouse model with a truncated version of *Mecp2* which contains the first 308 amino acids and hence is called *Mecp2*³⁰⁸ (Shahbazian et al., 2002a). This truncated *Mecp2* protein preserves the MBD, TRD, and both nuclear localization signals, but lacks the C-terminal domain which includes important phosphorylation sites. The *Mecp2*^{308/y} mouse model displays a classic albeit milder RTT phenotype that recapitulates many of the features of RTT but display an extended survival (up to one year) and more modest phenotype trajectory that starts late in life, at approximately five months, in the form of tremor, myotonic jerks, seizures and forelimb stereotypic movement and clasp. *Mecp2*^{308/y} mice also display impairments in hippocampus-dependent spatial memory as well as social memory (Moretti et al., 2006). In contrast to *Mecp2*-null models, these mice are fertile and exhibit normal body and brain weights

with no detectable morphological changes in the peripheral tissues or in the CNS. Heterozygous female *Mecp2*^{308/+} display milder and more variable phenotype features even at one year old.

A cell-type specific knockout study in which *Mecp2* was silenced specifically in inhibitory GABAergic cells revealed a range of subtle RTT-like neuropsychiatric phenotypes (table 1-1) including autistic-like repetitive behaviours (Chao et al., 2010). In another study in which MeCP2 was silenced in tyrosine hydroxylase-containing neurons, mice were found to display motor abnormalities and breathing problems including an increased incidence of apnoeas suggesting that dysfunction in aminergic systems may be responsible for some RTT-like breathing phenotypes (Samaco et al., 2009). A more recent mouse model of RTT was generated by insertion of missense mutation in *Mecp2* to replace amino-acid threonine T158 with methionine to mimic one of the most common missense mutations in human (Bienvenu and Chelly, 2006). *Mecp2*^{T158M/y} male mice showed RTT-like phenotypes that were similar, however less severe, compared to the *Mecp2*-null mice with slightly extended survival (Goffin et al., 2012) suggesting that a single *MECP2* mutation could be almost as detrimental as complete absence of the protein.

1.5 Cellular alterations in RTT patients and animal models

In addition to the gross neurological and behavioural abnormalities observed in RTT, a number of structural changes in the brain were also observed in RTT patients as well as in *Mecp2* knockout mice. In RTT patients, the most obvious features are a reduced brain size and weight with subtle changes in neuronal packing density and neuronal morphology, e.g. reduced dendritic branching complexity and changes in spine density and morphology (Armstrong et al., 1995, Bauman et al., 1995). Similar changes are observed in *Mecp2*-null mice (Chen et al., 2001) with an evidence of both cell autonomous and non-cell autonomous changes in neuronal morphology (Kishi and Macklis, 2010). *Mecp2* level was also reported to regulate number of excitatory synaptic connections (Chao et al., 2007) and axonal guidance (Degano et al., 2009). Electrophysiological studies revealed relatively modest alterations in the salient electrical properties of cortical neurons (Dani et al., 2005) although more pronounced changes are

reported in subcortical regions (Bauman et al., 1995). In contrast, a robust body of evidence exists for changes in synaptic signaling, affecting both excitatory and inhibitory amino acid neurotransmission (Kline et al., Dani et al., 2005, Nelson et al., 2006, Medrihan et al., 2008). Regarding inhibitory connections, loss of *Mecp2* has been shown to reduce quantal GABA release consistent with a presynaptic reduction in neurotransmitter content (Chao et al., 2010). This may account for the tendency for seizures to occur in the RTT brain. In addition to changes in the baseline properties (frequency and amplitude) of synaptic events, several studies have reported deficits in both short- and long-term forms of synaptic plasticity (Le Roith, 1997, Moretti et al., 2006, Guy et al., 2007, Weng et al., 2011). Interestingly, synaptic plasticity appears normal in young *Mecp2*-mutant mice (Guy et al., 2007), but becomes progressively more impaired with the disease progression in older mice (Guy et al., 2007, Weng et al., 2011). The exact mechanism by which absence of functional *Mecp2* in the nucleus produces a synaptic deficit phenotype remains to be established.

1.6 Reversibility and treatment strategies for the RTT-like phenotype

The conventional view is that abnormalities in brain development during critical periods of growth and maturation will produce aberrations in the nervous system with subsequent essentially irreversible neurological and psychiatric features due to the limited ability of the brain to generate new neurons or to radically rewire itself. However, a number of studies of animal models of diseases ranging across Down syndrome (Fernandez et al., 2007, Rueda et al., 2008), fragile X syndrome (McBride et al., 2005, Dolen et al., 2007), and Angelman syndrome (van Woerden et al., 2007) are beginning to show an unexpected propensity for phenotypic reversal, even in adult mice (Ehninger et al., 2008). This propensity has also recently been reported in RTT (Guy et al., 2007, Derecki et al., 2012).

RTT is considered to result from a failure of neurons to mature, a developmental process, and / or of their failure to maintain a mature phenotype, a maintenance process, (Kishi and Macklis, 2004, Palmer et al., 2008, Degano et al., 2009). MeCP2 is also present in astrocytes and other non-neuronal cell types in the brain, albeit at much lower levels (Schmid et al., 2008). Although a deletion and a neuron-specific expression of *Mecp2* studies in mice show that the

dominant mutant phenotype is principally due to absence of MeCP2 in neurons (Chen et al., 2001, Guy et al., 2001, Luikenhuis et al., 2004), loss of MeCP2 function in astrocytes leads to altered release of neurotrophic factors, changes to dendritic outgrowth (Ballas et al., 2009, Maezawa et al., 2009) and contribute to non-cell autonomous aspects of RTT pathology. Moreover astrocyte-specific *Mecp2* delayed activation rescued RTT-like phenotypes in *Mecp2* knockout mice (Lioy et al., 2011) and bone marrow transplantation of WT microglia into pre-symptomatic *Mecp2*^{-y} mice arrested the progression of the RTT-like phenotype (Derecki et al., 2012).

In considering whether the phenotype is reversible or even preventable, three scenarios must be considered. Firstly, since neurons lacking MeCP2 display long-term survival and since neurons seem to require MeCP2 throughout their lives, it is possible that the introduction of normal MeCP2 or therapeutic strategies targeting MeCP2-related signaling might restore function and, thereby, reverse deficits seen in RTT. Alternatively, it may be that MeCP2 is essential for neuronal development during a specific time window, after which damage caused by its absence is permanent. A third scenario combines both of these ideas, whereby certain RTT-like features can be rectified in the mature nervous system if cells begin expressing MeCP2 whilst other features are critically dependent upon the presence of MeCP2 during essential, developmentally inflexible, processes and are thus insensitive to simple restoration of MeCP2 or other intervention beyond a critical period.

1.6.1 Reversibility of the RTT-like phenotype in *Mecp2* knockout mice models

Mouse models of RTT have played an important role in studying the requirement for *Mecp2* in different cell types and at different stages of development as well as in testing the reversibility of RTT-like phenotypes. For instance, Luikenhuis and colleagues have created an animal model in which *Mecp2* coding sequence was cloned into exon 1 of the tau locus to allow neuronal-specific expression of *Mecp2* in WT as well as *Mecp2*-null mice. This report showed that *Mecp2*-null mice heterozygous for the transgene displayed a modest over-expression of *Mecp2* transgene and an absence of the RTT-like phenotype. However the same study showed that WT and *Mecp2*-null mice homozygous for the transgene

showed severe overexpression of *Mecp2* transgene (2-4 fold of the WT level) that was associated with profound motor dysfunction (Luikenhuis et al., 2004). This experiment provided evidence of a critical requirement for MeCP2 in neurons but it also highlighted the importance of maintaining MeCP2 protein expression at an appropriate level, which has therapeutic significance when considering potential gene therapy strategies. In another study, (Giacometti et al., 2007), early brain-specific activation of *Mecp2* under either nestin (drive *Mecp2* expression on pre-mitotic cells) or tau (drive expression of *Mecp2* in post-mitotic neurons) promoter resulted in prolonged lifespan, normalized bodyweight, delayed development of motor deficits and improved motor activities that had been reported in *Mecp2*-null mice (Chen et al., 2001). On the other hand delayed forebrain activation of *Mecp2* showed modest effects compared to the whole brain activation. These results suggest that the introduction of *Mecp2* to the nervous system under artificial promoters is sufficient to enable a modest amelioration of RTT-like phenotypes and to prolong life span.

In another study, Guy and colleagues (Guy et al., 2007) created a mouse model in which the endogenous *Mecp2* gene is silenced by insertion of a lox-Stop cassette but which can be conditionally activated (cre mediated Stop cassette excision) following tamoxifen injection. Importantly, this enabled the activation of *Mecp2* at its endogenous locus and under the control of its own promoter and regulatory elements. The control mice *Mecp2*^{cre-stop/y} (no tamoxifen-induced activation of *Mecp2*) typically developed the RTT-like phenotype with premature mortality, however hemizygous male mice showed no RTT-like phenotype when treated with tamoxifen in the first 4 weeks of life (presymptomatic) and showed robust symptom reversal and dramatically enhanced survival if treated once symptoms had developed. Furthermore, heterozygous female mice (the accurate model of RTT in humans) displayed a dramatic improvement of RTT-like phenotypes, a normalization of bodyweight and a restoration of synaptic plasticity deficits, even when treated as fully adult mice (>6 months). These findings confirm the propensity for phenotypic reversal, at least in the mouse model. This reversibility may bring into question the categorization of RTT as a neurodevelopmental disorder as it suggests that MeCP2-deficiency during brain development does little lasting damage. However, it remains to be established whether improvement in overt signs (tremor, locomotion, abnormal breathing

etc.) is accompanied by improved cognition and other behavioural correlates. Nevertheless, a following study by the same authors show improvement in a wide range of locomotor and respiratory phenotypes as well as evidence for structural remodelling in the brain following *Mecp2* activation (Robinson et al., 2012). These mouse genetic studies suggest that there is the opportunity, even in the fully mature nervous system, to modulate MeCP2 levels or target downstream processes by pharmacological means to prevent, or reduce the severity of, the condition. Interestingly, recent complementary experiments in an adult onset model of RTT (tamoxifen-induced excision of a floxed *Mecp2* allele) suggest that MeCP2 is critical for ongoing neurological function in the adult nervous system and that potential therapies for RTT are likely to be required throughout life (McGraw et al., 2011).

In contrast to the significant reversal seen following a global reintroduction of *Mecp2*, studies focusing on more restricted expression of *Mecp2* and using promoters other than the endogenous *Mecp2* promoter have shown a more modest effect. For instance, *Mecp2* expression under either Ca^{2+} /calmodulin-dependent protein kinases II (CamKII) or enolase promoter in the forebrain and cerebellum/striatum respectively was unable to prevent the occurrence of the RTT-like phenotype in *Mecp2*^{-y} mice (Alvarez-Saavedra et al., 2007). However *Mecp2* expression under the control of CamKII promoter in the forebrain of *Mecp2*^{-/+} female mice revealed improvement of the mobility and locomotor activity to WT levels (Jugloff et al., 2008). It is unclear from these studies whether the sustained deficits result from an inherent irreversibility due to neurodevelopmental aberrations or to dysfunction of regions or cell types in the brain still devoid of *Mecp2*, or to the exogenous promoters driving cellular *Mecp2* expression at levels outside the physiological range, or to other unknown mouse-specific processes.

Mecp2 is a widely expressed protein which is especially abundant in post-mitotic neurons (Skene et al., 2010). The neurological phenotype of RTT together with the fact that neuron-specific deletion of *Mecp2* resulted in RTT-like phenotypes suggests that neurons are the key contributor to RTT phenotypes (Chen et al., 2001, Guy et al., 2001). However glia lacking *Mecp2* negatively affects neurons in a non-cell autonomous manner (Ballas et al., 2009, Maezawa et al., 2009). Interestingly delayed astrocyte-specific activation of *Mecp2* in *Mecp2*-null mice

resulted in improved locomotion, anxiety levels and normalized the breathing pattern with great extension of the life span (Lioy et al., 2011). This study emphasises the importance of glia in both pathogenesis and reversal of RTT. In support of this notion is the recent study that showed the ability of bone marrow transplantation of WT microglia in *Mecp2*-null mice to arrest disease progression and extend the survival of *Mecp2*^{-y} mice (Derecki et al., 2012).

In addition to targeting *Mecp2* itself, genetic approaches in mice have also been used to explore interactions with other signaling processes in the brain. Bdnf (brain-derived neurotrophic factor) is a neurotrophic factor whose expression is proposed to be regulated by *Mecp2* protein (Chen et al., 2003b, Martinowich et al., 2003). Neural activity leads to phosphorylation of *Mecp2*, which correlates with the transcriptional induction of Bdnf. It has been reported that *Mecp2*-null mice display lower levels of Bdnf protein and that Bdnf knockout mice also exhibit some of the RTT-like phenotypes including hindlimb clasping and reduced brain weight (Chang et al., 2006). To explore the potential involvement of Bdnf in RTT pathogenesis a *Mecp2* and Bdnf double knock out mouse line was created (Chang et al., 2006). This was found to result in an earlier onset of RTT-like features and lethality. In contrast, *Mecp2*-null mice in which Bdnf is overexpressed resulted in a delayed onset of RTT-like signs and a significantly increased life span. These experiments suggest that increasing the level of Bdnf expression could influence the disease progression in RTT.

1.6.2 Treatment strategies for RTT

The demonstrated reversibility of the *Mecp2* knockout phenotype in *Mecp2*-STOP mice (Guy et al., 2007), as described above, has stimulated a good deal of activity in exploring therapeutic approaches designed both to reverse existing dysfunction in RTT and to prevent its onset. In addition to the question of which of these two basic approaches to take therapeutically, there is also the question of where in the pathogenetic pathway to target the therapy. Two main categories of intervention suggest themselves - targeting the primary underlying cause (i.e. a loss of function mutation in *MECP2*) or targeting processes further downstream in the pathway. In the following sections I review the potential for such therapeutic approaches and describe any progress thus far.

1.6.2.1 Pharmacological approaches in RTT - current challenges

Many groups have argued that identifying factors that are downstream of MeCP2 function and targeting those pharmacologically is the most sensible approach to developing rational therapies in RTT. Nevertheless it is unlikely for drug molecules to replace the, yet unknown, function of MeCP2. The widely believed proposition that MeCP2 has distinct 'target genes' whose expression becomes significantly aberrant in the absence of functional MeCP2 has little corroborated support (Skene et al., 2010). If MeCP2 truly functions to sense/interpret the DNA methylation signal then the action of MeCP2, or more specifically the precise dysfunction caused by its absence, will be uniquely dependent on the methylation status within a given neuronal type or indeed individual neuron. Moreover, the high abundance of MeCP2 together with the ubiquity of DNA methylation suggests that candidates for targeting its core chromatin-binding function therapeutically will be multiple and diverse (Skene et al., 2010). Furthermore, it is unclear which of the various reported changes in gene expression, brain neurochemistry, neuronal / synaptic morphology, cellular / synaptic function, and network electrical activity patterns (Pintaudi et al., Zhang et al., 2008, D'Cruz et al., 2010) in the RTT brain are a primary result of MeCP2 dysfunction and which may represent secondary effects. Identifying the primary molecular dysfunction in RTT and the important and tractable downstream changes in signaling processes remains an important challenge.

The brain signaling pathway that has received most attention in relation to MeCP2 to date is the neurotrophic factor Bdnf (brain-derived neurotrophic factor) whose level shows consistent changes in the RTT brain (Chen et al., 2003b, Martinowich et al., 2003). Moreover, overexpressing Bdnf ameliorates key symptoms in *Mecp2*-null mouse (Chang et al., 2006). Therefore, Ogier and colleagues tested the ampakine CX546, a positive modulator of AMPA receptors and known enhancer of Bdnf levels (Lauterborn et al., 2000) in *Mecp2*-null mice. Ampakine was able to restore normal breathing pattern and respiratory minute volume (Ogier et al., 2007). This study is consistent with the hypothesis that elevation of Bdnf level is associated with improved phenotype and supports the concept of targeting Bdnf signaling in RTT. Ampakine-induced Bdnf up-regulation was able to reverse deficits in synaptic plasticity and to improve the long-term memory in animal model of Huntington disease, however with no effect on the

impaired locomotor activity (Simmons et al., 2009). Therefore it will be interesting to find out whether ampakines or novel TrkB receptor ligands may improve other features of the *Mecp2*-null phenotype.

Table 1-1 Mapping the effect of *Mecp2* deletion or activation in the RTT mice models. Adopted from (Gadalla et al., 2011).

Intervention								
Stage:	Early (prenatal/early postnatal)					Late (post-onset)		
Location:	Neuronal subset	Neuronal subset	Neurons	All CNS	Global	Brain-region	Global	Global
								
Objective:	Prevent MeCP2 expression in specified cells		Deliver MeCP2 to MeCP2-ve cells			Drive MeCP2 expression in specified cells	Deliver <i>Mecp2</i> to <i>Mecp2</i> -ve cells	Deliver <i>Mecp2</i> to <i>Mecp2</i> -ve astrocyte
Strategy:	GAD65 promoter drives cre to delete floxed <i>Mecp2</i> in GABAergic neurons	TH promoter drives cre to delete floxed <i>Mecp2</i> in aminergic neurons	Tau-promoter drives <i>Mecp2</i> transgene expression	Nestin-cre activates exogenous, PGK promoter-driven <i>Mecp2</i> by STOP cassette deletion	Tamoxifen re-activates native <i>Mecp2</i> by STOP cassette deletion	Region-specific promoters enhance <i>Mecp2</i> in specific brain regions	Tamoxifen re-activates native <i>Mecp2</i> by STOP cassette deletion	Tamoxifen re-activates native <i>Mecp2</i> by STOP cassette deletion in astrocyte
Result:	•Autistic-like behaviours •↓GABA transmission	•↓ Motor function •breathing problems	Prevent phenotype (Motor dysfunction etc with over-expression)	•↑ life span •↑ nocturnal activity •↑ brain / body weight	Prevent phenotype	•↑ survival •↑ nocturnal activity	Rescue of Rett phenotype in symptomatic mice	Rescue of Rett phenotype in symptomatic mice
Refs.	Chao 2010	Samaco 2009	Luikenhuis 2004	Giacometti 2007	Guy 2007	Luikenhuis 2004	Guy 2007	Lioy 2011

Another growth factor that has attracted attention is a derivative of IGF1 (insulin-like growth factor 1). Full length IGF1 which is important in neuronal maturation and as a regulator of synaptic plasticity, is widely expressed in the brain and its function is to regulate neuronal survival and synaptic maturation (Bondy and Cheng, 2004). IGF1 signaling is reduced in RTT patients as well as in *Mecp2*-null mice as a consequence of elevated levels of the IGF-binding protein 3 (Itoh et al., 2007). The N-terminal tripeptide of IGF1 (known as GPE) has neuromodulatory and neuroprotective effects and administration to *Mecp2*-null mice significantly extended the survival and improved locomotor activity and cardiorespiratory function. Moreover, at the cellular level, it increased PSD-95 (a major postsynaptic density protein and synaptic marker) labelling, cortical spine density and the amplitude of the excitatory post synaptic currents (Tropea et al., 2009). Nevertheless, treated mice developed all the characteristic RTT-

like features and died prematurely. In addition, full-length IGF1 increased the number of glutamatergic synapses in neurons that were differentiated from pluripotent stem cells taken from RTT patients (Marchetto et al.). Recombinant IGF1 is available as a clinical formulation and is currently undergoing initial phase clinical trials in RTT patients (<http://clinicaltrials.gov/ct2/show/record/NCT01253317?term=rett+syndrome>).

1.6.2.2 Neurotransmitter systems – monoamines

Another transmitter system that has attracted attention in RTT is the monoamines. Monoamines (noradrenaline, serotonin and dopamine) are important regulators of brainstem function whose levels have been reported to be decreased in brain biopsies taken from RTT patients (Brucke et al., 1987, Lekman et al., 1989). This reduction was also observed in *Mecp2*-null mice in conjunction with reduced levels of the primary synthesizing enzyme tyrosine hydroxylase in the brain, peripheral neurons and the adrenal medulla (Viemari et al., 2005, Roux et al., 2008, Roux et al., 2010). *In vitro* application of noradrenaline to the brainstem of *Mecp2*-null mice, which displayed irregular rhythms, stabilized the respiratory network rhythmogenesis (Viemari et al., 2005) suggesting a potential role of monoamine in RTT therapy. In a follow up experiment, administration of Desipramine (an antidepressant which increases noradrenaline levels by blocking its re-uptake) to *Mecp2*-null mice resulted in delayed onset of breathing abnormalities in young animals and improvement of respiratory phenotype (apnoeas) in symptomatic mice (Roux and Villard, 2007, Zanella et al., 2008). However, whilst Desipramine treatment improved respiratory function and extended the lifespan of *Mecp2*-null mice (from a modest increase up to double), it failed to alter growth curves or, surprisingly, levels of noradrenaline (Zanella et al., 2008).

1.6.2.3 Neurotransmitter systems – glutamate

Glutamate is the primary excitatory transmitter in the central nervous system. Loss of MeCP2 is associated with structural and functional changes in the glutamatergic synapses with consistent reduction in various forms of short and long-term synaptic plasticity in *Mecp2*-null mice brains. Neuron-to-neuron signaling and the neurotoxic actions of glutamate released from microglia are

suggested to contribute to the onset and progression of RTT (Maezawa and Jin, 2010). Mice lacking *Mecp2* show altered NMDA subunit distribution within glutamatergic synapses (Maliszewska-Cyna et al., 2010). NMDA receptors are key component of many forms of synaptic plasticity and are important in excitotoxic processes. Memantine is a weak non-competitive antagonist of the NMDA receptor and is used in Alzheimer's disease therapy by virtue of its proposed antagonism of sustained pathological activation of NMDA receptors and promotion of synaptic plasticity through reducing synaptic noise (Frankiewicz and Parsons, 1999). In a recent report, Weng and colleagues (Weng et al., 2011) showed that the progressive reduction in both short and long term forms of synaptic plasticity seen in *Mecp2*-mutant hippocampus can be partially reversed *ex vivo* using clinically relevant concentrations of memantine. However, when applied *in vivo*, memantine failed to show any improvement in RTT-like phenotypes suggesting that the improvement seen at the synaptic level is not reflected when considering the overall phenotype. However, it is possible that memantine may be useful in targeting other aspects of RTT such as the cognitive impairment.

1.6.2.4 Neurotransmitter systems - GABA

GABA (gamma-aminobutyric acid) is the major inhibitory neurotransmitter in the brain. The selective silencing of *Mecp2* in the GABA-releasing neurons revealed that *Mecp2* is crucial for their normal function (Zhang et al., Chao et al., 2010). Dysfunction of GABA signaling is suggested to mediate some of the autism-like behaviours as well as other RTT-like phenotypes including altered locomotor activity, motor function and breathing patterns (Chao et al., 2010). Previous report has shown that increased GABA level by using GABA reuptake blocker improved respiratory phenotype in *Mecp2*-null mice. In addition, the combination of GABA reuptake blocker and serotonin 1a receptor agonist completely rescued the breathing abnormalities in *Mecp2*^{-/+} heterozygous females (Abdala et al., 2010). Moreover, Pre-treatment with midazolam (a positive allosteric modulator of several common GABAA receptor subtypes) resulted in a reduction in apnoeas, that take place after hypoxic or hypercapnic exposure (Voituron et al., 2009), and reduction in the prolonged inspiration events (Voituron et al.) in *Mecp2*-null mice (Voituron and Hilaire). This data

indicates that drugs targeting GABAergic neurotransmission may be of important therapeutic benefits in RTT patients.

1.6.2.5 Drugs targeting *MECP2* mutations

In addition to targeting downstream systems that are disrupted in the absence of functional MeCP2, another pharmacological approach would be to target, further upstream, the immediate consequences of the specific mutation responsible for the MeCP2 abnormal functions in the particular patient. Many patients carry nonsense mutations in *MECP2* (e.g. p.R168X, p.R255X, p.R270X), which are associated with premature stop codons (PSCs). Agents, such as aminoglycoside antibiotics, which permit ribosomal read-through of PSCs during translation would enable production of full length functional protein (Martin et al., 1989, Manuvakhova et al., 2000). Aminoglycoside-induced read-through has been applied in some clinical applications such as Duchenne muscular dystrophy (Malik et al.) and cystic fibrosis (Howard et al., 1996, Bedwell et al., 1997). Based on these previous studies and considering the fact that up to ~40% of typical RTT patients with *MECP2* mutations have one of the nonsense mutations (Philippe et al., 2006), aminoglycosides seem a promising avenue by which to achieve a restoration of full length functional MeCP2. In cultured cell line aminoglycosides were able to produce full length Mecp2 protein from cells expressing different type of Mecp2 nonsense mutations, e.g. R168X and R255X, however with variable expression levels dependent on the type of mutation and the drugs used (Popescu et al., Brendel et al., 2009). The low read-through efficiency together with the known toxicity of these drugs indicates that the currently available aminoglycoside drugs are unlikely to represent a new therapeutic approach. Nevertheless a new generation of aminoglycoside-related compounds with relatively high readthrough efficiency and less toxic effect such as PTC124 (Welch et al., 2007) and NB54 (Nudelman et al., 2009) could be more promising, However little is known about the ability of these compounds to cross the BBB and so their likely efficiency in treating CNS disorders including RTT is unknown.

1.6.2.6 Environmental and epigenetic factors

Exposure to an enriched environment (EE), by increasing social stimulation and increasing the complexity of housing through additional nesting material

(Nithianantharajah and Hannan, 2006), can delay the onset and progression of neurological signs in a range of disease models including models of Huntington disease (Hockly et al., 2002) and Alzheimer disease (Jankowsky et al., 2005). Moreover, EE is known to result in a number of morphological changes in the brain (increased cortical thickness, dendritic branching and spine density) and promotes neurogenesis and the production of various neurotrophic factors (Leggio et al., 2005). At the molecular level, EE is also known to alter the expression of a large number of genes (Rampon et al., 2000) and brain proteins (McNair et al., 2007). Clinical studies suggest that modification of the environment may have useful application in the management of children with RTT (Lotan and Shapiro, 2005). Furthermore, exposure of pre-symptomatic *Mecp2*-null mice to EE resulted in reduced motor coordination deficits and increased *Bdnf* level in *Mecp2*^{-/+} heterozygous females (Kondo et al., 2008) and in *Mecp2*^{-y} male mice (Lonetti et al., Nag et al., 2009). Although the exact mechanism by which EE influences aspects of RTT-like phenotypes is unclear. These results however suggest that epigenetic modulators may be a possible route to therapeutic intervention. In support of this notion is the recent study which demonstrated that RTT-like anxiety phenotypes can be mirrored by local administration of a histone deacetylase inhibitor (Adachi et al., 2009). Future discovery of new therapeutic compounds that can specifically target abnormal transcriptional repression may be useful in treating RTT close to the upstream end of the pathogenic process.

1.6.3 RTT therapeutic strategies at the level of the gene

1.6.3.1 Reactivation of the normal allele

As mentioned above, *MECP2* is located on the X chromosome and is subject to X chromosome inactivation (XCI), such that in each cell in a heterozygous female RTT patient expresses only the normal (thus having an MeCP2 +ve phenotype) or only the mutant *MECP2* allele (thus having an MeCP2 -ve phenotype, in the case of substantial loss of function mutations), never both. This process is usually random and results in an approximately 50:50 mixture of cells of each type although ratios may vary somewhat from tissue to tissue and between individuals. Studies of the distribution of brain cells expressing the normal and mutant *Mecp2* alleles have revealed that in this critical tissue *Mecp2* -ve cells

tend not to be clustered but intermingle with the *Mecp2* +ve cells in a fine-scale mosaic pattern (Guy et al., 2007).

A number of studies have reported skewing of the XCI ratio away from 50:50 in RTT patients (Schanen et al., 1997, Knudsen et al., 2006). It is well known that the rare familial cases of RTT are usually explained by the fact that mothers of these patients carry the causative mutation but are highly skewed towards expression of the normal allele (Villard et al., 2001). A study investigating the direction and extent of skewing in sporadic RTT cases (Archer et al., 2007) found that most of the included patients had some degree of skewing towards expression of the normal allele and that the direction and extent of XCI alone explained approximately 20% of the variance in severity of the disorder. The conclusion that in several patient tissues there may be a tendency of selective survival advantages for *MeCP2* +ve cells does need to be verified in view of the fact that most skewing studies have been conducted in peripheral tissues such as blood with much higher cell turnover and that the ratio may not be the same in affected brain regions. There is at least some evidence to suggest that similarly skewed patterns are found in brain in the mouse models however (Young and Zoghbi, 2004, Smrt et al., 2011).

One strategy for delivering *MECP2* to those cells expressing the mutant allele could be to encourage the re-activation of the inactive X to allow expression of the normal allele in the same cells. Results of studies conducted before the X inactivation process was understood suggested that simple chemical interventions (application of 5-azacytidine) designed to reduce genomic methylation levels could result in activation of X-linked genes in cell culture models (Mohandas et al., 1981). However, this approach is unlikely to be applicable. Amongst the likely problems that may be encountered are that if the entire inactive X is re-activated, the X-linked gene dosage problem, for which X inactivation evolved, will supervene and pathological levels of gene expression are likely to result at many loci. If the re-activation can be targeted only to the *MECP2* locus or the immediate vicinity, that might avoid the general dosage problem; however, there are currently no obvious resources that can be used to target re-activation in this way, and neither are there any ways to target only those cells that have inactivated the normal allele.

1.6.3.2 RTT therapeutic strategies at the level of the gene - gene therapy

Another approach at the level of the gene is gene therapy. The scope of this study is focusing on the potential application of gene therapy in RTT mice models, therefore in the next section I will give an overview on gene therapy principles and RTT propensity and challenges to this approach. Finally I will discuss possible delivery vectors that could have potential in treating RTT.

1.7 Gene therapy

Gene therapy is a promising approach for treating multiple disorders including infectious, genetic, neurologic diseases and cancer (Karlsson, 1991, Blomer et al., 1996). Generally this approach deploys delivering new genetic instructions into target tissues to compensate for aberrant or missing genes or to convey a new function. Gene therapy remains the only hope of cure for many patients with inherited and acquired diseases that cannot be treated with conventional methods, e.g. drugs, recombinant proteins or transplantation. Gene therapy for genetic disorders provides treatment at the molecular level to fix the primary underlying cause of the disorders instead of tackling variable secondary effects.

1.7.1 Types of gene therapy

Gene therapy of the monogenic disorder comprises two main types; the first is to introduce new genetic material (transgene) into germ cells (sperms or ova) to fix an inherited genetic disorder allowing the transgene to eventually pass to any future offspring. This type of therapy has many ethical problems and has not implemented so far. The second type involves introducing the transgene into somatic cells to restrict the transgene action only to the treated patient without subsequent inheritance. Thus somatic gene therapy is similar to other conventional pharmacological interventions. The therapeutic transgene could be applied to somatic cells by *ex vivo* or *in vivo* methods. The *ex vivo* method includes transfecting target cells *in vitro* with the gene of interest followed by re-implantation of transfected cells, however this approach is limited by the accessibility of the target organs/cells. *In vivo* approaches include direct delivery of the transgene to target cells by systemic or local application which requires a vehicle to facilitate gene delivery.

Essential requirements should be fulfilled in a given disorder to be a candidate for gene therapy such as; identification of the underlying genetic defect, presence of a correcting gene, availability of vehicles or vectors and suitable method of delivery to transduce target tissues or cells (Nathwani et al., 2004). Therefore the success of gene therapy is dependent on the ability of a vector to deliver the transgene to the target cells at efficient levels. Gene transfer to somatic cells can be achieved through using non-viral or viral vectors.

1.7.1.1 Non-viral methods

These methods involve either direct introduction of the naked plasmid DNA into the target cells, by gene gun (Yang et al., 1990) or electroporation (Rols et al., 1998), or encapsulating the DNA within an artificial lipid sphere with an aqueous core (liposome) that is capable of transferring therapeutic DNA through the target cell's membrane (Felgner et al., 1987). These methods are simple and easy to produce with reduced toxicity, however they are less effective for *in vivo* transgene delivery and usually mediate Relatively short term gene expression (Li and Huang, 2000)

1.7.1.2 Viral vectors

Sustained transgene expression is needed for the treatment of many diseases. Viruses have developed a way of encapsulating and delivering their genome to human cells in a pathogenic manner, therefore especial attention has been paid to viral vectors. Recombinant viral vectors are designed to replace the disease-causing- and replication-responsible genes with a transgenic cassette containing the gene of interest and an appropriate promoter. An ideal vector for gene delivery should be capable of entering target cells and transferring the transgenic cassette to the host nucleus (with or without integration into the host genome) as well as conveying enduring expression with minimal induced-toxicity. The number of viruses whose genomes can be manipulated to generate viral vectors are steadily increasing and include; retroviruses, adenoviruses, adeno-associated viruses and herpes simplex virus (Hermens and Verhaagen, 1998). Each specific vector group has its own advantages and disadvantages for human gene transfer. For example adenoviruses transduce cells very efficiently and have a large cloning capacity but they also strongly trigger the host-immune

response and produce transient gene expression. Retroviruses despite producing enduring gene expression are unable to transduce non dividing cells (with the exception of lentiviruses). Adeno-associated viruses convey long-term expression and do not activate the immune system, however they have a very limited cloning capacity (Walther and Stein, 2000).

1.7.2 Gene therapy application for RTT

1.7.2.1 RTT Propensity to gene therapy

As previously described, Rett syndrome is caused mainly by dysfunctional mutations in the *MECP2* gene whose encoding sequences, isoforms and resultant protein products are well studied. The lack of effective conventional therapeutic approaches and a lack of understanding of the downstream effects of MeCP2 highlight the importance of tackling this disorder at the genetic level. This, along with the reported phenotype reversibility of RTT-like phenotypes in *Mecp2* knockout mice models makes RTT an attractive candidate for gene therapy. The major objective of this therapy will be to deliver a working copy of *MECP2* to as many affected brain cells) as possible to raise function (at both molecular and cellular level) above a threshold required for improvement of the clinical picture. A preliminary attempt to use adenovirus to deliver a construct driving *Mecp2* expression in the striatum of *Mecp2*-null mice reported decreased motor deterioration and restoration of voluntary motor activity (Kosai, 2005). However, this study has never been followed up, reported in detail or repeated. Rastegar and colleagues (Rastegar et al., 2009) demonstrated the potential for lentiviral transgene delivery to improve the phenotype of *Mecp2*-null neurons derived from neuronal stem cells in culture. These neurons displayed increased dendritic growth and branching than non-transduced controls. The same authors also showed the endogenous *Mecp2* promoter to be a sensible choice in driving cell type-appropriate expression thus avoiding overtly ectopic patterns of expression.

1.7.2.2 Challenges for gene therapy application for RTT

However encouraging these results are, there are many challenges to overcome for this approach to be successful including; finding an appropriate vector, transducing sufficient cells, avoiding transgene repression and avoiding overexpression of exogenous MeCP2 in the mosaic female brain.

Whilst MeCP2 is expressed throughout the body, particular attention has been directed to the brain as brain-specific deletion in a mouse model resulted in a RTT-like phenotype whereas brain-specific expression of MeCP2 prevented/rescued RTT-like phenotypes in RTT mice models. MeCP2 functioning in a mainly cell-autonomous manner, therefore MeCP2 has to be expressed in each individual cell for proper cellular function. In addition, a recent study showed a positive correlation between the degree of phenotype rescue and the number of cells expressing endogenous *Mecp2* after being activated in RTT mice models (Robinson et al., 2012). Given that the RTT phenotype results from effects on post-mitotic neurons with long lifespans and cannot simply be fixed by delivery of cells with the right characteristics into the tissue, it is clear that if gene therapy is to work it will have to involve *in vivo* delivery, which is not a trivial undertaking. The current lack of viral vector that can achieve widespread delivery of *Mecp2* transgene across the BBB with transduction efficiency capable of producing therapeutic benefits represents one of the major hurdles for meaningful gene therapy application for RTT. However several groups are actively developing such tools for delivery of genes encoding MeCP2, particularly for use in the mouse models described above, but to date there are no reports that viral vector-based delivery of *Mecp2* to the brain of *Mecp2*-null mice can rescue any aspects of the RTT phenotype.

Maintaining MeCP2 expression levels within a physiological level is important for normal function and is one of the more difficult challenges. It has been shown that elevated levels of MeCP2 may be detrimental, since patients with duplication of Xq28 in regions spanning the *MECP2* locus show a range of neurological features including altered head growth rates, ataxia, seizures and mental retardation (Meins et al., 2005, Van Esch et al., 2005, Friez et al., 2006). Similarly, mice overexpressing *Mecp2* show behavioural changes. While mice with modest overexpression of MeCP2 show motor coordination impairment, cognitive deficits and anxiety-like phenotype (Collins et al., 2004, Na et al., 2012), mice expressing higher (2-4) fold levels of *Mecp2* in neurons display tremors and motor dysfunction (Luikenhuis et al., 2004). In the mouse *Mecp2* reactivation study (Guy et al., 2007) it was assumed that removal of the STOP cassette would not have a large effect on later expression levels of *Mecp2* driven by its endogenous promoter and regulatory elements and that expression would

effectively be at WT levels in each rescued cell. Gene therapy approaches will therefore have to deliver an extra copy of *MECP2* to each cell that becomes transduced, while avoiding a significant multiplicity of infection, which could lead to large numbers of cells overexpressing MeCP2 at high levels. Even in cells transduced by a single virus particle and expressing MeCP2 from a single extra copy of the gene, the fact that female patients (and heterozygous mice) are a mosaic of MeCP2 expressing and non-expressing cells due to X-inactivation itself causes problems. Virus particles delivering *Mecp2*-expressing constructs to cells expressing the mutant allele are unlikely to cause problems, but those delivering constructs to cells expressing the WT allele could cause overexpression.

Two strategies to avoid overexpression-induced toxicity in the female cellular mosaic network of *Mecp2* expression have been devised. In one strategy, the construct itself is designed in such a way that pre-existing expression of MeCP2 leads to the transgene not being expressed. One potential means for doing this is to design a highly efficient MeCP2 binding target into the promoter driving transgene expression in the hope that this would stimulate heterochromatin formation and long-term repression of the transgene. In cells expressing the mutant allele, this shutdown would not occur until sufficient transgenic MeCP2 had built up in the cell to produce a negative feedback effect on its own expression. The other strategy, employed by (Zhou et al., 2006), is to design a construct that includes an agent that will suppress endogenous MeCP2 expression while leaving the transgene to do its work. A polycistronic construct incorporating a siRNA that will suppress both WT and mutant MeCP2 translation from endogenous mRNA was designed. Base changes in the sequence of the *MECP2* transgene in the same construct ensured that translation of the mRNA from exogenous *Mecp2* transgene was not suppressed. Both these approaches can be seen as varieties of the ‘suppression and replacement’ strategy currently being developed for a range of dominant disorders, but modified for use in relation to an X-linked gene.

Based on the previous challenges, the development of an appropriate vector for gene delivery is the success limiting step in any future attempt for gene therapy application in RTT. Therefore in the next part of this chapter, I will discuss the characteristic features, advantages and disadvantages of Lentivirus- and Adeno-associated virus-based vectors as potential tools for *Mecp2* gene delivery.

1.8 Lentiviruses

Lentiviruses include a range of primate (e.g. human immunodeficiency viruses [HIV-1 and 2], and simian immunodeficiency viruses [SIV]) and non-primate viruses (e.g. feline immunodeficiency virus [FIV] and equine infectious anemia virus [EIAV],) viruses. Lentiviruses are very attractive tools for gene therapy due to; (1) the ability to integrate into the host genome and produce enduring gene expression (Trowbridge et al., 1980); (2) the relatively large cloning capacity that makes these vectors suitable for application in many disorders (where large gene transfer is required); (3) the ability to transduce dividing and non-dividing cells (e.g. neurons, hepatocytes and myocytes); (4) the ability to produce transgene expression with a minimal immune response (Walther and Stein, 2000).

The lentivirus genome is composed of structural, regulatory and accessory genes flanked by two long terminal repeats (LTRs). The structural genes are; (1) *gag*, which produces three proteins; Matrix, capsid and nucleocapsid (figure 1-4). These proteins are important for virion assembly and maturation; (2) *pol* gene, which produces enzymes responsible for replication and integration to the host genome (protease, reverse transcriptase and integrase); (3) *env* gene, which encodes for the glycoprotein envelope that is essential for viral binding and entry into the host cells. The genome also encodes some regulatory proteins such as Rev, which is responsible for nuclear export of mRNAs that encode the viral structural protein, and Tat protein, which regulates post transcriptional elongation of viral mRNAs (Wei et al 1998). Another group of genes includes; *vif*, *vpr*, *vpu* and *nef*. Proteins encoded by these genes are not essential for virus replication and are therefore called accessory genes (Zufferey et al., 1997).

1.8.1 Lentivirus-based vectors

The preliminary design of replication incompetent lentivirus-based vectors is based on isolation of the *cis*-acting elements in virus genome (non-coding region necessary for vector RNA synthesis, packaging, reverse transcription, and integration) in one plasmid (vector cassette) whereas the *trans* elements encoding enzymatic, structural, and accessory proteins are incorporated in another plasmid, packaging cassette, (Naldini et al., 1996b). The envelope

encoding sequences are contained in a third separate vector (envelope cassette). Virus production is carried out by concomitant transfection of human embryonic kidney cells with the three plasmid cassettes followed by virus collection and concentration (detailed virus production protocol is discussed in chapter 2).

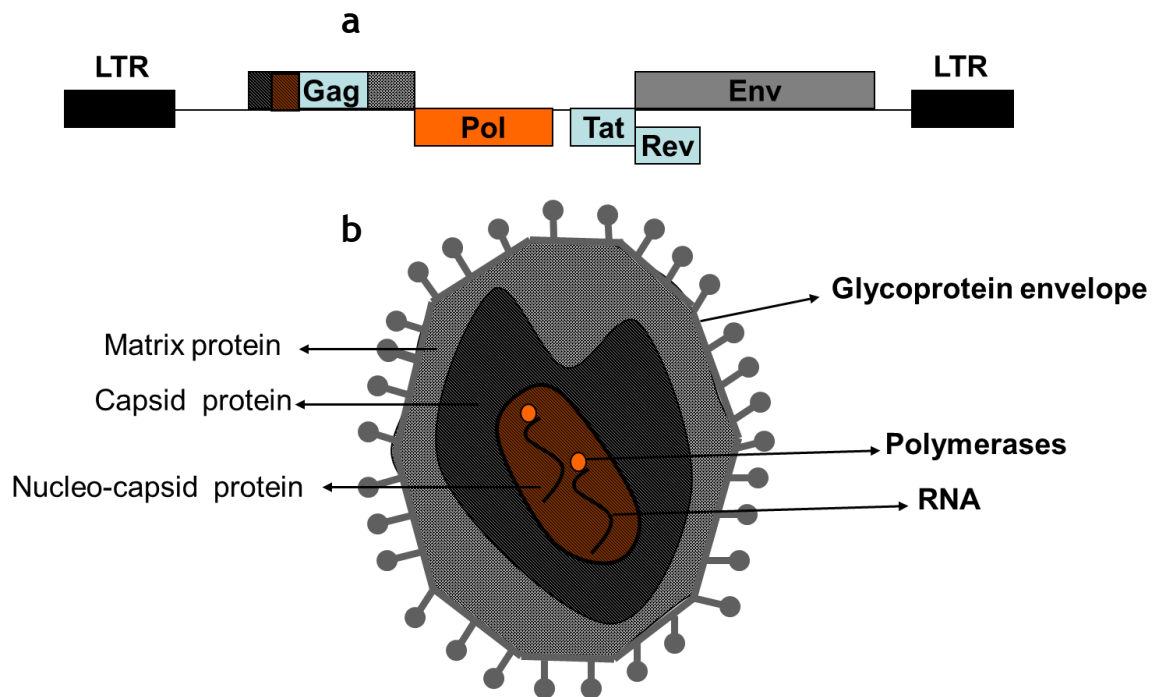


Figure 1-4 Genomic structure of WT lentiviruses.

(a) Representative diagram showing genomic structure of the lentivirus. Lentivirus genome consists of 3 structural genes (gag, pol and env), regulatory genes (tat and rev) and accessory genes (not shown) flanked between two LTRs. (b) representative diagram of lentivirus particles showing the main structural proteins; env, matrix, capsid and nucleocapsid encapsulating 2 single stranded virus RNA. LTR; long terminal repeat.

1.8.1.1 The vector cassette

The lentivirus-based vector cassette encodes the full-length vector RNA which contains all cis-acting elements and the transgene expression cassette (includes the heterologous promoter and the transgene of interest, figure 1-5a). The cis-elements include (1) 3` LTR and 5` LTR that helps nuclear localization and integration into the host genome as well as acting as a promoter (Toyama et al., 1992); (2) 5` UTR which contains the primer binding site (PBS), splice donor site, packaging signal, rev-response element (RRE), and splice acceptor; and (3) a 3` UTR containing a poly purine tract (PPT) and the 3` LTR.

1.8.1.2 The packaging cassette

The packaging cassette of the lentivirus-based vector encodes all trans-elements (expressed from gag and pol genes), which involve structural and enzymatic proteins required for vector particle production and transduction of target cells. The initial packaging cassette (first generation vector) retained all structural proteins, except Env, together with the accessory proteins (Naldini et al., 1996a, Naldini et al., 1996b). However the structure of this cassette has been further modified to increase the biosafety of lentivirus-based vectors.

1.8.1.3 The envelope cassette

The parental lentivirus envelope protein restricts the viral tropism to CD4 receptor-expressing cells. In order to increase lentivirus tropism, the parental envelope was substituted with vesicular stomatitis virus G protein (VSV-G) (Akkina et al., 1996) which extends the vector tropism to include many cell types *in vitro* and *in vivo*. Moreover the VSV-G envelope helps stabilization of the vector particles, thus enabling vector concentration by ultracentrifugation. In addition, it directs vector cellular entry to an endocytic pathway that compensates for the absence of the viral accessory proteins (Aiken, 1997). However the presence of complement and antibody mediated immune response against the VSV-G envelope decreases the efficiency of systemic administration of VSV-G- pseudotyped lentivirus-based vectors (DePolo et al., 2000). Pseudotyping lentivirus-based vectors with envelope proteins other than VSV-G, e.g. Rabies virus glycoprotein, allow peripheral administration of the virus with axonal retrograde spread to the central nervous system (Mazarakis et al., 2001, Mentis et al., 2006).

Packaging of the vector cassette (transgenic cassette flanked by 2 LTRs, figure 1-5a) to the viral proteins occurs in human embryonic kidney cells with subsequent viral assembly and release to the culture media. These virus particles are capable of transferring the expression cassette to target cells *in vitro* and *in vivo*. Lentivirus cellular entry starts by binding of the envelope glycoprotein to a specific receptor (which defines the viral tropism) on the cell membrane (Maddon et al., 1988). The viral membrane then fuses with the cellular membrane with disassembly of matrix and capsid proteins and

subsequent delivery of nucleoprotein complex (nucleocapsid-binding viral genome) inside infected cells (figure 1-5b). In the cytoplasm of the host cell, single stranded viral RNA is converted to linear double-stranded DNA by reverse transcription. Viral integrase facilitates permanent integration of the double-stranded DNA to the host genome (Sakai et al., 1993). Transcription from the provirus (integrated virus genome) results in production of mRNA transcripts that encode for the gene of interest and lack all virus structural genes. These lentivirus based vectors are therefore considered replication incompetent.

1.8.2 Biosafety of lentivirus-based vectors

The ultimate aim of transgene delivery with lentivirus-based vector is to achieve transduction events without disturbing normal function of the transduced cell. However many potential hazards could emerge from this transduction, such as; insertional mutagenesis and generation of replication competent lentivirus. Several methods are deployed to reduce the potential risk of insertional mutagenesis such as the use of zinc finger technology (Bibikova et al., 2001) to direct the insertion of lentivirus based vectors to a specific site in the genome or the development of a non-integrating lentivirus-based vectors, in which the vector persists as an episome without integration into the host genome. Interestingly, the non-integrating vector achieved stable expression in non-dividing cells (Rahim et al., 2009). To decrease the risk of generation of replication competent virus, the structure of the packaging cassette was modified by deletion of all accessory genes, important for virus replication *in vivo*, except Tat and Rev Proteins (Zufferey et al., 1997). To augment vector biosafety, the Tat encoding gene was deleted from the packaging cassette with further split of gag/pol and rev into two separate plasmids (Dull et al., 1998). This constitutes the third generation vector in which the risk of the virus becoming replication competent is reduced by increasing the minimal number of recombination events necessary for generation of replication competent vector to three, thus substantially increasing biosafety. A further modification involves a deletion in the downstream long terminal repeat (LTR) which, after transduction, leads to transcriptional inactivation of the upstream LTR and considerably reduces the risk of vector mobilization and recombination, self-inactivating design, (Zufferey et al., 1998, Bukovsky et al., 1999).

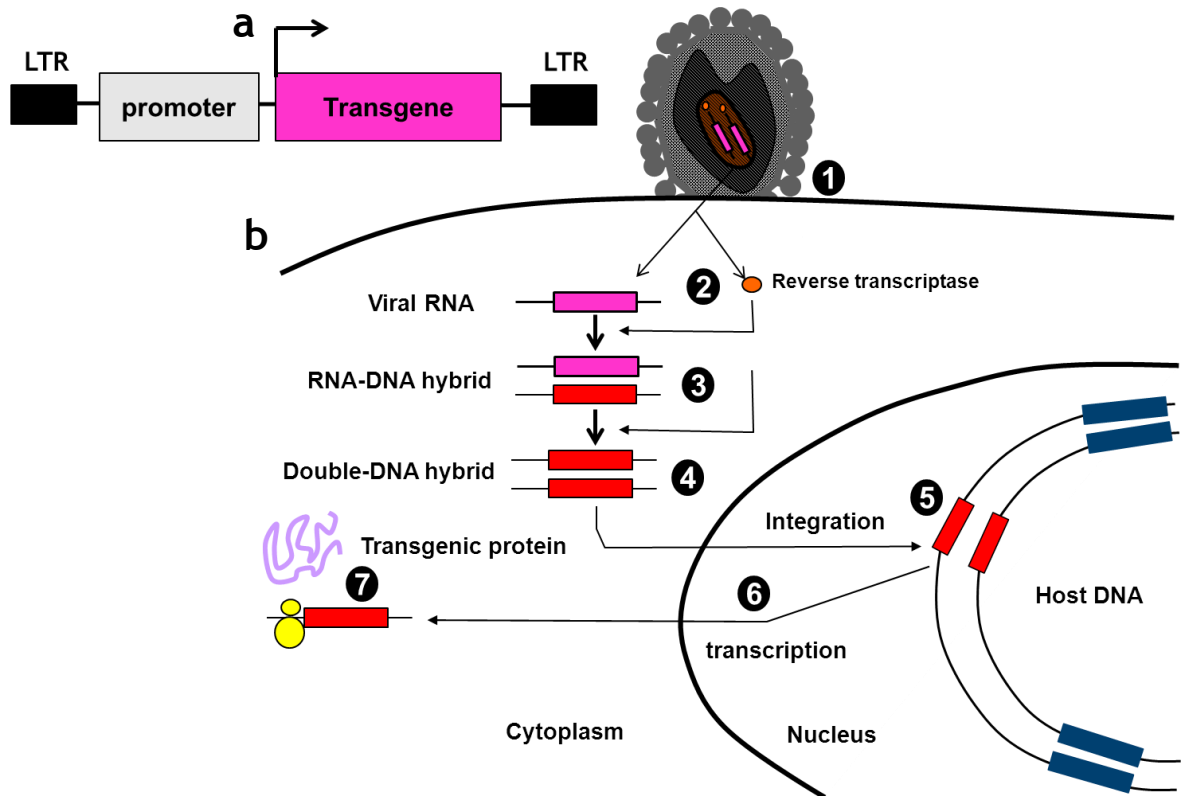


Figure 1-5 Lentivirus-based vector, structure and transduction.

(a) Representative diagram showing structure of lentivirus-based vector. The transgene cassette (promoter and gene of interest) are flanked by the 2 LTRs. (b) Representative diagram showing the steps of lentivirus transduction; (1) virus entry, (2) release of the provirus to the cytoplasm of infected cells, (3) formation of the complementary DNA strand by reverse transcriptase, (4) formation of double stranded DNA, (5) nuclear localization and integration to the host genome, (6) transcription of the lentivirus mRNA and (7) transgene expression.

1.8.3 Application of lentivirus-based vectors in neurological disorders and its tractability in RTT.

Lentivirus-based vectors are attractive tools for treating several disorders including; genetic and metabolic disorders as well as various forms of cancer. This is in part, because of their ability to transduce a wide range of tissues including the CNS, kidneys, muscle, heart and hematopoietic system. Transgene delivery to the CNS by lentivirus is particularly challenging as it requires invasive surgical methods/intervention to achieve direct CNS delivery. Despite the requirement to deliver into what is an extremely delicate structure, the enduring nature of lentiviral transgene expression nevertheless avoids the necessity for repeated administration.

Lentivirus-based vectors have been extensively used in preclinical trials to investigate their potential for treating neurological disorders. For instance, lentivirus-mediated delivery of tyrosine hydroxylase, aromatic L-amino acid decarboxylase, and guanosine 5'-triphosphate cyclohydrolase 1 in the striatum improved motor deficits in an animal model of Parkinson (Jarraya et al., 2009). In the same context, lentivirus-mediated delivery of ciliary neurotrophic factor prevented striatal degeneration in a rat model of Huntington disease (de Almeida et al., 2001). Another study showed the ability of lentivirus pseudotyped with the rabies virus glycoprotein coat to deliver survival motor neuron 1 protein into the lower motor neurons in an animal model of spinal muscular atrophy with subsequent improvement of the motor activity and extended survival (Azzouz et al., 2004b).

Lentivirus-based vectors meet most of the criteria required for *Mecp2* gene delivery in RTT (table 1-2). Firstly, *Mecp2* can be easily cloned into a lenti-vector backbone, with sufficient space left for large or complex promoters (e.g. GFAP), to drive cell-type specific expression of *Mecp2*. The vector also benefits from a relative ease of particles production and the generation of high titre preparation. Secondly, Lentiviruses are able to transduce both neurons and glia which are the main contributors to RTT pathogenesis. Thirdly, Lentivirus integrates into the host genome providing stable long-term transgene expression (Bienemann et al., 2003) and with a low incidence of transgene repression (Lois et al., 2002). This is critical in RTT as *Mecp2* is necessary for the normal function of adult neurons (McGraw et al., 2011). Other attractive features of lentivirus based vectors are that they (independent of insert) do not alter the electrophysiological properties of transduced cells (Dittgen et al., 2004), and they elicit a minimal immune response both in the brain and systemically (Abordo-Adesida et al., 2005). One important limitation of lentivirus-based vectors is that they cannot pass the blood brain barrier (BBB). This means that any brain delivery attempts will involve direct brain injections which are not practical as there is only limited spread of viral particles from the injection site but global expression of *Mecp2* in the brain is required. A previous study showed lentivirus-based vectors were able to deliver exogenous *Mecp2* into neurons in culture with a pattern of expression similar to endogenous *Mecp2* (Rastegar et al., 2009). However, the functional consequences of this expression have not

been evaluated. Lentivirus could still be useful for local *Mecp2* delivery to the brain to investigate potential rescue of brain region-specific phenotypes.

Table 1-2 Comparison between lentivirus- and AAV-based vectors as a potential tools for *Mecp2* delivery

	Lentiviruses	Adeno-associated viruses serotype 9 (AAV9)
Type of cells transduced	Both can transduce dividing and non-dividing cells with high efficiency	
Ability to accommodate <i>Mecp2</i>	Mecp2 encoding sequences (1500 bp) is within the cloning capacity of lenti vector (8,000 bp) and Adeno-associated virus (4,600bp)	
Particle Size	~100-120nm	22-25nm
Ability to cross the BBB	Cannot pass BBB	Efficiently cross BBB after IV administration
Viral tropism in the mouse brain	Transduce mainly neurons but also glia	Transduce mainly neurons (neonatal injection) and both neurons and glia (adult injection)
Advantages	<ul style="list-style-type: none"> • Integrate into the host genome (may be undesirable) • Long-term expression • Minimal immune response 	<ul style="list-style-type: none"> • Accessible method of delivery (IV) • Minimal risk of insertional mutagenesis • Widespread after local or systemic administration
Disadvantages	<ul style="list-style-type: none"> • Potential for insertion mutagenesis • Limited spread after focal application • limited application approaches/need for invasive CNS delivery 	<ul style="list-style-type: none"> • Relatively short term expression • Limited cloning capacity • Variable immune response stimulation

1.9 Adeno-associated virus

Adeno-associated virus (AAV) is a small (22-25 nm), nonenveloped virus. It is a member of the family parvoviridae and classified as a dependovirus because it requires the presence of helper virus in order to replicate (Daya and Berns, 2008). The majority of humans are seropositive for AAV infection which in the absence of helper virus can establish latency by site-specific integration into chromosome 19q13.4 (Kotin et al., 1992). The effectiveness of AAV as a vehicle for gene therapy comes from; (1) the ability to transduce dividing and non-dividing cells; (2) wide range of cellular tropism; (3) low immunogenicity; (4) stable transgene expression and (5) absence of disease production in humans (McCarty et al., 2004).

The AAV/2 genome is the most studied AAV serotype and all AAV-based vectors developed so far are based on AAV/2 backbone. It comprises a linear, single-stranded DNA of 4.7 kb (Srivastava et al., 1983). The structure of the genome is composed two inverted terminal repeats (ITRs) flanking two open reading frames (ORF) (figure 1-6a). ITRs are the origin of replication and act as a priming site for synthesis of the complementary strand by DNA polymerase. Moreover they are also involved in AAV genome packaging, transcription and site-specific integration (Daya and Berns, 2008). The left ORF contains the Rep (replication) gene that encodes four Rep proteins, Rep78, Rep68, Rep52 and Rep40. Rep78 and Rep68 are produced under the control of the P5 promoter and act as regulatory proteins and are essential for virus replication (Pereira et al., 1997). Rep52 and Rep 40 are produced under the control of the P19 promoter and are responsible for the accumulation of single-stranded viral DNA used for packaging inside AAV capsids. The right ORF contains the Cap (capsid) gene (figure 1-6a) that encodes for three capsid proteins (VP1, VP2 and VP3 in 1:1:10 molar ratio) and are produced under the P40 promoter (Grieger and Samulski, 2005a).

1.9.1 AAV-based vector transduction

In the current AAV based vector (figure 1-6b), the encoding sequences for cap and rep are replaced by the transgene cassette (the promoter and the gene of interest) flanked by the two ITRs (vector cassette) that constitute the cis signal essential for packaging and priming for generation of the second strand

(Samulski et al., 1982, Schnepf et al., 2005). Other posttranscriptional regulators are also included to control transgene expression. The packaging cassettes are split into two plasmids, one to supply the encoding sequences for rep and cap genes and the other to provide the adenovirus helper genes (E4, VA and E2A). Production of the virus is accomplished by triple transfection of human embryonic kidney cells with the vector and packaging cassettes as described in chapter 2 (Gray et al., 2011a).

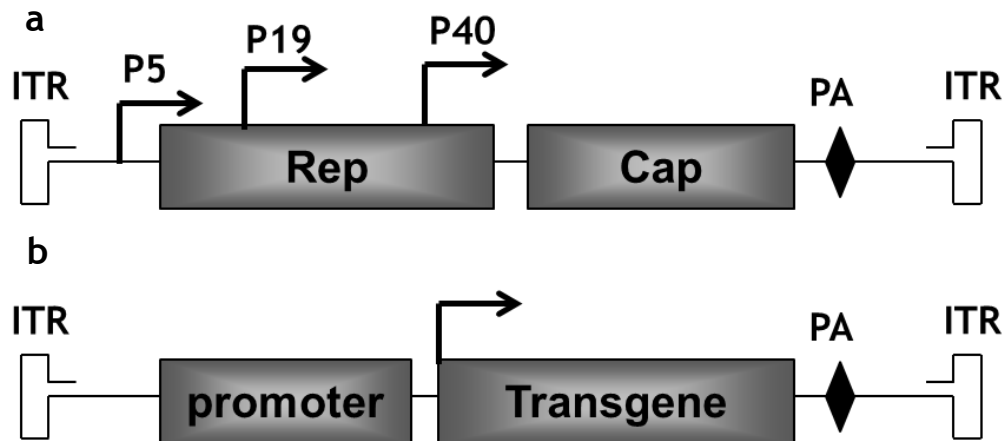


Figure 1-6 Genomic structure of the WT AAV and AAV-based vector.

(a) Representative figure showing the genomic structure of AAV wild-type virus. Two main structural genes, rep and cap flanked by two ITRs. Different rep and cap transcripts produced from their respective promoter (P5, P19 and P40, arrows). (b) Structure of AAV-based vector in which the expression cassette replaced rep and cap genes and still flanked by the 2 ITRs. PA; polyadenylation signal, ITR; inverted terminal repeat.

AAV cellular entry starts by the virus binding to heparan sulfate proteoglycan receptors on the cell surface (Summerford and Samulski, 1998), followed by viral internalization inside the cells (figure 1-7). Afterwards, AAV virus is either engulfed by endocytic vesicles and cleared or escapes these endocytic vesicles and achieves successful infection (Duan et al., 1999). Intracellular trafficking of AAV using microtubules is further enhanced by cellular signaling such as RAC1 and phosphatidylinositol 3-kinase pathway activation (Sanlioglu et al., 2000). The mechanism of directed nuclear transport of AAV particles is not clear. However it could be mediated through a nuclear pore complex- dependent /or independent mechanisms (Hansen et al., 2001). For successful transgene expression the single stranded DNA packaged in the AAV vector must be converted to a double stranded DNA. The generation of the second strand of DNA is accomplished either by; *de novo* synthesis of the second strand or by strand

annealing (SA) of complementary strands from two infecting viruses (figure 1-7, (Nakai et al., 2000). AAV packages either the plus or minus DNA strand with equal efficiency (Berns, 1990). However precluding the SA pathway (by packaging ssAAV by either positive or minus strand only) showed no impact on the transduction efficiency of ssAAV indicating *de novo* synthesis play a major role in second strand synthesis during vector transduction (Zhong et al., 2008). Inside the nucleus the rAAV genome requires synthesis of the complementary strand to start gene expression. Failure of AAV transduced cells to achieve transgenic expression is mainly due to their inability to generate the complementary strands and this is therefore considered as a rate limiting step in the AAV vector transduction process (Miao et al., 2000).

1.9.2 Self-complementary AAV

The key steps in rAAV transduction process are virus trafficking to the nucleus and second-strand generation (Ferrari et al., 1996). Generation of the second strand is followed by a transient period of genome instability that compromises gene expression (Wang et al., 2007). Two of these critical steps can be circumvented by packaging AAV with both strands (sense and non-sense) as a single molecule to form self-complementary AAV (scAAV). This enables the two complementary strands to produce a dimeric inverted repeat genome (Carter et al., 1972). scAAV vectors display a substantial increase in transduction efficiency and in the speed of onset of transgene expression compared to ssAAV vectors (McCarty et al., 2001). The relatively low transduction efficiency observed in ssAAV is because some of the transfected cells are not competent to generate the secondary strand which is mandatory for gene expression. In contrast, the formation of the second strand is independent of the host-cell DNA synthesis in scAAV (McCarty et al., 2001). scAAV vector also displays rapid onset and an approximately 15 fold increase in transgene expression compared to the ssAAV (Ren et al., 2005). The limiting factor for extensive applications of scAAV in the field of gene therapy is the reduction of the cloning capacity to approximately half that of the ssAAV vector. Despite this drawback scAAV still has the potential to be useful in a number of applications and this limitation can be partially overcome through reduction/optimization of the size of promoter and transcription regulatory elements (Wu et al., 2008) and by using AAV capsids

that can accommodate inserts with larger genome sizes, e.g. capsid 5, (Grieger and Samulski, 2005b).

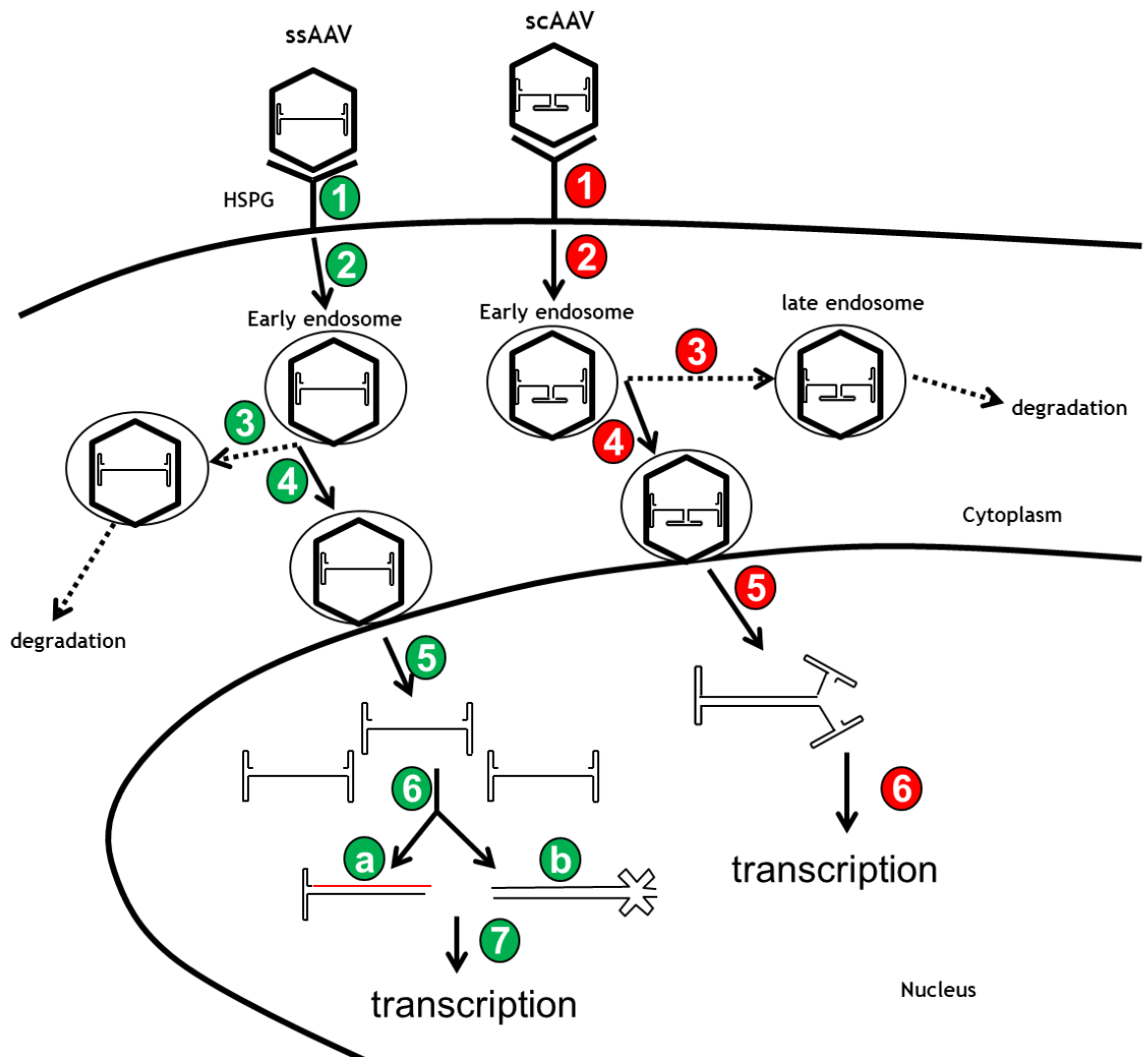


Figure 1-7 AAV-based vector transduction.

Representative diagram showing the transduction of AAV-based vector; (1) virus binding to heparin sulphate proteoglycan, (2) virus endocytosis to the early endosome followed either by (3) maturation to late endosome and degradation or (4) escape early endosome and (5) translocation to the nucleus. (6) in the case of ssAAV (green circles), the single stranded DNA must be converted to double stranded DNA either by *de novo* synthesis (6a) or strand annealing between plus and minus strands (6b) followed by (7) transcription of the transgene. Whereas, in the case of scAAV (red circles), once inside the nucleus it can bypass 2nd strand synthesis via intramolecular annealing and start transcription faster than the ssAAV vector. HSPG; heparin sulphate proteoglycan, ssAAV; single stranded Adeno-associated virus, scAAV; self-complementary Adeno-associated virus.

1.9.3 AAV capsids

Despite the extended infectivity of the AAV2 capsid in many tissues and cells, certain cells still cannot be infected with AAV2 (Gigout et al., 2005). The use of different AAV serotypes in a pseudo-typing approach (the genome of one ITR serotype being packaged into a different serotype capsid) has allowed extended tissue tropisms. Analysis of the difference in transduction efficiency and expression levels between AAV capsids 1-9 revealed that AAV virus pseudotyped with capsid 7 and 9 displayed the highest expression levels whereas the quickest onset of expression was achieved by AAV capsids; 1, 6, 7, 8 and 9. Among all investigated capsids, AAV capsid 9 showed the best viral genome distribution and the highest protein levels (Zincarelli et al., 2008). Another study showed the high transduction efficiency of AAV capsid 8 and 9 in the liver, skeletal muscle, pancreas after IV injection with additional relatively high cardiac tropism for AAV9 virus (Inagaki et al., 2006).

Gene delivery to the CNS is very challenging due to the presence of the BBB which impedes large drug molecules, many proteins and viruses from passively crossing into the brain. The BBB is an important element to protect the brain from different pathogens and toxin. However, in doing so it also, represents a barrier for many viral-based gene delivery applications. Gene delivery to the brain has been accomplished through direct brain injection of the vector to the target area, both in animal and in human studies. However, this approach is very challenging and may require more than one injection site to produce a therapeutic effect. In addition, transient disruption of the BBB using hyperosmotic drugs such as mannitol permits gene delivery to the brain using small-sized vector (McCarty et al., 2009). Recently AAV capsid 9 has emerged as a potential vector for gene delivery to the brain after peripheral injection and this can be achieved without the necessity for disrupting the BBB (Duque et al., 2009, Foust et al., 2009). This ability to transduce the CNS was further improved by the generation of the scAAV9 vector, which is 10-100 time more efficient than the ssAAV9 vector (Gray et al., 2011c). Therefore this scAAV9 vector has been the focus of several studies to determine the transduction efficiency and cell-type specific tropism after different routes of administration.

Foust and colleagues showed that peripheral administration of scAAV9 to neonatal mice transduces mainly neurons however adult peripheral injection produces mixed glia and neuronal transduction (Foust et al., 2009). The authors explained this age-dependent differential cell tropism to be due to the presence of a fully developed BBB in adult mice that relatively increases the exposure of glia, but not neurons, to the virus through the astrocyte-foot processes. In contrast, the neuronal tropism in neonates is probably due to the undeveloped nature of the BBB at this age which allows the virus to spread throughout the brain. Saunders and colleagues disagree with the previous explanation because the BBB is fully functional in neonatal mice and they attribute the neuronal tropism in neonates to the low number of glia relative to neurons in the developing brain at this time point (Saunders et al., 2009). Nevertheless these results disagree with a recent study that showed high glial transduction after peripheral injection of scAAV9 in neonatal mice (Rahim et al., 2011). Moreover a recent quantification study in the rodent brain showed that adult peripheral injection of scAAV9 could also produce high neuronal transduction (2X glial transduction; (Gray et al., 2011c). Interestingly the same study showed that peripheral injection of scAAV9 virus in non-human primates resulted in limited brain transduction and decreased neuronal transduction. However it is not clear whether the reduced transduction efficiency in the brain is a dose-dependent effect and whether it can be augmented by dose modification.

1.9.4 Clinical applications and potentials in RTT

The recent advances in vector /capsid design of the Adeno-associated virus-based vectors has led to extensive preclinical and phase 1 clinical studies to implement these vectors in the treatment of various human diseases (Warrington and Herzog, 2006). Published data from recent human clinical trials has shown AAV-based vectors to produce significant therapeutic effects in the treatment of cystic fibrosis (Wagner et al., 1998, Moss et al., 2004) and Hemophilia B (Kay et al., 2000, Manno et al., 2003). However these trials have also uncovered some restrictions to the current vectors including; limitations in the biological effect, immune response stimulation, induction of liver transaminases, and inefficient transduction of progenitor cells. Many CNS disorders are being tested for potential AAV mediated gene therapy, including; amyotrophic lateral sclerosis (Azzouz et al., 2000, Kaspar et al., 2005), spinal muscular atrophy (SMA) (Valori

et al., 2010), Huntington disease (McBride et al., 2003, Kells et al., 2004), lysosomal storage disorders (Sferra et al., 2004), Parkinson`s disease (Eslamboli et al., 2005, Feigin et al., 2007) and Canavan`s disease (Klugmann et al., 2005).

AAV is very promising in the case of RTT gene therapy (Tables 1-1) as; it can cross the blood-brain barrier, especially pseudo-typed with AAV9 capsid (Foust et al., 2009), infect neurons efficiently, mediate long-term transgene expression (Herzog et al., 1997, Arruda et al., 2005, Jiang et al., 2006) and does not integrate in a random fashion into host chromosomes (the vector DNA usually persisting as an episome in the nucleus) with accompanying safety benefits (Duan et al., 1998, Nakai et al., 2001). In spite of achieving high neuronal transduction, great attention has to be given to the transcription levels of *Mecp2* as overexpression is predicted to be detrimental. On the other hand, the disadvantages of this vector include immune system stimulation and potential issues of the endurance of transgene expression over the long term.

Summary and aims

Rett syndrome is not uncommon neurodevelopmental/ maintenance disorder that occurs mainly in girls and is characterized by neurological, motor and social disabilities. Dysfunctional mutations in *MECP2* gene are responsible for > 95% of typical RTT cases and also implicated in other neurological conditions. Mice models of RTT have been invaluable tools to help understand the underlying pathological changes occurring in RTT at the cellular and molecular levels and help to evaluate the efficacy of possible therapeutic interventions. The observed phenotype reversibility shown in these mice models, after reactivation of endogenous *Mecp2*, highlights the potentials for treating and or preventing RTT in patient. There is no current curative treatment for RTT and the exact function of *Mecp2* and its downstream effects is not clear. For these reasons, therapeutic intervention at the *Mecp2* gene level either by reactivation of the inactive X chromosome, which contains a normal *Mecp2* allele or by viral-mediated delivery of exogenous copy of normal *Mecp2* offer attractive possible strategies. Lentivirus- and AAV-based delivery systems have been shown to have good potentials for introducing various transgenes to the CNS and suggest a

possible application for these vectors in delivering exogenous as a first step to developing gene therapy strategies in RTT models.

Therefore the main aim of my PhD is to investigate the potential of gene therapy in RTT by investigating the viral-mediated delivery of *MECP2* in genetic mouse models of RTT. Specific goals were as follows:

- 1 To develop lentivirus-based vectors with various promoters and tag epitopes to enable *in vitro* and *in vivo* expression of exogenous *Mecp2*. To further examine the transduction efficiency, pattern and levels of transgenic *Mecp2* expression and to ascertain the phenotypic consequences that result.
- 2 Investigating the potentials of ssAAV9-based vector mediated delivery of *MECP2* in modifying the trajectory of RTT-like phenotypes in *Mecp2*-deficient mice.
- 3 To quantify the transduction efficiency and cellular protein levels achieved by AAV9-mediated *MECP2* delivery.
- 4 To examine the potential for overexpression-related toxicity and identify the threshold of *Mecp2* overexpression that is tolerable.
- 5 Testing whether increasing the transduction efficiency through implementing the scAAV9 vector could achieve more therapeutic benefits on RTT-like phenotype.

The overall objective of my thesis research was thus to take the first step in developing a gene therapy-based approach in Rett syndrome.

Chapter 2

Materials and methods

2.1 General materials

2.1.1 Enzymes and reagents

Table 2-1 list of enzymes

Enzymes	Supplier
GoTaq hot start Polymerase	Promega
2xThermo-start high performance PCR master mix	Thermo-scientific
Phire hot start DNA polymerase	NEB
Crimson Taq DNA Polymerase	NEB
T4 DNA ligase	Invitrogen
T4 DNA ligase	NEB

Table 2-2 list of the Kits and their suppliers

Kits	Supplier
Rapid DNA ligation kit	Roche
Qiaquick PCR purification kit	Qiagen
Qiaquick gel extraction kit	Qiagen
Qiaprep spin miniprep kit	Qiagen
Qiagen plasmid maxi kit	Qiagen

2.1.2 Primers

All the primers listed below are supplied from Sigma Aldrich except the first two primers that were supplied from Eurofins MWG/Operon

Table 2-3 Oligonucleotide list

Primer name	Nucleotide sequences (5' → 3')
Fpr-MECP2 (Nhe1) PCR	TTTGCTAGCATGGCCGCCGCTGCC
Rpr-MECP2-FLAG(BamH1) PCR	AAAGGATCCGCCTTGTCATCGTCGTCCTTGTA GTCGCTAACTCTCTCGGT
Fpr -pCDNA <i>RFP</i> -(Seq)T7	TAATACGACTCACTATAGGG
Rpr -pCDNARFP (Seq) BGH	TAGAAGGCACAGTCGAGG
Fpr pEGFP-C1(MECP2-E1) Seq	GACAACCACTACCTGAGC A
Rpr pEGFP-C1(MECP2-E1) SEq	CCACAACCTAGAATGCAGTG
Fpr-pcdnaMecp2RfpSeq	AGTCATCGCTATTACCATGGTGATGC
Fpr- pLL4MECP2RFPSeq	TTTCGGCATTCTGCACGCTTC
Rpr-pLL4MECP2RFPSeq	GGATCCAGAGGTTGATTATCG
Fpr-plenti-syn Seq	ACCACGCGAGGCGCGAGATAG
Fpr BamH1LentiGFPMCS2	AAAGGATCCGGCGCGCCTAGGCGATCGCTAGCA TGGTGAGCAAG GC
Rpr EcoR1LentiGFPMCS2	GAATTCTTAATTAACACCGGCGGTCCGCTACTTGTA CAGCTC
FprNot1BDNF promoter	GCGGCCGCTTTCACCTTGTAAACCATCAGCCC
Rpr Nhe1BDNF promoter	GCTAGCGCGAGAGCAGTCCTCTCCTCGGTGAAT
Fpr Not1 Mecp2 promoter	GCGGCCGCTAGCAAATAAATGAATAGAGAGGGG AGC
Rpr Nhe1 Mecp2 promoter	GCTAGCTTTCGGACGGGTTTTACCACAGCC
Fpr WRE seq	ATCACTCTCGGCATGGACG
Rpr WRE seq	GCCAGGCACAATCAGCAT
Fpr BDNF promoter seq	GCTCGCTTCACGAGATT
Rpr BDNF promoter seq	GGTGGTGCAGATGAACT
New P5	TGGTAAAGACCCATGTGACCCAAG

New P6	TCCACCTAG CCTGCCTGTACTTTG
P7	GGCTTGCCACATGACAAGAC

Table 2-4 List of Bacterial strains

Bacterial strains	Supplier
DH5 alpha cells sub cloning eff/1ML	Invitrogen
XL1 Blue Competent Cells	Agilent

Table 2-5 List of the vectors

Vector name	Type	Encoded product	Source
pCDNA(+) zeo RFP	Mammalian	<i>RFP</i>	Prof. Manuela Zaccolo Balliol college, University of Oxford, UK.
pLenti-syn1- <i>GFP</i>	Lenti-virus	<i>GFP</i>	Prof. Kumlesh Dev Trinity college, Dublin, Ireland.
pLenti-PGK- <i>GFP</i>	Lenti-virus	<i>GFP</i>	Prof. Kumlesh Dev Trinity college, Dublin, Ireland.
pRSV-40 <i>Mecp2_e1</i>	Mammalian	mouse <i>Mecp2_e1</i>	prof. Adrian Bird University of Edinburgh, UK.
pRSV-40 <i>Mecp2_e2</i>	Mammalian	mouse <i>Mecp2_e2</i>	prof. Adrian Bird University of Edinburgh, UK.

2.2 General solutions

All chemicals below without specified origins were supplied from Merck Ltd. (BDH laboratories, UK) or Sigma-Aldrich Company Ltd. (Sigma, UK).

2.2.1 Phosphate buffer (PB) Solution

2.2.1.1 0.2 M PB

Ingredients

- Solution A: 37.44 g of $\text{NaH}_2\text{PO}_4 (2\text{H}_2\text{O})$ in 1200 ml H_2O
- Solution B: 84.90 g of Na_2HPO_4 in 3000 ml H_2O

Add 1120 ml of solution A to 2880 ml of solution B and mix well. Adjust pH to 7.4 with either HCl or NaOH. Add 3000 ml distilled water to the final solution.

2.2.1.2 0.1 M PB

0.1 PB was made by 50/50 (v/v) dilution with distilled water.

2.2.1.3 0.3 M PBS

100 ml of 0.2 M phosphate buffer, Distilled water 1900 ml and NaCl 36 g.

2.2.2 1x TBE

Trizma base (90 mM), Orthoboric acid (90 mM) and EDTA (2 mM).

2.2.3 1kb DNA ladder

1Kb DNA ladder (NEB, N3232)

2.2.4 5x DNA loading dye

SDS 0.5% (w/v), Xylene cyanol 0.25% (w/v), Bromophenol blue 0.25% (w/v) and Ficoll^R 400 1.5% (w/v) in 3x TBE.

2.2.5 Ethidium Bromide

Stock solution: 10 mg/ml in H₂O (Sigma, E-1510).

2.2.6 TE buffer

10 mM Tris-HCl and 1mM EDTA (pH 8.0).

2.2.7 Ampicillin solution

Stock solution of 25 mg/ml in distilled water. Aliquots of 1 ml of the stock are kept at -20°C freezer. Final concentration is 50 µg/ml.

2.3 Bacterial solutions

2.3.1 Luria-Bertani (LB) medium

3 % (w/v) Bacto-tryptone, 0.5% (w/v) Bacto-Yeast extract and 1% (w/v) NaCl.

2.3.2 LB agar

LB medium plus 7-10% agar (w/v).

2.3.3 SOB media

2% (w/v) Bacto-tryptone, 0.5% (w/v) Bacto-Yeast extract, 10 mM NaCl, 0.25 mM KCl, 10 mM MgCl₂ and 10 mM MgSO₄, PH = 7.0. Sterilized by autoclaving.

2.3.4 SOC media

SOB media with 0.04 % (w/v) glucose.

2.4 Solutions for DNA plasmid preparation (Alkaline lysis methods)

2.4.1 Solution I (resuspension solution)

50 mM glucose, 25 mM Tris-HCL (pH 8.0) and 10 mM EDTA.

2.4.2 Solution II (Lysis solution)

0.2 N NaOH and 1% SDS.

2.4.3 Solution III (neutralization solution) 3M KAC

294.45 g potassium acetate and 115 ml glacial acetic acid in a final volume of 1 liter of water.

2.5 Methods

2.5.1 Restriction endonuclease digestion of plasmid DNA

Restriction digests were carried out to generate DNA fragments for either ligation or validation of the insert size of a recombinant plasmid. Double restriction digest reactions (containing two different enzymes in the same buffer) were carried out whenever possible to minimize the DNA loss that accompanies sequential simple restriction digests. Table 2-6 demonstrates the components of each restriction digest reaction.

Table 2-6 Components of the restriction digestion reaction

Reagent	Volume
Restriction buffer	2.5 μ l
DNA	? μ l (1 μ g of plasmid DNA)
Enzyme 1	1 μ l
Enzyme 2	1 μ l
Water	top u to 25 μ l
Final volume	25 μ l

All reaction components were thoroughly mixed by pipetting up and down several times then pulse spun. The reaction mixture was incubated at 37°C for 1-2 hours depending on the enzyme used.

2.5.2 Ligation reaction

DNA ligase was used to clone various gene encoding sequences into different vector backbones. Insert to vector molar ratio of 3:1 is mostly used to set up the reaction mix. 50 ng of the vector was used per reaction and the amount of the insert was calculated using the following formula: amount of insert in ng = amount of the vector (50 ng) X molar ratio (3) X insert size / vector size. The reaction conditions are summarized in the following table 2-7. A control reaction which contains all the ligation reaction components except the insert was also performed.

Table 2-7 Components of the ligation reaction

Reagent	Ligation reaction	Negative control
Ligation buffer	4µl	4µl
Insert	Estimated from the above formula	-
Vector	50ng	50ng
T4 ligase	1 µl	1 µl
Water	top up to 20 µl	
Total volume	20 µl	20 µl

Ligation reactions were carried out at 26°C for one hour for sticky-end ligation and at 16°C overnight for blunt-end ligation. These conditions and reaction reagents were varied according to which ligase enzyme was used.

2.5.3 Preparation of chemically competent cell

E-Coli, DH5α, bacterial cells were spread on an antibiotic-free LB agar plate and incubated overnight at 37°C. A single colony was picked and sub-cultured in 5 ml LB medium followed by an overnight incubation at 37°C in the shaking incubator. To generate a large volume of bacterial culture, 3 ml of the overnight culture was added to 200 ml of LB medium and incubated for another 2-3 hours at 37°C in the shaking incubator. The optical density (OD) of the culture was tested every 30 minutes until it reached 0.6-1.0. The culture medium was spun down at 3000 rpm for 15 minutes at 4°C to precipitate the bacterial pellet. The pellet was then fully

re-suspended in 80 ml of 0.1 M MgSO₄ by pipetting up and down several times on ice. To remove the MgSO₄ solution, the solution was centrifuged at 3000 rpm for 15 minutes at 4°C. Lastly the bacterial pellet was re-suspended in 2ml of ice-chilled 0.1M CaCl₂. Aliquots of 50 µl of the competent DH5α were stored at -80°C in cryo-protective tubes.

2.5.4 Heat shock transformation of chemically competent *E-Coli*

Two 50 µl aliquots of competent cells were defrosted on ice for 15 minutes. 10-100 ng of the vector or 5 µl of the ligation-mix was added to the cells and gently mixed by gentle pipetting up and down several times on ice, then left undisturbed for 30 minutes. The competent cells were then exposed to a heat shock by transferring them from ice to pre-heated water bath at 42°C for 30-45 seconds then incubated on ice for a further 3 minutes. 900 µl LB or SOC medium was added to the transformed cells and they were then incubated for 60-90 minutes at 37°C in the shaking incubator. 100 µl of the transformed competent cells were plated on the pre-warmed LB agar plate with appropriate antibiotic and incubated overnight at 37°C.

2.5.5 Plasmid mini-preparation (alkaline lysis)

A single bacterial colony was chosen and sub-cultured in 5 ml of LB medium with ampicillin (final concentration of 50 µg/ml) in a loosely capped 50 ml tube and incubated overnight at 37°C with vigorous shaking (200-250 rpm). The bacterial culture was spun down at 13000 rpm for 2 minutes at room temperature to harvest the bacterial pellet. 100 µl of ice-cold solution 1 (resuspension solution) was used to fully resuspend the bacterial pellet by either vortexing or pipetting up and down followed by incubation for 5 minutes at room temperature. 200 µl of solution II (lysis solution) was then added to the tube to lyse the bacterial cells. The tube was mixed gently by inversion, to avoid excessive shearing of the genomic DNA, and incubated on ice for 5 minutes.

To isolate the plasmid DNA from the genomic DNA, 150 µl of ice-chilled solution III (neutralization solution) was added to the tube and mixed by vortex then incubated on ice for 5 minutes. The mixture was centrifuged at 13000 rpm for 10 minutes at room temperature. The supernatant, containing the plasmid DNA,

was transferred to another tube and incubated with 1 μ l of 10 mg/ml RNase A for 15 minutes at 37°C. 500 μ l phenol/ chloroform was added and mixed vigorously by vortex. The aqueous top layer was then obtained by centrifugation at 13,000 rpm for 10 minutes at room temperature. Precipitation of plasmid DNA was carried out by adding 1/9 volume of 3 M sodium acetate and 2.5 volume of absolute alcohol followed by vortex and centrifugation at 13000 rpm for 10 minutes at room temperature. Lastly the DNA pellet was washed with 70% ethanol and centrifuged for 2-3 minutes. The pellet then air dried and resuspended in 20-30 μ l of TE buffer solution.

2.5.6 Making glycerol stock

For long term storage of the bacterial cells containing the plasmid of interest, 500 μ l of the overnight culture was added to 500 μ l of 50% glycerol (filtered sterilized) and mixed by vortex giving a final concentration of 25% glycerol. This mixture was incubated for 30 minutes at 37°C in the shaking incubator followed by storage at -80°C.

2.5.7 Determination of DNA concentration

The concentration and purity of DNA in aqueous solution were estimated by measuring the UV absorbance of the solution at wavelength of 200-300nm using Nano drop 1000. An optical density of 1 corresponds to 50mg/ml of DNA in the solution. The purity of the DNA samples was measured by comparing the ratio of the OD at 260nm (OD_{260}) to 280nm (OD_{280}). An OD_{260}/OD_{280} ratio of 1.8-2.0 is taken as an acceptable level of purity. The base line of the Nano-drop1000 was corrected using TE buffer as a blank.

2.5.8 Polymerase chain reaction (PCR) for transgene amplification

Standard PCR reactions were carried out to amplify various transgenes used in this study. Restriction sites usually added to the amplified PCR by the forward and reverse primers. The components and concentration of the PCR are included in table 2-8. The reactions were set up in 0.2 ml PCR tubes (Themoscientific). The PCR conditions varied according to the polymerase type, primers and the size of the constructs to be amplified.

Table 2-8 Components of the PCR reactions

Reagent	Volume
PCR buffer	10 μ l
dNTPs mix	X μ l (0.25 μ M)
Forward primer	x μ l (0.5 μ M)
Reverse primer	x μ l (0.5 μ M)
DNA template	x μ l (100 pg-1 ng)
Polymerase	1 μ l
Water	top up to 50 μ l
Final volume	50 μ l

The PCR reaction mix was incubated in the Gene Amp thermal cycler (PCR system 9700; Applied Biosystems, UK) using the following standard amplification conditions that are listed in table 2-9.

Table 2-9 Standard PCR condition

Step	Temperature	Duration
Initial denaturation	94 °C	5 minutes
x30 cycles		
Denaturation	94 °C	30 seconds
Annealing	55-60 °C (dependent on the T_M of the primers)	30 seconds
Extension	72 °C	dependent on the type of the polymerase
Final extension	72 °C	10 minutes
Hold	4 °C	α

2.5.9 Agarose gel electrophoresis

DNA molecules were separated according to their size by agarose gel electrophoresis. A solution of 0.8-1 % (w/v) agarose in 0.5 X TBE buffer was prepared in a microwave till the Agarose was completely dissolved. When the

TBE solution had cooled down (-40°C), Ethidium bromide was added to a final concentration of 200 ng/ml. Gels were poured in a horizontal tray and allowed to set at room temperature for one hour. DNA samples were mixed with 5 X DNA loading dye and electrophoresed for one hour at 100-120 volts. An aliquot of a DNA size ladder (1.5-2 μg) was also electrophoresed and used as a marker. Separated DNA samples were visualized using an UV transilluminator (UV-TM-40; Upland, USA; wavelength 254nm) and photographed using Canon digital camera (PC1192; Japan).

2.6 Animals

2.6.1 Design of the *Mecp2*-KO mouse models

The *Mecp2*-knock out mouse models were created and supplied by prof. Adrian Bird's laboratory at the University of Edinburgh, Edinburgh, UK. The first model was generated by cre-lox mediated deletion of part of exons 3 and 4 of *Mecp2* gene to produce the *Mecp2*-null model (Guy et al., 2001). Several years later the second model was created by insertion of a NEO-STOP cassette into intron 2 of *Mecp2* to generate an incomplete *Mecp2* mRNA that precludes translation of *Mecp2* protein (*Mecp2*-stop model). This model allows selective deletion of the stop cassette to enable activation of endogenous *Mecp2* expression and is thus a functional knockout rather than structural knockout (Guy et al., 2007).

2.6.2 Breeding strategy of *Mecp2*-KO mice

Local *Mecp2*-KO colonies at University of Glasgow were established by breeding heterozygous *Mecp2*^{stop/+} and *Mecp2*^{-/+} females (C57BL/6 background) with WT males (BALB/C and B57BL/6 background respectively) purchased from Harlan laboratories (Shardlow, UK). All mice used in this work were hemizygous *Mecp2*^{stop/y} or *Mecp2*^{-/y} males and their WT male littermates. Different genotypes/genders that were created from the mating of *Mecp2*^{-/y} females with WT males are summarized in table 2-10. Offspring genotypes were determined by PCR. Mice were housed in groups of 2-3, maintained on a 12-hour light/dark cycle and provided with food and water ad libitum. All experiments were conducted in accordance with the European Communities Council Directive (86/609/EEC) and a project license with local ethical approval under the UK Scientific Procedures Act (1986).

Table 2-10 Breeding scheme for *Mecp2* knockout mice

Females	Male WT (<i>Mecp2</i> ^{+/y})				
<i>Mecp2</i> ^{-/+}	sex	Male	Male	Female	Female
	genotype	WT <i>Mecp2</i> ^{+/y}	hemizygous <i>Mecp2</i> ^{-/y}	WT <i>Mecp2</i> ^{+/+}	heterozygous <i>Mecp2</i> ^{-/+}
<i>Mecp2</i> ^{stop/+}	sex	Male	Male	Female	Female
	genotype	WT <i>Mecp2</i> ^{+/y}	hemizygous <i>Mecp2</i> ^{stop/y}	WT <i>Mecp2</i> ^{+/+}	heterozygous <i>Mecp2</i> ^{stop/+}

2.6.3 Genotyping

2.6.3.1 DNA extraction

Genomic DNA was extracted from either tail samples (mice neonates) or ear samples (adult mice) using DNareasy™ reagent (ANACHEM Ltd.UK). Ear or tail samples were added to 20 µl of DNareasy buffer then incubated in a GeneAmp thermal cycler (PCR system 9700; Applied Biosystems, UK) under the manufacturers` recommended conditions (table 2-11).

Table 2-11 DNA extraction conditions

Temperature	Duration
75 °C	5 minutes
96 °C	2 minutes
20 °C	hold

2.6.3.2 PCR verification of mouse genotypes

PCR reactions were carried out to genotype offspring in each litter. For each genomic DNA sample two PCR reactions were performed, the first reaction using primers specifically designed to anneal with the WT *Mecp2* allele (P5 and P7) and the second reaction using primers that anneal with the KO *Mecp2* allele (P5 and P6). The reaction set up and PCR conditions are summarised in tables 2-12.

Table 2-12 PCR reaction sets for genotyping of *Mecp2*-null mice and their WT littermates

Reagent	WT set	<i>Mecp2</i> -null set
Thermo-start HP PCR master mix	13 μ l	13 μ l
Forward primer	P5 (0.4 μ M)	P5 (0.4 μ M)
Reverse primer	P7 (0.4 μ M)	P6 (0.4 μ M)
DNA template	5ng-10ng	5ng-10ng
Water	9 μ l	9 μ l
Final volume	26 μ l	26 μ l

The PCR reactions were carried out in GeneAmp thermal cycler (PCR system 9700; Applied Biosystems, UK). The reaction conditions are summarized in table 2-13.

Table 2-13 PCR conditions for genotype discrimination

Step	Temperature	Duration
Initial denaturation	94° C	15 minutes
	X30 cycles	
Denaturation	94° C	45 seconds
Annealing	60° C	45 seconds
Extension	72° C	1 minute
Final extension	72° C	10 minutes
Hold	4° C	α

PCR products were separated by agarose gel electrophoresis. PCR products for the P5/P7 primer set (WT allele) are 416bp, and PCR products for the P5/P6 primer set (*Mecp2*-KO allele) are 470bp.

2.6.4 Phenotype severity score

Mecp2 KO mice were phenotyped weekly after weaning (postnatal day 21-23) according to the scoring system developed by (Guy et al., 2007). The score uses six cardinal features of the RTT-like phenotype as a semi-quantitative measure

for the disease trajectory. These features are; mobility, gait, hind limb claspings, tremor, breathing abnormality and general appearance. Each of these feature scores 0 for a phenotype indistinguishable from WT, 1 for mild phenotype and 2 for severe phenotype (table 2-14) with total score ranging between 0-12. Tremor and breathing are observed while the mouse is standing still whereas hind limb claspings is tested by suspending the mouse by the base of the tail with the mouse supporting itself by its forelimbs.

Table 2-14 Detailed phenotype severity score of *Mecp2* KO mice

Phenotype features	Scores	
	1	2
Mobility	Reduced movement or prolonged freezing periods	No spontaneous movement
Gait	Wider than WT or reduced pelvic elevation “waddling” gait	Tremor when feet are lifted, walks backwards or lifting both rear feet at once
Hindlimb claspings	Hindlimbs are drawn into the midline (without touching) or one leg is drawn into the trunk.	Both legs are pulled into the midline tightly or touching body
Tremor	intermittent mild tremor	continuous or violent tremor
Breathing	short periods of rapid breathing or pauses in breathing	very irregular breathing - gasping or panting
General conditions	eyes dull, coat dull/un-groomed	eyes crusted or narrowed, piloerection or hunched posture

2.7 Hippocampal dissociated cell culture.

Hippocampal dissociated neuronal cell culture was conducted according to (Greenwood et al., 2007)

2.7.1 Animal

Pups (postnatal day 1-3) from;

- Mouse; *Mecp2*^{stop/Y} males, *Mecp2*^{stop/+} females and their WT littermates.
- Rat (used occasionally during the course of the study)

2.7.2 Materials

Enzymes and media used for cell culture are listed in table 2-15.

Table 2-15 Materials for dissociated hippocampal cell culture

Materials	Supplier
Poly-L-lysine	Sigma
L-Glutamine	Sigma
Neurobasal-A medium	Invitrogen
B27 medium	Invitrogen
Bovine serum albumin (BSA)	Invitrogen
Papain	Sigma

The components of the cell culture buffer that used during preparation of the hippocampal cell culture are listed in table 2-16.

Table 2-16 Components of the cell culture buffer

Compound	Working concentration	g/L
NaCl	116 mM	6.78
KCl	5.4 mM	0.40
NaHCO ₃	26 mM	2.18
NaH ₂ PO ₄	1.3 mM	0.16
MgSO ₄ .7H ₂ O	1 mM	0.25
CaCl ₂ .2H ₂ O	1 mM	0.15
EDTA.2Na.2H ₂ O	0.5 mM	0.15
Glucose	25 mM	4.5

The PH of the Cell culture buffer is =7.4

2.7.3 Method

Each mouse pup was euthanized by intra-peritoneal injection of a lethal dose of pentobarbital Na⁺ (Euthatal; Merial Animal Health Ltd., Harlow, UK). The pup was then decapitated, the skin was removed, and the skull was opened by making three cuts, two horizontal cuts through the foramen magnum and one longitudinal cut through the sagittal suture of the skull. The brain was removed and placed on a pre-sterilized (with 70% alcohol) filter paper (figure 2-1). The brain was cut through the midline into 2 halves, using a No. 11 scalpel blade, followed by dissection of the hippocampus, which was kept in a pre-chilled buffer in a 35 mm petri-dish. The hippocampus was chopped into small pieces by scalpel blade and the pieces were transferred to 15 ml falcon tube containing pre-warmed filtered-sterilized Papain (7.5 mg in 5 ml of the buffer) and incubated for 20 minutes at 37°C in the water bath. The papain was then inactivated by mixing with pre-warmed BSA (60 mg in 6 ml of the buffer). The cell suspension was centrifuged at 3000 rpm for 4 minutes at room temperature to remove any residual papain. The pellet was resuspended in 1 ml of complete neuro-basal medium (supplement with 2% B27 and 1% L-Glutamine). 100 µl of the cell suspension was plated on a poly-L-lysine-coated 12mm sterilised cover slip and incubated for one hour at 37°C, 5% CO₂. One hour later 1 ml of complete neuro-basal media was added to the cover slip containing petri dish and incubated at 37°C, 5% CO₂.

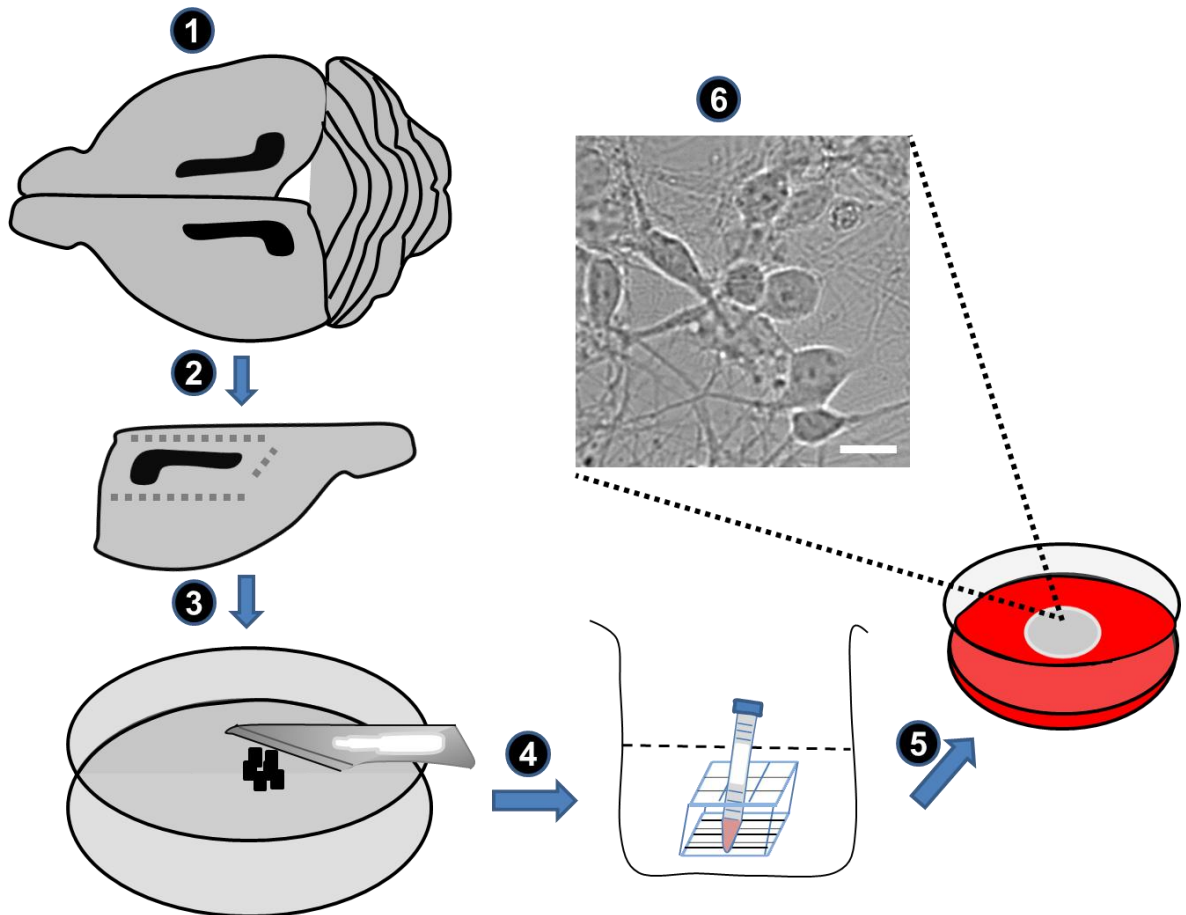


Figure 2-1 Hippocampal dissociated cell culture

Diagram showing preparation steps of the hippocampal dissociated cell culture. The brain of a P1-3 mouse pup was extracted (1) and the hippocampus was cut out (2) and chopped using a scalpel blade into small pieces (3). The hippocampal pieces were then incubated in papain followed by neutralization by BSA (4). The dispersed cells were plated on the coverslips in a 35 mm petri-dish with 1ml of neuro-basal media (5). (6) Micrograph showing bright field image of 7 days old hippocampal dissociated neuronal culture. Scale bar in 6 = 10 μm .

2.8 Calcium phosphate transfection

Ca^{2+} phosphate transfection of dissociated neuronal cultures was carried out according to Jiang et al 2004 (Jiang et al., 2004)

2.8.1 Materials

Table 2-17 Materials for Ca^{2+} phosphate transfection

Materials	Supplier
Neuronal dissociated cell culture	
Neuro basal-A media	Invitrogen
CaCl_2	Riedel-de-Haen

2X HEPES (pH 7.2)	Fisher-scientific BP
5X Kynurenic acid (stock, 10mM)	Sigma
Acidic 10% CO ₂ equilibrated culture medium	

2.8.2 Preparation of the transfection mix (for single coverslip)

Plasmid DNA (1-4 µg) was diluted in 1XTE buffer (PH = 7.3) to a final volume of 45 µl and mixed gently by vortex. 5 µl of 2.5 M CaCl₂ in 10 mM HEPES (to give a final concentration of 250 mM CaCl₂) was added in drop-wise fashion to the DNA/TE solution and mixed gently by vortex. This DNA/CaCl₂/TE (50 µl) solution was added to 50 µl of 2X HEBS (HEPES Buffered Saline) pH 7.2 and mixed by pipetting up and down. The mix containing tube was wrapped in tin foil and incubated at room temperature for 30 minutes with intermittent vortexing for 2-3 seconds every 5 minutes to allow formation of the transfection precipitate.

2.8.3 Preparation and transfection of the cell culture.

To protect neurons against the excitotoxic effect of Ca²⁺ ions, 50 µl of 10 mM Kynurenic acid (an NMDA receptor antagonist) was mixed with 200 µl of the conditioned neuro-basal medium (conditioned by the cultured neuronal cells) to make enough volume for one well of a 24 well plate. The cover slip to be transfected was transferred to this well and incubated at 37°C, 5% CO₂ until the transfection mix become ready. 50 µl of the transfection precipitate was added in a drop-wise fashion to the cover slip and mixed to ensure that the precipitate completely covered the cover slip. The culture was then incubated for 1-3 hours at 37°C, 5% CO₂. After that the transfected cover slip was transferred to a fresh well of 24 wells plate containing 1ml of acidic 10% CO₂ equilibrated culture medium and incubated at 37°C, 5% CO₂ for 15-20 minutes. A single wash of the cover slip with unconditioned medium is recommended to remove any traces of kynurenic acid. The transfected cover slip was finally transferred to a fresh well of 24 wells plate containing 500 ul of the conditioned medium and incubated at 37°C, 5% CO₂ for 24 hours.

2.9 Generation of Lentivirus particles

Lentivirus production was carried out according to (Kuroda et al., 2009)

2.9.1 Materials

Table 2-18 Materials for the generation of lentivirus particles

Material	Supplier
Human embryonic kidney (HEK) 293T/17 cells	ATCC
Sodium pyruvate	Sigma
L-Glutamine	Invitrogen
Fetal bovine serum (FBS) heat inactivated	Sigma
Phosphate buffer solution (PBS) 1X w- out calcium	Invitrogen
Pen-Strep 10K units	Invitrogen
DMEM medium (high glucose, no glutamine, with sod. pyruvate	Sigma
Trypsin/ EDTA 0.25%	Sigma
Optimem medium	Invitrogen
Polyethylenimine (PEI)	Sigma
Trypan blue solution (0.4%)	sigma
Plasmid pMD2.G	Addgene
Plasmid pMDLg/pRRE	Addgene
Plasmid pRSV-Rev	Addgene
Nunc Cryo-tube vial	sigma
TC flask 150 cm ² vented	Corning
Syringe filter 0.2um 25mm dia.	Sartorius

2.9.2 Preparation of HEK 293T/17 cells

2.9.2.1 Recovery of HEK 293T cells from liquid nitrogen

Gradual recovery of HEK293T is critical to minimize cell death. One vial of HEK293T-containing medium was taken from storage in liquid nitrogen and transferred to the cell culture lab on dry ice. The vial was kept at room temperature (approximately 22 °C) for two minutes before being incubated in a pre-heated water bath at 37 °C till the cell-containing media became fully defrosted. The vial was wrapped in an alcohol-soaked tissue (70% EtoH) and transferred to a sterilized fume hood to prevent contamination. The contents of the vial was added to 9 ml of pre-conditioned (37 °C, 5% CO₂) complete DMEM medium (DMEM with 10% FBS, 1% L-Glutamine, 1% Pen-Strept and 1% Sodium pyruvate) and centrifuged at 4000 rpm for 4 minutes at room temperature. The supernatant was discarded and the cell pellet was dispersed in 1 ml of complete pre-conditioned media by pipetting up and down. The dispersed cells were then added to 30 ml of preconditioned complete media in a T150 cm² flask and incubated at 37 °C, 5% CO₂. After 24 hours, the medium was changed and cell growth was monitored.

2.9.2.2 Passage of HEK293T cells

HEK293T cell passage was carried out to maintain the cells in the log phase of growth to ensure maximum growth rate and avoid over confluence and subsequent cell death. Cell confluence of 75-80 % was considered as optimal for cell passage. To passage HEK293T cells, the culture media was removed and the cells were washed with pre-heated (37 °C) PBS to remove any residual serum-containing medium. To induce cellular detachment from the flask, 3 ml of trypsin was added to the cell layer and mixed then incubated at 37 °C, 5% CO₂ for 3 minutes. To inactivate the trypsin, 7 ml of pre-warmed (37 °C) complete medium was added and mixed by pipetting up and down several times to fully disperse the cells. HEK293T cell suspension was then transferred to a 50 ml falcon tube. To determine the cell count, 20 µl of HEK293T cell suspension was mixed with 20 µl of Trypan blue dye and 8 µl of this mix was placed on each counting chamber of a haemocytometer slide (LW Scientific, Inc. 800/726-7345) to determine the cell numbers per ml. Afterwards, a defined cell number was added to preconditioned complete medium-containing flasks.

2.9.3 Lentiviral vector particles preparation

2.9.3.1 Preparation of HEK293T cells

24 hours before transfection, HEK293T cells were passaged and 8×10^6 cells were plated in a T150 cm² flask and incubated overnight at 37 °C, 5 % CO₂. A number of 6-8 flasks were prepared in the same way. HEK293T cell confluence was monitored before transfection and only flasks that had 80-85% confluence were used for virus generation.

2.9.3.2 Preparation of the transfection solutions

The following volumes are sufficient for one T150 cm² flask.

Recipe 1(Optimem PEI)

1 µl of 10 mM PEI was added to 5 ml of Optimem in a 50 ml Falcon tube and mixed by inversion several times. The mixture was filtered and sterilized using a 0.2 µm syringe-filter.

Recipe 2 (Optimem DNA)

Lentivirus-based vectors containing the gene of interest together with the packaging plasmids (table 2-19) were added to 5 ml of Optimem in a 50 ml Falcon tube (figure 2-2) and mixed by inversion. The mixture was filtered and sterilized by 0.2 µm syringe-filter.

Table 2-19 Vectors concentration for Lentiviruses generation

Plasmid name	Concentration / T150 cm ² flask
Lentiviral vector	40 µg
Packaging plasmid(pMDLg/PRRE)	20 µg
Envelope plasmid (pMD ₂ G)	10 µg
Rev plasmid (pRSV-Rev)	10 µg

To generate transfection precipitates, the PEI-containing Optimem (recipe 1) was added drop by drop to the DNA-containing Optimem (recipe 2). Both recipes were mixed by inversion and incubated for 20-30 minutes at room temperature in the fume hood to help formation of the transfection mix.

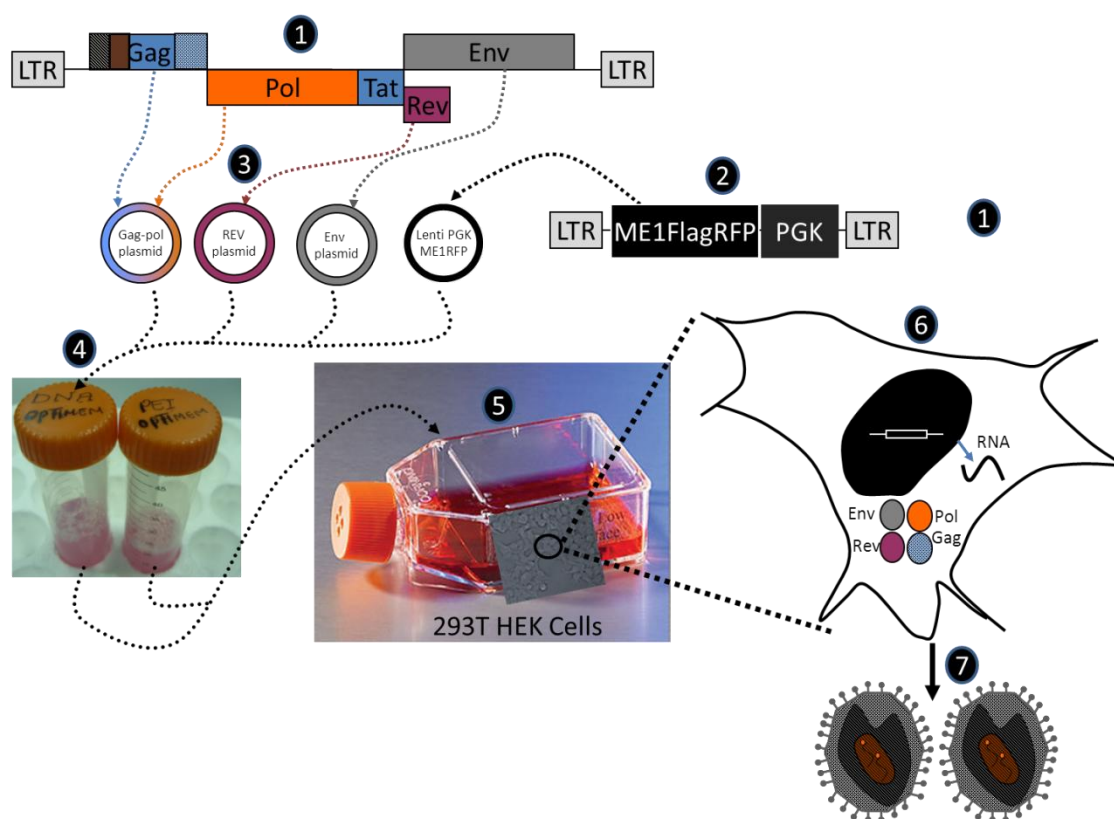


Figure 2-2 Generation of lentivirus particles

Schematic diagram showing the steps of lentivirus production. (1) shows the structural genes of the lentivirus (Gag, Pol, Rev and Env) located between both LTRs. (2) shows the structure of the lenti-vector backbone with all structural genes replaced by the gene of interest (e.g. *ME1FlagRFP*) between the two LTRs. (3) To generate lentivirus particles, all essential genes were supplied *in-trans* by 3 different vectors. (4) Transfection precipitates were carried out by mixing positively charged PEI with negatively charged DNA. (5) Transfection precipitate was added to HEK293T cells for 4 hours followed by 48 hours incubation. (6) Diagram of HEK293T cells showing the production of the virus RNA which is then packaged into viral proteins followed by viral assembly and release to the culture medium.

2.9.3.3 Transfection of HEK293T cells

To transfect HEK293T cells with the transfection mixture, the culture medium was replaced by 10 ml of the transfection mix. The flask was swirled gently to ensure that the transfection fluid covered all cells. The flask was then incubated at 37°C, 5% CO₂ for 4 hours to allow transfection of HEK cells. To confirm the

presence of transfection precipitates, the cells were visualized under the microscope and the presence of small black dots on and in-between the cells was confirmed. Finally the transfection mix was replaced by 30 ml of pre-conditioned complete DMEM medium and incubated at 37°C, 5% CO₂ for 48 hours.

2.9.4 Collection of lentivirus particles

Two batches of the virus containing media were collected; the first batch of lentivirus was collected after 48 hours. The culture medium containing the particles was transferred to a 50 ml falcon tube and replaced by 30 ml of pre-warmed fresh complete DMEM medium and incubated for another 24 hours under the same conditions. To remove cellular debris, the virus containing medium was centrifuged at 4000 rpm for 5 minutes at 4°C. The supernatant was filtered-sterilized by 0.2µm syringe-filter and stored at 4°C for further processing. The second batch of the virus was collected 24 hours after the first batch and processed in the same way. HEK293T cells were treated with Virkon and discarded.

2.9.5 Concentration of the Virus particles

To concentrate the virus particles, virus containing medium from the first and second batch were mixed together followed by spinning at 27000 rpm for 2 hours at 4°C in the pre-cooled Beckman ultracentrifuge. The supernatant was carefully discarded and the virus pellets (yellow and sometime difficult to see) were re-suspended in 5 ml of pre-chilled DMEM medium and incubated on ice for 20 minutes before being vigorously dispersed by vortexing. The content of all six ultracentrifuge tubes were added together in one tube and re-centrifuged at 27000 rpm for 2 hours at 4°C. The supernatant was discarded and the virus pellet was dispersed in 100 µl of pre-chilled PBS and incubated overnight at 4°C followed by final vigorous dispersion of the virus particles by vortex and pipetting up and down. 10 µl Aliquots were then stored at -80°C in a cryo-protective tubes.

2.9.6 Titration of lentivirus particles

2.9.6.1 First method

0.5 X 10⁵ of HEK293T cells/coverslip were plated on 6 poly-L-Lysine coated coverslips in 24 well tissue culture plates. After 24 hours one coverslip was used to estimate the total cell count per coverslip. One cover slip was used as a control (non-transduced) and the remaining four coverslips were transduced with a series of increasing amounts of virus particles (1, 2, 4 and 8 µl). After 72 hours the cells were fixed with 4% PFA and screened for RFP expression. The number of RFP expressing cells was counted and the titre was calculated according to the following formula;

$$\frac{\text{Number of HEK293T cells X percentage of RFP positive cells X1000}}{\text{Volume of virus (}\mu\text{l) used for transduction}}$$

The resulting titre will be presented as (infection unit) IU/ml

2.9.6.2 Second method

HEK293T cells were prepared as described above. On the day of transduction, the complete DMEM medium was discarded and replaced by 1ml of fresh complete DMEM containing a serial dilution of the virus particles in 10² to 10¹⁰. After 72 hours the numbers of RFP-positive cells were counted in each dilution and the titre was calculated according to the following formula;

$$\text{Virus titre (IU/ml)} = \text{virus dilution} \times \text{number of RFP-positive cells.}$$

2.10 Adeno-associated virus production

Adeno-associated virus particles (AAV9) has been generated, titrated and supplied by Dr. Steven Gray, Jude Samulski Lab UNC Gene Therapy Center, USA.

Recombinant AAV vectors were generated using HEK293 cells grown in serum-free suspension conditions in shaker flasks, using proprietary methods developed at the UNC Gene Therapy Center Vector Core facility. In brief, single-stranded or self-complementary AAV particles (AAV2 serotype vector backbone packaged

into AAV9 serotype coats) were produced from suspension HEK293 cells (ATCC# CRL 1573) transfected using polyethyleneimine (Polysciences) with the following helper plasmids (pXX6-80 (Xiao et al., 1998), pGSK2/9) plus the ITR-flanked transgene construct (pTR-CBA-*GFP*, pTR-CBA-*hMeCP2*, or pSJG-MeP-*hMeCP2*, respectively). The CBA constructs utilized a CMV enhancer, chicken beta actin promoter, shortened SV40 intron, and SV40 polyadenylation sequence (Gray et al., 2011b). The MeP construct used a truncated 229 bp murine MeCP2 promoter (Gray et al., 2011a) and the bovine growth hormone polyadenylation signal. All *MECP2* constructs utilized the human *MECP2_e1* minigene with a C-terminal Myc epitope tag. Forty-eight hours post-transfection, cell cultures were centrifuged and supernatant was discarded. The cells were resuspended and lysed by sonication, as described in (Grieger et al., 2006). DNase (550 U) was added to the lysate and incubated at 37°C for 45 minutes, followed by centrifugation at 9400 x g to pellet the cell debris and the clarified lysate was loaded onto a modified discontinuous iodixanol gradient followed by column chromatography, or purified by a step CsCl gradient centrifugation followed by a discontinuous CsCl gradient centrifugation. Both purification methods provide equivalent high levels of purity and *in vivo* transduction efficiency (Gray et al., 2011c). Purified vectors were dialyzed in 1x PBS with 5% D-sorbitol and a final NaCl concentration of 350 mM. Titer was obtained by both dot blot (Grieger et al., 2006) and qPCR.

2.11 Stereotaxic brain injection

To drive expression of exogenous *Mecp2*flagRFP in the hippocampus of the *Mecp2*^{stop/y} mouse, animals were anaesthetized with inhalational anaesthesia (Halothane) and after full loss of consciousness, their head was shaved and cleaned with 70% alcohol-soaked gauze. The mice were fixed on the stereotaxic frame using ear and mouth bars. Body temperature was monitored by insertion of a rectal probe. The skin was cut by scissors and the skull bone was softened using a bone drill followed by removal of the vault bone that covers the injection coordinates. An Injection glass pipette 25-30 µm in diameter was used, under the dissection microscope, to inject 0.3-0.6 µl of the virus/sit very slowly (over 5 minutes) using pressure pump. The injection pipette was kept in place for 2-3 minutes to minimize virus reflux. The skin was sutured and the mouse was injected intramuscularly with analgesic and was given a soft diet and kept in a 37°C incubator overnight to help the post-operative recovery.

2.12 Neonatal injection

For neonatal delivery of AAV9/*MECP2*, male littermates were sexed at birth (post-natal day 0-2) and received either facial vein injection of 30 μ l of scAAV9/*MECP2* or direct bilateral brain injections of sc/ssAAV9/*MECP2* virus (3 μ l/site) into the neuropil via a 33 g needle (Finescience) connected to 10 μ l Hamilton syringe by a very thin tube. The brain injection sites were over the temporal cortex, approximately 1-2 mm lateral from the midline, anterior to lambda and 2mm in depth. Injection was carried out slowly (over approximately 30 second) and the injection needle was kept in place for 30-60 seconds to minimize virus reflux. Immediately after injection, the pups were wrapped in the home cage bedding materials to prevent mother rejection. Non-injected female pups were also kept in the same cage to prevent mother distress. Three weeks after injection mice were weaned and ear-tagged for genotype verification and were then weekly phenotyped as previously described.

2.13 Immunohistochemistry (IHC)

To detect /study protein expression in different tissue sections, mice were deeply anaesthetised with sodium pentobarbital (Euthatal) at a dose of 100 mg/kg body weight (Merial Animal Health Ltd., Harlow, UK). After the animals were fully anaesthetised, the chest was opened immediately and the heart was explored. The perfusion needle was inserted in the left ventricle and a small cut to the right atrium was made to allow washing out of the blood and the excess fixative. Mice were first perfused with mammalian ringer or 0.1M PBS until their livers were cleared followed by perfusion with 300 ml of 4% paraformaldehyde (PFA) in 0.1M PBS. After complete fixation (evidenced by tail and limb rigidity) brains and other organs were dissected. All organs were then post-fixed in the same fixative for 5 hours before being transferred to 30% sucrose in 0.1M PBS and stored overnight at 4°C. Brain, spinal cord and other organs were embedded in 3% agar in water (w/v) and subsequently sectioned at 40-70 μ m using a vibrating microtome (Leica VT1200, Leica UK). Sections were washed three times in 0.3 M PBS followed by blocking using 15% normal goat serum in 0.3 M PBS with 0.3% Triton X100 for one hour at room temperature. Sections were incubated with primary antibody (table 2-20a) for 48 hours on a shaker at 4°C. The primary antibodies were then washed off (3 x 0.3 M PBS) followed by an

overnight incubation with the secondary antibodies (table 2-20b) at 4°C. Finally sections were incubated with DAPI (Sigma, 1/1000) dilution (v/v) in 0.3 M PBS for 30 minutes at room temperature and mounted with Vectashield (Vector labs, UK).

Table 2-20 Primary and secondary antibodies used in IHC

Antibody	Dilution	Supplier
(a) Primary antibodies		
Mouse anti-Flag tag	1/500	Abcam
Mouse anti-Mecp2	1/500	Sigma
Rabbit anti-Mecp2	1/500	Millipore
Rabbit anti-Myc tag	1/500	Abcam
Mouse anti Neu-N	1/500	Sigma
Rabbit Anti-GFAP	1/200	Abcam
Rabbit anti-Mecp2(S421)	1/10000	Greenberg lab
Chicken Anti-MAP2	1/200	Millipore
Rabbit anti-acetylated H4	1/1000	Millipore
Mouse anti-H4	1/1000	Abcam
Goat Anti-ChAT	1/100	Abcam
Sheep anti-GFP	1/1000	Santa Cruz
(b) Secondary antibodies		
Alexa fluor 488 goat anti-mouse	1/500	Invitrogen
Alexa fluor 488 goat anti-rabbit	1/500	Invitrogen
Alexa fluor 488 donkey anti-sheep	1/500	Santa-cruz
Alexa fluor 546 goat anti-mouse	1/500	Invitrogen
Alexa fluor 546 goat anti-rabbit	1/500	Invitrogen
Alexa fluor 647 goat anti-mouse	1/500	Invitrogen
Alexa fluor 647 goat anti-rabbit	1/500	Invitrogen
Alexa fluor 647 goat anti-chicken	1/500	Invitrogen
Alexa fluor 647 donkey anti-goat	1/500	Invitrogen

2.14 Image analysis

Expression patterns, transduction efficiency and transgene level quantification (intensity measurements) were carried out on image stacks captured using a Zeiss LSM710 laser confocal microscope. Z-series were taken at 0.6-1.3 μm intervals through the section of interest using a 40x or 60x objectives.

To estimate transduction efficiency, the ratio of Myc-positive nuclei relative to DAPI-stained nuclei in random fields was obtained from the hippocampus (CA3 region), layer 5 of primary motor cortex, thalamus, hypothalamus, brainstem and striatum. To assess the percentage of transgenic expression in neurons, the ratio of Myc-immunopositive to NeuN-immunopositive cells were determined. To quantify the amount of transgene product WT mice were injected with virus particles (lenti or AAV9) and at the end of the experiment these mice were perfused and their brains were sectioned as described above. RFP fluorescence or anti-Myc antibodies were used to identify the transduced cells whereas anti-Mecp2 immunofluorescence was used for intensity measures of the cellular Mecp2 level. ImageJ software (<http://rsbweb.nih.gov/ij/>) was used to determine mean MeCP2-channel fluorescence intensity within transduced and non-transduced cells within a 15 micron optical section.

Nuclear volume estimation was made by serial reconstruction of nuclei in a Z-series (0.6 μm) using ImageJ. The DAPI channel was used to define the nuclear boundary and the transduction status of cells discriminated by the presence or absence of anti-Myc immunolabelling for AAV9-based experiment and with RFP fluorescence expression in Lentivirus-based experiments.

2.15 Treadmill motor challenge test

Treadmill motor test was carried out using the DigiGait imaging system (Mouse Specifics, Boston, MA) as described (Kale et al., 2004). Digital videos were captured as mice were challenged to run at varying speeds (10 and 25cm/s) on a transparent treadmill. Mice were contained within a plexiglass chamber (figure 2-3), with front and rear bumpers, that was placed on top of the treadmill to ensure the animals remained visible to the camera at all times. Mice were given 1-2 minutes to accommodate before starting the test. The treadmill belt was

cleaned with 70 % EtOH after each run. A run was considered as successful if the animals could run at the set speed for 10 consecutive steps (~ 2 seconds) without sliding back and hitting the rear bumper with their hindquarters.



Figure 2-3 DigiGait apparatus

An image showing the DigiGait apparatus that was used for the treadmill test. Mice were challenged to run on a transparent treadmill belt (white arrow) and their movement were captured by a camera fixed underneath the belt. Mice were kept in the view of the camera by front and rear bumpers (black arrows).

2.16 Open Field Testing

Motor function and anxiety were evaluated using the well-established open field test (Choleris et al., 2001). Mice were placed in the centre of a 60 cm diameter arena (with opaque wall that the mouse cannot see outside, figure 2-4) and allowed to ambulate freely for 40 minutes during which time the experimenter left the room. The arena was filmed using an overhead digital camera and the mouse was tracked using Ethovision 3.1 tracking software (Noldus Inc., Leesburg, VA). The digital track produced by the animal was then analysed by the software and various motor and anxiety parameters were calculated. All animals tested were between 9-11 weeks old.

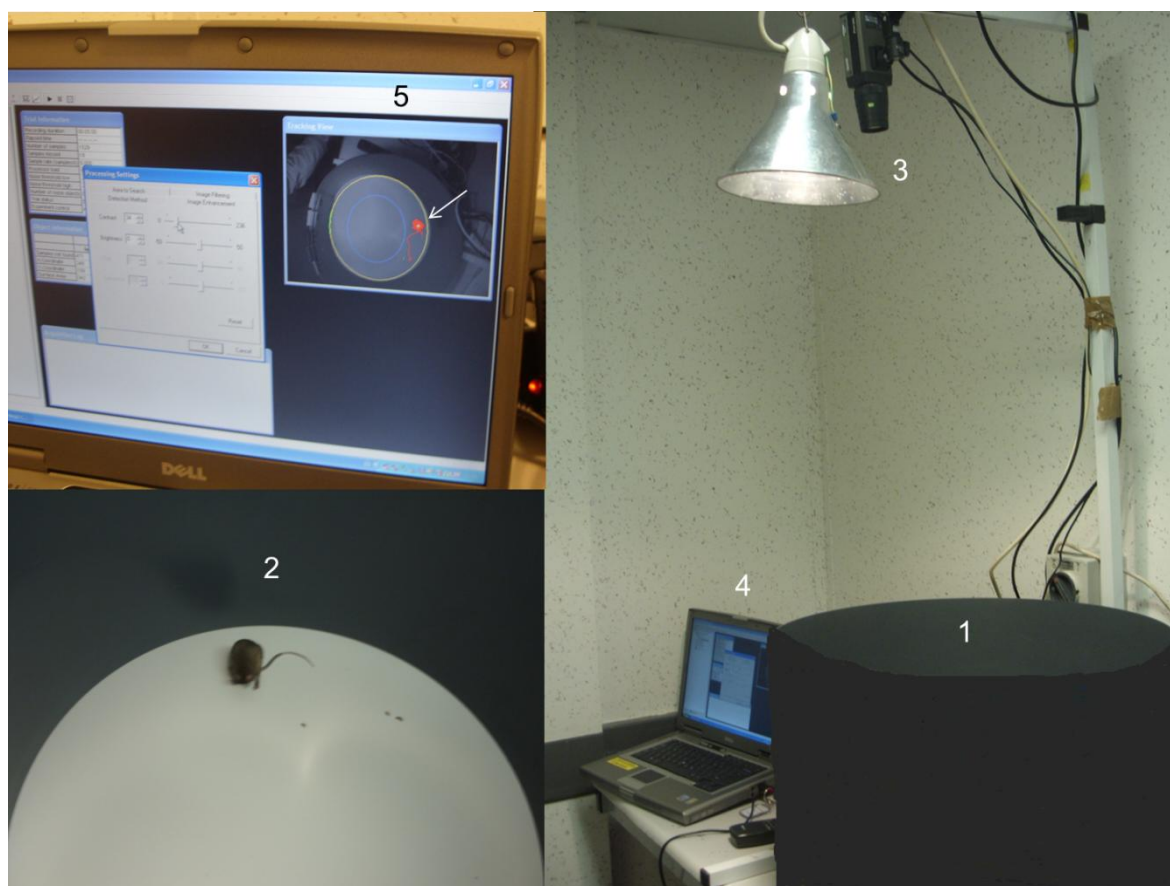


Figure 2-4 Open field test
 Images showing the open field test. (1 and 2) show The open field arena. (3) Camera fixed on the top of the arena to trace mice movement. (4 and 5) the movement was tracked and analysed by Ethovision 3.1 tracking software.

2.17 Whole body plethysmograph

Respiratory phenotype was determined in a conscious and unrestrained animal using whole body plethysmography (EMMS, Bordon, U.K.). Animals were placed inside a plexiglass chamber (figure 2-5) for 20 minutes to become adapted to the environment after which their breathing was monitored for 30 minutes. A continuous bias airflow supply allowed the animal to be kept in the chamber for extended periods of time. Pressure changes caused by alterations in the temperature and humidity of the air as it enters and leaves the subjects lungs were detected by a pressure transducer. This analogue signal was amplified and converted to a digital display by the custom software to produce a waveform representing the breathing pattern of the animal. This waveform was then exported and analysed using pClamp 10.2 (Molecular Devices inc., California, USA). Pressure changes were calibrated by injecting 1ml of air via syringe. Respiratory waveforms were analysed for frequency, frequency variability and

the presence of abnormal breaths /apnoeas (expiratory pauses >3 breaths (Lioy et al., 2011)).

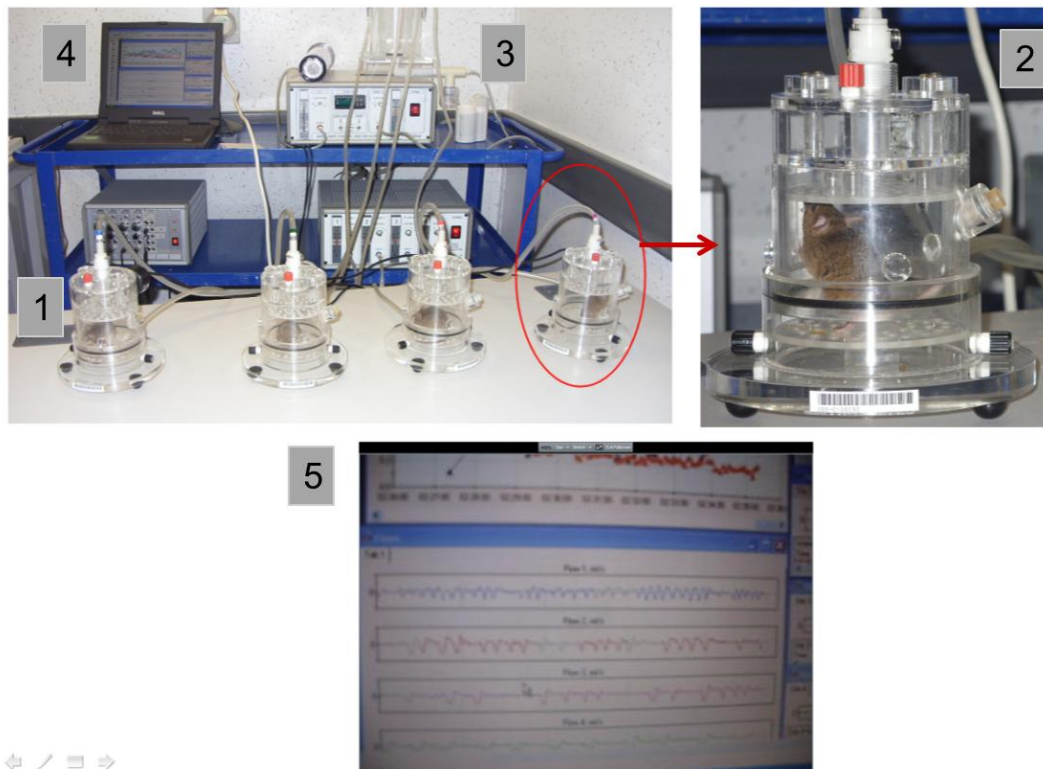


Figure 2-5 Whole body plethysmograph apparatus
 Images of the whole body plethysmograph used for assessment of the breathing phenotype. (1 and 2) plexiglass chambers. (3) Source for air supply. (4 and 5) changes in the chambers transmitted by pressure transducer to be analysed by (EMMS, Bordon, U.K.) software.

2.18 Statistical analysis

Differences between treatment groups were analysed using 2-way ANOVA, repeated measures ANOVA, one way ANOVA, Fisher's exact test, or Student's T-test where appropriate. $p < 0.05$ was used to define statistical significance.

Chapter 3

Generation of Lentivirus vector-based approach to deliver exogenous *Mecp2* *in vitro* and *in vivo*

3.1 Introduction

The characteristic neurological phenotype in RTT patients (Neul et al., 2010) and in *Mecp2* knockout mouse models (Chen et al., 2001) in addition to the rescue of RTT-like phenotypes in mouse models by delayed activation of endogenous *Mecp2* in the brain suggests that RTT can be potentially treated at the gene level by introducing a functional copy of *Mecp2* into the brain. Therefore the availability of functional copy of *Mecp2* and suitable viral vector that can transfer *Mecp2* into brain cells (neurons and glia) is important to test this approach.

Lentiviral vectors are useful tools for transgene delivery to the brain as it can transduce neurons with enduring gene expression (Trowbridge et al., 1980, Blomer et al., 1996). Lentiviral vectors contain only the *cis* elements required for nuclear targeting and integration to the host genome whereas all viral genes responsible for viral infection and assembly are supplied in *trans* by number of plasmids to generate replication incompetent virus.

Mecp2_e1 is the most abundant *Mecp2* isoform throughout the brain (Dragich et al., 2007) and is translated more efficiently *in vivo* compared to *Mecp2_e2* (Kriaucionis and Bird, 2004). Mutations in exon1 (only translated in *Mecp2_e1*) cause neurological manifestation and affect *Mecp2_e2* translation (Mnatzakanian et al., 2004, Saxena et al., 2006). A recent report showed that *Mecp2_e2* is more up regulated during neuron-induced toxicity and its forced overexpression enhanced apoptosis in healthy neurons, moreover knocking down *Mecp2_e2* achieved a neuron-protective effect (Dastidar et al., 2012). Therefore I decided to focus on using *Mecp2_e1* minigene in this study.

Fluorescent proteins (FPs) are widely used to study cell dynamics and as a marker for fusion proteins to help identify their cellular location, expression level and interactions. Red fluorescent proteins (*RFP*), used in conjunction with the well-established green fluorescent protein (*GFP*), broadens the spectrum of protein labelling and permits protein-protein interaction studies, however a wide range of FP variants has now been generated that covers nearly the entire visible spectrum (Rizzo et al., 2009). *RFP* has a maximum of fluorescence emission above 558 nm and absorption maximum at 583 nm (Wachter et al., 2010). *RFP* has been used, through recombinant DNA technology, to visualize many proteins *in vitro* (Park et al., 2007) and *in vivo* (Brolund et al., 2011) without reports of altered dynamic changes (e.g. misfolding or abnormal conformational changes). The *RFP* induced fluorescence allows rapid visualization and characterization of the fused protein in the real time and in fixed material without the need for immunolabelling reaction.

Several epitopes have been used for labelling recombinant proteins to reveal their cellular location, expression level and posttranslational alterations. Flag-tag was the first generated 8 amino acid polypeptide to be used for protein tagging. It helps protein localization and can be employed for immunocytochemistry and for western blot analysis. The FLAG tag is more hydrophilic than other common epitope tags and is therefore not likely to cause abnormal folding of the tagged proteins (Braun, 1995).

3.2 Study aims

The main aim of the work described in this chapter was to develop a lentiviral vector system with various promoters to enable delivery of tagged *Mecp2_e1* encoding sequences into the brain of *Mecp2* knockout mice. The specific objectives of this study are:

- I. To generate a fusion construct in which *Mecp2_e1* (*ME1*) minigene is tagged at the C-terminal with Flag-epitope and *RFP*. This construct should permit tracing exogenous *Mecp2* expression in real time and in fixed tissues.

- II. Cloning of *ME1FlagRFP* fusion construct into lentiviral vectors with various promoters including; the synapsin1 (*syn1*), neuron specific, or the phosphoglycerate kinase (PGK), ubiquitous, promoter.
- III. Generation of Lentivirus particles to enable exogenous *Mecp2_e1* delivery into *Mecp2* deficient cells *in vitro* and *in vivo*.

3.3 Generation of lenti-syn1/PGK-*ME1FlagRFP* vectors

3.3.1 Creation of *ME1FlagRFP* fusion construct

pCDNA3.1 Zeo(+) *RFP* (pCDNARFP) is a mammalian expression vector (5.678 kb) that contains the red fluorescence protein (*RFP*) gene (678 bp) cloned between *BamH1* and *EcoR1* restriction sites under the control of CMV promoter (figure 3-1). Analysis of the multiple cloning sites of this vector showed the presence of *Nhe1* restriction site upstream to the RFP encoding sequences. On the same time, mapping the restriction sites in *ME1Flag* sequences showed that *Nhe1* and *bamh1* sequences are not present in this construct. Therefore *Nhe1* and *EcoR1* are suitable restriction enzymes to create sticky ends of both *ME1Flag* and pCDNARFP vector for future cloning.

To create *ME1 with C-terminal FlagRFP* (figure 3-1), a polymerase chain reaction (PCR) was used to amplify *ME1* (1.5 kb) minigene from pRSV40- *ME1* vector using Forward primer (Fpr), 5` TTT GCTAGC ATG GCC GCC GCT GCC 3`, that contains an *Nhe1* restriction site (underlined) and reverse primer (Rpr), 5` AAA GGA TCC GC CTT GTC ATC GTC GTC CTT GTA GTC GCT AAC TCT CTC GGT` 3, that contains *Flag-tag* coding sequences (double underline) and *BamH1* restriction site (single underline). Two base pairs (grey colour) were added to this primer to keep the downstream RFP on frame. This primer also precludes the *ME1* stop codon to allow read-through the downstream flag-tag and RFP encoding sequences (figure 3-1). Gel electrophoresis of the PCR product resulted from this reaction showed a band size of approximately 1.5 kb which is corresponding to the expected *ME1* band-size (figure 3-2).

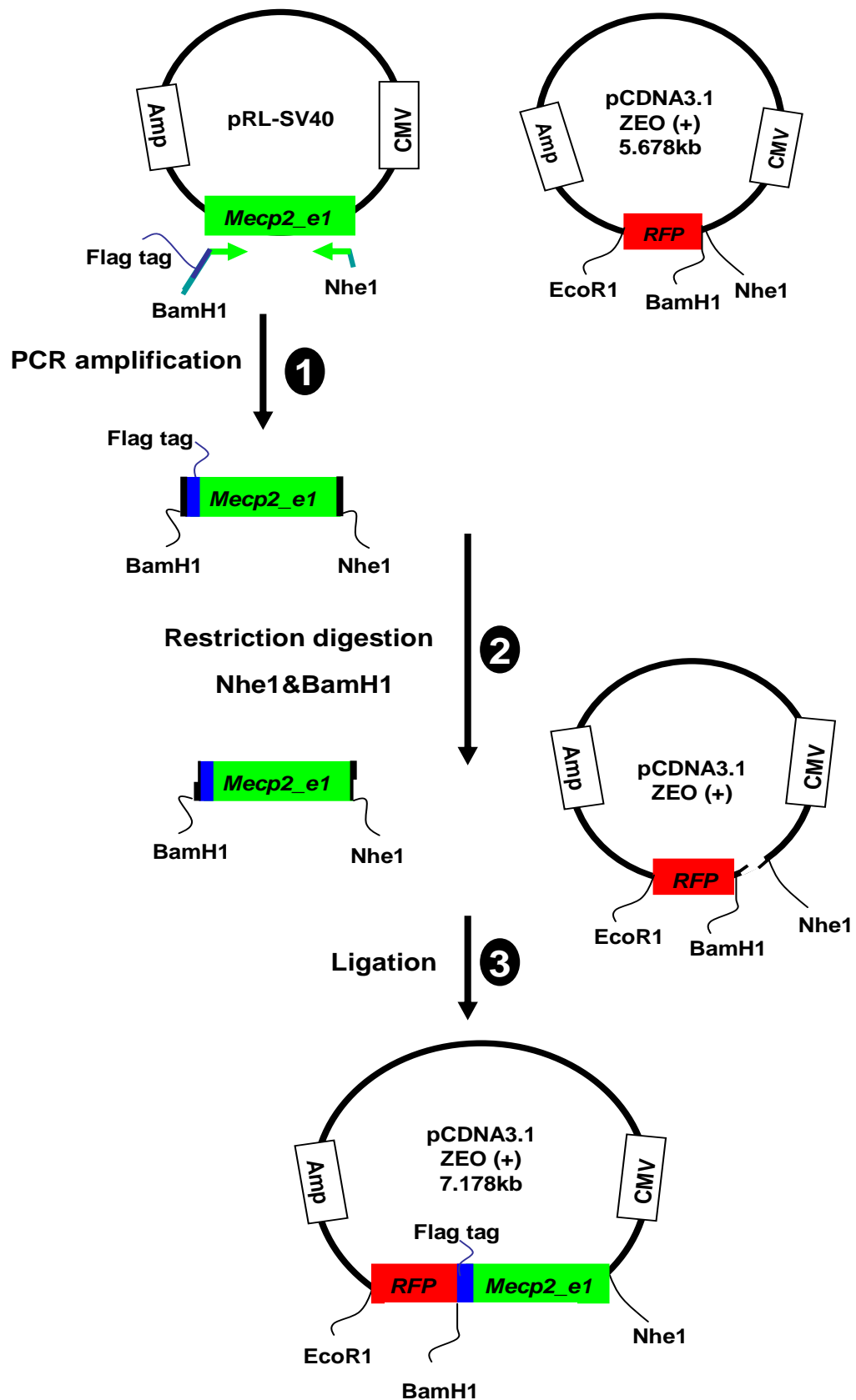


Figure 3-1 Cloning strategy of *ME1FlagRFP* fusion construct
 Simplified cartoon showing the cloning steps of *Mecp2* encoding sequences into pCDNARFP vector (1) *ME1* minigene with C-terminal Flag-tag coding sequences (*ME1Flag*) was amplified by PCR. (2) *ME1Flag* construct and pCDNARFP vector were cut by *EcoR1* and *BamH1* restriction enzymes. (3) Ligation reaction was performed to insert *ME1Flag* fusion construct at the N-terminal end of the *RFP* to generate pCDNAME1FlagRFP plasmid. Amp; Ampicillin resistance gene, CMV; Cytomegalovirus promoter.

In order to clone the *ME1Flag* fusion construct to the N-terminal end of the *RFP*, both the PCR product and the pCDN*RFP* vector were cut by *Nhe1* and *BamH1* restriction enzymes to create compatible sticky ends. The PCR product was then cleaned to remove residual primers and buffers using PCR cleaning kits (Qiagen). The pCDN*RFP* vector was cut from the gel and purified using gel extraction kits (Qiagen). Both doubly cut insert and vector (molar ratio of 3:1 respectively) were ligated together using T4 DNA ligase enzyme.

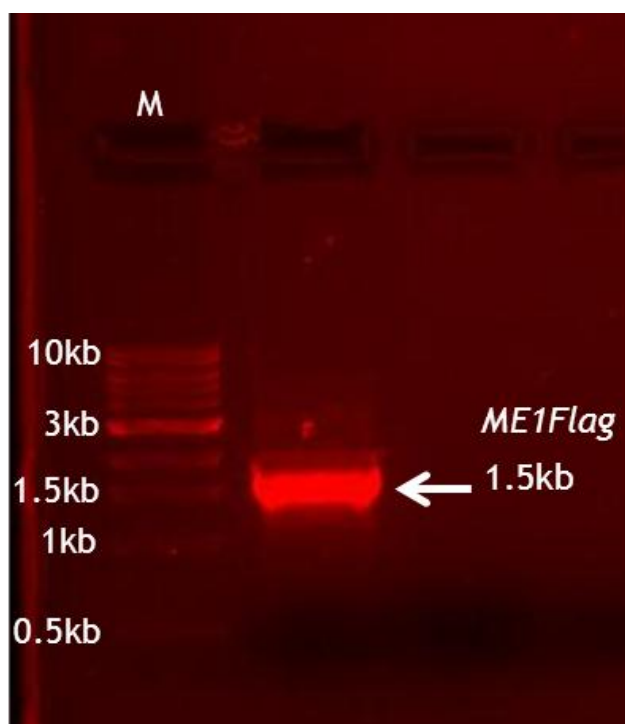


Figure 3-2 PCR amplification of *ME1Flag* fusion construct. Gel image showing the resulting PCR product after amplification of *ME1Flag* fusion construct. The PCR product size is 1.5 kb which is equivalent to the size of *ME1Flag* coding sequence. M; 1 KB DNA ladder.

3.3.2 Validation of the pCDN*ME1FlagRFP* construct

The ligation reaction was transformed and plated onto ampicillin plates (50 µg/ml, see chapter 2). The Plasmid DNA preparation was then carried out for all resulting colonies (N = 9). In order to identify plasmids that contain the new construct (*ME1Flag*), 0.1-1ng of each plasmid was used as a template for a PCR reaction using the same Fpr and Rpr primers that were used to amplify *ME1Flag* sequences. A parallel PCR reaction using the pRSV-40*ME1* plasmid as a template was carried out (positive control). Six of the plasmids generated PCR products of 1.5 kb band size; this was comparable to the positive control band size,

suggesting that *ME1Flag* encoding sequences were successfully cloned into pCDNARFP vector (figure3-3).

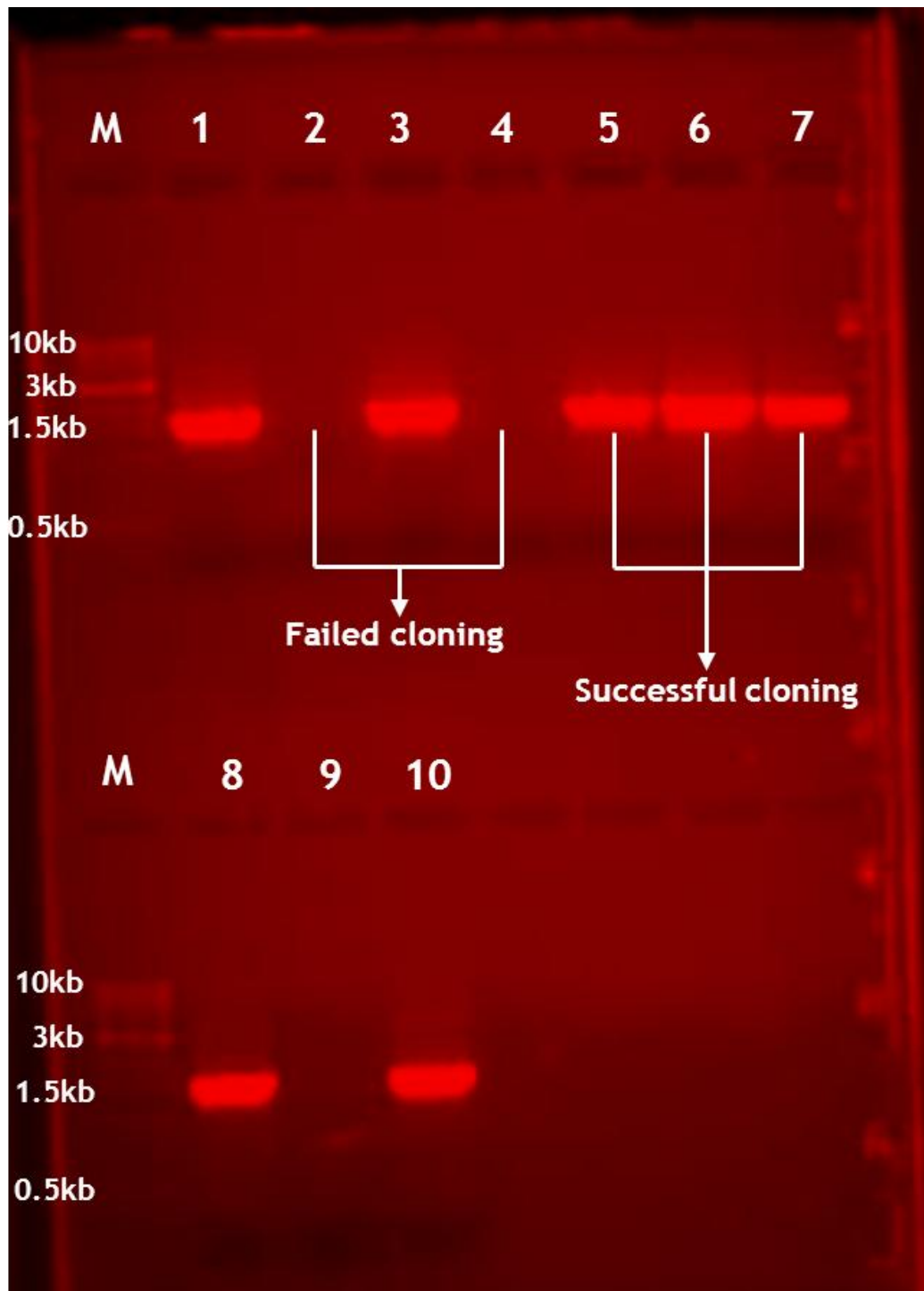


Figure 3-3 PCR verification of pCDNARFP vectors for successful cloning of *ME1Flag* fusion construct.

Gel image showing PCR amplification of *ME1* minigene from plasmid DNA preparations obtained after the transformation with the ligation mix of *ME1Flag* and pCDNARFP vector. Lane 1 shows the positive control reaction with band size of 1.5kb (*ME1* minigene). Lanes 2, 4 and 9 show no PCR band suggesting failed cloning process. Lanes 3, 5-8 and 10 show PCR bands (1.5kb) that are equal to the *ME1* minigene band size and similar to the positive control band, indicating successful cloning of *ME1Flag* fusion construct into pCDNARFP vector. M; 1 kb DNA ladder.

To further confirm the structure of the new pCDNARFP vector after successful cloning of *ME1*Flag fusion construct (henceforth referred to as pCDNAME1FlagRFP) 1 µg of this plasmid was examined by restriction digest using restriction enzymes (*Nhe1*, *BamH1* and *EcoR1*) that flank the fusion construct (figure3-4A). *BamH1* and *EcoR1* double restriction digest gave rise to two bands, sized 0.6 and 6.5 kb (figure3-4B), which are corresponding to the size of the RFP gene and pCDNAME1Flag vector respectively. *Nhe1* and *BamH1* double restriction digest resulted in two bands sized 1.5 and 5.6 kb, which are equivalent to the *ME1* gene and to pCDNARFP vector respectively. Finally, *Nhe1* and *EcoR1* double restriction digest produced two bands, sized 2.1 and 5.0 kb which are equal to the size of the *MR1*FlagRFP and pCDNA vector respectively. These results, together with the previous PCR data indicate the successful generation of a new vector construct (figure 3-5) that contains the *ME1* minigene with a C-terminal flag-tag and *RFP* under the control of the CMV promoter in the pCDNA vector. The new plasmid pCDNAME1FlagRFP was also sequenced used primers that anneal to specific sequences on the vector backbone and flank *ME1*FlagRFP fusion construct confirmed the presence of *ME1*FlagRFP construct with 100% sequence identity to that of *ME1* (GenBank accession No. NM_001081979.1) and *RFP* (GenBank accession No. EF212309.1) sequences.

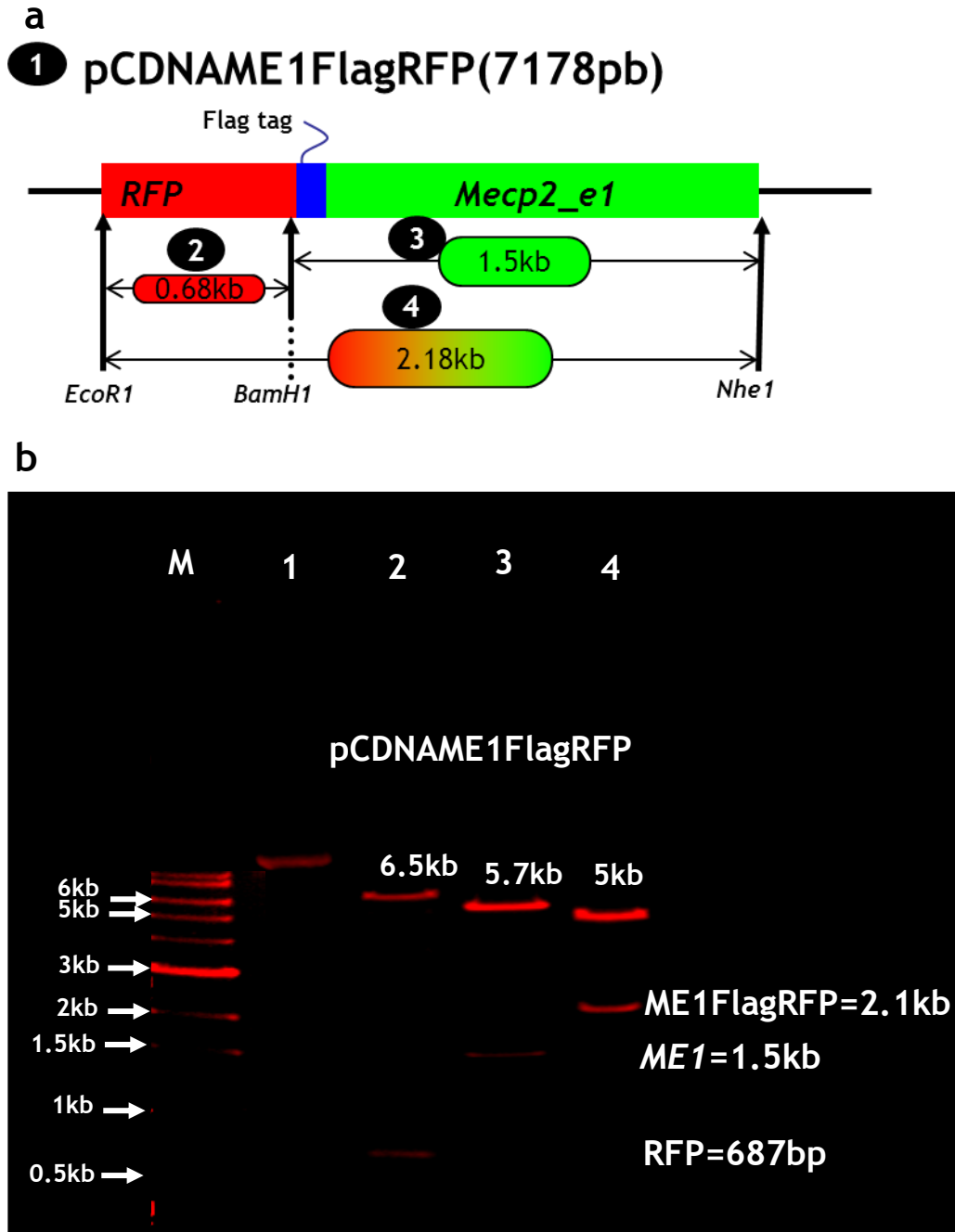


Figure 3-4 Restriction digest validation of pCDNAME1FlagRFP.
(A) Diagram showing the expected band-sizes after restriction digestion of pCDNAME1FlagRFP with *Nhe1*, *EcoR1* and *BamH1*. **(B)** Gel image showing the bands size after restriction digest (RD). Lane 1 shows undigested vector. Lane 2 shows RD with *BamH1* and *EcoR1* that gives 2 bands sized 6.5 and 0.687 kb which represents the pCDNAME1Flag vector and the *RFP* gene respectively. Lane 3 shows RD with *Nhe1* and *BamH1* that produced bands sized 5.7 and 1.5 kb representing pCDNARFP vector and *ME1Flag* fusion construct respectively. Lane 4 shows RD with *Nhe1* and *EcoR1* that resulted in generation of bands sized 5 and 2.1 kb corresponding to pCDNA vector and *ME1FlagRFP* fusion construct respectively. M; 1 kb DNA ladder.

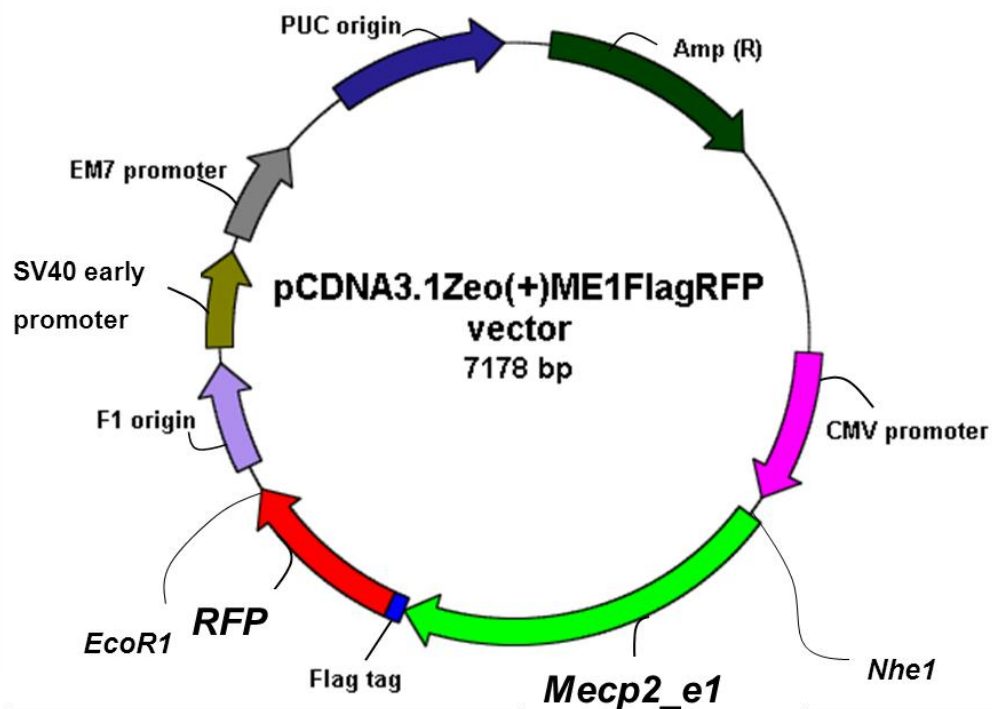


Figure 3-5 pCDNA(+)/Zeo/ME1FlagRFP vector map.

A simplified plasmid map of the pCDNAME1FlagRFP vector showing the C-terminal flag-tagged ME1 minigene that was incorporated in frame with the N-terminal end of the RFP gene between Nhe1 and BamH1 restriction sites. This fusion construct is under the control of CMV (ubiquitous) promoter. Amp, ampicillin resistance gene, expressed under EM7 and SV40 promoters. F1 and PUC are the origins of replication in E-Coli.

3.3.3 Cloning of ME1FlagRFP fusion construct into Lentivirus vector backbone

To enable *Mecp2* delivery into *Mecp2* deficient cells, I decided to clone ME1FlagRFP fusion construct into lentiviral backbone which is known to produce high transduction efficiency *in vitro* and *in vivo*. Two lentiviral vectors were used in this study; one contains the synapsin1 promoter (neuron-specific) and the second one contains the PGK (ubiquitous) promoter. Restriction mapping of the lentiviral vectors showed the presence of two unique restriction sites; *Nhe1* and *EcoR1* flanking the EGFP encoding sequences (figure 3-6). The same restriction sites are also flanking the ME1FlagRFP fusion construct in the pCDNAME1FlagRFP vector. Therefore to clone ME1FlagRFP fusion construct into lentiviral vectors, both pCDNAME1FlagRFP and lentiviral vectors were restriction digested with *Nhe1* and *EcoR1* restriction enzymes to generate compatible sticky ends. Lentiviral vectors and ME1FlagRFP bands were cut from the gel and gel extracted using gel extraction kits and ligated together using T4 DNA ligase.

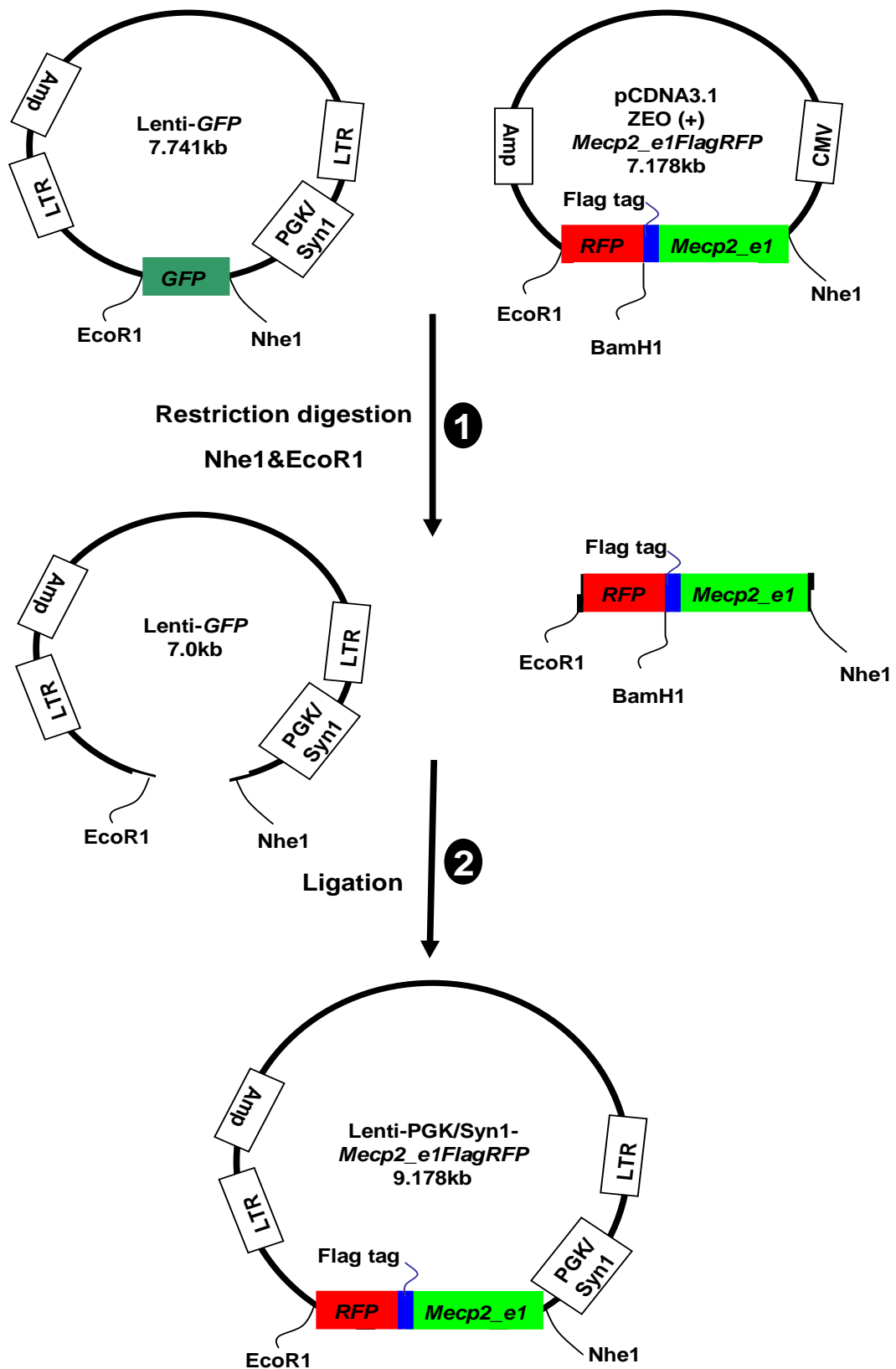


Figure 3-6 Cloning strategy for *ME1FlagRFP* fusion construct insertion into lentiviral vector backbones.

ME1FlagRFP fusion construct was cloned using *EcoR1* and *Nhe1* restriction enzymes. EGFP gene was cloned into lentiviral vectors using the same restriction enzymes. (1) Compatible sticky ends were generated in lentiviral vectors and *ME1FlagRFP* fusion construct by double RD with *Nhe1* and *EcoR1*. (2) DNA gel extraction was followed by ligation of the linearized lentiviral vectors and *ME1FlagRFP* construct to create new plenti-PGK/Syn1-*ME1FlagRFP* vectors.

3.3.4 Confirmation of lenti-PGK/syn1-*ME1FlagRFP* constructs

To verify the cloning of the *ME1FlagRFP* fusion construct into the lentiviral vectors, all the bacterial colonies grown on the transformation plates were sub cultured and the plasmid DNA was extracted. PCR reactions using primers specific for *ME1Flag* sequences were used to confirm the presence of *ME1Flag* sequences in the lentiviral vectors. Analysis of the electrophoresis gel showed PCR product size of 1.5kb (figure 3-7) which are equivalent to the size of *ME1Flag* sequences, suggesting that *ME1FlagRFP* sequences are successfully cloned into both lenti-PGK and Lenti-syn1 vectors (these constructs hereafter referred to as plenti-PGK-*ME1flagRFP* and plenti-syn1-*ME1FlagRFP*).

For additional confirmation of successful *ME1FlagRFP* insertion into the lentiviral vectors, both plenti-PGK-*ME1FlagRFP* and plenti-syn1-*ME1FlagRFP* were restriction digested with *Nhe1* and *EcoR1* restriction enzymes (figure 3-8A). Both vectors showed two bands; one is equal to ~ 2.2kb (figure 3-8B) which is equivalent to the *ME1FlagRFP* band size and the other band is 7.0 kb which is equal to lentiviral vector backbones. Final validation of the plenti-PGK/syn1-*ME1FlagRFP* Vector constructs (figure 3-9) was carried out by plasmid DNA sequencing (figure 3-10). Alignment of the fusion construct sequence and mouse *Mecp2_e1* (Gen Bank accession No. NM_011081979.1) and *RFP* (Gen Bank accession No. EF212309.1) nucleotide sequences revealed complete identity between the sequences

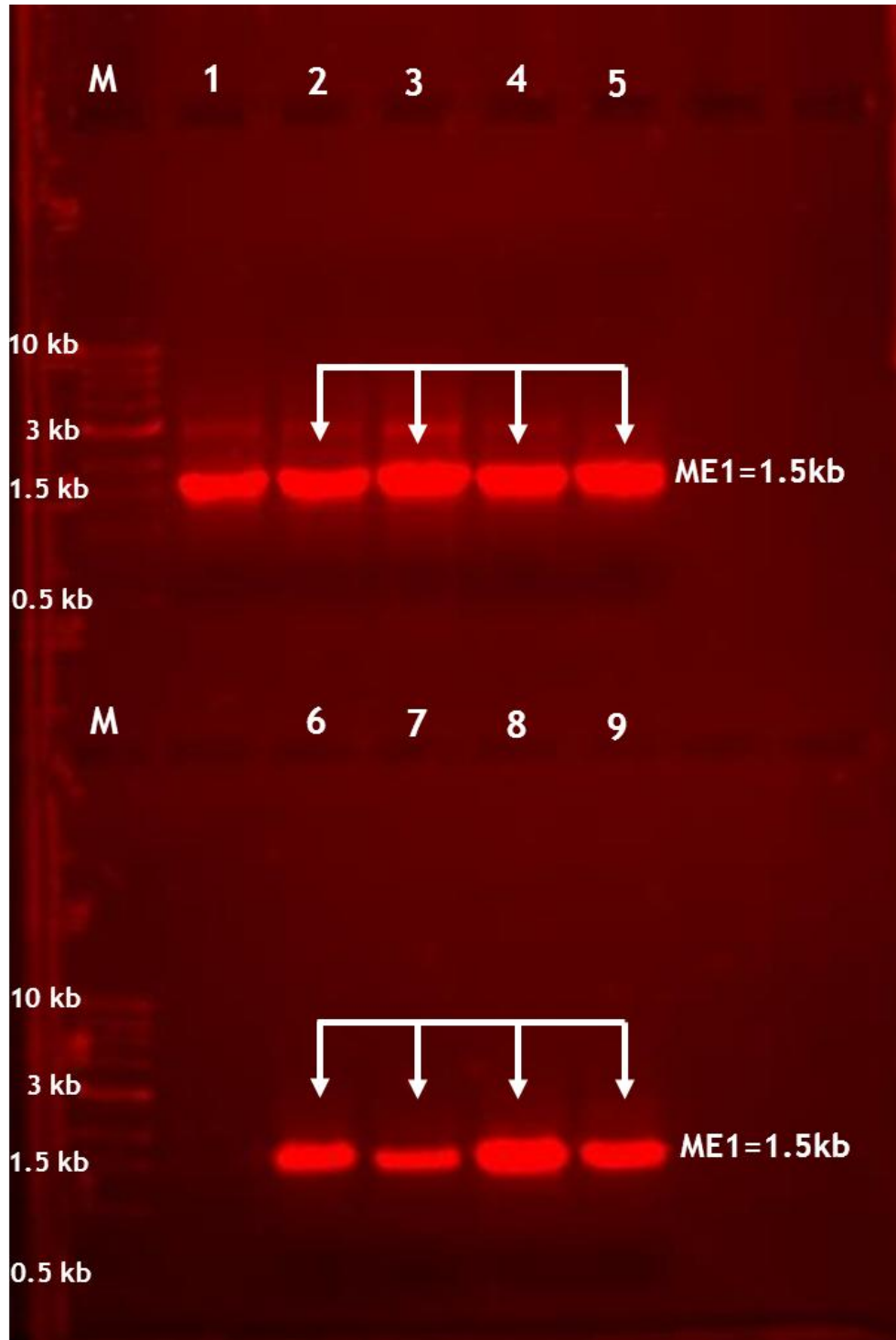


Figure 3-7 PCR validation of lenti-PGK-*ME1*FlagRFP

Gel image shows PCR amplification of *ME1* minigene to validate the creation of the plenti-*ME1*FlagRFP constructs. Lane 1 shows the positive control. Lane 2-5 show reactions based on the proposed plenti-PGK-*ME1*FlagRFP plasmids, presence of *ME1* equivalent bands size indicates successful cloning. Lane 6-9 show PCR reactions based on the proposed plenti-Syn1-*ME1*FlagRFP plasmid templates, presence of bands size equal to *ME1* band (1.5kb) denotes positive cloning. M; 1 kb ladder.

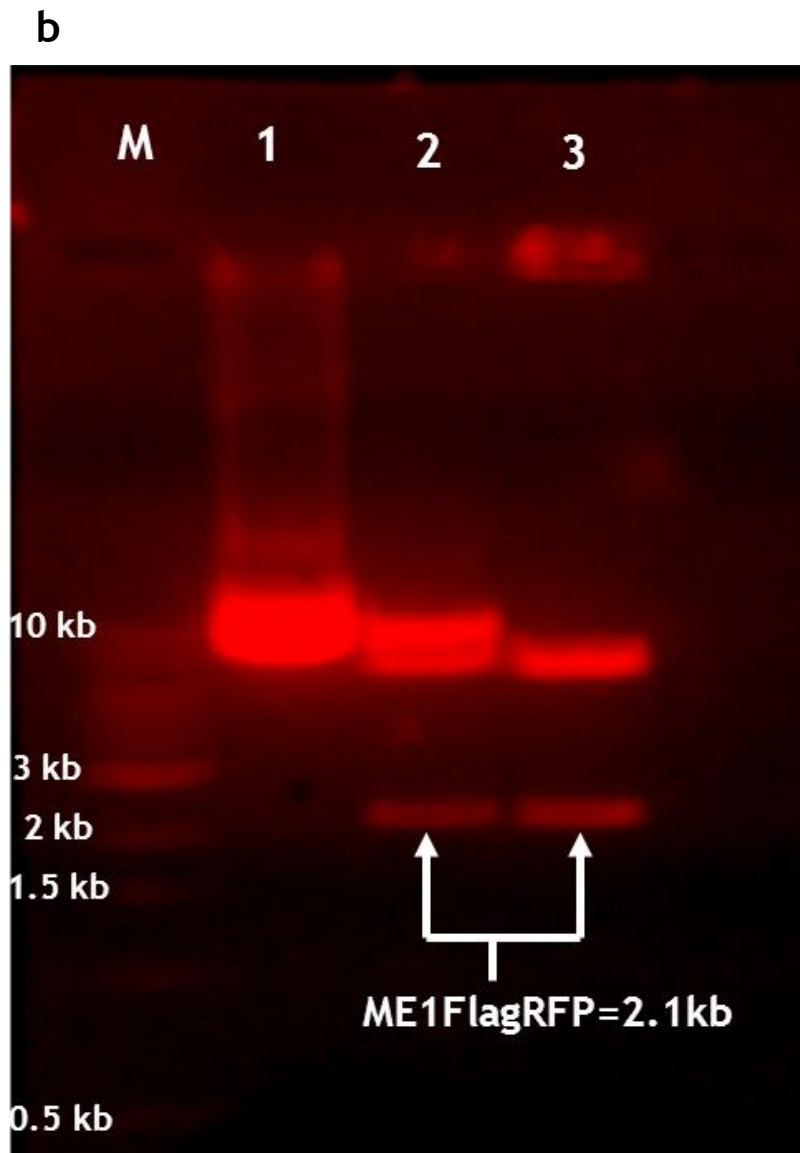
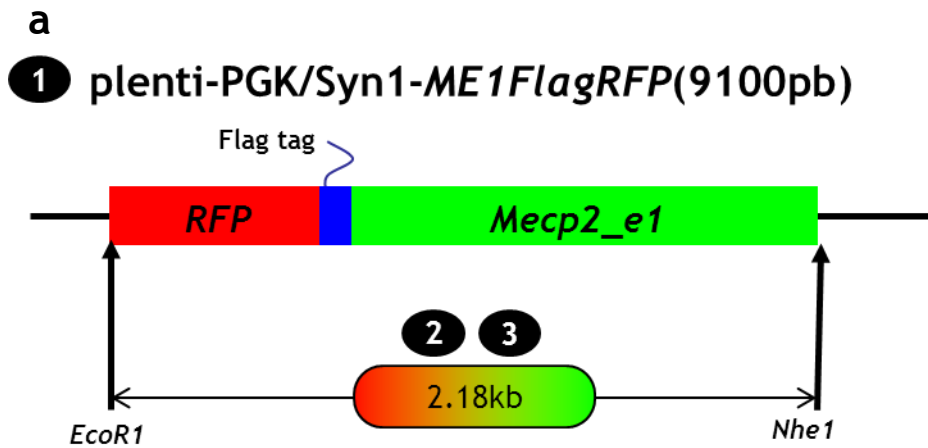


Figure 3-8 Restriction digest confirmation of plenti-PGK/syn1-*ME1FlagRFP*.
 (a) Diagram showing the expected band sizes after restriction digest of lentiviral vectors. (b) Gel image showing restriction digest of lenti-vectors by *Nhe1* and *EcoR1* enzymes. Lane 1 shows the undigested vector plenti-PGK-*ME1FlagRFP*. Lane 2 shows restriction digest of plenti-PGK-*ME1FlagRFP* that show; one band at 2.1 kb (*ME1FlagRFP*) and another band at 7kb that represents plenti-PGK vector. The extra band at 7 kb could possibly be an open circular uncut vector. Lane 3 shows restriction digest of plenti-syn1-*ME1FlagRFP* that shows 2 bands; one at 2.1kb that represents *ME1FlagRFP* and the other at 7kb that represents plenti-syn1 vector. M; 1 kb DNA ladder.

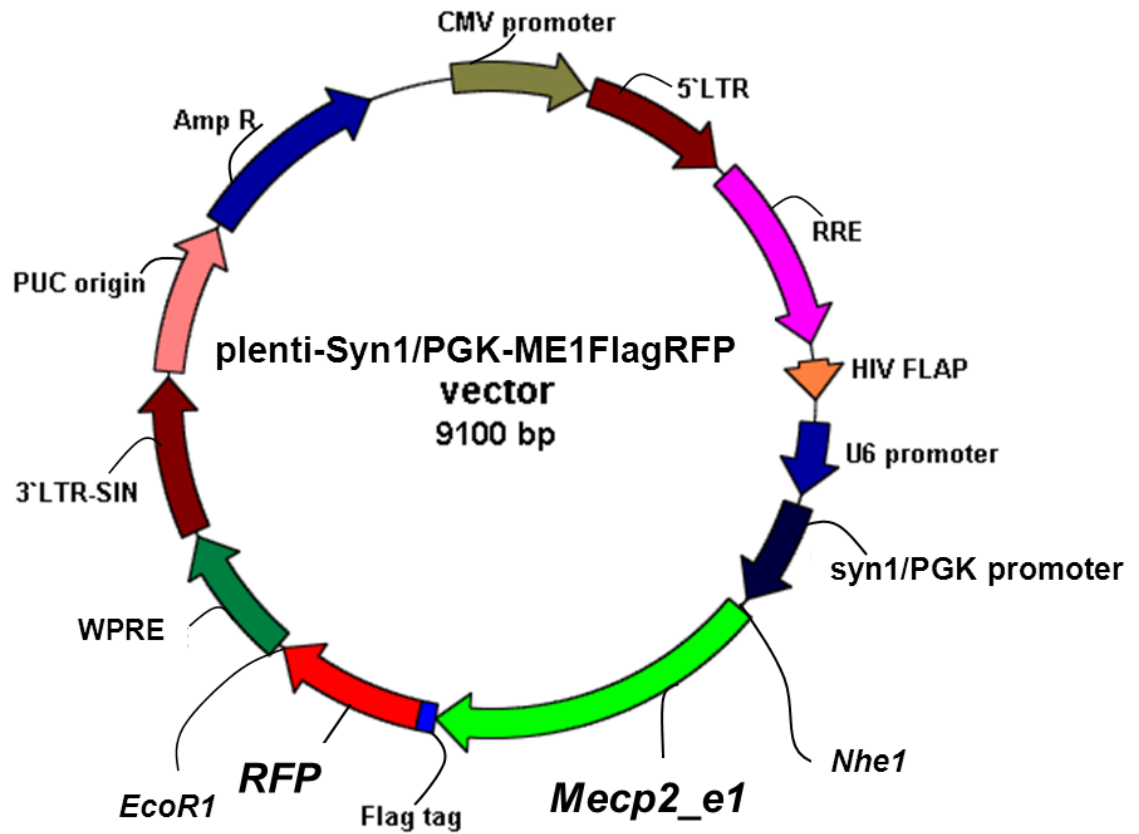


Figure 3-9 plenti-PGK/syn1-ME1FlagRFP vector map.

Plasmid map showing the main components of Lentivirus based-vectors. *ME1* with a C-terminal FlagRFP fusion was inserted downstream to either the PGK (ubiquitous) or the synapsin1 (neuron specific) promoter. Both the transgene and the promoter are incorporated between both LTRs (essential for integration into the host genome).

```

plenti-ME1FlagRFP      CCGGGGCTAGCATGCGCCCGCTGCCGCCACCGCCCGCCCGCCCGCCGAGCGGAG 180
Mecp2                  -----ATGCGCCCGCTGCCGCCACCGCCCGCCCGCCCGCCGAGCGGAG 49
                        *****
plenti-ME1FlagRFP      GAGGAGGAGGAGGCGAGGAGGAGACTGGAGGAAAAGTCAGAAGACCAGGATCTCCAGG 240
Mecp2                  GAGGAGGAGGAGGCGAGGAGGAGACTGGAGGAAAAGTCAGAAGACCAGGATCTCCAGG 109
                        *****
plenti-ME1FlagRFP      GCCTCAGAGACAAGCCACTGAAGTTTAAAGAAGCGAAGAAAAGACAAGAAGGAGGACAAAG 300
Mecp2                  GCCTCAGAGACAAGCCACTGAAGTTTAAAGAAGCGAAGAAAAGACAAGAAGGAGGACAAAG 169
                        *****
plenti-ME1FlagRFP      AAGGCAAGCATGAGCCACTACAACCTTCAGCCACCATTCTGCAGAGCCAGCAGAGGCGAG 360
Mecp2                  AAGGCAAGCATGAGCCACTACAACCTTCAGCCACCATTCTGCAGAGCCAGCAGAGGCGAG 229
                        *****
plenti-ME1FlagRFP      GCAAAGCAGAAACATCAGAAAGCTCAGGCTCTGCCCCAGCAGTGCCAGAAGCCTCGGCTT 420
Mecp2                  GCAAAGCAGAAACATCAGAAAGCTCAGGCTCTGCCCCAGCAGTGCCAGAAGCCTCGGCTT 289
                        *****
plenti-ME1FlagRFP      CCCCCAAACAGCGCGCTCCATTATCCGTGACCGGGGACCTATGTATGATGACCCACCT 480
Mecp2                  CCCCCAAACAGCGCGCTCCATTATCCGTGACCGGGGACCTATGTATGATGACCCACCT 349
                        *****
plenti-ME1FlagRFP      TGCCTGAAGGTTGGACACGAAAGCTTAAACAAGGAAGTCTGGCCGATCTGCTGGAAGT 540
Mecp2                  TGCCTGAAGGTTGGACACGAAAGCTTAAACAAGGAAGTCTGGCCGATCTGCTGGAAGT 409
                        *****
plenti-ME1FlagRFP      ATGATGTATATTTGATCAATCCCAGGGAAAAGCTTTTCGCTCTAAAGTAGAATTGATG 600
Mecp2                  ATGATGTATATTTGATCAATCCCAGGGAAAAGCTTTTCGCTCTAAAGTAGAATTGATG 469
                        *****
plenti-ME1FlagRFP      CATACTTTGAAAAGGTGGGAGACACCTCCTTGACCCTAATGATTTTGACTTCACGGTAA 660
Mecp2                  CATACTTTGAAAAGGTGGGAGACACCTCCTTGACCCTAATGATTTTGACTTCACGGTAA 529
                        *****
plenti-ME1FlagRFP      CTGGGAGAGGAGCCCTCCAGGAGAGAGCAGAAACCACCTAAGAAGCCAAATCTCCCA 720
Mecp2                  CTGGGAGAGGAGCCCTCCAGGAGAGAGCAGAAACCACCTAAGAAGCCAAATCTCCCA 589
                        *****
plenti-ME1FlagRFP      AAGCTCCAGGAAGTGGCAGGGGTGCGGGACGCCCAAGGGAGCGGCACTGGGAGACCAA 780
Mecp2                  AAGCTCCAGGAAGTGGCAGGGGTGCGGGACGCCCAAGGGAGCGGCACTGGGAGACCAA 649
                        *****
plenti-ME1FlagRFP      AGGCAGCAGCATCAGAAGGTGTTTCAGGTGAAAAGGGTCTGGAGAAGAGCCCTGGGAAAC 840
Mecp2                  AGGCAGCAGCATCAGAAGGTGTTTCAGGTGAAAAGGGTCTGGAGAAGAGCCCTGGGAAAC 709
                        *****
plenti-ME1FlagRFP      TTGTTGTCAAGATGCCTTTCCAAGCATCGCCTGGGGTAAGGGTGAGGAGGTGGGGCTA 900
Mecp2                  TTGTTGTCAAGATGCCTTTCCAAGCATCGCCTGGGGTAAGGGTGAGGAGGTGGGGCTA 769
                        *****
plenti-ME1FlagRFP      CCACATCTGCCAGGTCATGGTGATCAAACGCCCTGGCAGAAAAGCGAAAAGCTGAAGCTG 960
Mecp2                  CCACATCTGCCAGGTCATGGTGATCAAACGCCCTGGCAGAAAAGCGAAAAGCTGAAGCTG 829
                        *****
plenti-ME1FlagRFP      ACCCCAGGCCATTCCTAAGAAGCGGGTAGAAAGCCTGGGAGTGTGGTGGCAGCTGCTG 1020
Mecp2                  ACCCCAGGCCATTCCTAAGAAGCGGGTAGAAAGCCTGGGAGTGTGGTGGCAGCTGCTG 889
                        *****
plenti-ME1FlagRFP      CAGCTGAGGCCAAAAGAAAGCCGTGAAGGAGTCTTCCATACGGTCTGTGCATGAGACTG 1080
Mecp2                  CAGCTGAGGCCAAAAGAAAGCCGTGAAGGAGTCTTCCATACGGTCTGTGCATGAGACTG 949
                        *****
plenti-ME1FlagRFP      TGCTCCCCATCAAGAAGCGCAAGACCCGGGAGACGGTCAGCATCGAGGTCAAGGAAGTGG 1140
Mecp2                  TGCTCCCCATCAAGAAGCGCAAGACCCGGGAGACGGTCAGCATCGAGGTCAAGGAAGTGG 1009
                        *****
plenti-ME1FlagRFP      TGAAGCCCCTGCTGGTGTCCACCCTTGGTGAGAAAAGCGGGAAGGGACTGAAGACCTGCA 1200
Mecp2                  TGAAGCCCCTGCTGGTGTCCACCCTTGGTGAGAAAAGCGGGAAGGGACTGAAGACCTGCA 1069
                        *****
plenti-ME1FlagRFP      AGAGCCCTGGGCGTAAAAGCAAGGAGAGCAGCCCAAGGGGCGCAGCAGCAGTGCCTCCT 1260
Mecp2                  AGAGCCCTGGGCGTAAAAGCAAGGAGAGCAGCCCAAGGGGCGCAGCAGCAGTGCCTCCT 1129
                        *****
plenti-ME1FlagRFP      CCCCACCTAAGAAGGAGCACCATCATCACCACCATCACTCAGAGTCCACAAAGGCCCCCA 1320
Mecp2                  CCCCACCTAAGAAGGAGCACCATCATCACCACCATCACTCAGAGTCCACAAAGGCCCCCA 1189
                        *****
plenti-ME1FlagRFP      TGCCACTGCTCCCATCCCCACCCACCTGAGCCTGAGAGCTCTGAGGACCCATCAGCC 1380
Mecp2                  TGCCACTGCTCCCATCCCCACCCACCTGAGCCTGAGAGCTCTGAGGACCCATCAGCC 1249
                        *****
plenti-ME1FlagRFP      CCCCTGAGCCTCAGGACTTGAGCAGCAGCATCTGCAAAGAAGAGAAGATGCCCCGAGGAG 1440
Mecp2                  CCCCTGAGCCTCAGGACTTGAGCAGCAGCATCTGCAAAGAAGAGAAGATGCCCCGAGGAG 1309
                        *****
plenti-ME1FlagRFP      GCTCACTGGAAGCGATGGCTGCCCAAGGAGCCAGCTAAGACTCAGCCTATGGTCGCCA 1500
Mecp2                  GCTCACTGGAAGCGATGGCTGCCCAAGGAGCCAGCTAAGACTCAGCCTATGGTCGCCA 1369
                        *****
plenti-ME1FlagRFP      CCACTACCACAGTTGCAGAAAAGTACAAACACCGAGGGGAGGAGAGCGCAAAGACATTTG 1560
Mecp2                  CCACTACCACAGTTGCAGAAAAGTACAAACACCGAGGGGAGGAGAGCGCAAAGACATTTG 1429
                        *****
plenti-ME1FlagRFP      TTTTCATCTCCATGCCAAGGCCAAACAGAGAGGAGCCTGTGGACAGCCGACGCCGTGA 1620
Mecp2                  TTTTCATCTCCATGCCAAGGCCAAACAGAGAGGAGCCTGTGGACAGCCGACGCCGTGA 1489
                        *****
plenti-ME1FlagRFP      CCGAGAGAGTTAGC--- 1634
Mecp2                  CCGAGAGAGTTAGCTGA 1506
                        *****

```

```

plenti-ME1FlagRFP      GACTACAAGGACGACGATGACAAGGCGGATCCGATGGCCTCCTCCGAGGACGTCATCAAG 60
RFP                    -----ATGGCCTCCTCCGAGGACGTCATCAAG 27
                        *****
plenti-ME1FlagRFP      GAGTTCATGCGCTTCAAGGTGCGCATGGAGGGCTCCGTGAACGGCCACGAGTTCGAGATC 120
RFP                    GAGTTCATGCGCTTCAAGGTGCGCATGGAGGGCTCCGTGAACGGCCACGAGTTCGAGATC 87
                        *****
plenti-ME1FlagRFP      GAGGGCGAGGGCGAGGGCCGCCCTACGAGGGCACCCAGACCCCAAGCTGAAGGTGACC 180
RFP                    GAGGGCGAGGGCGAGGGCCGCCCTACGAGGGCACCCAGACCCCAAGCTGAAGGTGACC 147
                        *****
plenti-ME1FlagRFP      AAGGGCGGCCCTGCGCTTCGCTGGGACATCCTGTCCCCTCAGTTCAGTACGGCTCC 240
RFP                    AAGGGCGGCCCTGCGCTTCGCTGGGACATCCTGTCCCCTCAGTTCAGTACGGCTCC 207
                        *****
plenti-ME1FlagRFP      AAGGCCTACGTGAAGCACCCCGCGACATCCCCGACTACTTGAAGCTGTCCTTCCCCGAG 300
RFP                    AAGGCCTACGTGAAGCACCCCGCGACATCCCCGACTACTTGAAGCTGTCCTTCCCCGAG 267
                        *****
plenti-ME1FlagRFP      GGCTTCAAGTGGGAGCGCGTGAAGTTCGAGGACGGCGCGTGGTGACCGTGACCCAG 360
RFP                    GGCTTCAAGTGGGAGCGCGTGAAGTTCGAGGACGGCGCGTGGTGACCGTGACCCAG 327
                        *****
plenti-ME1FlagRFP      GACTCCTCCCTGCAGGACGGCGAGTTCATCTACAAGGTGAAGCTGCGCGGCACCAACTTC 420
RFP                    GACTCCTCCCTGCAGGACGGCGAGTTCATCTACAAGGTGAAGCTGCGCGGCACCAACTTC 387
                        *****
plenti-ME1FlagRFP      CCCTCCGACGGCCCGTAATGCAGAAGAAGACCATGGGCTGGGAGGCTCCACCGAGCGG 480
RFP                    CCCTCCGACGGCCCGTAATGCAGAAGAAGACCATGGGCTGGGAGGCTCCACCGAGCGG 447
                        *****
plenti-ME1FlagRFP      ATGTACCCCGAGGACGGCGCCCTGAAGGGCGAGATCAAGATGAGGCTGAAGCTGAAGGAC 540
RFP                    ATGTACCCCGAGGACGGCGCCCTGAAGGGCGAGATCAAGATGAGGCTGAAGCTGAAGGAC 507
                        *****
plenti-ME1FlagRFP      GGCGGCCACTACGACGCCGAGGTCAAGACCACCTACATGGCCAAGAAGCCCGTGCAGCTG 600
RFP                    GGCGGCCACTACGACGCCGAGGTCAAGACCACCTACATGGCCAAGAAGCCCGTGCAGCTG 567
                        *****
plenti-ME1FlagRFP      CCCGGCGCCTACAAGACCGACATCAAGCTGGACATCACCTCCCACAACGAGGACTACACC 660
RFP                    CCCGGCGCCTACAAGACCGACATCAAGCTGGACATCACCTCCCACAACGAGGACTACACC 627
                        *****
plenti-ME1FlagRFP      ATCGTGAACAGTACGAGCGCGCCGAGGGCCGCCACTCCACCGCGCCTAAGAATTCSTC 720
RFP                    ATCGTGAACAGTACGAGCGCGCCGAGGGCCGCCACTCCACCGCGCCTAA----- 678
                        *****

```

Figure 3-10 Sequence alignment of *ME1FlagRFP* to the mouse *Mecp2_e1* and *RFP* encoding sequences.

ME1 sequence was compared to mouse *Mecp2_e1* sequence (NM_001081979.1, yellow colour). Whereas the cloned *RFP* gene sequence was compared to *RFP* sequences (EF212309.1, red colour). Flag sequence was confirmed upstream to the *RFP* gene (green colour). Two nucleotide bases (blue colour) were included to keep *RFP* in frame. Restriction endonuclease sites that were used for generating the fusion construct are underlined (*Nhe1*, *BamH1* and *EcoR1* respectively). The *Mecp2* start codon (purple colour) is used to start translation whereas the stop codon (grey colour) of the *RFP* is used to stop translation. * indicates identical nucleotide

3.3.5 Delivery of exogenous *Mecp2* into hippocampal cell culture using Ca^{2+} phosphate transfection method.

To test the ability of plenti-*ME1FlagRFP* plasmids to express exogenous *Mecp2* *in vitro*, dissociated rat hippocampal cell culture was transfected with either plenti-PGK-*ME1FlagRFP* or plenti-syn1-*ME1FlagRFP* plasmids using Ca^{2+} phosphate transfection method (chapter 2). *Mecp2FlagRFP* expression was investigated 17 hours post-transfection. Live image analysis showed that the *RFP* fluorescence was localized to the nuclei of cultured cells (figure 3-11). To further confirm the nuclear localization of the transgene, cultured neuronal cells were fixed with 4% PFA and stained with DAPI. *RFP* fluorescence (indicator of exogenous *Mecp2*) was co-localized with DAPI-stained nuclei indicating nuclear targeting. These results confirmed that both lentiviral vectors are able to express exogenous *Mecp2* and

that this exogenous protein recapitulates similar expression pattern, *in vitro*, to that of the endogenous *Mecp2*.

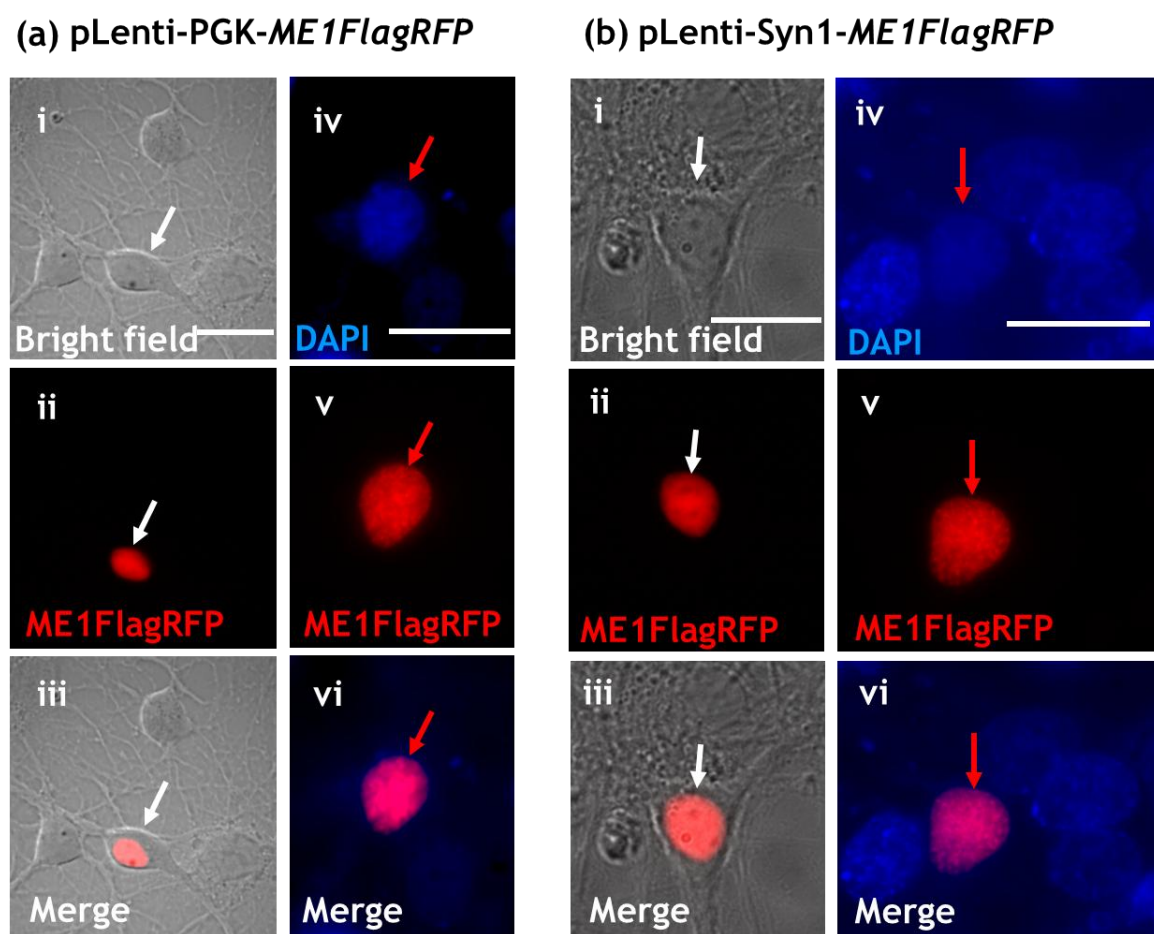


Figure 3-11 Lenti-PGK/syn1-*ME1FlagRFP* vectors express *ME1FlagRFP* fusion protein in hippocampal dissociated culture. Micrographs showing exogenous *ME1FlagRFP* expression in the rat hippocampal dissociated culture. Culture was transfected with (a) plenti-PGK-*ME1FlagRFP* or (b) plenti-syn1-*ME1FlagRFP* using Ca^{2+} phosphate transfection. (i-iii) Live images showing the RFP fluorescence that is confined to the nuclei of the cultured hippocampal cells (White arrows). (iv-vi) cultured cells were fixed with 4% PFA and stained with DAPI. RFP fluorescence is co-localised with DAPI-stained nuclei indicating nuclear targeting of the exogenous *Mecp2* (red arrows). Scale bar = 20 μm .

3.3.6 Generation and titration of Lentivirus particles

To generate Lentivirus particles, human embryonic kidney cells (HEK293T) were transfected with plenti-*ME1FlagRFP* plasmids together with packaging plasmid to supply the essential viral proteins (chapter 2). To test the efficiency of the viral particles, HEK293T cells were transduced with 1 μl of the concentrated particles. After 72 hours the culture was fixed with 4% PFA and stained with DAPI. RFP fluorescence was observed in the nuclei of HEK cells; however, transduction efficiency was shown to be low (figure 3-11a) as indicated by the low percentage of cells expressing the transgene compared to DAPI-stained

nuclei. High virus titre is required to achieve high transduction efficiency, especially for the *in vivo* studies. Therefore I optimized the virus production protocol by increasing the quantity of virus containing media (through increasing the number of transfected culture flasks) with subsequent consecutive concentration using the ultracentrifuge. The virus particles generated by the adjusted protocol displayed high transduction efficiency (figure 3-11b) with virus titres between 10^7 and 10^8 IU/ml.

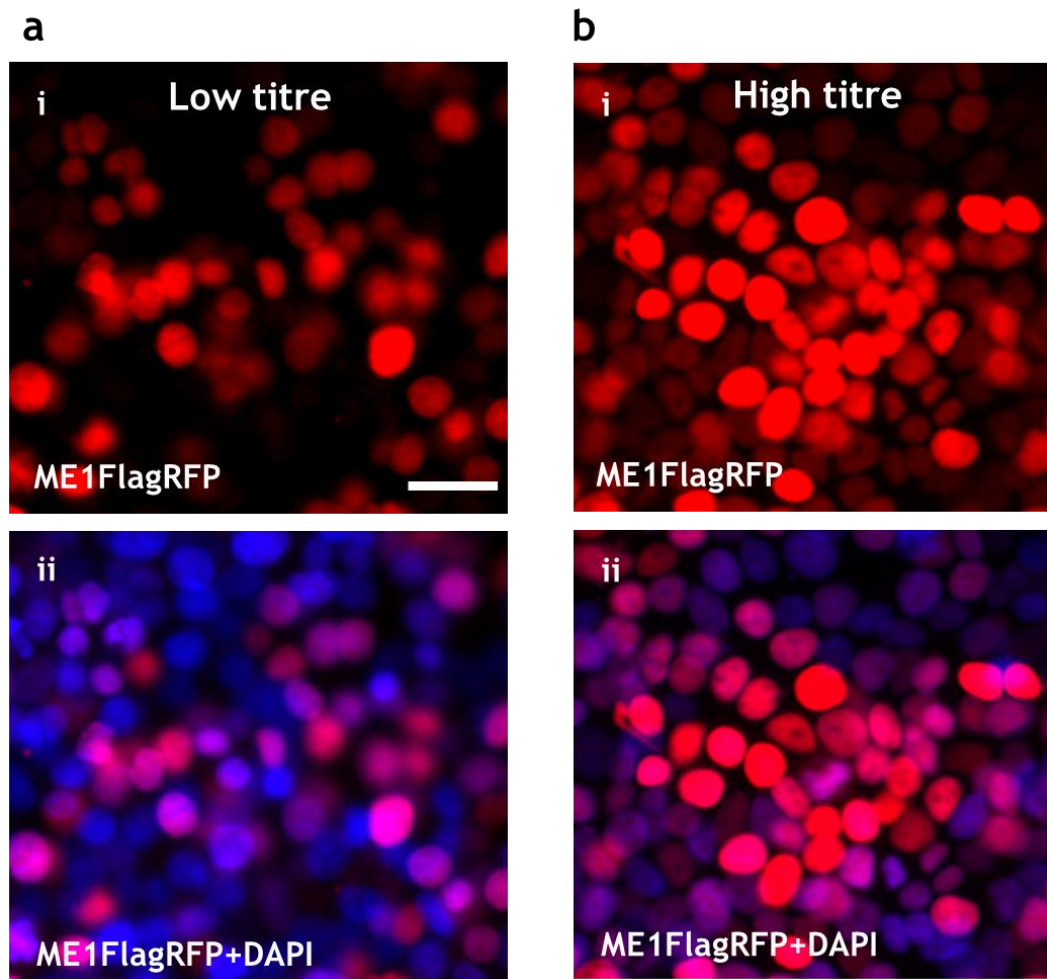


Figure 3-12 HEK293T cells transduced with lenti-PGK-*ME1FlagRFP* virus particles. Micrograph showing the transduction efficiency of lentivirus particles in HEK cells. 1 μ l of the concentrated virus was used for transducing HEK cells. (a) Low viral titre displayed lower transduction efficiency (as indicated by low number of transgene expressing (red) cells (i) compared to DAPI-stained nuclei (blue) (ii)). (b) Increased transduction efficiency (i) after the production of high titre viruses with the majority of DAPI-stained nuclei showing transgene expression (ii). Note some cells are brighter than others probably as a result of differences in the multiplicity of infection. Scale bar = 20 μ m.

3.3.7 Time course expression analysis of lenti-mediated delivery of *Mecp2*

To study the expression time course of the Lentivirus-derived products *in vitro*, dissociated hippocampal neuron cultures (N = 2) were transduced with 1 μ l of 10⁷ IU/ml (10⁴ IU) of lenti-syn1-*ME1FlagRFP*. Cover slips were fixed with 4% PFA at 24, 84, 72, 96 and 120 hours post-transduction and stained with DAPI. Images of 6-8 random fields were captured and the percentage of transduced cells counted as a proportion of the number of DAPI-stained nuclei at each time point (figure 3-12). *ME1flagRFP* expression was detectable as early as 24 hours after lenti-transduction (3.4 \pm 1.3%). The number of transgene expressing cells increased steadily but not linearly with time to 25.3 \pm 2.4% after 120 hours of transfection.

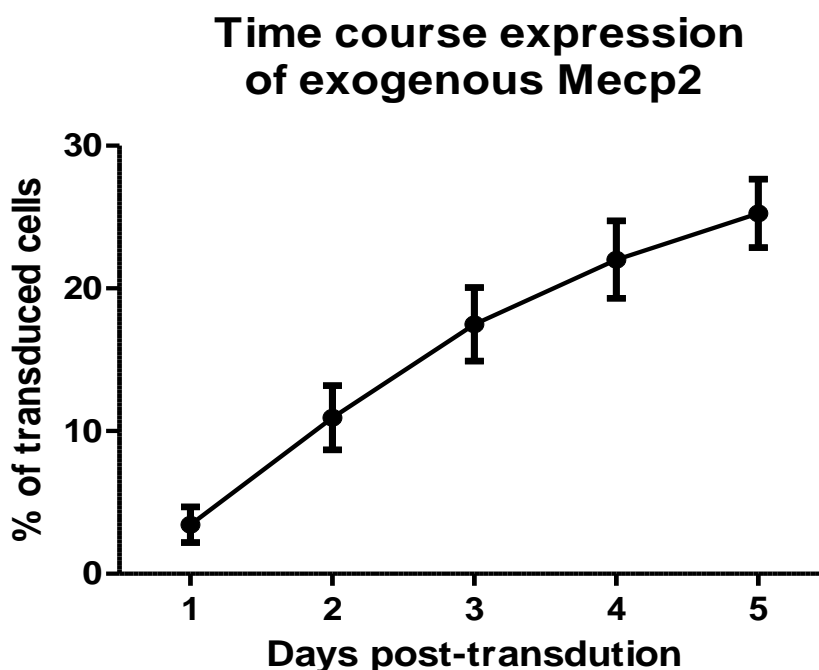


Figure 3-13 Time course expression analysis of exogenous *Mecp2*. Plot showing transduction efficiency over time of lenti-syn1-*ME1FlagRFP* in neuronal cell culture. Note that transgene expression was observed after 24 hours with marked increase in the transduction efficiency after 5 days. Data are presented as mean \pm SEM.

3.4 Discussion

The monogenic nature of RTT combined with studies showing phenotypic reversal after delayed reactivation of the *Mecp2* gene (Giacometti et al., 2007, Guy et al., 2007) makes RTT an attractive target for gene therapy. However, in order to study potential therapeutic applications, cloning of the *Mecp2* minigene into viral vectors was essential to achieve high transduction efficiency and to

allow *in vivo* studies. MeCP2 protein has two isoforms; MeCP2_e1 and MeCP2_e2 that result from alternative splicing of exon one (Kriaucionis and Bird, 2004). Both isoform were previously thought to have identical function, however a recent report has shown that overexpression of *Mecp2_e2* but not *Mecp2_e1* induces neuronal apoptosis and death in cultured cells (Dastidar et al., 2012). Therefore I generated a fusion construct containing *Mecp2_e1* encoding sequences combined with a Flag-epitope tag and *RFP* gene.

The importance of the *ME1FlagRFP* fusion construct is that it enables tracking of exogenous *Mecp2* expression in real time (by RFP fluorescence) so that studies addressing electrophysiological properties can be conducted on transduced (RFP-positive) and non-transduced cells (RFP-negative) to test the effect of exogenous *Mecp2* on the electrical properties of null cells. It also helps in discriminating exogenous and endogenous *Mecp2* in WT cells thus helping to measure and adjust the amount of exogenous *Mecp2* expression in transduced cells. This is important to avoid overexpression related toxicity. These tags also allow immunolabelling detection of exogenous *Mecp2* in fixed tissues by using anti-Flag or anti-RFP antibodies.

The rescue of RTT-like phenotype after delayed activation of *Mecp2* in mouse brain (Giacometti et al., 2007) indicates that any attempt at treating RTT at the gene level should utilise delivery methods capable of transferring *Mecp2* into the brain. Rastegar and colleagues have shown the ability of retrovirus- and lentivirus- based vectors to drive expression of *Mecp2* in neuronal stem cells and dissociated neuronal culture, respectively (Rastegar et al., 2009). However this study was confined to dissociated neuronal culture with no data regarding *in vivo* expression or levels of exogenous *Mecp2* in transduced cells. Therefore I decided to clone a *ME1FLAGRFP* fusion construct into Lentiviral vectors under the control of either the *syn1* or the PGK promoter. *Syn1*, which drives neuron-specific expression of *Mecp2*, was chosen as a previous report has shown that neuron-specific expression of *Mecp2* was able to rescue RTT-like phenotypes in *Mecp2* knockout mice (Luikenhuis et al., 2004). The PGK promoter, which drives expression in both neurons and glia, was chosen based on the growing evidence for the role of glia in RTT pathogenesis (Ballas et al., 2009) and the reported rescue of RTT-like phenotype after glia-specific activation of *Mecp2* in *Mecp2* knockout mice (Lioy et al., 2011).

Ca²⁺ phosphate transfection of rat neuronal dissociated culture using lenti-syn1/PGK-ME1FlagRFP plasmids showed that the Mecp2FlagRFP fusion protein recapitulates the same expression pattern of the endogenous Mecp2 in rats (nuclear targeting with diffuse localization to the euchromatic chromosome without tendency to concentrate in distinct areas of the genome) (Lewis et al., 1992, Nan et al., 1996) without ectopic expression. Mouse neuronal cultures transfected with the same vectors produced an exogenous Mecp2FlagRFP fusion protein that followed the same pattern as the endogenous Mecp2 expression in mouse cells (nuclear localization with characteristic heterochromatin localization, chapter 4) (Lewis et al., 1992, Nan et al., 1996, Nan et al., 1997) indicating that the expression of the fusion product follows the same expression pattern and sub-nuclear localization as the endogenous Mecp2 in different species. This data also confirms that cloning of the RFP in the C-terminal end of Mecp2 does not interfere with the regular cellular and subcellular localization of the transgene.

Ca²⁺ phosphate transfection has been reported to display low transfection efficiency *in vitro* (Goetze et al., 2004, Karra and Dahm, 2010) and is not applicable for *in vivo* studies, therefore production of Lentivirus particles was necessary for conducting *in vivo* studies in the animal model of RTT syndrome. Initial attempts to generate lentivirus particles showed relatively low titre as indicated by low transduction efficiency in HEK cells. These virus particles were generated by harvesting virus containing medium obtained from a single 150 cm² flask and spinning it down by the ultracentrifuge to precipitate the virus pellet which was then re-suspended in 600 µl of PBS. To increase the titre, I modified this protocol by scaling up the number of transfected HEK cells to 8 times the number used in the initial protocol and re-suspending the final pellet in a smaller volume of PBS. This modification increased the virus titre from 10⁴ to 10⁷-10⁸ IU/ml.

Time course experiments were also conducted to study the onset and expression course of lenti-mediated Mecp2 expression. RFP fluorescence was detected 24 hours post-transduction with gradual increases in the percentage of Mecp2FlagRFP expressing cells over time. Previous report showed that lenti-mediated transgene expression in cell culture shows peaks after both 6 hours and 3 days of transduction (Wang et al., 2005). However very early expression of

the transgene could be due to pseudo-transduction (the protein is transferred passively within the viral particles) and is not true transduction (Nash and Lever, 2004). Technical issues precluded monitoring of early expressing cells over time to discriminate true transduction (persistent expression) from pseudo-transduction (fading of expression with time due to limited half-life of the passively transferred protein). The delayed detection of *Mecp2*RFP expression in some cells could be explained by; (1) reduced viral uptake into the cells (electrostatic repulsion between lentivirus and neuron cell surface as both of them are negatively charged)(Swaney et al., 1997, Jensen et al., 2003, Denning et al., 2012), (2) difference in the transcription machinery in the transduced cells, (3) the variability in the onset of neuronal cell recovery (cells were transduced 24 hours after culture) (4) the variability in the multiplicity of infection (MOI) i.e. number of virus copies per cell. Cells with low MOI require more time to produce a detectable level of *Mecp2*RFP(Wanisich and Yanez-Munoz, 2009).

The fact that even after 5 days the maximum transduction efficiency was around 30% of DAPI-stained nuclei can be explained partially by the low virus titre that was used in this experiment and also to the fact that *syn1* is a relatively weak promoter (require more time to build up detectable protein level (Glover et al., 2002) and drives expression only in neurons thus excluding glia that might be transduced but not expressing the transgene.

In this chapter I have generated a Lentivirus-based vector to drive expression of exogenous *Mecp2* in *Mecp2 knockout* as well as WT cells to help investigate the potential therapeutic effects of this approach in both *in vitro* and *in vivo* models of Rett syndrome.

Chapter 4

Lentivirus-mediated delivery of *Mecp2* *in vitro* and *in vivo* in a mouse model of Rett syndrome

4.1 Introduction

Previous studies have shown that rescue of RTT-like phenotypes in the *Mecp2* knockout mouse model at the gene level is achievable by delayed activation of a conditionally silenced endogenous *Mecp2* (Giacometti et al., 2007, Guy et al., 2007). Thus introducing a functional copy of *Mecp2* through viral vectors to neurons or glia or both of them could be a potential therapeutic avenue for RTT. In the last few years huge progress has been made in the field of gene therapy through improving vector design and discovering/optimizing many tissue-specific promoters (Boulos et al., 2006, Gray et al., 2011b). Previous report, based on a published abstract, showed improvement in the locomotor activity after local delivery of exogenous *Mecp2* in the striatum of *Mecp2*-null mice (Kosai, 2005), however this work has never been published as a full study paper. In addition, neurons that have been differentiated from *Mecp2*-transduced neuronal stem cells taken from a *Mecp2*^{-/+} heterozygous female mouse, displayed improvement in dendritic arborization and spine density (Rastegar et al., 2009).

As described in chapter 3, I have generated lentivirus-based vectors to drive expression of *Mecp2*-e1 isoform as a fusion construct with RFP and Flag-epitope. These vectors were designed to enable exogenous *Mecp2* expression under the synapsin1 promoter to drive neuron-specific expression (Boulos et al., 2006) of *Mecp2* because it has been shown that lacking *Mecp2* in neurons only resulted in RTT-like phenotypes (Chen et al., 2001) whereas delayed activation of *Mecp2* only in neurons rescued RTT-like phenotypes (Luikenhuis et al., 2004) in *Mecp2* knockout mouse model. Recently it has been reported that absence of *Mecp2* in glia negatively affects normal neuronal growth (Ballas et al., 2009) and interestingly delayed activation of *Mecp2* in glia only rescued RTT-like phenotype in *Mecp2* knockout mouse model (Lioy et al., 2011). Therefore I generated lentivirus-based vector to drive expression of *Mecp2* in both neurons

and glia under the control of the PGK (housekeeping) promoter (Hannan et al., 1993, Wang et al., 2008). In this chapter I utilised these constructs to investigate the potentials benefits of exogenous *Mecp2* expression in *Mecp2* knockout mice *in vitro* and *in vivo*.

Many theoretical obstacles impede considering gene therapy as a real highly potential approach for RTT therapy; firstly, the transduction efficiency should be high enough to compensate for the global absence of *Mecp2*. Secondly the expression pattern of exogenous *Mecp2* should be similar to that of the endogenous *Mecp2* (Nan et al., 1996). Thirdly, the cellular levels of exogenous *Mecp2* protein should be crucially maintained at a near physiological level to minimize the overexpression-related toxicity (Collins et al., 2004, Luikenhuis et al., 2004, Na et al., 2012). Finally, the exogenous *Mecp2* should be able to recapitulate the molecular characteristics of the endogenous *Mecp2* protein e.g. site-specific phosphorylation at S421 (Zhou et al., 2006).

Another possible application of lenti-mediated *Mecp2* expression is to provide a *Mecp2*-overexpression model. Such a model will enable investigation of the effect of *Mecp2* overexpression on cellular morphology and function. Moreover it helps investigating the effect of *Mecp2*-overexpression on other nuclear proteins. *Mecp2* is one of the most abundant nuclear proteins in post-mitotic neurons and its absence is associated with alteration in the expression pattern of other nuclear proteins (Skene et al., 2010). Previous reports showed that the total level of histone1 (H1) protein is elevated in *Mecp2*-null mice (Nan et al., 1997) whereas other studies reported changes in the chromatin remodelling through changes in the acetylation state of H3 (Shahbazian et al., 2002a, Skene et al., 2010) and H4 (Wan et al., 2001) in *Mecp2*-null cells. In this study I tested the potential effect of *Mecp2* overexpression in the WT brain on cellular levels and acetylation state of histone 4 protein that could provide more understanding of protein dynamic changes in the nucleus in the presence of abnormally high level of *Mecp2*.

In this chapter I examined the efficiency of lentivirus-mediated delivery of *Mecp2* as a potential therapeutic tool. This work includes initial validation of transgene expression *in vitro* and the phenotypic consequences of the *in vivo* transgene delivery to the CNS of *Mecp2* knockout mice.

4.2 Study aims

The main aim of the work described here was to examine the ability of lentiviral vectors to deliver *Mecp2* into neurons and glia *in vitro* and *in vivo*. This work was further extended to study the effect of delivering exogenous *Mecp2* into the brain of *Mecp2*^{stop/y} mice on RTT-like phenotypes at the cellular and organismal levels. The specific objectives of this study are:

1. To investigate the ability of the lentivirus-based vectors described in chapter 3 to drive exogenous *Mecp2* expression in neurons *in vitro* and *in vivo*.
2. To determine the transduction efficiency and cellular levels of protein expression after *in vitro* and *in vivo* administration.
3. To evaluate the effect of brain-specific delivery of exogenous *Mecp2* on the organismal and cellular RTT-like phenotype in *Mecp2*^{stop/y} mice.
4. To establish a model of *Mecp2* overexpression at the cellular level and to study the effect of overexpressing *Mecp2* on the level of other nuclear proteins, particularly Histone 4.

4.3 Methods

To study the potential of lenti-mediated *Mecp2* expression *in vitro* and *in vivo* in *Mecp2* knockout mice, *Mecp2_e1* minigene was tagged at its C-terminal with Flag-tag epitope and *RFP* gene. This fusion construct was then cloned into lentivirus-based vector backbones under either, neuron-specific synapsin1 or generic PGK promoter (figure 4-1). Lentivirus particles were generated as described in chapter 2.

Hippocampal dissociated neuronal cultures were prepared from P0-3 pups from *Mecp2*^{stop/y} mice. The mouse was decapitated and the hippocampus was removed, chopped into small pieces, incubated in papain for 20 minutes before being cell dispersal by pipetting. The dissociated neurons were then plated on poly-L-lysine coated cover slips and maintained in a 5% CO₂ incubator at 37°C.

The culture was fixed with 4% paraformaldehyde followed by immunocytochemistry staining.

Stereotaxic brain injection of *Mecp2*^{stop/y} and WT mice was carried out at the age of 8 weeks (mildly symptomatic *Mecp2*^{stop/y} mice). The details of the injection coordinates and the volume of injected viruses will be discussed later in this chapter. Brain coronal sections were prepared using a vibratome then immunolabelled with various antibodies to confirm transgenic expression. Images were taken using a confocal microscope and analysed by Image J software (see chapter 2).

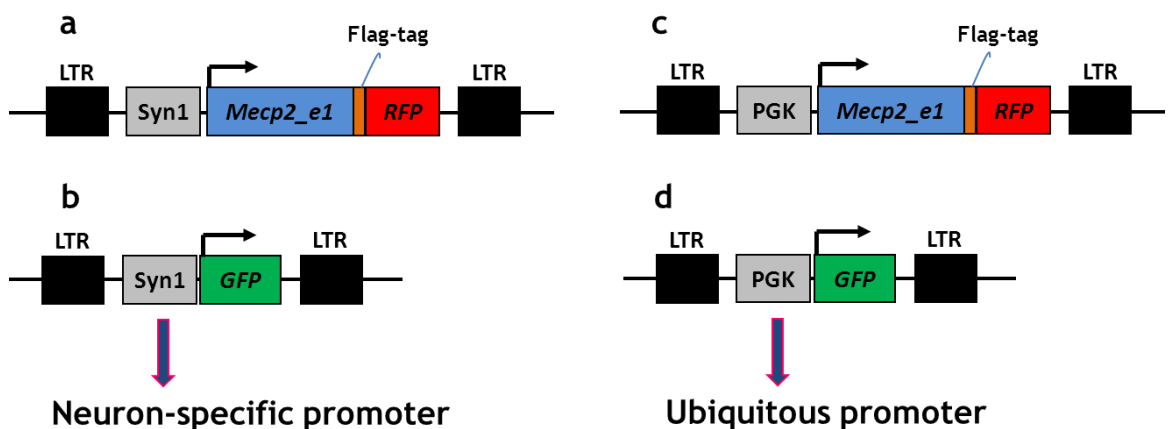


Figure 4-1 Lentivirus-based vector constructs

Representative figure showing designs of lentivirus-based vectors utilized in this study. (a) *Mecp2_e1* (ME1) *FlagRFP* fusions construct was cloned into Lentiviral vector under neuron-specific synapsin1 promoter. (b) *GFP* gene was cloned in the same vector backbone to be used as a control vector. (c) and (d) are similar vectors to (a) and (b) respectively, however synapsin1 is replaced by the housekeeping PGK promoter. LTR; long terminal repeat, syn1; synapsin1 promoter, PGK; phosphoglycerate kinase promoter, RFP; red fluorescent protein, GFP; green fluorescent protein.

4.4 Results

4.4.1 Lenti-mediated delivery of *ME1FlagRFP* to cultured neuronal cells

4.4.1.1 Neuron-specific expression of *Mecp2* in the hippocampal dissociated cell culture

Primary hippocampal dissociated neuronal cultures were prepared from *Mecp2*-stop mice (Guy et al., 2007). Cultured hippocampal cells prepared from *Mecp2*^{stop/y} (hemizygous male) and *Mecp2*^{-/+} (heterozygous female) mice were transduced with 10⁴ IU of lenti-syn1-*ME1FlagRFP*. Seven days later, the cultures were fixed with 4% PFA and immunolabelled with anti-Flag, anti-*Mecp2* and anti-MAP2 (neuronal specific marker) antibodies and stained with DAPI. The results show that the Flag-tagged *Mecp2* protein was localised to the nucleus, as indicated by co-localization with DAPI (figure 4-2), and displayed discrete punctate heterochromatin targeting with no evidence of ectopic (non-nuclear) cellular expression (figure 4-2). Anti-*Mecp2* labelling further confirms the exogenous *Mecp2* expression and showed that the transgene is the only source of detectable *Mecp2* in *Mecp2*^{stop/y} mice as indicated by the presence of detectable *Mecp2* immunofluorescence only in Flag-immunopositive nuclei. Co-immunolabelling with a neuronal marker MAP2 showed that exogenous *Mecp2* is only expressed in neurons as evidenced by expression of the transgene in MAP2-positive cells and not in MAP2-immunonegative cells (figure 4-2).

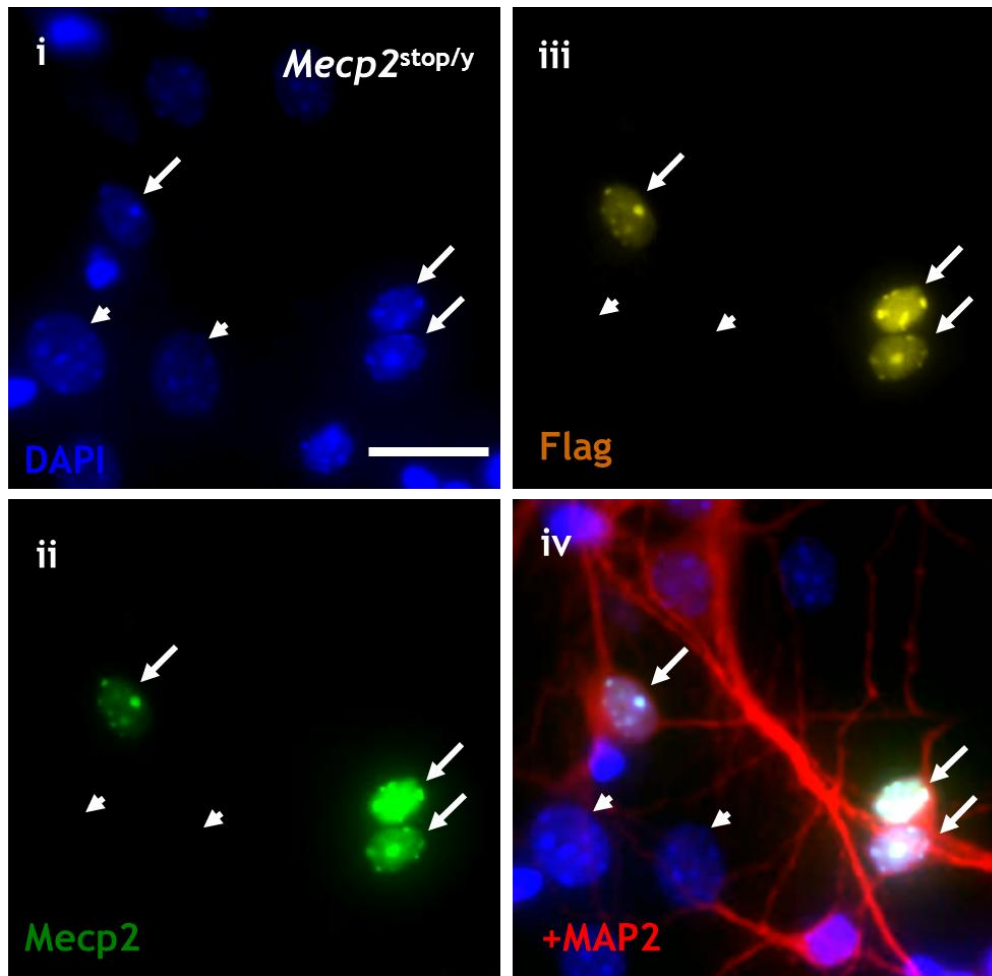


Figure 4-2 Synapsin1 promoter drove neuron-specific expression of exogenous Mecp2. Micrograph of primary hippocampal dissociated cell culture prepared from *Mecp2*^{stop/y} neonatal mouse. The culture was transduced after 24 hours with lenti-syn1-*ME1FlagRFP*. (i-iii) show labelling for nuclei (DAPI), anti-Mecp2 and anti-Flag antibodies respectively. (iv) Showed merge of i-iii together with immunolabelling for the neuronal marker MAP2. Arrows show examples of Flag-tagged Mecp2 expressed in neuronal nuclei and showing discrete heterochromatin-like punctate expression with no evidence of ectopic, non-nuclear, expression. Arrowheads indicate MAP2-immunonegative cells (presumed to be glia). Scale bar = 20 μ m.

4.4.1.2 Delivery of exogenous Mecp2 in *Mecp2*^{+/stop} female mosaic hippocampal cell culture

In *Mecp2*^{+/Stop} heterozygous female mice insertion of a stop cassette leads to silencing of one of the *Mecp2* alleles (Guy et al., 2007). This leads to mosaic expression of the endogenous Mecp2 due to random X-chromosome inactivation. The mosaic pattern of Mecp2 expression was indicated by the presence of a population of DAPI-positive cells showing absence of detectable Mecp2 expression (figure 4-3). Anti-Flag immunolabelling enables discrimination of cells expressing endogenous Mecp2 (Flag negative) from those expressing recombinant Mecp2 (Flag-immunopositive, figure 4-3). Anti-Mecp2 antibody is unable to distinguish between endogenous and exogenous Mecp2 in the transduced cells

and thus anti-Mecp2 immunofluorescence in transduced cells either represents exogenous Mecp2 alone (if the transduced cells are lacking endogenous Mecp2) or exogenous plus endogenous Mecp2 (if the transduced cells are expressing endogenous Mecp2).

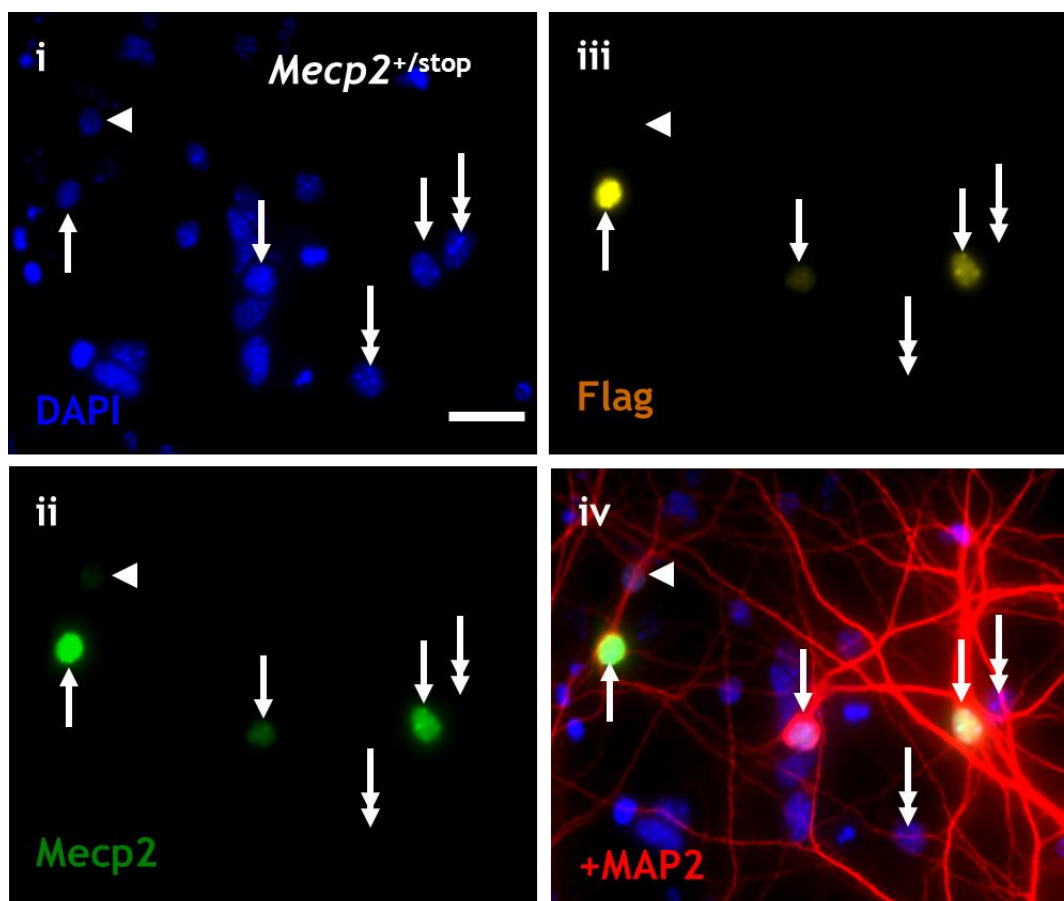


Figure 4-3 Neuron-specific expression of exogenous Mecp2 in $Mecp2^{+/stop}$ hippocampal cell culture.

Micrograph of primary hippocampal dissociated cell culture from $Mecp2^{+/stop}$ heterozygous female neonatal mice. The culture was transduced after 24 hours with lenti-syn1-*ME1FlagRFP* and stained with (i) DAPI, (ii) anti-Mecp2 antibody and (iii) anti-Flag antibodies to discriminate transduced cells. (iv) Merge of i-iii together with MAP2 immunolabelling. Note the mosaic expression pattern of endogenous Mecp2 as indicated by the presence of DAPI stained nuclei with a mixture of Mecp2 positive (arrows) and negative cells (arrows with double heads). Arrowhead points to cell expressing endogenous Mecp2 only. The arrows indicate transduced cells. Scale bars = 20 μ m.

4.4.1.3 Lenti-mediated delivery of *Mecp2* in neurons and glia under ubiquitous, PGK, promoter in hippocampal dissociated cell culture

Recent reports have suggested that glia may be an important factor in the RTT etiology (Ballas et al., 2009, Maezawa et al., 2009) and a more recent study has shown phenotypic rescue in a RTT mouse model after delayed activation of *Mecp2* in astrocytes only (Lioy et al., 2011). To deliver exogenous *Mecp2* into

neurons and glia, dissociated hippocampal cell culture was prepared from *Mecp2*^{stop/y} neonatal mice and transduced with 10⁵ IU of lenti-PGK-*ME1FlagRFP*. Seven days after transduction, the culture was fixed with 4% PFA and immunolabelled with anti-neuronal nuclear antigen (NeuN) antibody and DAPI. RFP fluorescence was used to discriminate transduced cells. The result of this experiment shows that lenti-PGK-*ME1FlagRFP* drove exogenous *Mecp2* expression both in neuronal (NeuN-immunopositive) and non-neuronal populations (NeuN-immunonegative, figure 4-4 A). The transduction efficiency of lenti-PGK-*ME1FlagRFP* was measured by counting the RFP positive cells, NeuN positive and DAPI stained nuclei in 12 random fields taken from 4 cover slips (N = 2 mice). The average percentage of cells transduced (*ME1RFP* expressing) was 75 ± 2.7% (mean ± SEM, N = 459 transduced cells of 614 DAPI-stained cells). NeuN-immunopositive cells represent 62 ± 2.5% whereas NeuN-immunonegative cells (presumed to be glia) constitute 38 ± 2.5 % of total *Mecp2RFP* expressing cells (figure 4-4b).

4.4.1.4 PGK promoter drove expression of high level of exogenous *Mecp2* in neurons in dissociated hippocampal cell culture

Mecp2 is one of the most abundant nuclear proteins with neurons expressing high level of *Mecp2* compared to glia (Skene et al., 2010). To determine exogenous *Mecp2* level expressed from the lenti-PGK-*ME1FlagRFP* construct in neurons and glia, intensity measures of *Mecp2RFP* fluorescence were measured (chapter 2) in NeuN-immunopositive cells and NeuN-immunonegative cell taken from 6 cover slips (N = 2 mice). The average fluorescence intensity of *Mecp2RFP* in NeuN-immunopositive cells was 116.1 ± 9.9 AU (mean ± SEM, N = 236 sampled cells) which is significantly ($p < 0.001$, unpaired t test) higher than the average *Mecp2RFP* intensity in NeuN-negative cells 46.9 ± 5.0 AU (N = 106 sampled cells, figure 4-4c).

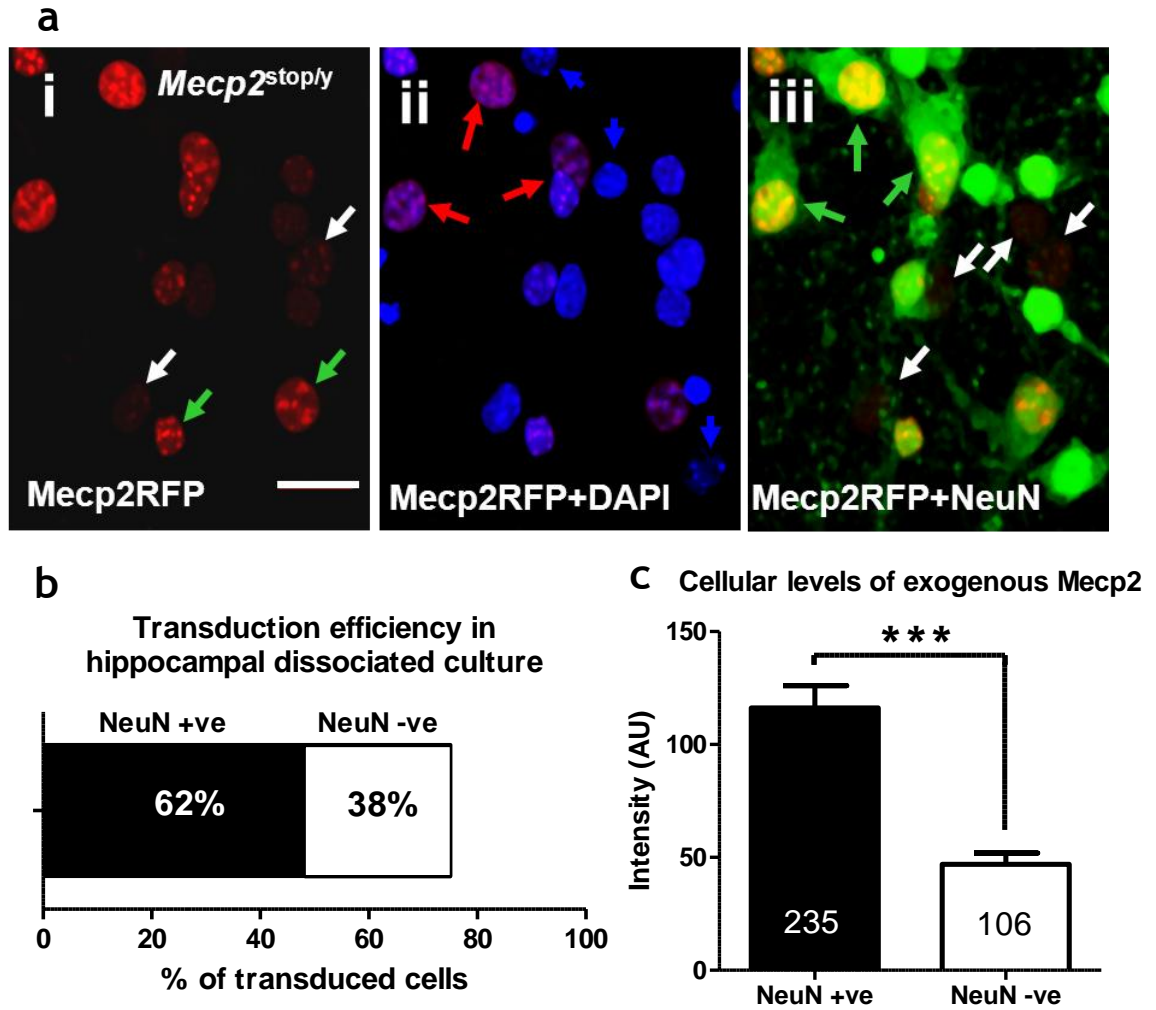


Figure 4-4 Lentivirus-based vector mediated high neuronal transduction of *Mecp2* in hippocampal dissociated cell culture.

(a) Micrograph of primary hippocampus neuronal culture from *Mecp2*^{stop/y} neonatal mice. The culture was transduced with 10^5 IU of lenti-PGK-*ME1FlagRFP*. (i) RFP fluorescence was used to discriminate the transduced cells. DAPI stain (ii) was used to determine the transduction efficiency (red arrows indicate transduced cells while blue arrows indicate non-transduced cells). Anti-NeuN antibody (iii) was used to show neuronal transduction (green arrows indicate neuronal expression whereas white arrows indicate glia expression). (b) Plot showing the total transduction efficiency (percentage of transgene-expressing cells relative to DAPI-stained cells) in dissociated cell culture and illustrates the relative proportion of exogenous *Mecp2* expression in neurons and glia (6 cover slips from 2 separate cultures). (c) Plot showing RFP fluorescence intensity as an indicator of exogenous *Mecp2* expression level, in neurons and presumed glia. Numbers on the columns indicate the numbers of sampled cells / group (6 cover slips. N = 2 mice). *** = $p < 0.001$, unpaired *t* test. Scale bar in (a) = 20 μ m.

4.4.2 *In vivo* injection of lenti-*ME1FlagRFP* viruses into the mouse brain

4.4.2.1 *In vivo* Neuron-specific delivery of exogenous *Mecp2* into the mouse brain

Brain-specific *Mecp2* knock out resulted in RTT-like phenotypes similar to that resulted from global *Mecp2* knockout (Chen et al., 2001, Guy et al., 2001) indicating the importance of this organ in RTT. Therefore it is clear that any attempt for gene therapy application in RTT should involve transgene delivery to the brain. To examine the ability of lentivirus to drive expression of exogenous *Mecp2* into the brain, 2 month old WT and *Mecp2*^{stop/y} male mice were injected with lenti-syn1-*ME1FlagRFP* to target the hippocampus (well-defined structure and easy to target) in one hemisphere and with lenti-syn1-*GFP* in the contralateral hemisphere as a control (figure 4-5a). 0.9µl of 10⁷ IU/ml (~10⁴ IU) were injected by stereotaxic brain injection (was kindly performed by Dr John Riddell, University of Glasgow, UK) into 3 different sites in each hemisphere (0.3 µl/site, table 4.1).

Table 4-1 Injection coordinates for the hippocampus stereotaxic brain injection

Injection sites	Bregma	Lateral	Depth
First	-1.5mm	1.08mm	2.2mm
Second	-1.25mm	1.56mm	2.2mm
Third	-1.75mm	2.08mm	2.1mm

To validate transgene expression, mice were transcardially perfused one week post-injection with 4% PFA in 0.1 M PBS. Coronal sections from the brain were immunolabelled with anti-Flag, anti-*Mecp2* and anti-GFP antibodies together with DAPI stain. Analysis of transgene expression showed that the majority of Flag-immunopositive or RFP fluorescent cells (left hemisphere) and GFP-immunopositive cells (right hemisphere) were located within the granule cell layer of the dentate gyrus (figure 4-5) with limited spread to the CA3 region of the hippocampus. Exogenous *Mecp2* expression was targeted to the nucleus and recapitulated the characteristic heterochromatin localization of endogenous

Mecp2 as indicated by nuclear co-localization with DAPI (figure 4-6a). Anti-Mecp2 staining of the WT sections showed two populations of cells, cells expressing the endogenous Mecp2 only (normal fluorescence intensity) and cells expressing endogenous and exogenous Mecp2 (relative greater fluorescence intensity, figure 4-5b). As expected anti-Mecp2 immunofluorescence in the GFP injected hemisphere of *Mecp2*^{stop/y} males showed absence of detectable endogenous Mecp2. In the lenti-PGK-*ME1FlagRFP* injected hemisphere however, immunolabelling for anti-Mecp2 was positive and co-localized with the Flag immunofluorescence, indicating that the presence of Mecp2 expression was due to exclusively exogenously delivered *Mecp2* (figure 4-5c).

4.4.2.2 **Syn1 promoter drove expression of exogenous Mecp2 at near-physiological levels *in vivo*.**

MeCP2 over-expression in patients (Meins et al., 2005, Van Esch et al., 2005) and mouse models (Collins et al., 2004, Luikenhuis et al., 2004) leads to a wide range of neurological deficits. In this study I quantified the cellular levels of exogenous Mecp2 expressed under the control of syn1 promoter in WT mice (based on the fluorescence intensity after immunolabelling with an anti-Mecp2 antibody). RFP fluorescence was used to discriminate between non-transduced (RFP-negative) cells that express the endogenous protein and the transduced (RFP-positive) cells that express endogenous and exogenous Mecp2, figure 4-6a). Transduced cells displayed Mecp2 levels that were 1.8 ± 0.07 AU (mean \pm SEM, N = 115 sampled cells from 9 brain sections, figure 4-6b) times greater than endogenous levels ($p < 0.001$, unpaired *t* test) in non-transduced cells (1.0 ± 0.02 AU, N = 130 sampled cells) which means that the levels of exogenous Mecp2 are about 85 % of the endogenous protein. Frequency distribution analysis of total Mecp2 levels showed that the non-transduced cells have tight endogenous Mecp2 expression (narrow peak, SD = 0.3 AU, figure 4-6c), whereas Mecp2 transduced cells displayed a broader range (wide peak, SD = 0.8 AU) of exogenous Mecp2 expression indicating modest variability in the expression levels.

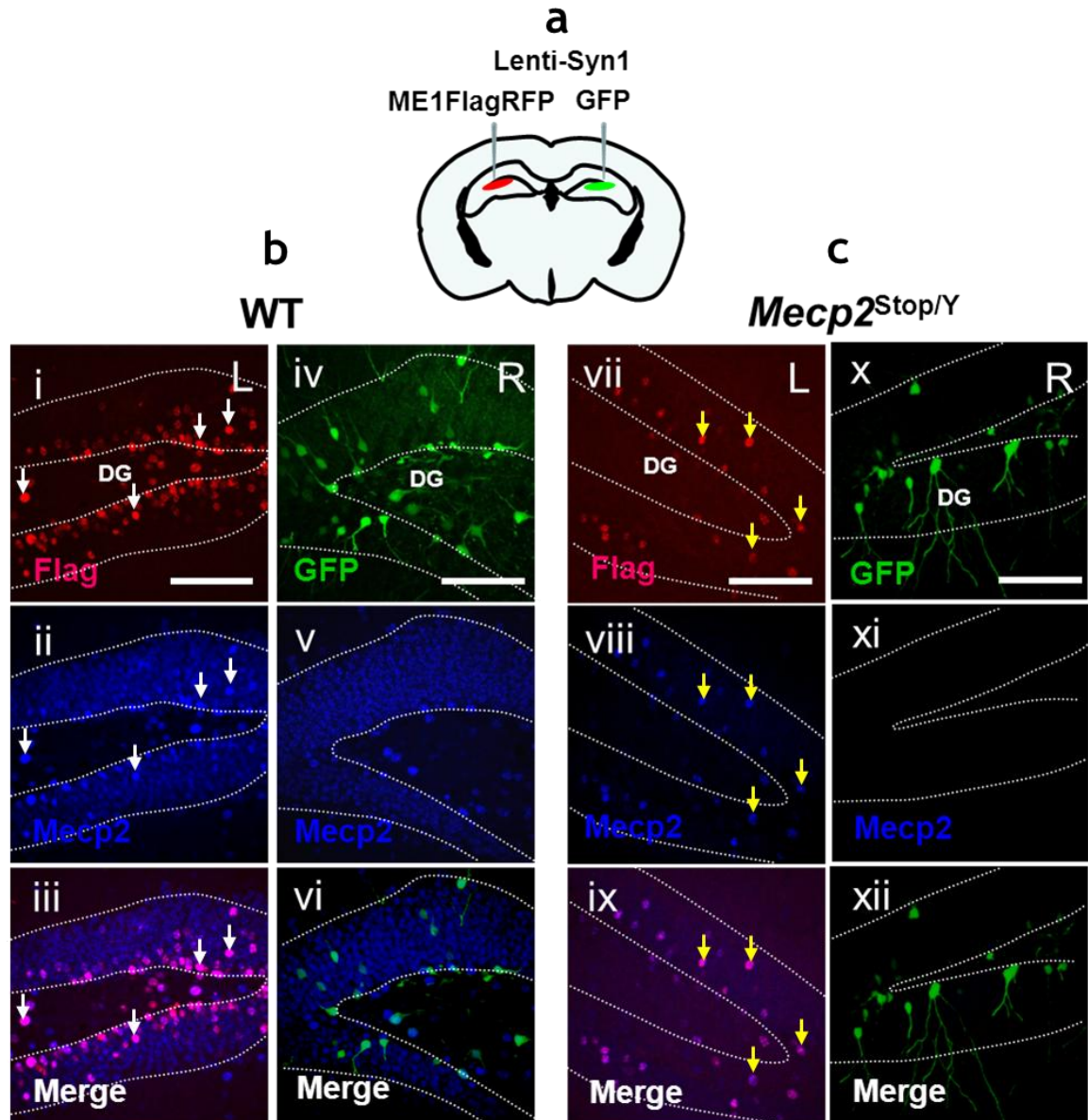


Figure 4-5 Lentivirus-based vector mediated exogenous *Mecp2* delivery into the hippocampus of *Mecp2*^{stop/y} and WT adult mice.

(a) Representative diagram showing the injection strategy. Lenti-syn1-*ME1FlagRFP* was injected into the left (L) hemisphere and lenti-syn1-*GFP* into the contra-lateral side (R). (b) Micrograph showing the expression of exogenous *Mecp2* (i-iii) and GFP (iv-vi) in the WT brain section. Transduced cells (co-localized with anti-Flag immunofluorescence) display high levels of anti-*Mecp2* immunofluorescence indicating presence of an extra protein that has been added by (exogenous) *Mecp2* expression (white arrows). (c) Micrograph showing exogenous *Mecp2* (vii-ix) and GFP (x-xii) expression in *Mecp2*^{stop/y} mouse brain. Note the absence of anti-*Mecp2* immunofluorescence in the GFP injected hemisphere whereas the exogenous *Mecp2* is the only source of anti-*Mecp2* immunofluorescence (yellow arrows). Scale bar = 100 μ m.

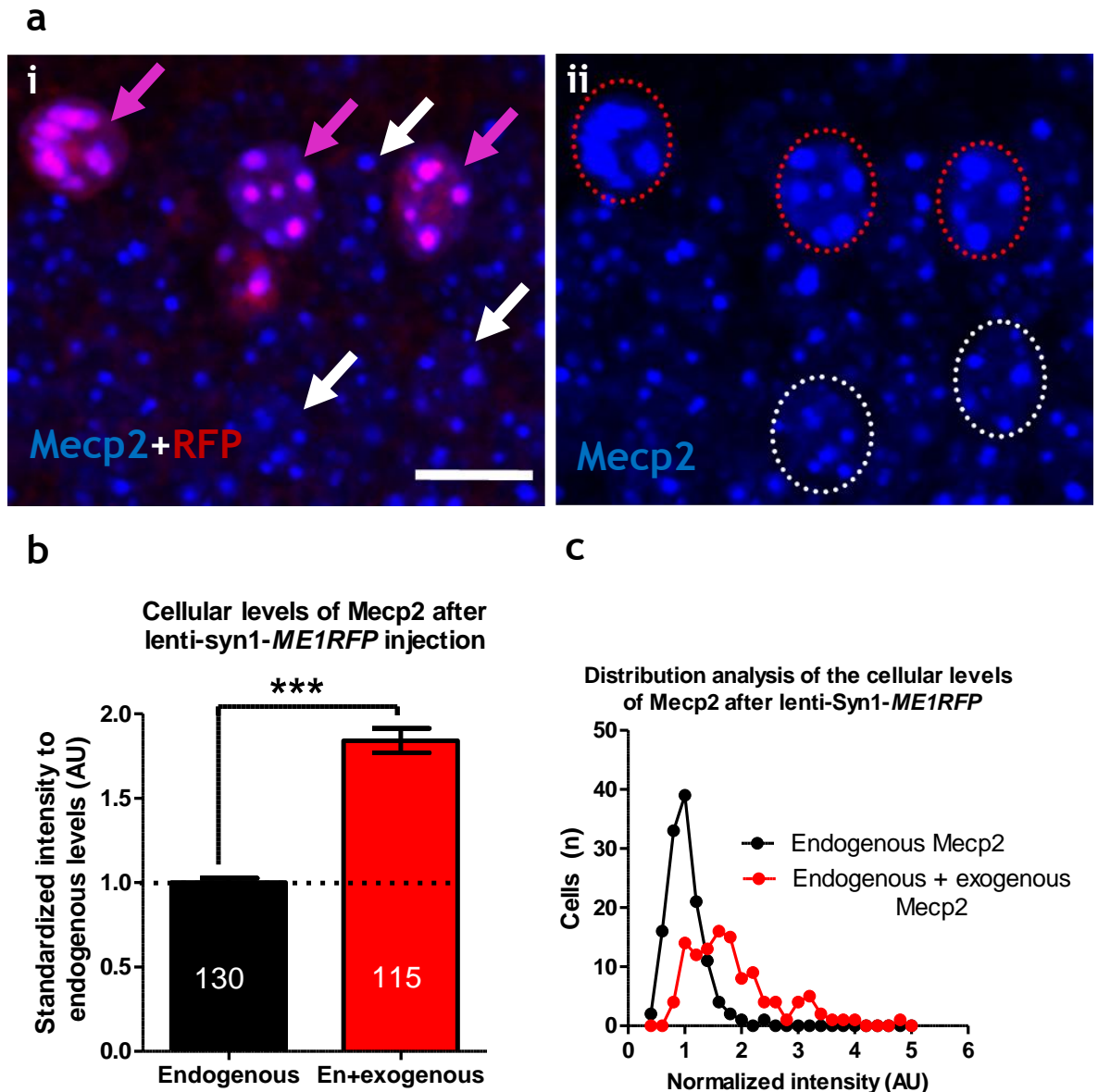


Figure 4-6 Syn1 promoter drove near-endogenous levels of exogenous Mecp2 *in vivo*. (a) Micrograph showing WT brain section after lenti-syn1-*ME1FlagRFP* injection. (i) RFP fluorescence discriminates between transduced (purple arrows) and non-transduced (white arrows) cells. (ii) Intensity of anti-Mecp2 immunofluorescence in transduced (red circles) and non-transduced (white circle) was used as a relative estimate for Mecp2 levels. (b) Plot showing Mecp2 immunofluorescence in non-transduced (endogenous level) and transduced cells (endogenous + exogenous Mecp2). Numbers on the columns indicate the numbers of sampled cells / group. Data was standardized to the average of the endogenous values and presented as mean \pm SEM. *** = $p < 0.001$, unpaired t test. (C) Frequency distribution of Mecp2 levels in transduced and non-transduced cells. Note the tight control of endogenous Mecp2 levels in the non-transduced cells (narrow peak). In contrast Mecp2 levels in transduced cells displayed wide peak, indicating variability in the expression level. Scale bar in (a) = 20 μ m.

To exclude the possible effect of Lentivirus transduction on the endogenous Mecp2 level, quantification of anti-Mecp2 fluorescence intensity in the GFP-transduced and non-transduced cells (figure 4-7a) showed cellular levels of Mecp2 expression in GFP-transduced cells equal to 0.94 ± 0.03 AU (N = 78

sampled cells from 9 brain sections, figure 4-7b) fold of the endogenous levels in GFP non-transduced cells (1.0 ± 0.02 AU, N = 140 sampled cells). Frequency distribution of *Mecp2* level showed that the GFP-transduced cells (SD = 0.3 AU) as well as the GFP non-transduced (SD = 0.3 AU) displayed a similar narrow range of endogenous *Mecp2* expression (figure 4-7c) indicating that lentivirus-based vector transduction has no detectable effect on the levels of endogenous *Mecp2* expression.

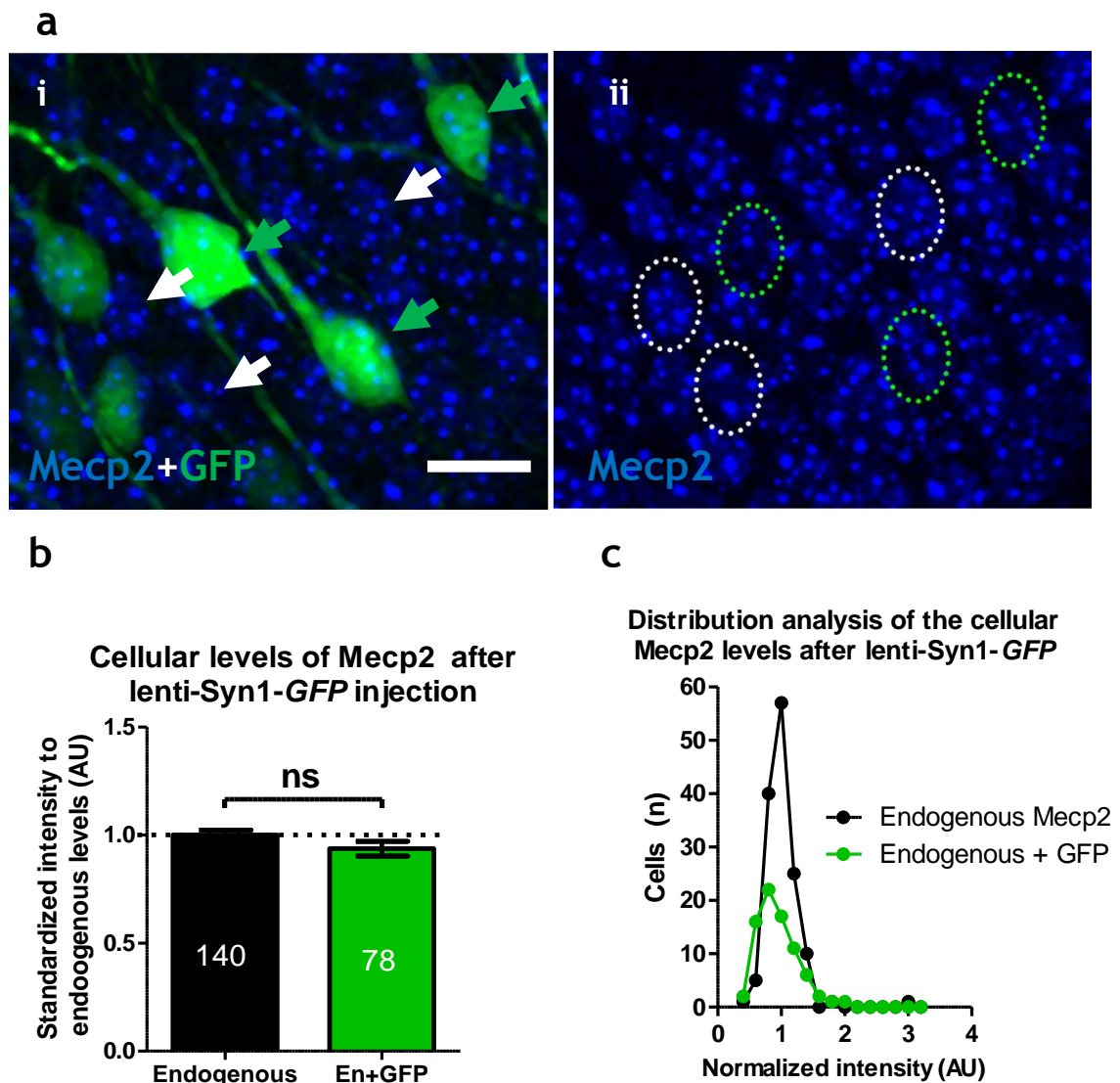


Figure 4-7 Lentivirus-mediated GFP expression showed no effect on the cellular levels of endogenous *Mecp2*.

(a) Micrograph showing WT brain section after lenti-syn1-GFP injection. (i) Anti-GFP antibody was used to discriminate transduced (green arrows) from non-transduced (white arrows) cells. (ii) Immunofluorescence intensity was used to quantify relative *Mecp2* levels in transduced (green circles) and non-transduced (white circle) was used as a measure for *Mecp2* level. (b) Plot showing the difference in *Mecp2* level between non-transduced (endogenous level) and GFP-transduced. Numbers on the columns indicate number of sampled cells / group. Data was standardized to the average of the endogenous values and presented as mean \pm SEM. ns; non-significant, En in (b); endogenous protein. (c) Frequency distribution plot of *Mecp2* level in the GFP-transduced and non-transduced cells showing similar distribution pattern with tightly controlled *Mecp2* expression levels. Scale bar in (a) = 20 μ m.

4.4.3 Transgenic expression of *ME1FlagRFP* in the CA1 region of the hippocampus under the control of the PGK promoter

The hippocampus constitutes a key part of the limbic system in the brain of humans and vertebrates. Studies of the hippocampus in *Mecp2* knockout mice have shown altered synaptic plasticity (Asaka et al., 2006, Weng et al., 2011) that were reversible by delayed activation of *Mecp2* (Guy et al., 2007). Alteration in the cellular morphology, such as decreased neuron nuclear-size, was also observed in the hippocampus of *Mecp2* knockout mice (Giacometti et al., 2007). Recent work published during the course of my research highlighted the unexpected contribution of glia in the development of RTT syndrome. In particular, studies showed that glia from the *Mecp2*-null mice were able to negatively affect the function of WT neurons when co-cultured together in the same media (Ballas et al., 2009). I therefore decided to inject lenti-PGK-*ME1FlagRFP* into the CA1 region of the hippocampus in order to test the potential rescue of the impaired synaptic plasticity and to investigate the effect of exogenous *Mecp2* on the pyramidal cell morphology. Eight week old *Mecp2*^{stop/y} (N = 4) mice were injected into the CA1 region of the hippocampus at the level of stratum pyramidale with lenti-PGK-*ME1FlagRFP* in one hemisphere and lenti-PGK-*GFP* viruses in the contra-lateral hemisphere as an internal control. 1.5 µl of 10⁸ IU/ml (1.5X10⁵ IU) of lentiviruses were injected into to each hemisphere (3 sites per hemisphere, 0.5 µl per site) according to the following coordinates (table 4-2).

Table 4-2 Injection coordinates for CA1 region of the hippocampus

Injection sites	Bregma	Lateral	Depth
First	-2mm	1.08mm	1.15mm
Second	-1.75mm	1.56mm	1.15mm
Third	-2mm	2.04mm	1.25mm

To confirm exogenous *Mecp2* delivery, one of the injected mice was transcardially perfused after one week with 4% PFA in 0.1M PBS and transverse coronal brain sections were immunolabelled with anti-Flag, anti-*Mecp2*

antibodies. Exogenous *Mecp2* expression was evident in the CA1 region of the hippocampus (figure 4-8a) with nuclear targeting and characteristic localization to the heterochromatin (figure 4-8b). Lentivirus mediated high transduction efficiency around the injection sites. The percentage of cells expressing the transgene was 83.5 ± 4.2 % of DAPI-stained nuclei (1941 transgene-expressing cells of 2359 DAPI-stained nuclei. N = 4 mice). However, the spread was limited and only covered approximately 41% of the CA1 region.

Whilst an original aim of the experiments was to compare synaptic plasticity in *Mecp2*^{stop/y} mice, all injected mice (N = 4) developed a severe tail lesion that necessitated culling them before any functional rescue (LTP) could be investigated. Mice that needed to be culled were perfused ~13 days after injection (minimum 8 days and maximum 18 days post-injection) and their tissues were used for further cellular and morphological analysis.

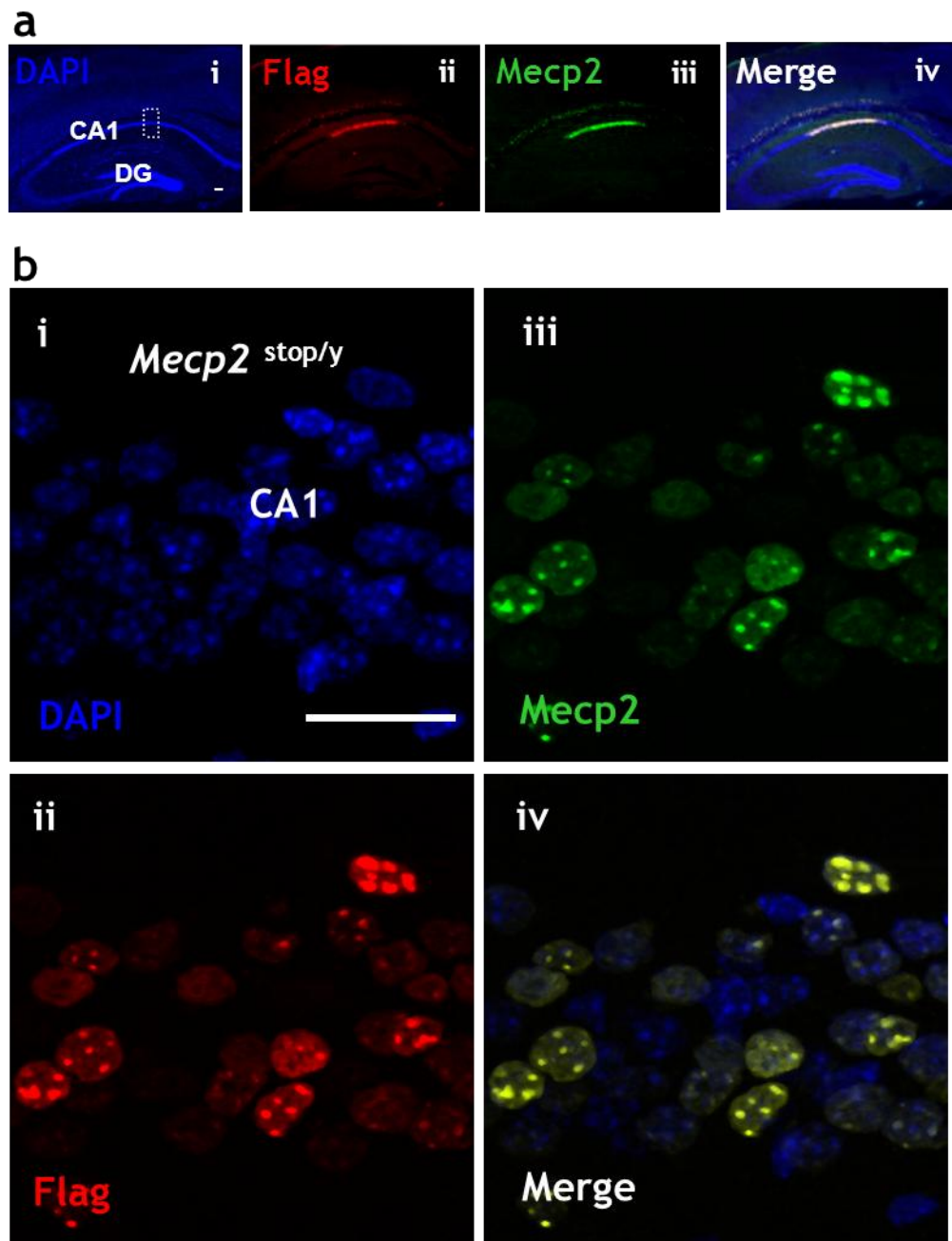


Figure 4-8 Lentivirus-mediated delivery of exogenous *Mecp2* to CA1 region of the hippocampus of *Mecp2*^{stop/y} mouse.

(a) Micrograph showing low power image of a coronal brain section taken from *Mecp2*^{stop/y} brain one week after lenti-PGK-ME1FlagRFP injection. Note the high transduction efficiency close to the injection site but limited spread. Box indicates high power image. (bi-iv) high power amplification image from the CA1 region shows; (i) staining with DAPI (ii) immunolabelling with anti-Flag antibody, (iii) immunolabelling with anti-Mecp2 antibody and (iv) is a merge of i-iii showing nuclear targeting of the transgene with characteristic localization to the heterochromatin. Scale bar = 200 μ m in (a) and 20 μ m in (b).

4.4.3.1 Lentiviruses with PGK promoter drove high neuronal expression of the exogenous *Mecp2*

To test the *in vivo* neuronal transduction efficiency of lenti-PGK-*ME1FlagRFP*, 50 μm thick sections from *Mecp2*^{stop/y} mice were immunolabelled with anti-NeuN and anti-GFAP (Astrocyte specific marker) antibodies. RFP fluorescence was used as a marker for transduced cells (figure 4-9). This data shows that the majority of transduced cells are NeuN positive with few transduced Astrocytes. This result indicates high neuronal tropism of lentiviruses regardless of the promoter type (syn1 or PGK) when injected using these coordinate at this age.

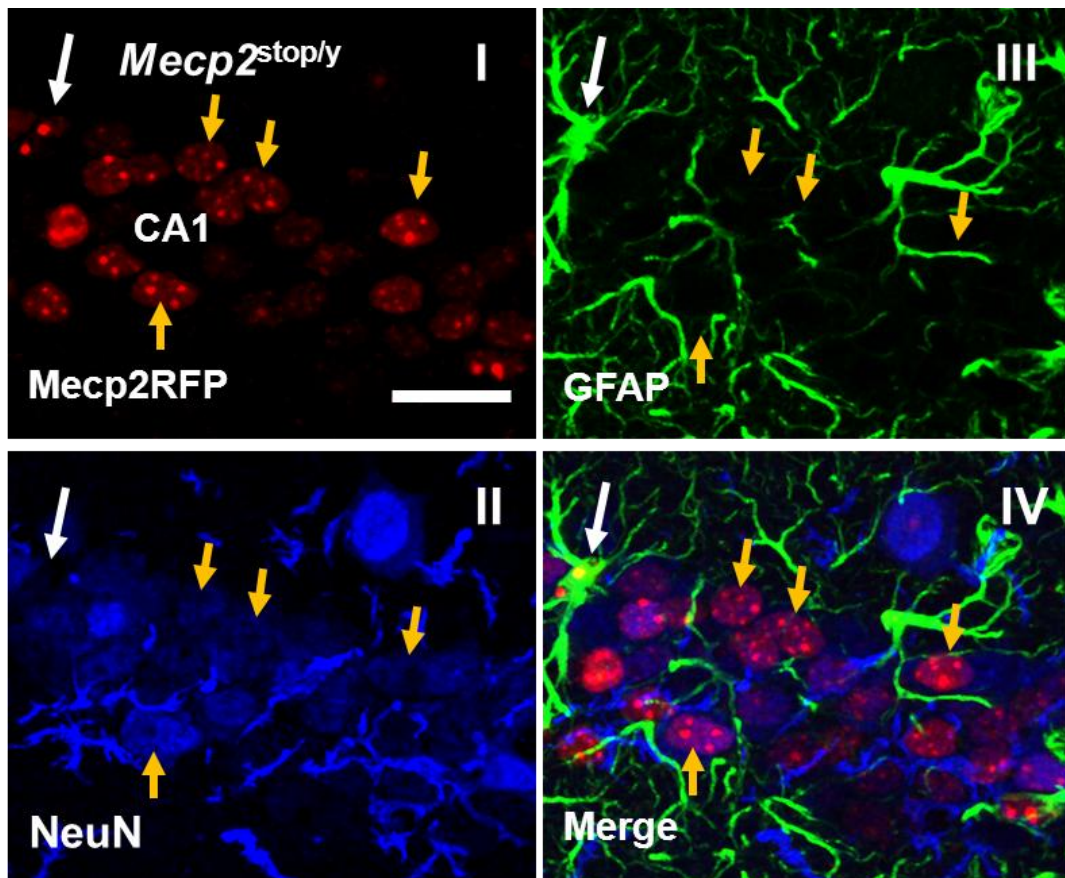


Figure 4-9 High neuronal tropism of Lentiviruses

Micrograph showing flattened confocal stack image from *Mecp2*^{stop/y} brain after lenti-PGK-*ME1FlagRFP* injection. (i) RFP fluorescence labels transduced cells. (ii-iii) show immunolabelling with anti-NeuN and anti-GFAP antibodies respectively. (v) is merge of (i-iii). Note the high neuronal transduction efficiency (yellow arrows) with very low glial expression (arrow). Scale bar = 20 μm .

4.4.3.2 Exogenous *Mecp2* rescued neuronal nuclear volume in *Mecp2*^{stop/y} mice

A characteristic hallmark of *Mecp2* deficiency, at the cellular level, is a reduction in neuronal nuclear volume (Giacometti et al., 2007, Johnson et al., 2011). In order to assess the potential changes of this cellular feature in cells in which *Mecp2* is reintroduced by lentivirus transduction, 3D nuclear reconstruction was carried out in ME1FlagRFP transduced and non-transduced (as an internal control) pyramidal cells of the CA1 region of *Mecp2*^{stop/y} mice. Non-transduced neurons (N = 4 mice) in *Mecp2*^{stop/y} mice showed significant ($p < 0.001$, one way ANOVA with tukey`s posthoc pairwise comparison) reduction of the nuclear volume (0.86 ± 0.04 AU fold of WT values, mean \pm SEM) compared to non-transduced cells in (N = 4) age-matched WT mice (1.0 ± 0.02 AU). ME1FlagRFP-transduced cells (N = 4 mice) displayed nuclear volumes of 1.0 ± 0.04 AU fold of WT values that were significantly ($p < 0.01$) larger than non-transduced cells (from the contra-lateral hemisphere as an internal control). In contrast there was no significant difference in the neuronal nuclear volume between *Mecp2*^{stop/y} pyramidal cells expressing exogenous *Mecp2* and that of WT age matched mice (Figure 4-10).

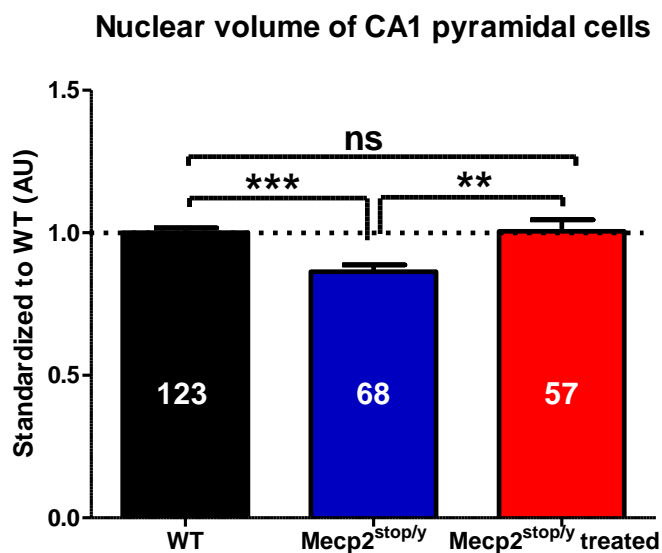


Figure 4-10 Exogenous *Mecp2* rescued nuclear volume in *Mecp2*^{stop/y} mice. Plot showing 3D nuclear volume measures of pyramidal cell layer of the CA1 area of the hippocampus of the *Mecp2*^{stop/y} (injected with lenti-PGK-ME1FlagRFP) and age-matched WT. Data was standardized to the average of the WT values and presented as mean \pm SEM. N = 4 mice/group. Numbers on the column refer to the number of sampled cells/group. *** = $p < 0.001$, ** = $p < 0.01$, one way ANOVA with tukey`s posthoc comparison.

4.4.3.3 Exogenous Mecp2 produced a modest increase in the nuclear volume of WT mice

The previous experiment demonstrated that exogenous Mecp2 rescued neuronal nuclear volume in *Mecp2*^{stop/y} mice to levels comparable to WT values. However it is not clear whether this change is due to expressing Mecp2 in cells lacking this protein or due to other downstream effect of the transgene. In order to test this effect, lenti-PGK-*ME1FlagRFP* was injected in the CA1 region of the hippocampus of 2 month old WT mice (N = 4) and the neuronal nuclear volume was examined two weeks later. 3D reconstruction of transduced CA1 pyramidal cell nuclei (RFP-positive) and non-transduced cells (RFP-negative) showed a modest, but significant ($p = 0.045$, unpaired t test), increase in the nuclear volume of transduced (1.1 ± 0.02 AU fold of WT non-transduced cells) compared to the non-transduced cells (1.0 ± 0.02 AU, figure 4-11).

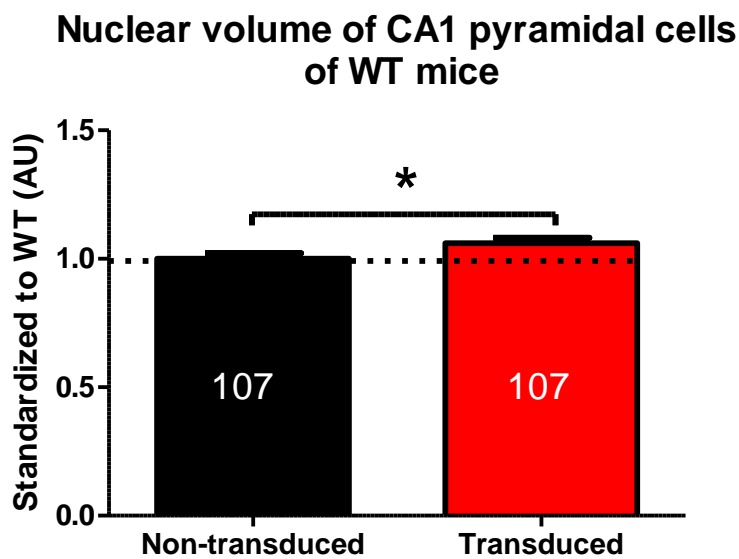


Figure 4-11 Exogenous Mecp2 increased pyramidal cells nuclear volume in WT mice. Plot showing 3D nuclear volume measures of CA1 pyramidal cells of the hippocampus of WT mice (N = 4). Data was standardized to the average of the WT (non-transduced) values and represented as mean \pm SEM. Numbers on the column refer to the number of sampled cells/group. * = $p < 0.05$, unpaired t test.

4.4.3.4 PGK promoter drove high levels of exogenous *Mecp2* *In vivo*

Maintaining the Level of *Mecp2* within physiological levels is critical in order to avoid the overt neurological deficits associated with *Mecp2* overexpression (Collins et al., 2004, Luikenhuis et al., 2004). I showed previously that synapsin1 promoter leads to expression levels of exogenous *Mecp2* approximately 85 % of the endogenous value in neurons (based on anti-*Mecp2* immunofluorescence intensity). Here I used the same approach to quantify the exogenous *Mecp2* protein levels expressed under the control of the PGK promoter. Analysis of the fluorescence intensity measurements of the anti-*Mecp2* immunofluorescence in transduced (RFP positive) and non-transduced (RFP negative) pyramidal cell nuclei in WT mice (figure 4-12a) revealed significantly ($p < 0.001$, unpaired t test) higher level of total *Mecp2* expression in transduced cells (3.173 ± 0.12 AU, mean \pm SEM, times the endogenous level) compared to non-transduced cells (1.0 ± 0.03 AU). This indicates that the PGK promoter drove expression of exogenous *Mecp2* protein in *Mecp2*^{stop/y} mice at a level approximately 2.1 fold higher than endogenous levels (figure 4-12b). Frequency distribution analysis of the total *Mecp2* levels showed that the non-transduced cells maintain the tightly controlled levels of endogenous *Mecp2* (SD = 0.38 AU), whereas *Mecp2* transduced cells displayed an extended range (SD = 1.37 AU) of *Mecp2* cellular levels indicating variable high expression levels (figure 4-12c).

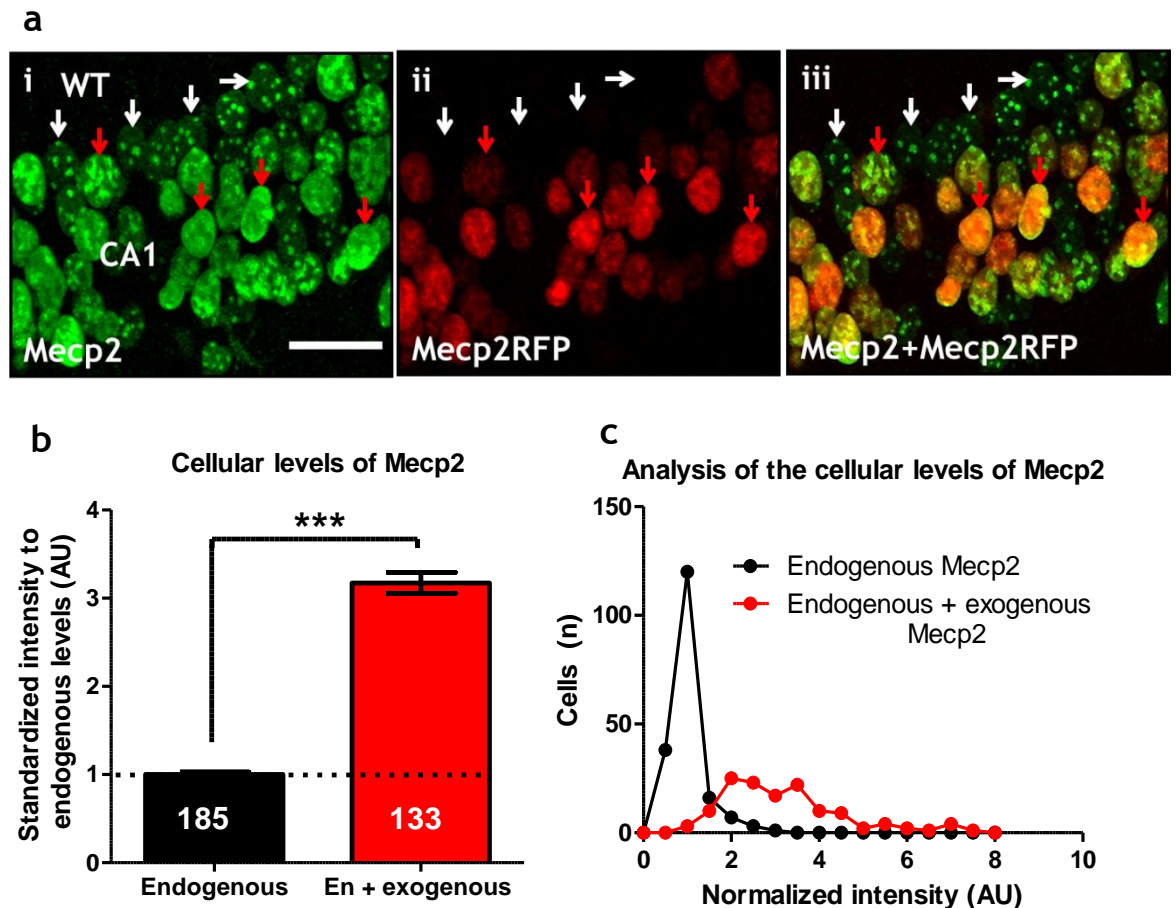


Figure 4-12 PGK promoter drove high levels of exogenous Mecp2 *in vivo*.

(a) Micrograph showing coronal brain section taken from WT mouse 2 weeks after lenti-PGK-*ME1FlagRFP* injection into the CA1 region. Section was immunolabelled with (i) anti-Mecp2 antibody. (ii) RFP fluorescence was used to identify the transduced cells. (iii) Merge of (i & ii). Red arrows indicate high levels of anti-Mecp2 immunofluorescence in transduced cells whereas white arrows indicate normal anti-Mecp2 immunofluorescence in non-transduced cells (express the endogenous Mecp2). (b) Plot showing Intensity measurements of anti-Mecp2 immunofluorescence in non-transduced (endogenous levels) cells and in transduced cells (N = 2 mice). (c) Frequency distribution of Mecp2 levels in transduced and non-transduced cells revealed extended levels of Mecp2 expression in transduced cells. Values are standardized to the average WT (non-transduced) values and presented as mean \pm SEM. Numbers in the columns in (b) indicate the numbers of sampled cells / group. *** indicates $p < 0.001$, unpaired *t* test. En; endogenous protein. Scale bar in (a) = 20 μ m.

4.4.4 Exogenous Mecp2 maintains phosphorylation at serine 421

The exact mechanism of action of Mecp2 at the molecular level is not fully understood. Previous studies have linked Mecp2 activity and interaction to site-specific phosphorylation particularly at serine 421 (S421) and S424 (Cohen et al., 2011). After neuronal activity-induced, Mecp2 was reported to be phosphorylated S421 with subsequent detachment from chromatin binding-sites to allow downstream expression of variety of genes (Chen et al., 2003b, Martinowich et al., 2003). However recent report has shown that proportion of

Mecp2 become phosphorylated while still attached to the chromatin (Na et al., 2012). I therefore decided to investigate whether exogenous Mecp2 is comparable, at the molecular level, to endogenous Mecp2, in terms of site-specific phosphorylation. Brain sections from *Mecp2*^{stop/y} mice (transduced into the CA1 region using lenti-PGK-*ME1FlagRFP*) were immunolabelled with anti-Mecp2 and anti-phosphorylated Mecp2 at serine 421 (pS421) antibodies (generous gift from Dr. Michael Greenberg laboratory, Harvard Medical School, USA). RFP fluorescence was used to distinguish transduced cells. These results show that Mecp2 phosphorylation at S421 persevered in the exogenous Mecp2 protein as indicated by co-localization between RFP fluorescence, anti-Mecp2, and anti-pS421 immunofluorescence (figure 4-13). However this phosphorylation in the exogenous Mecp2 was observed in the absence of induced neuronal activity.

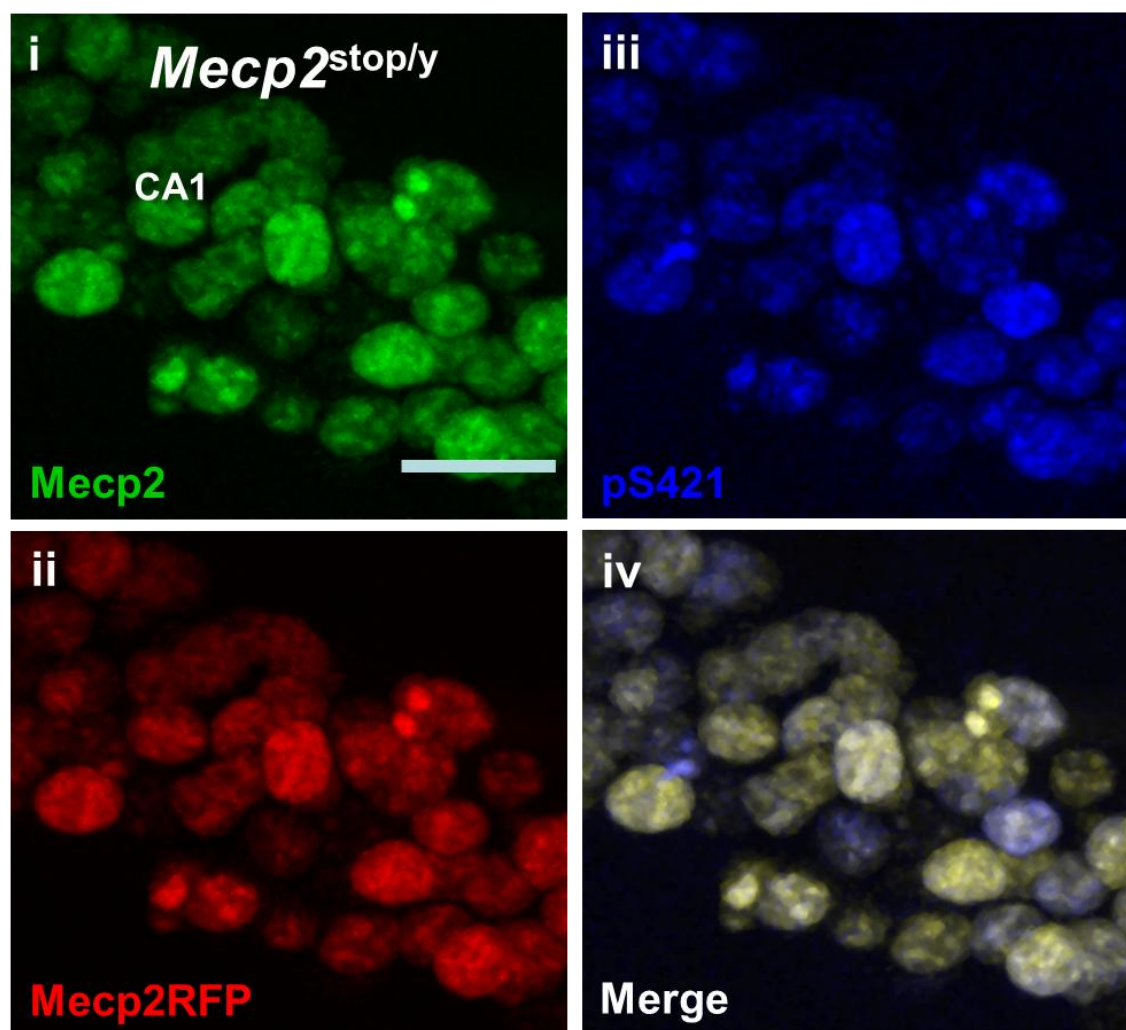


Figure 4-13 Exogenous Mecp2 maintains characteristic phosphorylation at S421
 Micrograph showing a flattened confocal stack taken from *Mecp2*^{stop/y} mice after lenti-PGK-*ME1FlagRFP* injection. Section was immunolabelled with anti-Mecp2 (i) and anti-pS421 (iii) antibodies. RFP fluorescence (ii) discriminate exogenous Mecp2 expression. Note that in the absence of neuron induced activity, exogenous Mecp2 becomes phosphorylated at S421 (iv merge). Scale bar = 20 μ m.

4.4.5 Exogenous Mecp2 is highly phosphorylated at S421

Mecp2 phosphorylation at S421 is normally neuronal activity-dependent with endogenous Mecp2 showing low levels of phosphorylation at this site under basal conditions. Therefore I decided to quantify the phosphorylation level of exogenous (transgenic delivered) Mecp2 relative to the basal level of phosphorylation of endogenous Mecp2. Sections from WT brains transduced into the CA1 region with lenti-PGK-*ME1FlagRFP* were immunolabelled with Anti-pS421 and anti-Mecp2 antibodies. RFP fluorescence was used to categorize transduced and non-transduced cells (figure 4-14). Fluorescence intensity measures of the anti-pS421 immunofluorescence were used to estimate cellular levels of pS421 protein. This result shows that the cellular levels of pS421 protein in transduced cells (6.6 ± 0.44 AU fold of the endogenous levels) was significantly ($p < 0.001$, unpaired t test) higher than the endogenous level (1.0 ± 0.04 AU) in non-transduced cells (figure 4-15a). Frequency distribution of pS421 levels in non-transduced cells showed tight control (SD = 0.58 AU) whereas the levels varied in the transduced cells (SD = 5.2 AU), indicating variable and high expression levels (figure 4-15b).

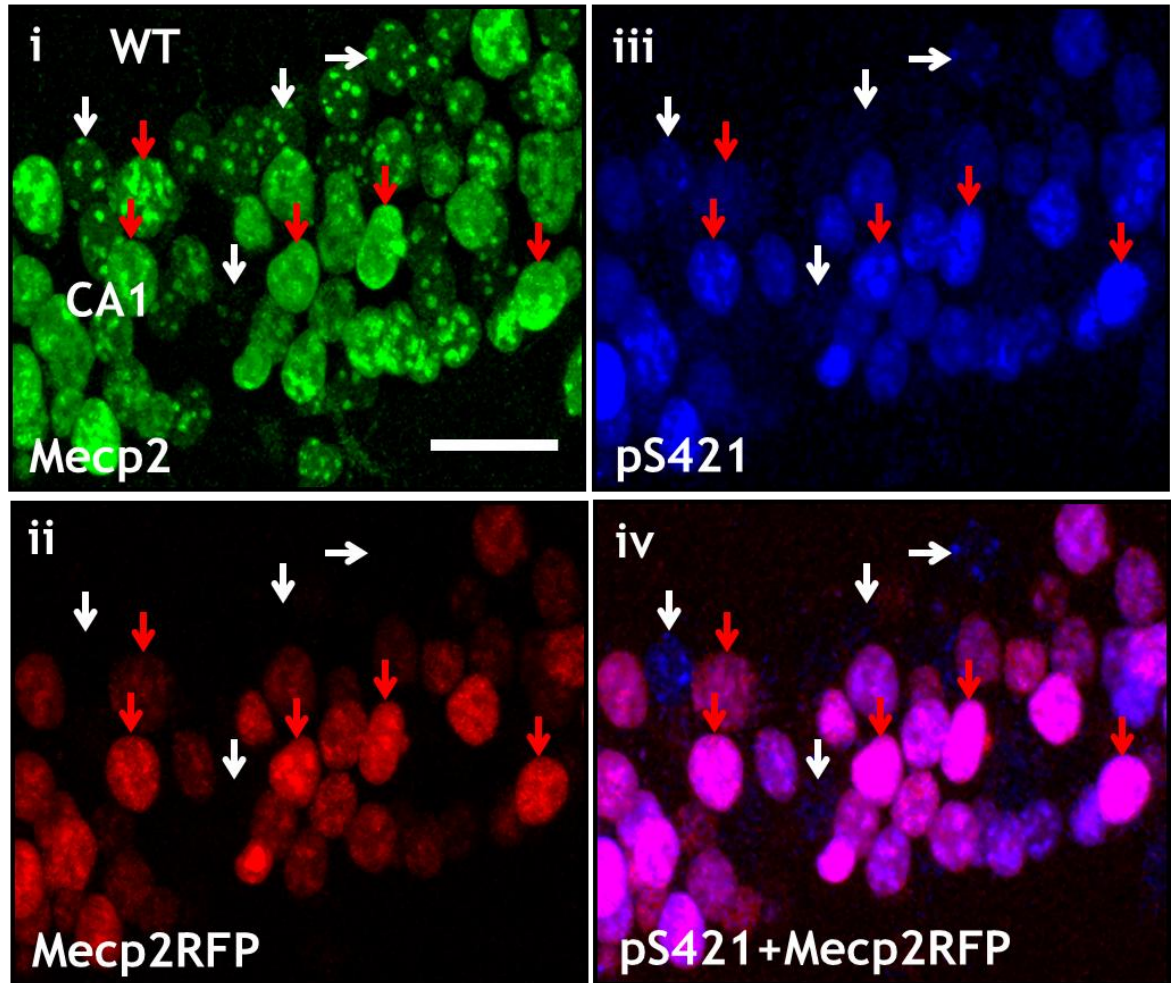


Figure 4-14 Exogenous Mecp2 expression and Mecp2-pS421 in WT mice. Micrograph showing coronal brain section taken from WT mouse 2 weeks after lenti-PGK-*ME1FlagRFP* injection into the CA1 region. Section was immunolabelled with (i) anti-Mecp2 (green), (ii) RFP fluorescence (red) was used to identify transduced cells and (iii) anti-pS421 (blue) antibodies. (iv) Merged (ii & iii) shows high anti-pS421 antibody signals in transduced cells (red arrows) relative to non-transduced cells (white arrows). Scale bar = 20 μ m.

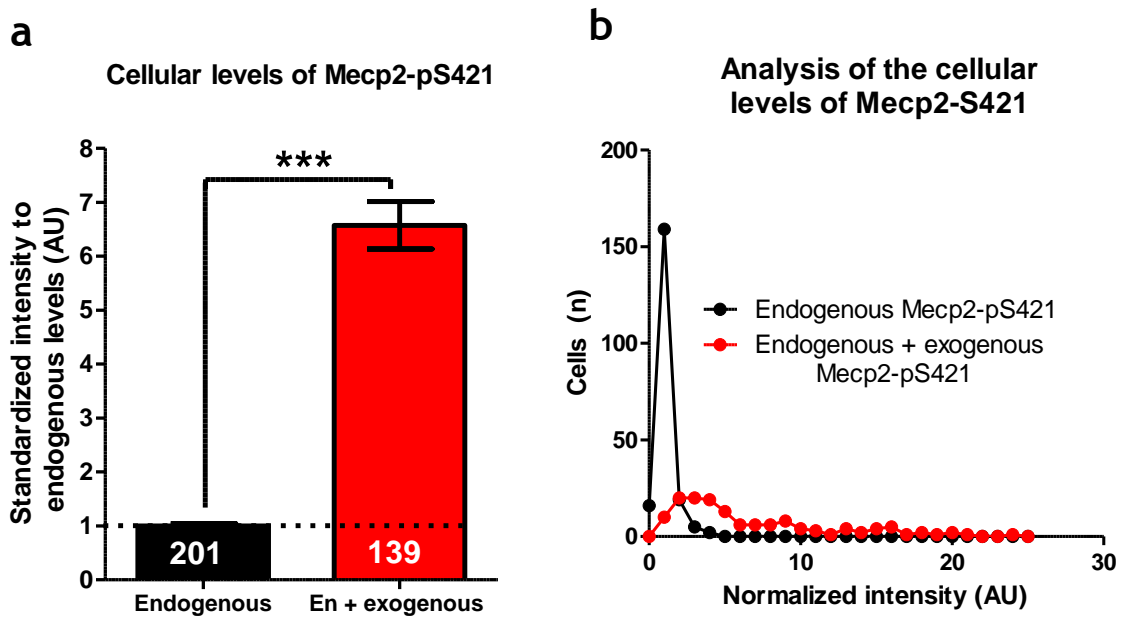


Figure 4-15 Exogenous Mecp2 expressing cells display high level of Mecp2-pS421 levels

(a) Plot showing Quantitative immunofluorescence of anti-pS421 immunofluorescence in non-transduced and transduced cells of CA1 region of the hippocampus (N = 2 mice). (b) Frequency distribution of pS421 immunofluorescence in transduced and non-transduced cells revealed closely regulated endogenous protein and extended expression range in the transduced cells. Values were standardized to the average WT (non-transduced) values and presented as mean \pm SEM. Numbers in the columns in (a) indicate the numbers of tested cells / group. *** indicates $p < 0.001$, unpaired t test. En; endogenous protein.

4.4.6 Neuronal overexpression of exogenous Mecp2 alters nuclear levels of histone 4

Previous studies have emphasized the potential interaction between Mecp2 and histones in the nucleus in both RTT patients (Wan et al., 2001) and Mecp2-null mice (Skene et al., 2010). In this study I investigated the effect of Mecp2 overexpression on the level of histone 4 (H4) and acetylated H4 (ACh4) level in CA1 region of the hippocampus of WT mice. Sections from mouse brains previously transduced with lenti-PGK-ME1FlagRFP were immunolabelled with anti-H4 and anti-ACh4 (binds to acetylated lysine residues, 5, 8, 12 and 16) antibodies. RFP fluorescence was used to identify transduced pyramidal cells. Cellular levels of ACh4 and H4 were estimated in the transduced and non-transduced cells by quantitative immunofluorescence (figure 4-16). The results show that the amount of the total H4 was significantly ($p < 0.001$, 2 way ANOVA, tukey`s posthoc pairwise comparison) reduced in the transduced cells (0.78 ± 0.014 AU, mean \pm SEM, times the endogenous level) compared to the non-

transduced cells, express endogenous level, (1.0 ± 0.01 AU, figure 4-17a). In parallel, the level of AchH4 was also significantly ($p < 0.001$, 2 way ANOVA) reduced in the transduced cells (0.79 ± 0.014 AU times the endogenous level) compared to the non-transduced cells (1.0 ± 0.01 AU, figure 4-16a). There was a positive correlation between the reduction in the level of total H4 and the AchH4 (figure 4-17b).

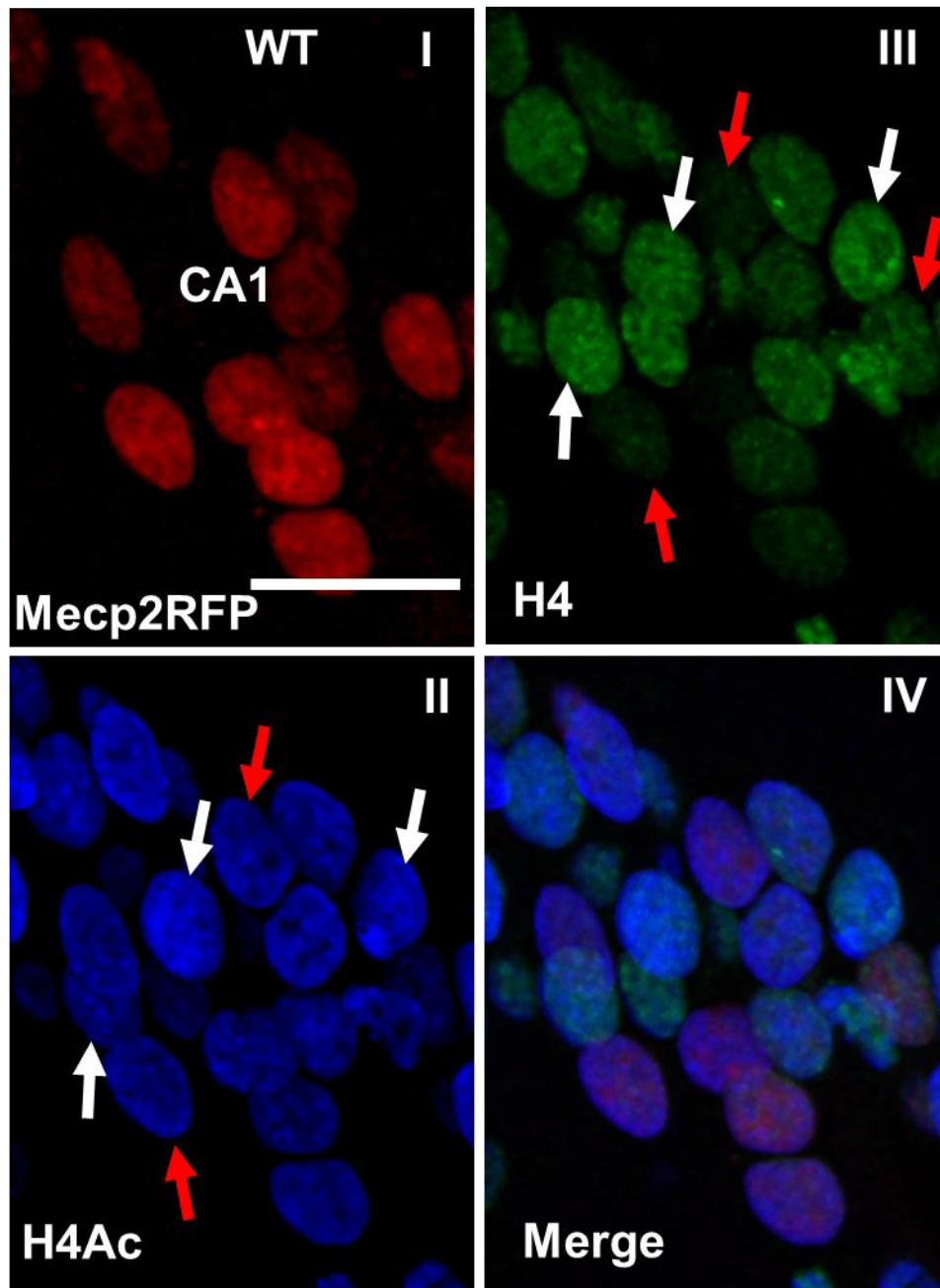
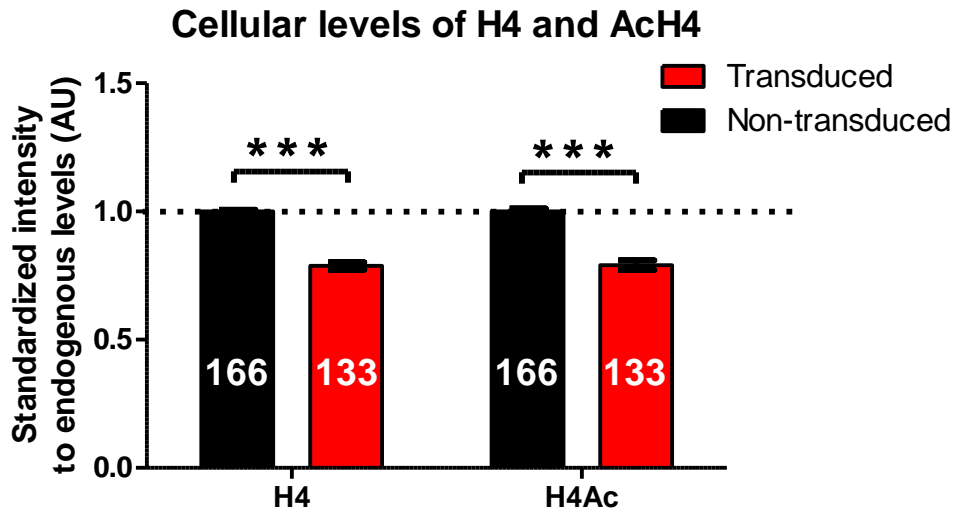


Figure 4-16 H4 and AchH4 cellular levels after Lenti-PGK-ME1-FlagRFP transduction
 Micrograph showing sections from the CA1 region of the hippocampus of WT mice (N = 2 mice) that were injected with lenti-PGK-ME1-FlagRFP at the pyramidal cell layer. Section was immunolabelled with anti-AchH4 (ii) anti-H4 (iii) antibodies whereas RFP fluorescence (i) discriminates the transduced (red arrows) and non-transduced cells (white arrows). Scale bar = 20 μ m.

a



b

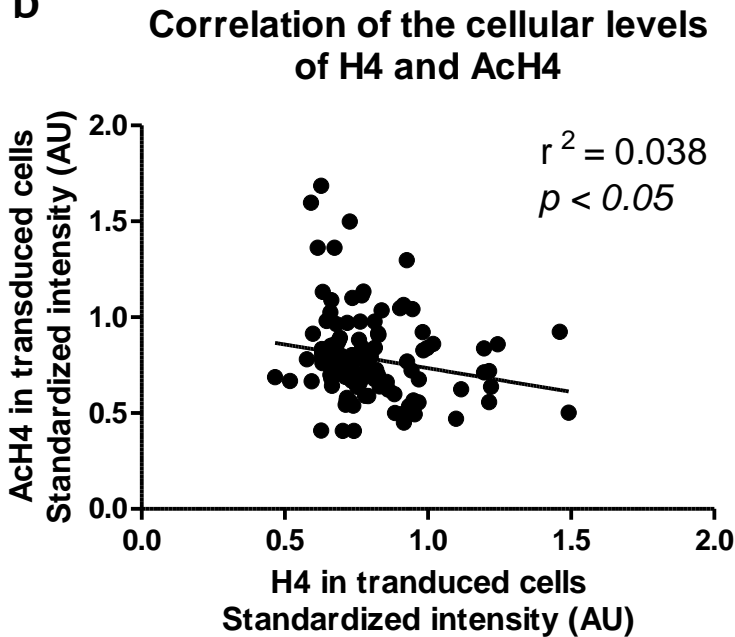


Figure 4-17 Altered cellular levels of H4 and AcH4 in *Mecp2* overexpressing pyramidal cells. (a) Plot showing the effect of exogenous *Mecp2* expression on the cellular levels of H4 and AcH4. Values are normalized to the endogenous levels (in non-transduced cells and presented as mean \pm SEM. Numbers on the columns indicate to the number of sampled cells / group. (b) Plot showing the correlation between cellular levels of H4 and AcH4 in the transduced cells. In (a) *** = $p < 0.001$, 2 way ANOVA with tukey's posthoc pairwise comparison.

4.4.7 Neonatal brain delivery of lenti-PGK-*ME1FlagRFP*

Mecp2 is globally expressed in the brain and peripheral tissue. However expression in the brain shows a special importance as brain-specific delayed activation of *Mecp2* rescued RTT-like phenotype in mouse models (Luikenhuis et

al., 2004, Giacometti et al., 2007). Stereotaxic brain injection of lenti-PGK-*ME1FlagRFP* in adult mice showed limited spread around the injection site indicating that lentivirus-mediated delivery has limited potential to deliver widespread expression of exogenous *Mecp2* in the adult mouse brain. As young animals have relatively large extracellular spaces that could allow more spread of the viral particles (Cetin et al., 2006), I therefore tested the potential of neonatal brain injection to produce a wider transgene spread across the brain. Neonatal pups (P0-2) were intracranially injected (chapter 2) with 3 μ l of 10⁸ IU/ml of lenti-PGK-*ME1FlagRFP* in each hemisphere (6 x 10⁵ IU / brain). Four weeks after injection, these mice were perfused with 4% PFA and brain sections were tested for the expression of the RFP. Serial coronal sections of the injected brains showed again that the majority of transduced cells were located very close to the ventricular wall with very limited parenchymal spread (figure 4-18).

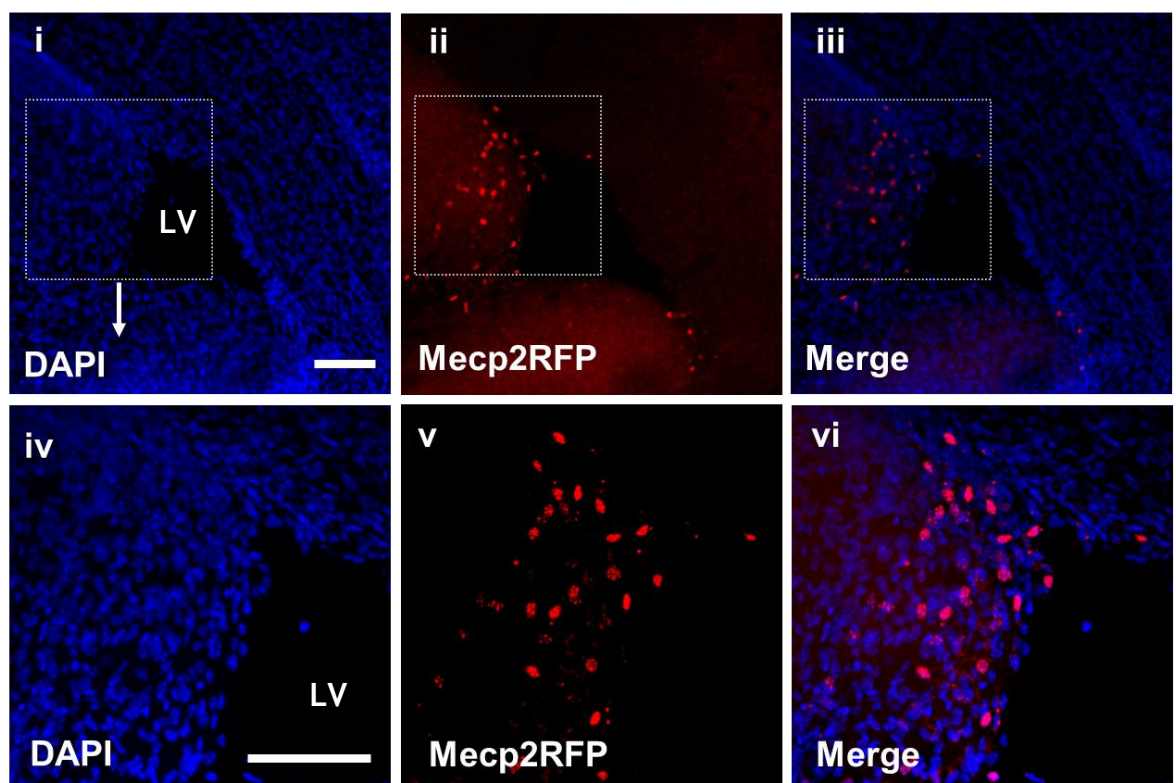


Figure 4-18 Neonatal intracranial injection of lenti-PGK-*ME1FlagRFP* resulted in limited transgene spread.

Micrograph showing the spread of exogenous *Mecp2* expression after direct brain injection in neonates. Section was stained with DAPI (i&iv) whereas RFP fluorescence was used to detect the extend of transgene expression (ii&v). (i-iii) low power image showing that the expression was confined to the wall of the ventricle with very limited parenchymal spread. box indicate high power image. (iv-vi) high power image showing the nuclear expression pattern of exogenous *Mecp2* and confirm the low transduction efficiency. LV; lateral ventricle. Scale bar = 100 μ m.

4.5 DISCUSSION

The unclear understanding of the molecular mechanism of *Mecp2* and its downstream effects make *Mecp2* replacement by gene therapy a potential therapeutic approach for Rett syndrome. However gene delivery methods as well as dosage issues are a major hindrance to this approach. Lentivirus-based vectors are a well-established and widely used system for gene delivery (Blomer et al., 1996, Azzouz et al., 2004a). Lentiviruses are particularly used because of their ability to transfect terminally differentiated neurons and provide long term stable transduction with minimal immune response stimulation (Kay et al., 2001, Li et al., 2010). In this study I have generated Lentivirus-based vectors that can drive expression of exogenous *Mecp2* *in vivo* and *in vitro* under two different promoters, the *syn1* promoter (neuron-specific) and the PGK promoter (ubiquitous). In agreement with Rastegar and colleagues (Rastegar et al., 2009), I showed that lenti-mediated exogenous *Mecp2* was targeted to the nucleus and showed a characteristic heterochromatin localization pattern similar to that of the endogenous *Mecp2* in mice (Nan et al., 1996). Exogenous *Mecp2* was mostly expressed in neurons in dissociated cell culture even under the control of the ubiquitously expressing PGK promoter. This could be explained by the natural neuronal tropism of Lentivirus (Lai and Brady, 2002) or due to a level of expression in transduced glia that was below the detectable limit (figure 4-4a). The transduced neurons expressed exogenous *Mecp2* at a relatively high level (2.5 fold) compared to glia. This expression pattern is consistent with the fact that endogenous *Mecp2* is mostly neuronal with ten times lower, however important, expression levels in glia (Ballas et al., 2009, Lioy et al., 2011) compared to neurons (Skene et al., 2010). The fact that the same vector drove different levels of exogenous *Mecp2* in neurons and glia could be partially explained by the increased multiplicity of infection in neurons due to viral neuronal tropism and partially by the difference in the transcription machinery in both populations of cells.

In vivo delivery of exogenous *Mecp2* in the hippocampus revealed nuclear targeting of the transgene with characteristic heterochromatin condensation. The transduction efficiency was high around the injection sites, however as in agreement with previous report (Brooks et al., 2002), the transgene showed limited spread from the injection sites. Large lentivirus particles (100-120 nm,

(Fleury et al., 2003) relative to the narrow extracellular space (40-60 nm, (Thorne and Nicholson, 2006) partially explain the limited spread of the transgene. The PGK promoter drove expression of exogenous *Mecp2* in neurons, mostly, and glial. Whereas, as reported before (Hioki et al., 2007), synapsin1 promoter was efficient in driving neuron-specific expression.

Endogenous *Mecp2* expression is very tightly controlled (Collins et al., 2004, Na et al., 2012) at the cellular level. Overexpression of *Mecp2* has been shown to lead to overt neurological deficits in Rett patients (Meins et al., 2005, Van Esch et al., 2005) as well as in the mouse model (Collins et al., 2004, Luikenhuis et al., 2004, Na et al., 2012). In this study I analysed the cellular expression level of exogenous *Mecp2* driven by two different promoters in the hippocampus. Synapsin1 promoter led to exogenous *Mecp2* expression levels that were very close to the physiological levels (0.8 fold of the endogenous level), whereas PGK promoter achieved a 2.2 fold of the endogenous levels. These results are particularly important in RTT females in which approximately half of the cells expressing the mutant allele (*Mecp2*-null cells) while the other half expressing the WT allele, therefore a transgene delivery strategy should be adopted to produce exogenous *Mecp2* at a therapeutic levels in the null cells without inducing overexpression toxicity in the normal cells (Zhou et al., 2006, Rastegar et al., 2009, Gadalla et al., 2011). My results suggest that *Mecp2* expression under PGK but not under synapsin1 promoter is more likely to produce an overt phenotype similar to the previously reported overexpression toxicity (Collins et al., 2004, Luikenhuis et al., 2004, Na et al., 2012). Optimizing the virus titre could help reduce the multiplicity of infection and, thus, expression levels (Wanisch and Yanez-Munoz, 2009). Combining segments from PGK promoter and syn1 promoter could help increase the expression power of syn1 promoter in a neuron-specific manner (Owens et al., 2002). Alternatively, *Mecp2* endogenous promoter (Adachi et al., 2005, Rastegar et al., 2009) or its core segment (Gray et al., 2011b) that have previously shown to recapitulate the expression pattern of endogenous *Mecp2* in neurons and glia, could potentially be used to achieve near physiological level of exogenous *Mecp2*.

Several studies have reported deficits in both short- and long-term forms of synaptic plasticity, which increase in severity as the neurological phenotype progress in *Mecp2* knockout mice (Asaka et al., 2006, Guy et al., 2007, Weng et

al., 2011). To test the ability of exogenous *Mecp2* to rescue this plasticity deficit, early symptomatic *Mecp2*^{stop/y} mice were injected with lentivirus-based vector to drive expression of *Mecp2* in the CA1 region of the hippocampus, so that plasticity at the Schaffer-collateral to CA1 pyramidal synapse could be assessed with and without the reintroduction of *Mecp2* in the postsynaptic neurons. Whilst the lenti-mediated delivery of *Mecp2* was successful, unfortunately, the injected *Mecp2*^{stop/y} mice developed a severe tail lesion and died/were culled before it was possible to investigate any functional rescue. The development of tail injury is not uncommon finding in *Mecp2* knockout mice, however its incidence increased after the stereotaxic brain injection which could be explained by an oversensitivity of *Mecp2* knockout mice to the anaesthetic or as a complication of the surgical procedures. Notably the WT mice injected with the same virus stock were normal, which indicates that virus particles are not likely to be involved in the etiology of this problem.

Neuronal nuclear volume measures within the CA1 region of the hippocampus revealed clear cellular changes in *Mecp2*^{stop/y} cells after exogenous *Mecp2* expression. The significant reduction in neuronal nuclear size has been reported previously (Giacometti et al., 2007, Johnson et al., 2011) and my results show that these morphological deficits are effectively normalized (comparable to WT) by reintroducing exogenous *Mecp2*. Interestingly the WT pyramidal cells transduced with exogenous *Mecp2* showed a modest increase in the nuclear volume compared to the non-transduced cells. Nuclear volume deficit in the *Mecp2*^{stop/y} cells could be explained by the fact that *Mecp2* is one of the most abundant nuclear proteins (Nan et al., 1997, Skene et al., 2010) so its absence could lead to volume shrinkage of the nuclei. Another possibility is that absence of *Mecp2* negatively affect normal cell growth and maturation which could be reflected as a smaller nuclear volume especially with the evidenced relationship between nuclear volume and overall soma size (Ledda et al., 2000). Exogenous *Mecp2* probably rescued the nuclear volume deficits by replacing absent nuclear protein and by enhancing cellular growth and maturation of the transduced neurons. The functional consequences of this volume changes needs to be investigated. However a recent report suggests that restoration of neuronal soma size due to *Mecp2* delayed activation is mirrored by changes in dendritic architectures and complexity (Robinson et al., 2012).

Mecp2 acts as a transcriptional repressor (Nan et al., 1997) and/or activator (Chahrour et al., 2008). The exact interaction of Mecp2 with the chromatin structures is not fully elucidated. Mecp2 is believed to bind specifically to the methylated CpG dinucleotide within the promoter regions of variety of genes (Nan et al., 1997, Skene et al., 2010). Upon neuronal induced activity Mecp2 was originally described to become phosphorylated at Serine 421 and subsequently detach from the promoter binding sites to allow downstream expression of genes (Chen et al., 2003a, Martinowich et al., 2003, Zhou et al., 2006). More recent studies from the same authors shows phosphorylation of Mecp2 at S421 rather acts as a global remodeling of the neuronal chromatin in response to neuronal activity (Cohen et al., 2011). Taken together with the fact that Mouse models with mutant S421 (A421) displayed cognitive impairments (Cohen et al., 2011), it was important to test the ability of the exogenous Mecp2 to maintain the appropriate phosphorylation regulation at S421. These results showed that the exogenous Mecp2 becomes phosphorylated at the S421 in the transduced cells in the *Mecp2*^{stop/y} mice under basal conditions. Zhou and colleagues reported phosphorylation of exogenous Mecp2 in organotypic slice culture after lenti-Mecp2 vector transfection, however this phosphorylation was induced either by membrane depolarization or glutamate application (Zhou et al., 2006). To validate the presence of basal level of S421 phosphorylation, lenti-PGK-*ME1FlagRFP* transduced WT mice were used to estimate the S421 phosphorylation level in non-transduced (basal) and transduced cells. My data shows that there is a detectable level of S421 phosphorylation at the basal level with the cells expressing exogenous Mecp2 displaying ~ 5.5 folds of the endogenous levels in non-transduced cells. The increased level of Mecp2 phosphorylation at S421 in the transduced cells could be explained by; (1) an overall increase in cellular levels of Mecp2 (by exogenous Mecp2), (2) transduced cells might become electrically more active compared to the non-transduced cells which could lead to more activity induced phosphorylation, (3) altered sensitivity of exogenous Mecp2 to neuronal activity and Ca⁺² signaling. However the effect of this increased phosphorylation on the neuronal morphology and function necessitates further investigation.

Previous studies have highlighted the potential effect of lacking Mecp2 on other nuclear proteins, particularly histone deacetylase (HDAC)-containing complexes

(Nan et al., 1998). *In vitro* studies showed that Mecp2 and histone1(H1) have the same pattern of distribution across the neuronal genome (Nan et al., 1997, Ghosh et al., 2010) with potential competition for the same binding sites as indicated by upregulated H1 levels (doubled) in the brain of Mecp2 knockout mice (Nan et al., 1997, Ghosh et al., 2010). Further effect of Mecp2 on the acetylation state of histone 3 (Shahbazian et al., 2002a, Skene et al., 2010) and histone 4 (Wan et al., 2001) has been reported. These data support the notion that Mecp2 is working as chromatin remodeling protein in addition to acting as a transcriptional regulator (Skene et al., 2010, Cohen et al., 2011). However the effect of Mecp2 was only investigated with regards to the acetylated forms of both H3 and H4 so it was unclear whether the increased acetylation status was due to an overall increase in the H3 and H4 levels or was a genuine increase in the acetylation process without affecting the total level of these proteins. I decided to address this question in the model of *in vivo* Mecp2 over-expression after lenti-PGK-ME1FlagRFP transduction in the CA1 region of the hippocampus of WT mice. My data shows that the cellular level of acetylated H4 (AcH4) was significantly decreased in cells over-expressing Mecp2 (transduced) which fits well with the previous report that showed hyperacetylation of H4 in the absence of Mecp2 in human (Wan et al., 2001), however quantification of the total H4 in the transduced cells displayed significant reduction in cellular level of H4 compared to the non-transduced cells. The reduction in the level of AcH4 was positively correlated to the reduction in the level of total H4 level. The parallel reduction in the cellular level of AcH4 in transduced cells shows that this reduction could be due to reduction in the total H4 level without altering the acetylation status of H4 protein. It also argues that the previous report of hyperacetylated H4 in cells lacking Mecp2 is probably due to increased level of H4 rather a genuine change of the acetylation condition. Identification of Mecp2 as a component/modulator of neuronal chromatin with various interactions with histone proteins highlights the potential benefits of chromatin modulator drugs in the treatment of RTT syndrome.

Lenti-mediated exogenous Mecp2 delivery by stereotaxic injection in the adult mouse brain displayed a limited spread around the injection sites (Blomer et al., 1997, Brooks et al., 2002). Mecp2 is globally expressed in the brain (Nan et al., 1997) and any attempt to rescue the RTT-like phenotype should produce

exogenous *Mecp2* in a reasonably high proportion of brain cells. Previous reports have described different methods to enhance lentivirus-mediated gene delivery to the CNS after peripheral administration, therefore I tried different methods to augment *Mecp2* delivery to the CNS by using lentivirus-based vectors. Firstly I tried delivery of lenti-syn1-*ME1FlagRFP* by intravenous injection in the tail vein of adult mice after the BBB was distributed by Mannitol injection (Ikeda et al., 2002, McCarty et al., 2009). Analysis of the brain tissue after 4 weeks of injection showed absence of RFP or anti-Flag immunofluorescence in different brain regions suggesting that lentivirus-based vector is not able to achieve brain transduction after peripheral injection. Secondly, lentivirus particles were pseudo-typed with rabies virus glycoprotein coat to enable retrograde transport to the CNS after peripheral intramuscular injection (Mentis et al., 2006, Federici et al., 2009). Despite achieving transgene expression in cultured neurons using lentivirus pseudotyped with the rabies coat, several attempts to deliver *Mecp2* under either syn1 or PGK promoter to the CNS via IM injection of this vector were not successful. Previous reports have shown that extracellular space is relatively larger in young animals compared to the adults, which could allow a better spread of viral particles in the brain parenchyma (Cetin et al., 2006), therefore I finally injected neonatal mice intracranially with lentivirus particles to enhance transgene spread in the brain. RFP fluorescence was detected in the brain after 4 weeks of injection but the transgene showed a limited spread in the brain parenchyma.

In this chapter I have provided an overview of the potentials of lentivirus-based vector approach in examining aspect of RTT pathology/rescue in *Mecp2* knockout mice. Despite failure to investigate functional rescue, however, at the cellular level it helps study the molecular function of *Mecp2* and its interaction with different nuclear proteins. Targeted expression of lenti-mediated exogenous *Mecp2* expression in CA1 region of the hippocampus of *Mecp2*-null mice rescued neuron nuclear volume deficits to a WT level. Lentiviruses also provide an easy *Mecp2* overexpression model to study the overexpression threshold without the need for generation of very sophisticated transgenic animal models. It could also be used to target *Mecp2* to specific brain regions in the *Mecp2* knockout mice (e.g. breathing centre and striatum (Kosai, 2005) in order to evaluate the potential for reversal of particular aspects of the RTT phenotype such as

respiratory or motor abnormalities. Thus whilst lentivirus-based vectors fulfil some of the necessary aspects of a viable gene therapy vector in RTT-gene therapy, the usefulness is restricted by the limited spread of Lentivirus in brain tissue compared to the global expression of *Mecp2*, makes Lentivirus based vectors inappropriate for seeking phenotype prevention/recovery which will require a vector with very high transduction efficiency and extended spread capabilities such as Adeno-associated virus-based vectors. The potential of these vectors in RTT-gene therapy will be addressed in detail in the next chapter.

Chapter 5

Improved Survival and Reduced Phenotypic Severity Following AAV9/*MECP2* Gene Transfer to Neonatal Male *Mecp2* Knockout Mice

5.1 Introduction

The genotype-phenotype pathway in RTT remains elusive and in the absence of a well-characterized set of downstream targets based on a known mechanism for MeCP2 action, a therapeutic strategy targeting the underlying causes of RTT more directly represents an attractive way forward. While there are multiple challenges facing its application in the clinical arena, gene-replacement therapy is a potential future treatment option for RTT patients, as postnatal activation of *Mecp2* in mice has been shown to lead to an improved phenotype (Luikenhuis et al., 2004, Giacometti et al., 2007, Guy et al., 2007) thus demonstrating that aspects of the disorder may be reversible and potentially preventable if early treatment can be instigated (Cobb et al., 2010, Gadalla et al., 2011).

MECP2 is expressed widely throughout the body but at particularly high levels in post-mitotic central nervous system (CNS) neurons postnatally (LaSalle et al., 2001, Shahbazian et al., 2002b, Zhou et al., 2006), and it has been demonstrated that activation of conditionally silent *Mecp2* only in specific populations of cells in the brain of *Mecp2*-null mice results in restoration of a broadly normal phenotype (Luikenhuis et al., 2004, Lioy et al., 2011). However, deletion of *Mecp2* in adult mice produces RTT-like phenotypes suggesting a persistent role of MeCP2 in adult neuronal function and a requirement for enduring expression on any therapeutic transgene (McGraw et al., 2011). It will thus be necessary for gene therapy approaches in RTT both to achieve widespread CNS delivery of a functional copy of *MECP2* and to maintain long-term expression (McGraw et al., 2011).

The lentivirus-based approach was able to drive expression of exogenous *Mecp2* in neurons (chapter 4), however the limited spread of the transgene observed

after *in vivo* injection of lentivirus in the brain of adult as well as neonatal mice impedes its application for global *Mecp2* expression. In contrast recombinant adeno-associated virus (AAV) pseudotyped with capsid 9 (AAV serotype 9) is particularly important because of its ability to spread widely and to cross the blood brain barrier and its high neuronal tropism especially after neonatal injection (Foust et al., 2009). AAV has been used in research and clinical gene-delivery studies primarily because it transduces non-dividing cells and confers stable gene expression (Arruda et al., 2005, Foust et al., 2009) without associated inflammation or toxicity.

5.2 Study aims

The main aim of the work described in the chapter was to assess the ability of ssAAV9-based vector to deliver *MECP2* to the *Mecp2*^{-/-} mouse brain. This work also extended to evaluate the effect of exogenous MeCP2 on RTT-like phenotypes at the cellular and organismal levels. The specific objectives of this study are:

- ❖ To test the ability of AAV9/*MECP2* virus particles to drive widespread expression of MeCP2 in the brain after direct brain injection in neonatal mice.
- ❖ To test the cellular level of exogenous MeCP2 in the transduced cells.
- ❖ To detect possible changes (improvement) in RTT-like phenotypes after early postnatal AAV9 mediated delivery of human *MECP2* in *Mecp2*-null mice.

5.3 Methods

To test the potential of Adeno-associated virus to deliver *MECP2* to the mouse brain, human *MECP2_e1* isoform coding sequences carrying a C-terminal Myc-tag was cloned into an adeno-associated virus 2 vector backbone and produced AAV particles with capsid 9 (AAV2/9) under the chicken beta actin (CBA) promoter (this construct hereafter referred to as AAV9/*MECP2*; figure 5-1a). ssAAV9/*GFP* vector was also generated to be used as a control.

To achieve high neuronal transduction of exogenous *MECP2* in mouse brain, a total of 6 μl of 8×10^{12} vector genome/ml was directly injected into the brain of male neonatal (P0-2) WT and *Mecp2*^{-y} mice.

The effect of exogenous *MECP2* on the organismal level was carried out by weekly (figure 5-1b) evaluating the disease progression using the RTT-like phenotype severity score.

Further assessment of motor (open field and treadmill test) and breathing (whole body plethysmograph) phenotypes were carried out between 8-11 weeks post injection (chapter 2).

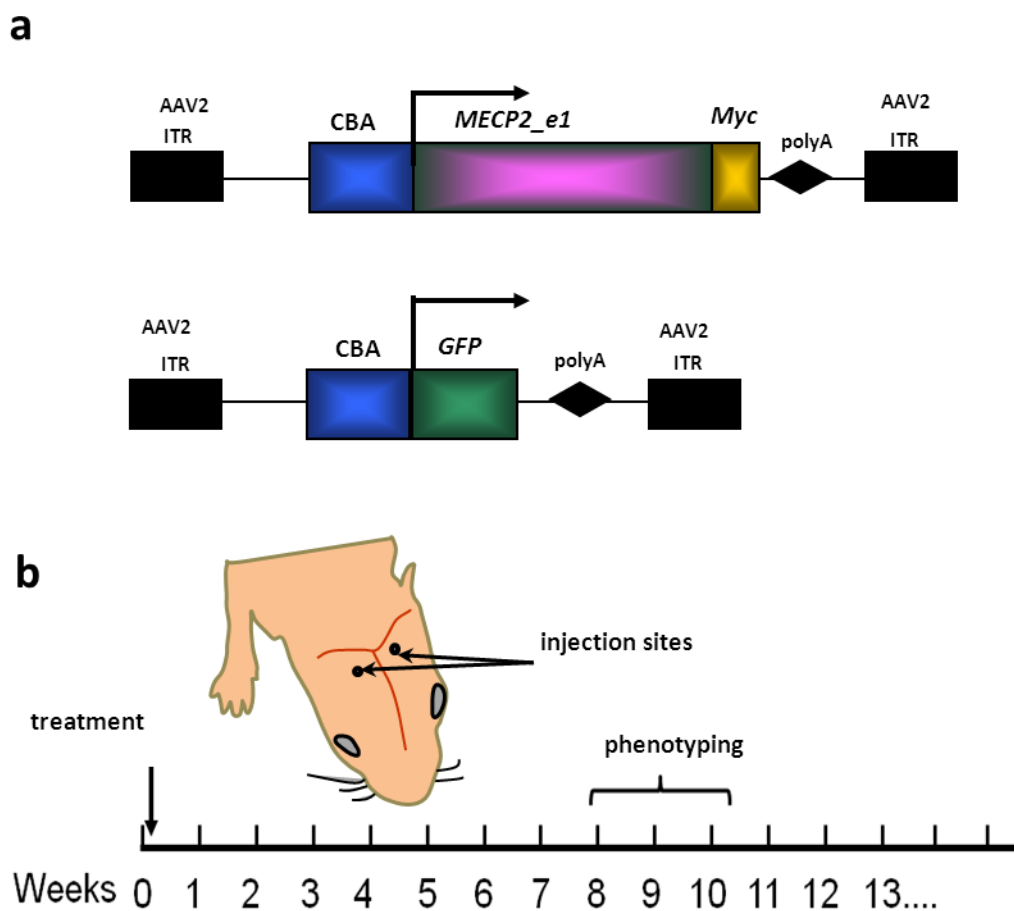


Figure 5-1 AAV vector-constructs and the experimental plan
(a) *MECP2_e1/Myc* fusion and *GFP* (control) constructs were cloned into AAV2 backbones under the control of CBA promoter. **(b)** Experimental plan in which male WT or *Mecp2*^{-y} mice were injected intracranially with AAV9/*MECP2* or AAV9/*GFP* at P0-2, scored for the progression of RTT-like signs from 3 weeks onwards and phenotyped quantitatively at weeks 8-11. PolyA; SV40 polyadenylation signal, CBA; chicken beta actin, ITR; inverted terminal repeat.

5.4 Results

5.4.1 Confirmation of genotypes in *Mecp2*-null mouse colony by PCR

To discriminate between *Mecp2*-null and WT allele, primers were used to amplify a 416 bp PCR product from WT allele (primers P5/P7) and a 470 bp product from *Mecp2*-null allele (primers P5/P6) (Guy et al., 2001). Ear samples from all mice were collected after weaning and genomic DNA was extracted and subjected to the previously described genotype protocol (chapter 2). Agarose gel electrophoreses (figure 5-3) was used to identify each mouse genotype (table 5-1). Two set of PCR reactions were carried out for each genomic DNA sample; the first is to detect the *Mecp2*-WT allele and the second is to detect the *Mecp2*-null allele. WT (male and female) and *Mecp2*-null mice display only one band with their corresponding reaction whereas the heterozygous females display PCR products with both reactions because female mice have both *Mecp2*-WT and *Mecp2*-Null alleles.

Table 5-1 Identification of mice genotype by PCR reaction

	Genotype	P5/P7 (WT allele)	P5/P6 (null allele)
Heterozygous female	<i>Mecp2</i> ^{+/-}	Positive	Positive
WT female	<i>Mecp2</i> ^{+/+}	Positive	Negative
Hemizygous male	<i>Mecp2</i> ^{+y}	Negative	Positive
WT male	<i>Mecp2</i> ^{+y}	Positive	Negative

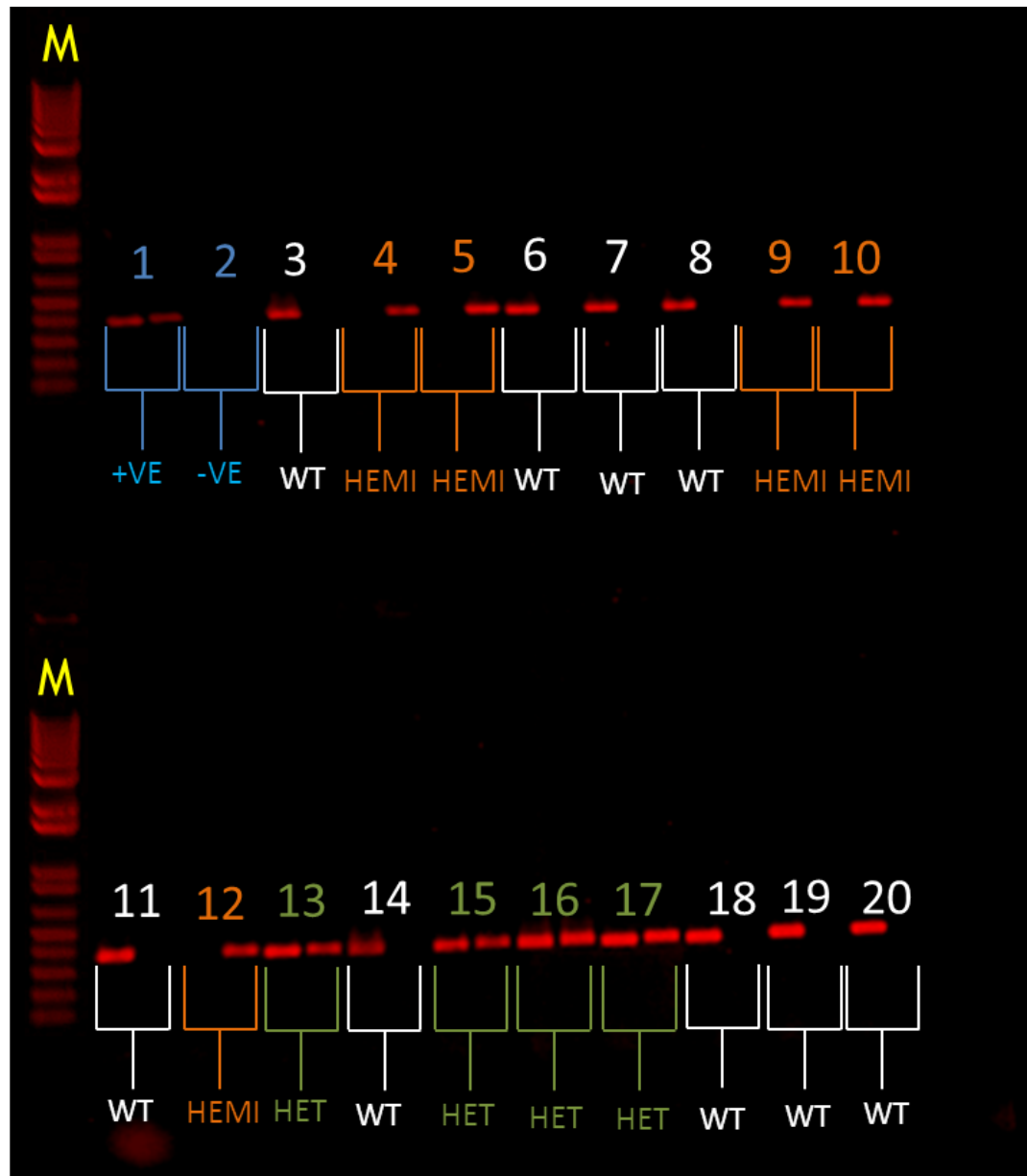


Figure 5-2 PCR identification of mice genotype

Representative gel image showing the PCR verification of mouse genotypes. Genomic DNA from heterozygous female was used as a template for a positive control PCR reaction (no.1) whereas PCR reactions without DNA template were used as a negative control (no.2). Each mouse genomic DNA has two sets of PCR reactions; the first reaction detects the WT allele and the second reaction detects *Mecp2*-null allele. Samples showing PCR bands on their first reaction are either WT males, e.g. no. 3&6, or WT females, e.g. no. 14&18 (white colour). Samples showing PCR bands on their second reaction are hemizygous males (orange colour). Finally samples showing 2 PCR bands in both PCR reactions are heterozygous females (green colours). M; 100bp DNA ladder.

5.4.2 Neonatal CNS injection of AAV9/*MECP2* resulted in widespread brain expression of MeCP2

To test the ability of AAV9 vector to deliver exogenous *MECP2* into the mouse brain, a WT mouse was perfused 12 weeks post-injection of AAV9/*MECP2* and brain parasagittal sections were immunolabelled with anti-Myc and anti-NeuN antibodies. Scanning different brain regions for exogenous MeCP2 expression

showed that the transgene (Myc-positive cells) was widely expressed across the brain (figure 5-3a). The expression of exogenous MeCP2 was mainly detected in NeuN -immunopositive cells in different brain regions suggesting putative neuronal expression (figure 5-3b-d).

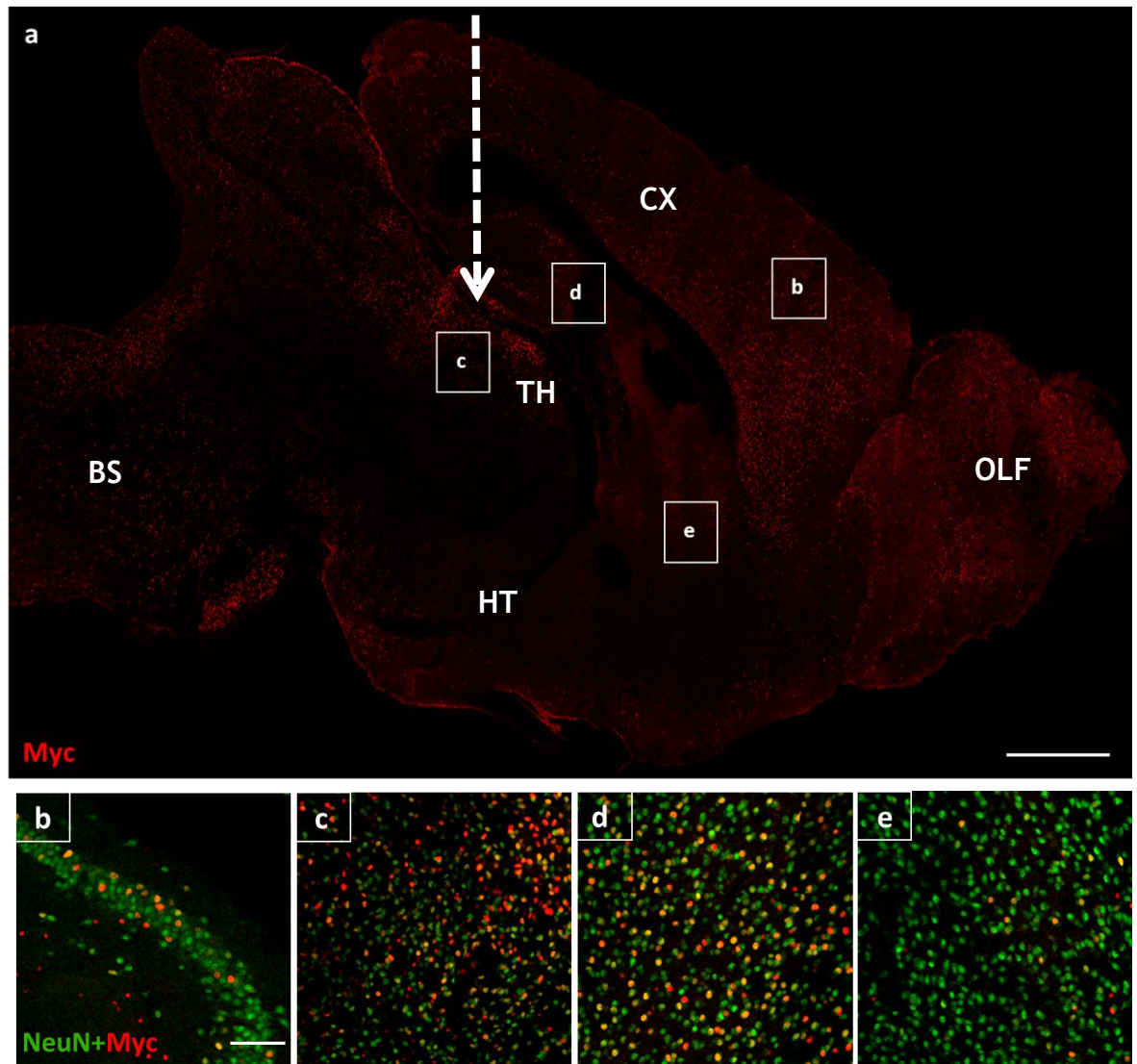


Figure 5-3 Widespread expression of exogenous MeCP2 across the brain following neonatal IC injection of ssAAV9/MECP2.

Representative micrograph (whole brain, parasagittal section) showing the distribution of transgene expression in a 12 week old WT mouse following bilateral brain injection. White dashed arrow indicates approximate injection site. (b) Higher power micrographs corresponding to boxes in (a) showing anti-Myc (transduced cells) and NeuN-immunolabelled cell populations. b; motor cortex, c; hypothalamus, d; hippocampus and e; striatum. Scale bars in (a) = 1mm and in (b) = 100 μ m. NeuN; neuronal nuclei antigen (Rbfox3), OLF; olfactory bulb, TH; thalamus, HT; hypothalamus, CX; cortex, BS; brainstem.

To measure the transduction efficiency across the brain, mice were perfused and brain coronal sections were immunolabelled with anti-Myc and anti-NeuN antibodies and stained with DAPI. The number of Myc-immunopositive cells DAPI-stained nuclei were counted in 18 random fields for each brain region (N = 4 mice) in different brain regions (figure 5-4a). The transduction efficiency varied between brain areas with the highest transduction efficiency observed in the hypothalamus (41.5 ± 11.3 % of all cells) and in the thalamus (37.2 ± 6.3 % of cells) and with the lowest efficiency seen in the striatum (6.8 ± 2.3 % of cells, figure 5-4b). High power images showed that the transgene was mostly expressed in neurons which represented 67 ± 11.8 % to 98 ± 0.8 % of all transduced cells indicating high transduction and/or expression in neuronal populations. In contrast, the proportion of transgene-expressing cells immunonegative for NeuN (presumed mostly to represent glia) was modest (range 0.5 - 6.0% of all transduced cells, figure 5-4b).

5.4.3 Neonatal CNS injection of AAV9/MECP2 resulted in spinal cord and liver expression of the exogenous MeCP2

I previously showed in (figure 5-4) the widespread transduction of AAV9/MECP2 throughout the brain after direct intracranial injection in neonatal mice. To test the ability of this virus to spread to the spinal cord, transverse sections were prepared from the lumbar spine and immunolabelled with anti-Myc and anti-Choline acetyl transferase (ChAT), a lower motor neuron marker, antibodies. Myc-immunopositive cells were observed in the lumbar section indicating the ability of AAV9/MECP2 to deliver expression to the spinal cord after direct brain injection. Co-labelling with anti-ChAT showed that the transgene was expressed in the lower motor neurons (figure 5-5a). I also asked whether AAV9 virus has the ability to transduce peripheral organs after direct brain injection. To answer this question, frozen sections from the liver were prepared and immunolabelled with anti-Myc antibody and DAPI. Interestingly, Myc-immunopositive cells that co-localized with DAPI were detected in the liver indicating extended spread properties of AAV9 to the peripheral organs after direct brain injection (figure 5-5b).

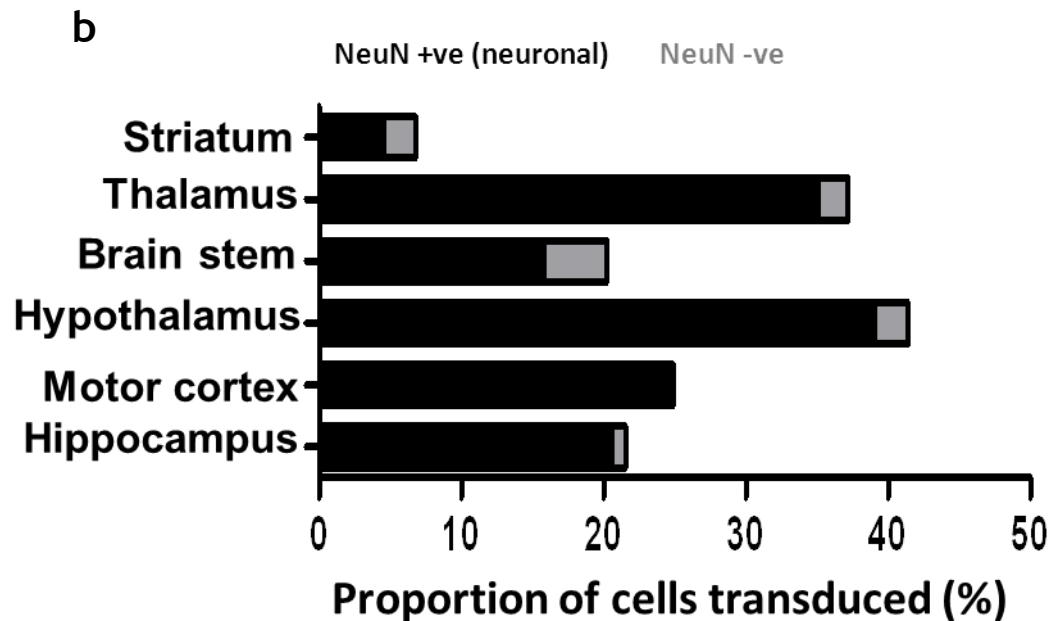
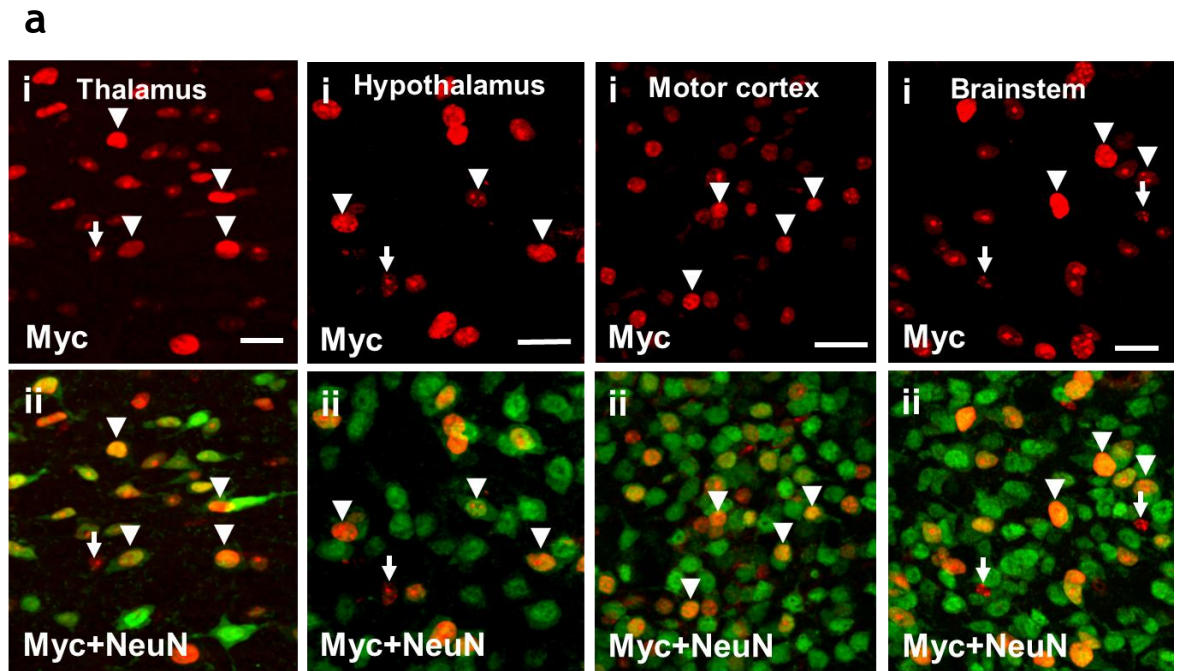


Figure 5-4 IC injection of AAV9/*MECP2* in neonatal mice produced high transduction efficiency across the brain.

(a) Micrographs showing brain coronal sections, that were immunolabelled with (a-i) anti-Myc antibody and (a-ii) anti-NeuN antibody. Exogenous MeCP2 expression was detected across the brain with high transduction efficiency in the NeuN-immunopositive cell population. (b) Quantification of the numbers of Myc-immunopositive cells (transduced) relative to the numbers of DAPI stained nuclei in different brain regions (N = 4 mice). The highest transduction efficiency was observed in the hypothalamus whereas the lowest transduction efficiency was observed in the striatum. Data is represented as mean \pm SEM. Scale bar in (a) = 20 μ m.

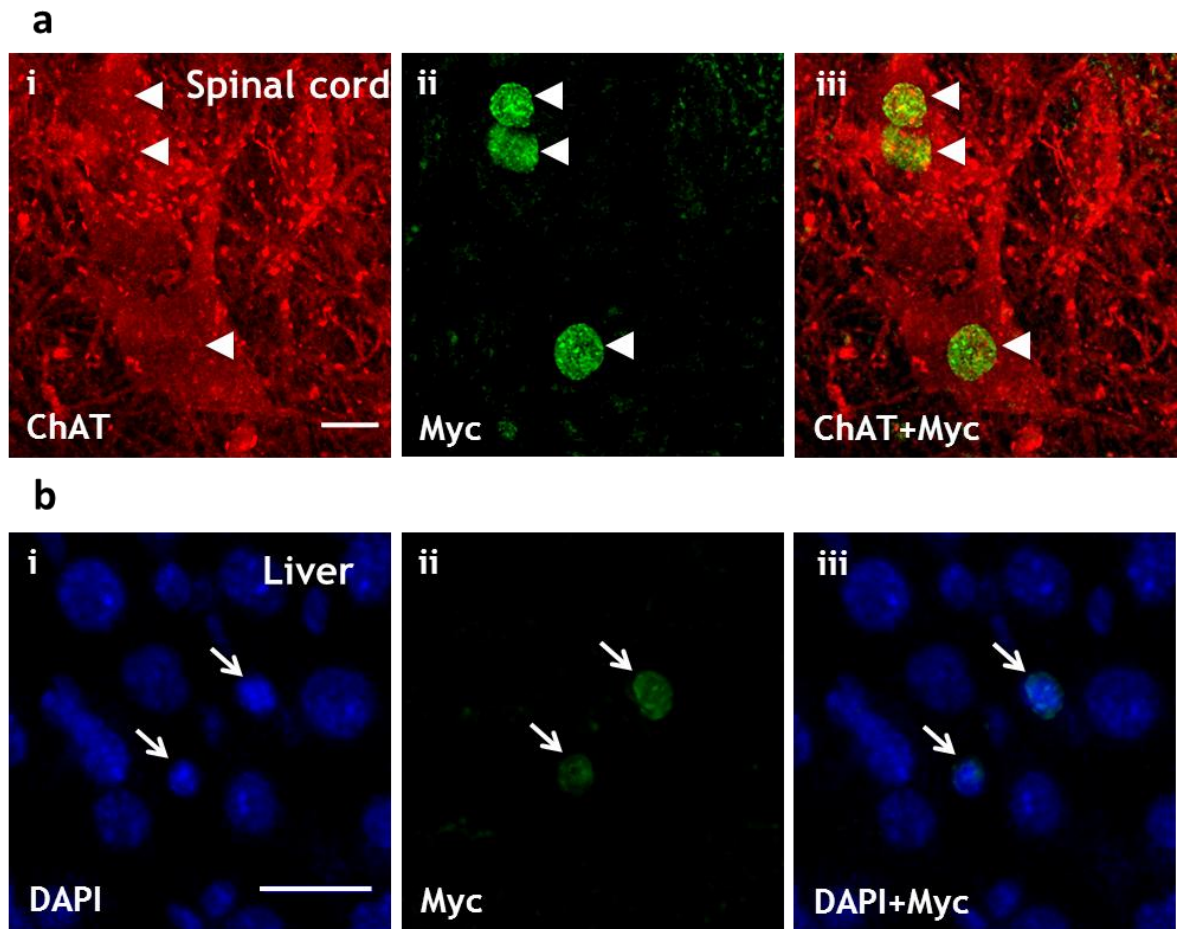


Figure 5-5 IC injection of AAV9/*MECP2* into neonatal mice led to widespread spinal cord and liver transduction.

(a) Representative images from the lumbar region of the spinal cord after direct brain injection of AAV9/*MECP2* in neonatal mice. Sections were immunolabelled with (i) anti-ChAT and (ii) anti-Myc antibodies. (iii) Merge of (i) and (ii). Arrowheads indicate expression of exogenous MeCP2 in the lower motor neurons as shown by the co-localization between Myc-immunopositive and ChAT-immunopositive cells. (b) Micrograph of a liver section taken from a mouse that was injected with AAV9/*MECP2* directly into the brain. Section was stained with (i) DAPI and (ii) anti-Myc antibody. (iii) Merge of (i) and (ii). Arrows indicate expression of exogenous MeCP2 in the liver. Scale bars = 10 μ m. ChAT; Choline Acetyl Transferase.

5.4.4 Neonatal brain injection of AAV9/*MECP2* resulted in MeCP2 expression at near-physiological cellular levels

Maintaining the normal cellular level of MeCP2 has become considered to be crucial for normal function as overexpression of *Mecp2* has a moderate phenotype in mice (Luikenhuis et al., 2004) and human chromosome Xq28 duplications involving *MECP2* result in a pronounced clinical phenotype (Meins et al., 2005, Van Esch et al., 2005). Therefore, to quantify the cellular level of the transgene product and relate this to endogenous MeCP2 levels, WT mice were injected postnatally (P0-2) with AAV9/*MECP2* and the resultant transgene product assessed by quantitative immunofluorescence after 12 weeks. Brain (N =

4) coronal sections were immunolabelled with anti-Myc and anti-MeCP2 (detect both endogenous and exogenous MeCP2 protein) antibodies. Analysis of MeCP2 immunofluorescence intensity in principal cells within hippocampal area CA3 (figure 5-6a) showed that the cellular levels of MeCP2 in transduced cells was 2.4 ± 0.08 AU (mean \pm SEM, N = 220 sampled cells) times the endogenous levels in non-transduced cells (1 ± 0.01 AU, N = 285 sampled cells). In layer V of primary motor cortex, the cellular level of MeCP2 in transduced cells was 2.05 ± 0.04 AU (N = 307 sampled cells) times the endogenous level in the non-transduced cells (1 ± 0.01 AU, N = 281 sampled cells). This data suggests that the exogenously-derived MeCP2 was being expressed at approximately 1-1.25 times the endogenous levels (figure 5-6b). Analysis of MeCP2 expression levels in the motor cortex (measured as immunofluorescence intensity) in transduced and non-transduced cells (N = 4 brains) revealed endogenous MeCP2 levels to be tightly regulated (narrow peak, SD = 0.1), while levels in transduced cells were higher and more broadly distributed (SD = 0.6, figure 5-6c).

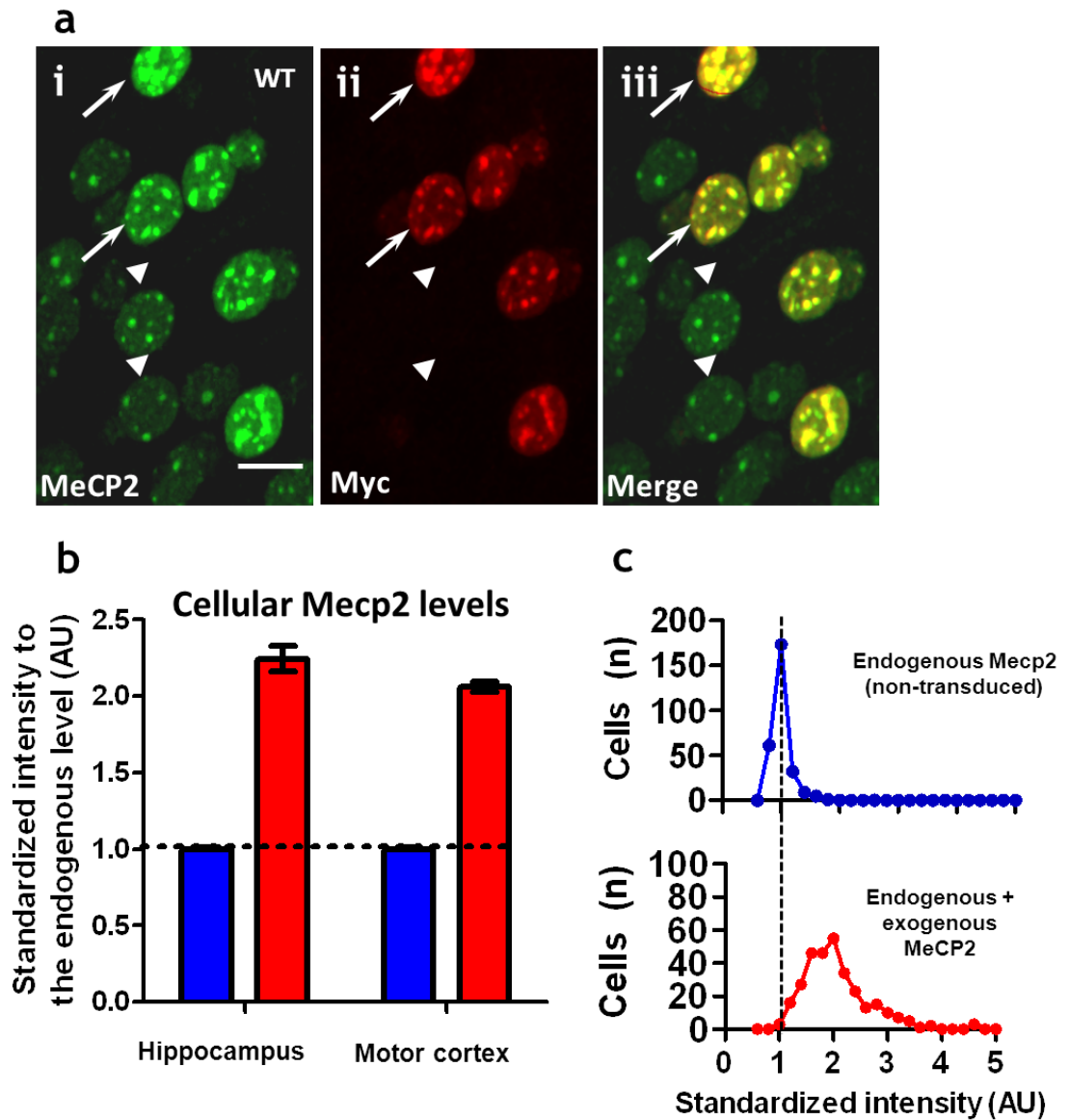


Figure 5-6 IC injection of AAV9/*MECP2* into neonatal mice produced exogenous MeCP2 levels close to that of the endogenous protein.

(a) Micrograph showing brain coronal section of 12 week old WT mouse that was injected at P0-2 with ssAAV9/*MECP2*. Section was immunolabelled with (i) anti-Mecp2 antibody and (ii) anti-Myc antibody. (iii) Merge of (i) and (ii). Arrows indicate transduced cells (express endogenous and exogenous MeCP2) whereas arrowheads indicate non-transduced cells (express endogenous MeCP2) in the CA3 region of the hippocampus. (b) Plot showing intensity measures of the anti-MeCP2 immunofluorescence in transduced and non-transduced cells in the (CA3) region of the hippocampus and in the primary motor cortex. (c) Distribution of MeCP2 levels (immunofluorescence intensity) in transduced and non-transduced cells of the primary motor cortex (N = 4 mice). Analysis revealed endogenous MeCP2 levels to be tightly regulated (narrow peak) while levels in transduced cells showed a broader and positively shifted distribution. Data is represented as mean \pm SEM. Scale bar in (a) = 10 μ m. AU; arbitrary units.

5.4.5 AAV9-mediated neonatal delivery of *MECP2* improved RTT-like phenotypes in *Mecp2*-null mice

To establish whether AAV-mediated gene delivery of *MECP2* can improve and/or prevent development of the RTT-like phenotype, *Mecp2*-null and corresponding WT littermate mice were injected intracerebrally at an early postnatal time point (P0/P2) with either AAV9/*MECP2* or AAV9/*GFP* (as a non-therapeutic control) and monitored over a 30 week experimental period. Weekly monitoring of these mice for overt RTT-like features using an established observational scoring system (Guy et al., 2007, Liroy et al., 2011, Weng et al., 2011) was carried out (figure 5-7). AAV9/*GFP* control-injected *Mecp2*-null mice showed the expected phenotype with motor/activity and other deficits apparent at 3 weeks and a steep increase in phenotype severity score over the subsequent weeks. In contrast AAV9/*MECP2*-treated null mice exhibited slower progression of the phenotype, whose mean severity reached a peak around 14 weeks and then decreased towards WT values. This decrease was in part due to sudden death in the most severely phenotypic mice, but also in part due to the lower and/or improving phenotype score in the longest-lived mice. There was no difference in severity score between WT mice injected with AAV9/*MECP2* and those injected with AAV9/*GFP* and scores in these two groups did not change significantly over the course of the study. It should be noted that the downward trajectory of severity in the AAV9/*GFP* control-injected *Mecp2*-null mice at 12 weeks is largely a result of the death of the most severely affected animals reducing the mean severity in the survivors rather than a tendency for the phenotype severity to peak and then reduce.

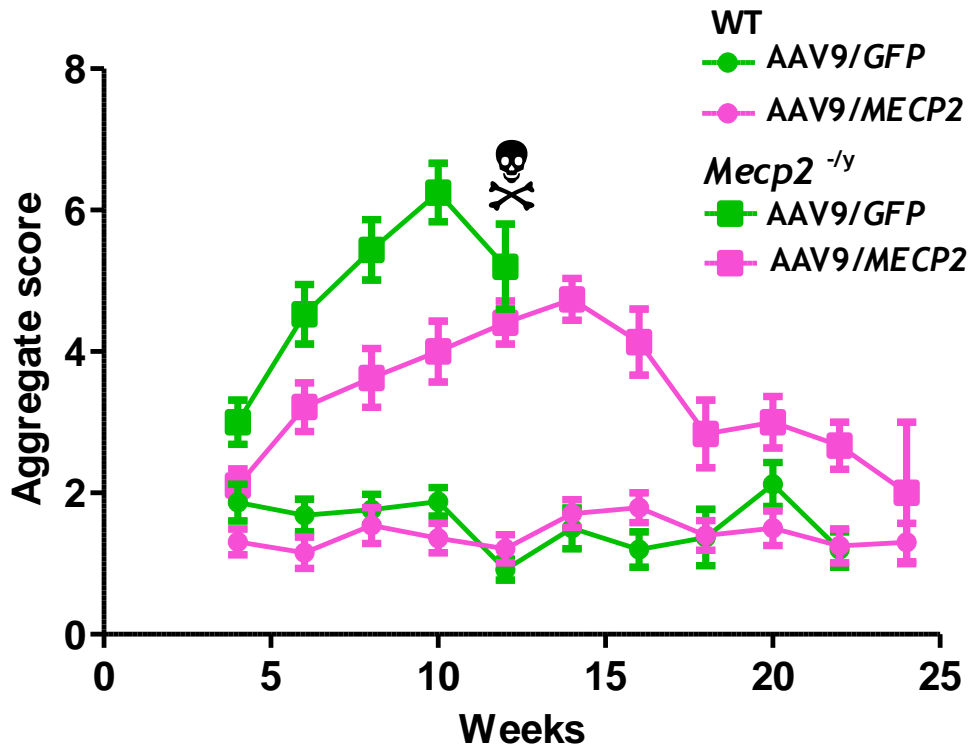


Figure 5-7 AAV9/*MECP2* neonatal injection reduced phenotype severity in *Mecp2*-null mice. Plot showing aggregate phenotype severity score of *Mecp2*-null and WT mice treated either with AAV9/*GFP* or AAV9/*MECP2*. The rate of phenotype progression in AAV9/*MECP2*-treated null mice (N = 14) was significantly ($p < 0.05$, Repeated measures ANOVA between weeks 3-12 with tukey's posthoc pairwise comparison) reduced compared to the aggressive phenotype trajectory seen in AAV9/*GFP*-injected control mice (N = 11). In contrast, WT mice injected with AAV9/*MECP2* (N = 12) or AAV9/*GFP* (N = 12) showed no difference between groups. ☠ Indicates that in the null untreated group, insufficient mice were still alive to plot the mean score after 12 weeks. Data is presented as mean \pm SEM.

5.4.6 AAV9-mediated neonatal delivery of *MECP2* prolonged life span in *Mecp2*-null mice

The reduced survival of *Mecp2*-null mice is one of the cardinal features of the RTT-like phenotype. Monitoring of the AAV9/*MECP2* and *GFP* treatment mice revealed that AAV9/*GFP*-treated null mice displayed markedly reduced survival, as expected for this model (Guy et al., 2001) (figure 5-8; median survival 9.3 weeks, range 5-19 weeks) whereas AAV9/*MECP2*-treated null mice showed significantly extended survival (median survival 16.6 weeks; range 7 to >30 weeks; $p < 0.0001$, Gehan-Breslow-Wilcoxon test). In the AAV9/*MECP2*-treated WT cohort, included to investigate the effect of overexpressing exogenously-derived MeCP2 in the brain, no mortality was observed. Two of 12 AAV9/*GFP*-treated WT mice died suddenly before the end of the study.

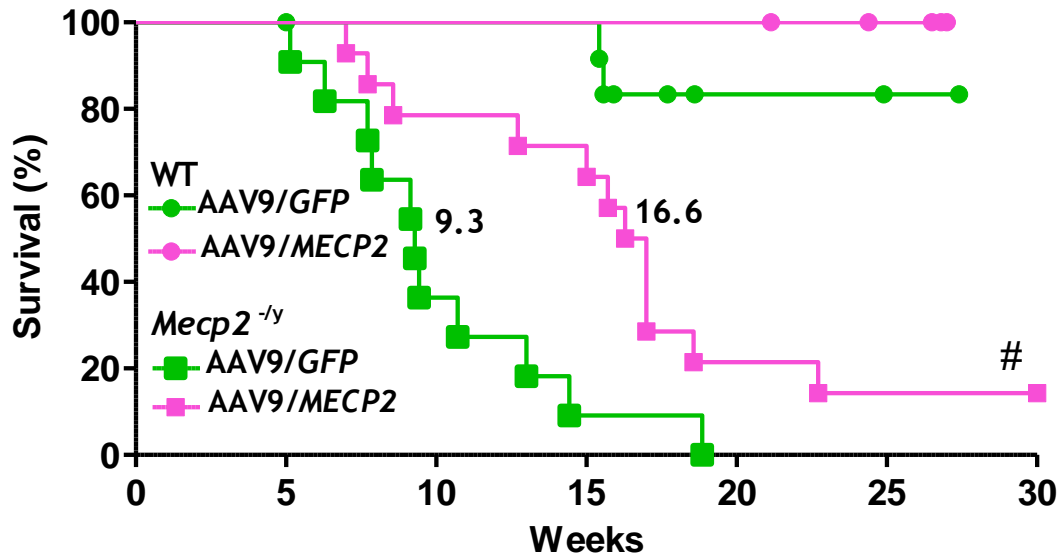


Figure 5-8 Prolonged survival of *Mecp2*-null mice after neonatal IC injection of AAV9/MECP2 Survival plot showing extended lifespan of *Mecp2*^{-/-} mice injected with AAV9/MECP2 (n = 14) compared to AAV9/GFP injected controls (n = 11). The median survival period was significantly increased from 9.3 weeks to 16.6 weeks (P<0.0001 Gehan-Breslow-Wilcoxon test). The plot also shows absence of lethality associated with overexpression of MeCP2 in AAV9/MECP2 treated WT mice (n = 12). AAV9/GFP-treated WT mice (n = 12) showed 2 unexplained sudden death at the age of 16 weeks. # indicates two AAV9/MECP2-treated *Mecp2*-null mice that survived to the end of the 30 week study.

5.4.7 Growth deficit persists after AAV9/MECP2 injection however stabilizes

As growth deficits are commonly observed in RTT (Neul et al., 2010) and low bodyweight is a prominent characteristic of *Mecp2*-null mice (Chen et al., 2001, Guy et al., 2001), growth was also monitored weekly in these mice, but the difference in bodyweight between AAV9/GFP control-injected *Mecp2*-null mice and AAV9/MECP2-treated *Mecp2*-null mice was not significant ($p > 0.05$ repeated measures ANOVA) despite a trend towards improved growth in the AAV9/MECP2-treated mice.

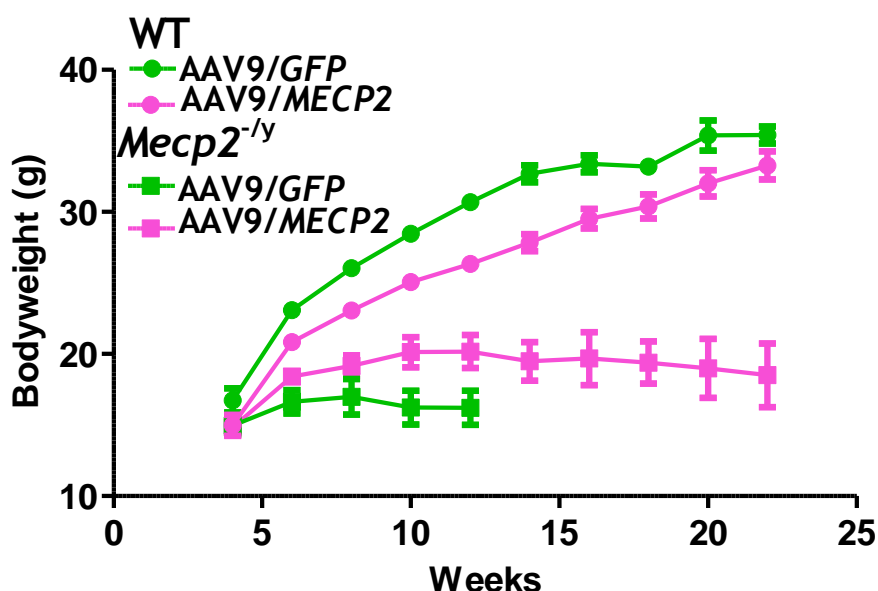


Figure 5-9 Persistent bodyweight deficit in *Mecp2*-null mice after AAV9/*MECP2* injection Plot showing bodyweight changes over time in WT and *Mecp2*-null mice after neonatal injection with either AAV9/*GFP* or AAV9/*MECP2*. There was a genotype effect (repeated measures ANOVA, $p < 0.05$) but no significant treatment effect.

5.4.8 AAV9-mediated neonatal delivery of *MECP2* improved motor phenotypes in *Mecp2*-null mice

5.4.8.1 Tread-mill test

Movement-related deficits constitute 3 of the 4 main criteria for RTT diagnosis (Neul et al., 2010) and represent a major feature of the syndrome in girls. Similarly, mobility and movement-dependent behaviour deficits constitute prominent characteristics of *Mecp2*-null mice (Chen et al., 2001, Guy et al., 2001). To explore the effect of AAV9/*MECP2* treatment on movement-related phenotypes, mice were subjected to analysis of their locomotory behaviour at 8-9 weeks using a treadmill device (chapter 2). Mice were challenged to perform on a treadmill at two different speeds (figure 5-10). There was a significant overall difference in performance between groups (10 cm/s, $p = 0.0013$; 25cm/s, $p < 0.0001$; Fisher's exact test). Challenged at the lower speed (10 cm/s), there was no significant difference between AAV9/*GFP*-treated and AAV9/*MECP2*-treated *Mecp2*-null mice (4/8 and 10/12 mice, respectively, could manage the task; Fisher's exact test, $p = 0.14$) in their ability to perform to criteria (achieving run for approximately 2 seconds, without sliding back on the running belt). When challenged using the more demanding high speed test (25 cm/s), none of the AAV9/*GFP*-treated *Mecp2*-null mice could perform to criteria

whereas 50% of AAV9/*MECP2*-treated *Mecp2*-null mice were still able to successfully complete the task, a significant difference in ability to perform in this test (0/8 vs 6/12 mice, respectively; Fisher's exact test, $p = 0.024$). All WT mice (both AAV9/*MECP2* and AAV9/*GFP* treatment groups) could perform at both speeds.

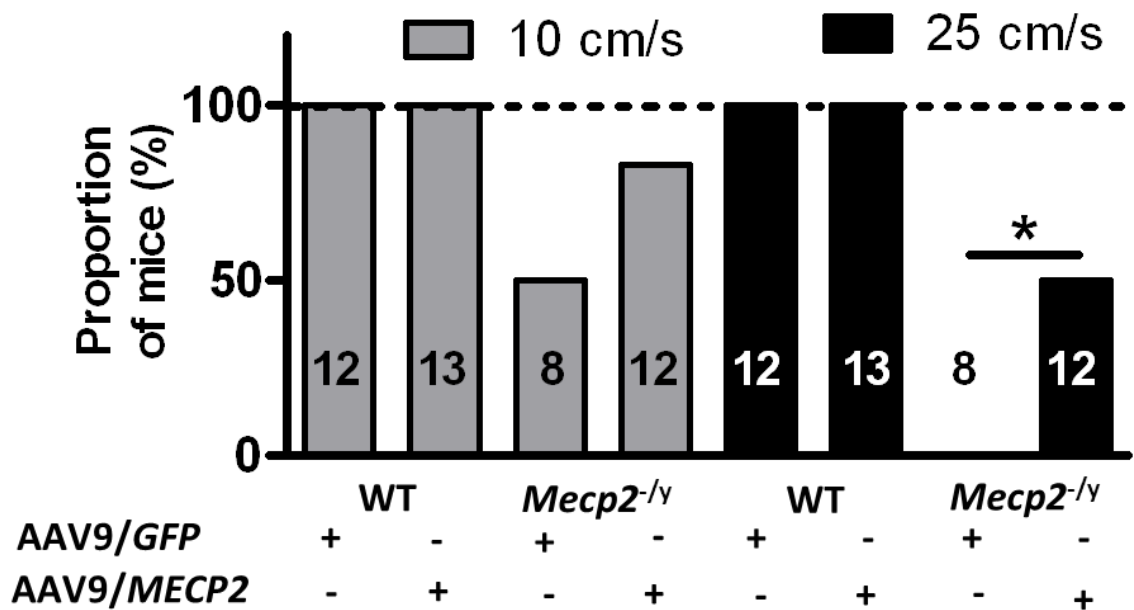


Figure 5-10 Treadmill motor test of *Mecp2*-null mice after neonatal injection of AAV9/*MECP2*. Plot showing the proportion of mice that were able to perform at two different speeds on a motorized treadmill. Numbers on the columns represent the number of mice included in each group. * $p < 0.05$, Fisher's exact test.

5.4.8.2 Open field test

To further study the motor behaviours in AAV9/*MECP2*-treated *Mecp2*-null mice and their AAV9/*GFP* treated control, an open field test was carried out at 9 weeks after injection. AAV9/*GFP*-treated *Mecp2*-null mice ($n = 6$) showed a significant deficit in locomotion-related parameters including; movement duration, total distance moved and mean velocity, compared to AAV9/*GFP*-treated WT controls (figure 5-11a-c; $n = 9$; all $p < 0.01$). In contrast, AAV9/*MECP2*-treated *Mecp2*-null mice ($n = 11$) were not significantly different from AAV9/*GFP*-treated WT controls ($n = 9$), while *post hoc* comparisons revealed significantly higher mean velocity and total distance moved parameters in the AAV9/*MECP2*-treated *Mecp2*-null mice than in the AAV9/*GFP*-treated *Mecp2*-null cohort (both $p < 0.05$).

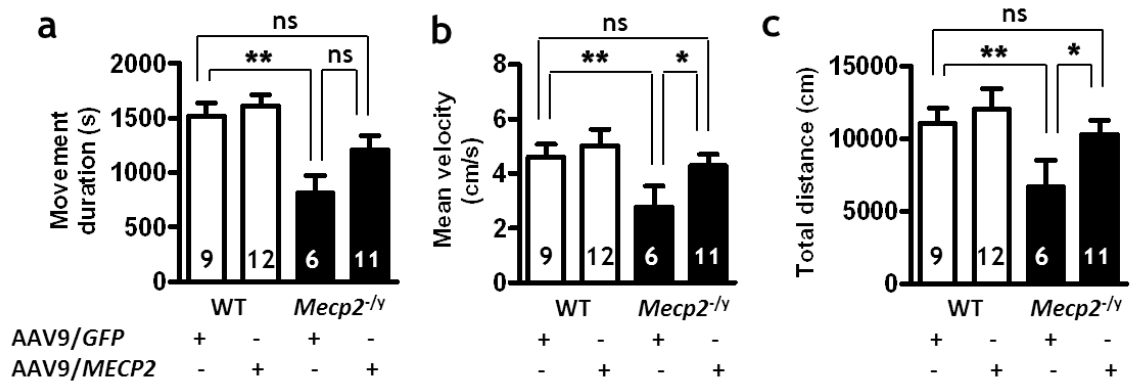


Figure 5-11 Motor-related measures of the open field test

Plots showing the motor related parameters of the open field test that was performed at 9-11 weeks following AAV9 injection. (a) Plot showing movement total duration (time during which the mice were producing detectable movement). (b) Plot showing mean velocity and (c) Plot showing the total distance moved. Numbers of animals per genotype/treatment group are shown within each bar. Open field measures were assessed by 2-way ANOVA with Tukey's *post hoc* comparisons. * $p < 0.05$, ** $p < 0.01$, ns = not significant.

5.4.8.3 Improved exploratory behaviours with no effect on the anxiety-related measures

In addition to ambulatory movement, we tested exploration and anxiety-related behaviour by assessing rearing frequency and time spent in the outer and central zones of the open field. AAV9/*GFP*-treated *Mecp2*-null mice showed a significantly reduced rearing frequency (figure 5-12a) compared to AAV9/*GFP*-treated WT mice ($p < 0.01$), while AAV9/*MECP2*-treated *Mecp2*-null mice showed increased rearing frequency relative to AAV9/*GFP*-treated *Mecp2*-null mice ($p < 0.05$). As with ambulatory movements, there was no difference between the WT treatment groups. There was no genotype or treatment significant difference between the studied groups in the anxiety related parameters by 2 way ANOVA ($p > 0.05$, figure 5-12b-c).

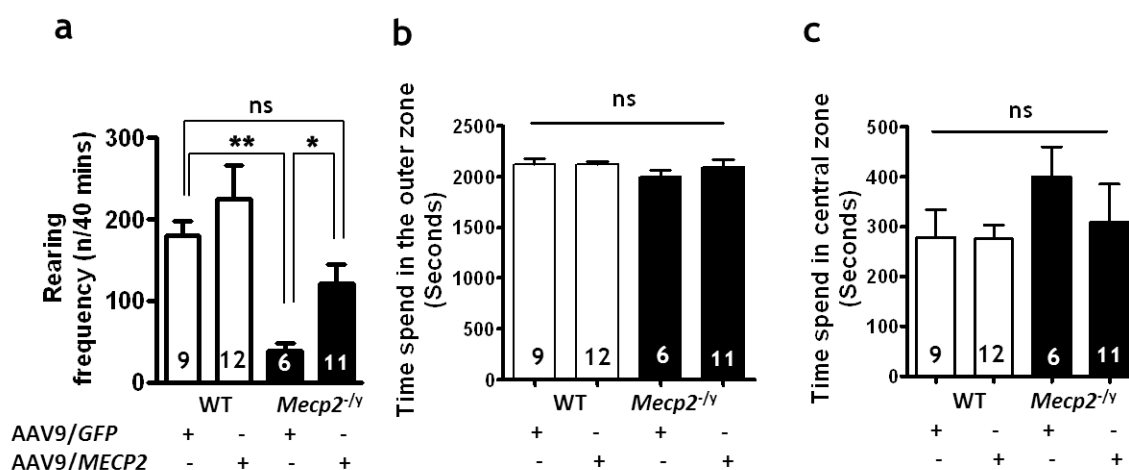


Figure 5-12 Exploratory and anxiety related measures of the open field test. Plots showing the exploratory and anxiety related parameters of the open field test that was performed at 9-11 weeks following AAV9/MECP2 or GFP injection. (a) Plot showing the rearing frequency which is an indicator of the exploratory behaviours. (b&c) plots showing the time spend in the outer zone and inner zone respectively which are indicators of anxiety. Numbers of animals per genotype/treatment group are shown within each bar. Open field measures were assessed by 2-way ANOVA with Tukey's *post hoc* comparisons. * $p < 0.05$, ** $p < 0.01$, ns; not significant.

5.4.9 AAV9/MECP2-treated Long-lived mice displayed consistent phenotype improvement.

As I showed before, AAV9/MECP2 treated *Mecp2*-null mice displayed extended survival compared to AAV9/GFP treated mice. Analysis of RTT-like phenotype severity score of the long-lived mice (> 22 weeks old) showed a gradual increase in the severity score, which achieved maximum value at the age of 14 weeks followed by steady reduction in the phenotype severity score, finally reaching levels comparable to WT. However these severity scores were less than the average phenotype severity score of *Mecp2*-null mice treated with AAV9/GFP at all-time points) (figure 5-13a). For further confirmation of this phenotype improvement, open field testing was carried out at the age of 22 weeks for the three survivors and the data was compared to their own data at the age of 11weeks. The data showed that the performances in the open field were very similar in motor and exploratory behaviour-related parameters at both ages which indicate persistent treatment effects (figure 5-13b-d).

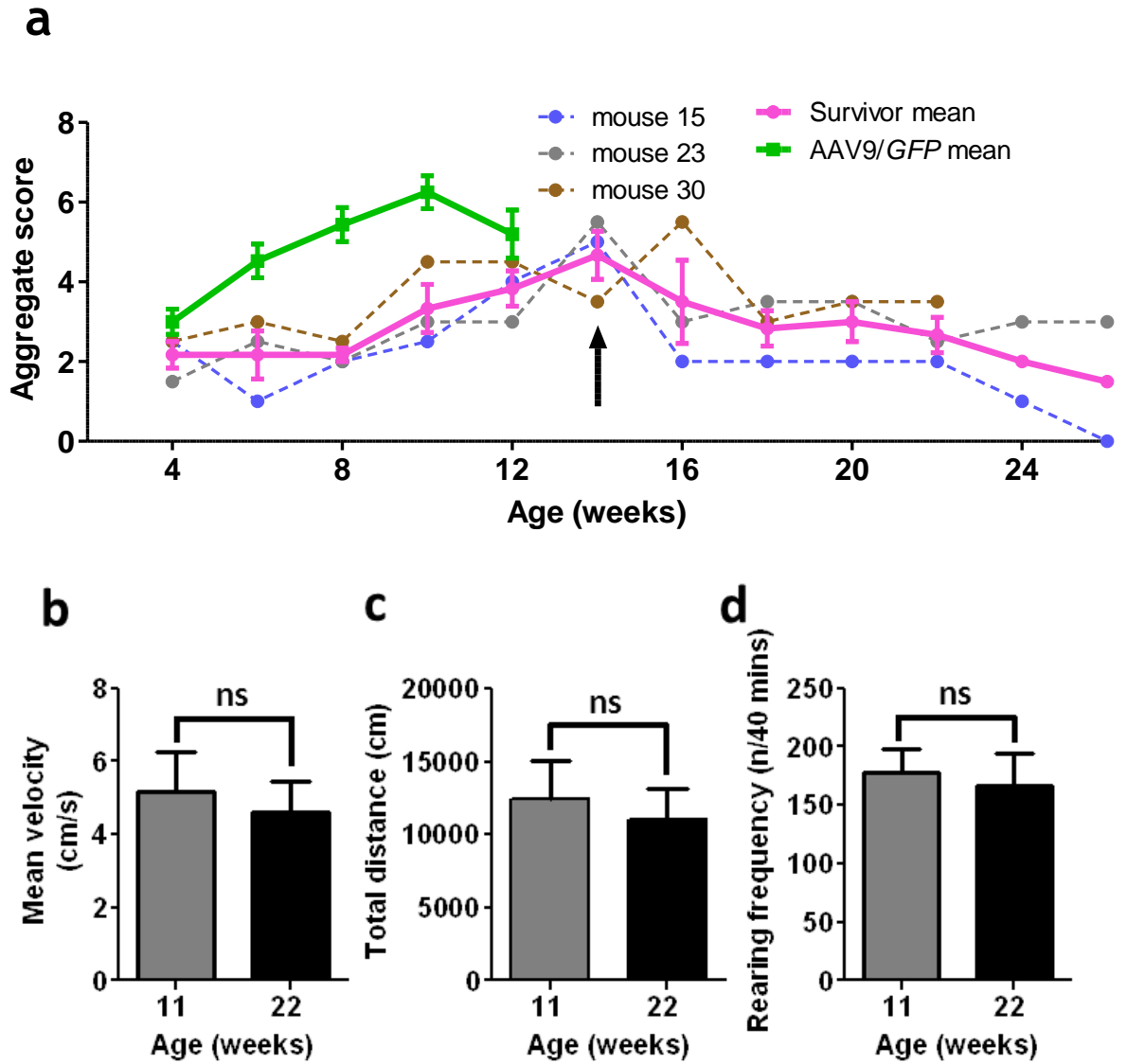


Figure 5-13 Phenotypic analysis of AAV9/*MECP2*-treated long-lived *Mecp2*-null mice. (a) Plot showing individual aggregate phenotype severity scores for the longest surviving mice (No. 15, 23 and 30). Numbers 15 and 23 survived to the end of the study (30 weeks; ie. 12 weeks beyond longest surviving AAV9/*GFP*-treated *Mecp2*^{fl/y} mouse) whilst number 30 died suddenly at 22 weeks. Black arrow indicates the peak mean severity score (around 14 weeks of age). (b-d) plots showing the performance of these mice on the open field test at two time points (11 and 22 weeks). Plots show data as mean \pm SEM. Statistical analysis was carried out by paired *t* test.

5.5 Overt respiratory phenotypes persist following AAV9-mediated neonatal delivery of *MECP2* to *Mecp2*-null mice

Apnoeas and abnormal breathing patterns were investigated using whole body plethysmography at 9 weeks following neonatal delivery of AAV9/*MECP2* or AAV9/*GFP*. *Mecp2*-null mice displayed a characteristic erratic breathing pattern with frequent apnoeas (figure 5-14a), in contrast to the regular baseline breathing pattern seen in both WT treatment groups. Overall, there was no difference in baseline respiratory frequency between genotypes or treatments (figure 5-14b; 2-way ANOVA, $p > 0.05$). An increased incidence of apnoeas (figure 5-15a) was observed in the *Mecp2*-null mice compared to the WT mice (2-way ANOVA, genotype main effect $p < 0.05$), but the AAV9/*MECP2*- and AAV9/*GFP*-treated mice did not differ. Similarly, higher breathing frequency variability (CV%; figure 5-15b) was observed in the *Mecp2*-null mice compared to the WT mice, but again the AAV9/*MECP2*- and AAV9/*GFP*-treated mice did not differ (2-way ANOVA, genotype main effect $p < 0.05$, treatment main effect $p > 0.05$, $n = 7-12$ mice per group).

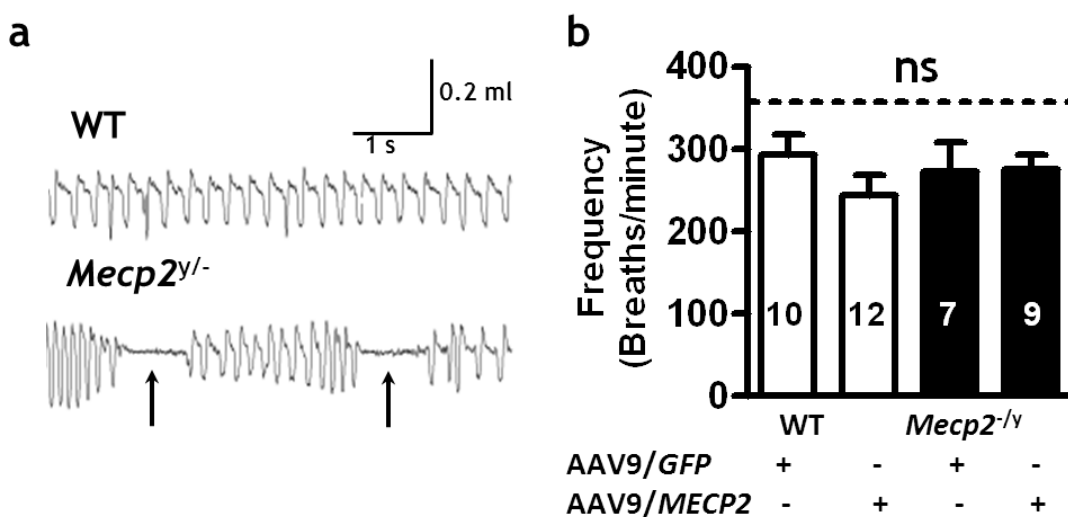


Figure 5-14 Persistent breathing phenotype in *Mecp2*-null mice after AAV9/*MECP2* injection (a) Representative whole-body plethysmograph traces showing regular and erratic breathing patterns/apnoeas (arrows) in WT and *Mecp2^{y/-}* mice respectively. (b) Baseline breathing frequency. Respiratory frequency was assessed by 2-way ANOVA with Tukey's *post hoc* comparisons. ns = not significant. Numbers of animals per genotype/treatment group are shown within each bar.

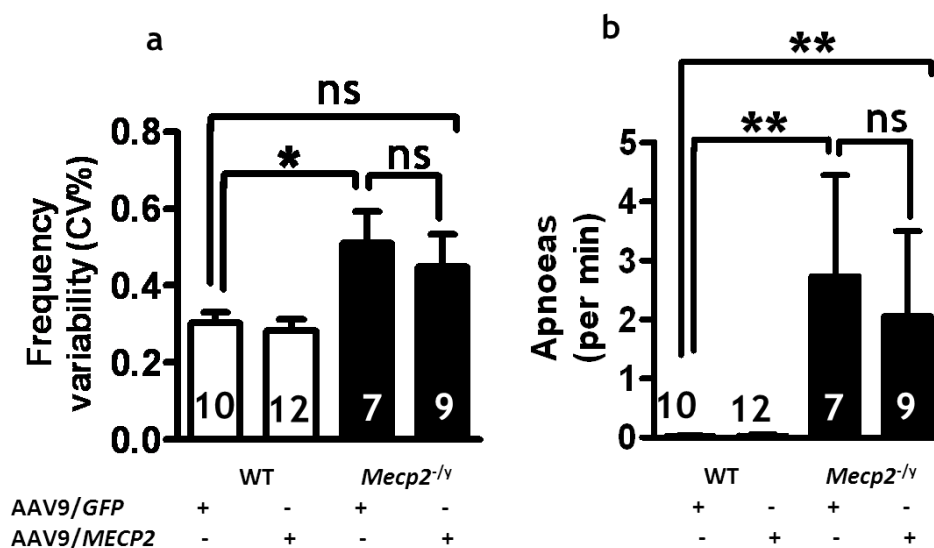


Figure 5-15 Breathing phenotype in *Mecp2*-null mice after AAV9/*MECP2* injection
(a) Plot showing the coefficient variability of the breathing frequency. **(b)** Plot showing the number of apnoeas/minutes (breath hold for more than 1 second). Numbers of animals per genotype/treatment group are shown within each bar. Breathing frequency variability and Apnoea frequency were assessed by 2-way ANOVA with Tukey's post hoc comparisons. * $p < 0.05$, ** $p < 0.01$, ns = not significant.

5.5.1 AAV9-mediated delivery of *MECP2* rescued the *Mecp2*-null nuclear volume phenotype

A consistent feature of MeCP2 deficiency at the cellular level is a reduction in nucleus volume (Giacometti et al., 2007, Johnson et al., 2011). In order to assess potential changes in this parameter, 3D nuclear volume measures were obtained for AAV9/*MECP2*-transduced and non-transduced granule cells of the dentate gyrus (figure 5-16a-b). Consistent with previous reports, non-transduced neurons in *Mecp2*-null mice showed nuclear volumes that were on average 69% of volumes in age-matched WT mice (figure 5-16c). In *Mecp2*-null mice AAV9/*MECP2*-transduced cells displayed nuclear volumes that were significantly larger (by 29% on average) than those of neighbouring non-transduced cells in the same brains, and the AAV9/*MECP2*-transduced cells showed no significant difference from values observed in non-transduced WT mice. Interestingly, in WT mice, AAV9/*MECP2*-transduced cells showed a modest (approx. 1.2-fold on average) but significant increase in nuclear volume relative to neighbouring non-transduced cells (figure 5-16d).

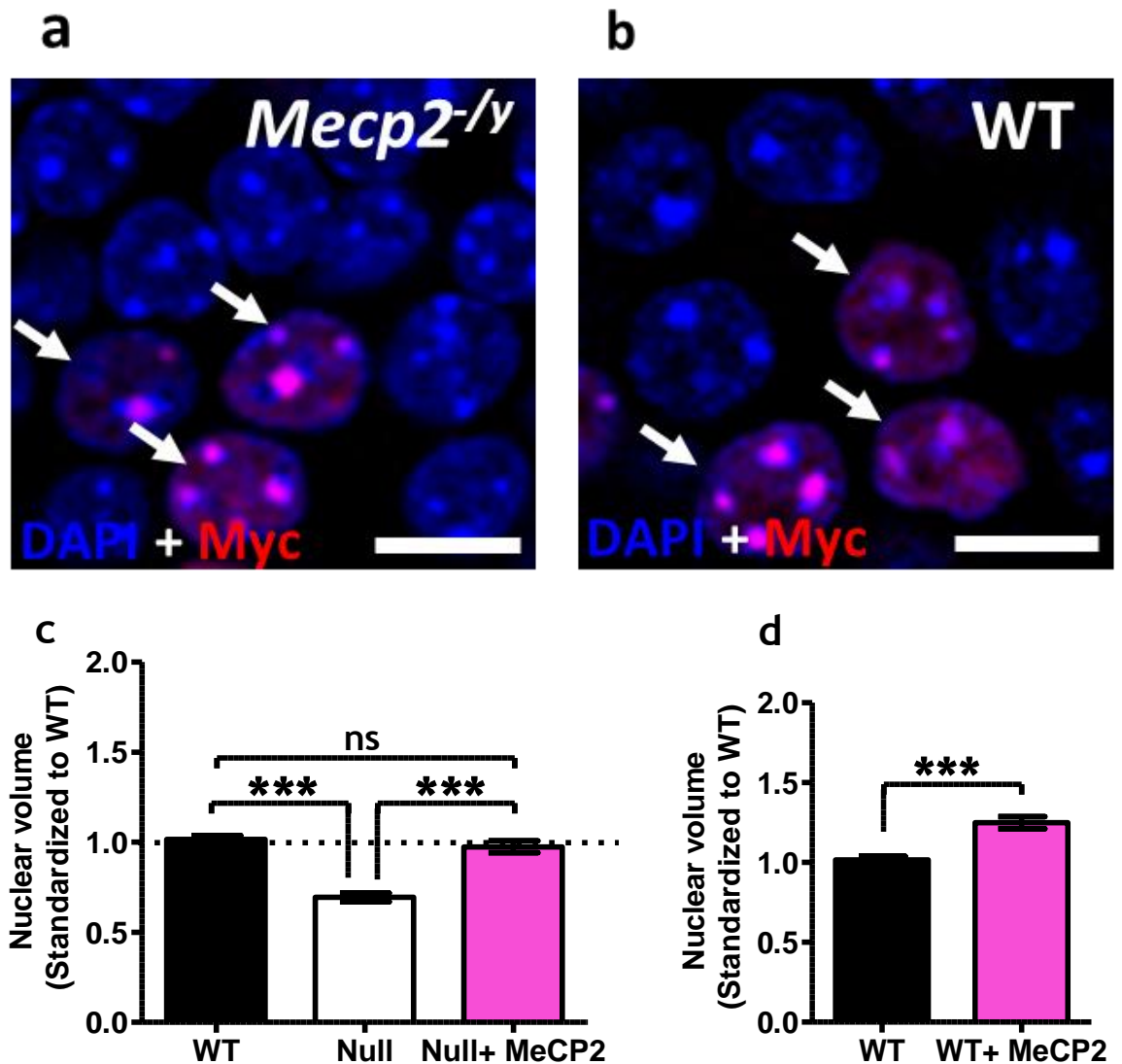


Figure 5-16 Increased nuclear volume in *Mecp2^{ly}* and WT mice after AAV9/MECP2 injection. (a&b) Representative images from the dentate gyrus of (a) WT and (b) *Mecp2*-null mouse at 12 weeks following AAV9/MECP2 injection. Sections were stained with DAPI (blue) and anti-Myc antibody (red). Arrows indicate transduced cells (purple). (c) Neuronal nuclear volume measurements of transduced and non-transduced cells of *Mecp2*-null mice (N = 3 mice) and age matched WT (N = 4 mice). (d) Neuronal nuclear volume measurements of transduced and non-transduced granular cells of WT mice (n = 4). Data was normalized to the mean volume in non-transduced WT cells and is represented as mean \pm SEM. Statistical analysis was carried out by 2-way ANOVA and Tukey's *post hoc* pairwise comparison. ***= $p < 0.001$. Scale bar = 10 μ m.

5.6 Discussion

Incomplete understanding of the precise molecular actions of MeCP2 continues to impede the development of rational therapeutic strategies for Rett syndrome. *MECP2* gene delivery is an obvious theoretical approach to overcoming the consequences of functional MeCP2 deficiency. I showed that early postnatal delivery of exogenous *MECP2* directly to the brain at transduction efficiencies in the range of ~7- 42%, depending on brain region, results in a substantial prolongation of lifespan (~80% increase in median survival) and a less aggressive trajectory of RTT-like phenotypes severity. Interestingly, a small number of mice survived to the end of the 30 week study period, well in excess of the average lifespan of the control *Mecp2*-null mice (lifespan was >3 fold greater for some AAV9/*MECP2*- treated mice). Furthermore, the longest-lived mice treated with the therapeutic vector also displayed a stabilization of the phenotype in terms of aggregate severity score and objective locomotor measures.

Male mice lacking MeCP2 in all cells display the most severe phenotype observable in any mouse model of RTT and thus provide an especially challenging system for assessing the potential of novel therapeutic approaches. Nevertheless, these data show that treatment with the AAV9/*MECP2* vector can influence phenotype progression and lifespan. In contrast to the observed beneficial impact on the RTT-like signs, AAV9/*MECP2*-treatment resulted in only a modest, non-significant increase in bodyweight of *Mecp2*-null mice compared to control-treated *Mecp2*-null mice, even for the most long-lived animals. This raises the possibility that the levels of transgene in relevant areas of the brain did not reach a threshold for affecting bodyweight or that reduced bodyweight in *Mecp2*-null mice is at least in part due to MeCP2 deficiency in peripheral organs rather than solely the brain.

An especially robust impact of treatment on the phenotype was observed in the motor behaviors measured, where exogenously-derived MeCP2 produced a substantial improvement in open field activity/locomotion and performance on a forced motor task in the *Mecp2*-null mice. The impaired locomotor activity observed in the control-treated *Mecp2*-null mice in the open field experiments can be explained by genuine motor disability, by an anxiety phenotype or by a lack of motivation. The complete inability of AAV9/*GFP*-treated mice to perform

when tested at the high speed on the treadmill and their partial ability to perform at low speed suggest the presence of a true motor defect in this forced challenge rather than inertia purely due to lack of motivation. This genuine motor impairment was ameliorated by AAV9/*MECP2* treatment. This effect was mirrored in the open field test whereby AAV9/*MECP2*-treated mice displayed significantly enhanced ambulatory activity. Locomotor improvement was accompanied by an increase in rearing frequency in AAV9/*MECP2*-treated mice suggesting additional improvement in exploration-related behaviours. Analysis of open field data from the long-term survivors collected on multiple occasions suggests that the locomotor phenotypes are not progressive throughout life in AAV9/*MECP2*-treated null mice (figure 5-13 a-d). Reports by other groups as to whether anxiety phenotypes, measured by open field test, are visible in young *Mecp2*-null mice have not revealed consistent observations (Pelka et al., 2006, Stearns et al., 2007, Lioy et al., 2011). We found no genotype or treatment differences in the proportion of time spent in the central zone of the open field.

The analysis of breathing was consistent with other reports that *Mecp2*-null mice exhibit a range of breathing phenotypes (Viemari et al., 2005) and mirrors the clinical picture where apneas and other breathing irregularities are characteristic and highly prevalent features of RTT (Neul et al., 2010). Previous studies have shown that postnatal activation of *Mecp2* globally (Robinson et al., 2012) or in glial cells (Lioy et al., 2011) can rescue abnormal breathing and this suggests that the respiratory phenotype is not solely the result of an earlier developmental deficit and is amenable to treatment at the level of causative gene function. The absence of any impact of AAV9/*MECP2*-treatment on breathing irregularity or on the incidence of apneas in the mutant mice in this study could be explained if, despite the widespread expression of exogenous MeCP2, the cells responsible for breathing rhythmogenesis or otherwise contributing to breathing regulation were transduced at very low levels.

MeCP2-deficiency is known to be associated with a wide variety of morphological and neurochemical changes in the brain (Gadalla et al., 2011). To examine the consequences of exogenous *MECP2* delivery, simple measures of cellular phenotype, including neuronal nuclear volumes within the dentate gyrus, were investigated. The significant reduction in neuronal nuclear volume in MeCP2-deficient cells has been reported previously (Giacometti et al., 2007, Johnson et

al., 2011) and my results show that this cell morphological measure can be effectively rescued by the expression of exogenously-derived MeCP2 at close to WT levels within the nucleus. Furthermore, the comparison within individual brains of neighbouring MeCP2-containing and MeCP2-deficient cells suggests that these changes represent a cell-autonomous effect. This would be consistent with the differences in nuclear volume and soma size in neurons containing MeCP2 and those lacking MeCP2 in the female heterozygote (*Mecp2^{+/-}*) mouse brain (Ho et al., 2008). The fact that nuclear volume was rescued after expression of exogenously-derived MeCP2 provides evidence for structural remodelling of neurons. Whether this remodelling also extends to changes in dendritic/axonal size and complexity, as shown for exogenously-derived MeCP2 in neuronal culture (Rastegar et al., 2009) and upon delayed activation of *Mecp2* in mature brains (Robinson et al., 2012), remains to be established.

Potentially serious complications have been attributed to MeCP2 overexpression (Luikenhuis et al., 2004, Van Esch et al., 2005, Friez et al., 2006). The present studies demonstrate the potential for delivering the MeCP2 protein transgenetically without overt overexpression-related toxicity, at least with the vector designs utilized in this study and with the delivery efficiencies achieved. This is demonstrated by the lack of any phenotypic deficits in WT mice injected as neonates with the ssAAV9/CBA-*MECP2* vector, which had approximately double normal levels of MeCP2 in transduced cells. The treated WT mice overexpressing MeCP2 displayed no difference from AAV9/GFP-treated WT controls in terms of survival, locomotor activity and breathing. However, these results cannot rule out the possibility of subtle or very delayed overexpression toxicity (Collins et al., 2004). Nevertheless, the same dose (conferring 1- to 1.25-fold of WT levels in null cells) in male RTT mice provided a significant behaviour and survival benefit. The implications of these findings are particularly important when considering this approach for RTT females (that have a mosaic network of cells expressing either normal or mutant *Mecp2* allele). Here, there is a concern that overexpression toxicity might result from an introduction of MeCP2 to cells expressing the WT endogenous gene while trying to achieve therapeutic levels of MeCP2 in the cells expressing the mutant allele. Our data shows that it may be possible to achieve a therapeutic outcome

without the associated overexpression toxicity using an appropriate vector and promoter system.

This work shows, at ‘proof-of-concept’ level, that exogenous MeCP2 can be delivered at a physiologically tolerable level via AAV2/9 vectors to the brain of *Mecp2*-null mice. Provision of MeCP2 from exogenous source has achieved a partial amelioration of the RTT-like phenotype and has prolonged the survival in *Mecp2*-null mouse model. Importantly, overexpressing exogenous MeCP2 was without apparent toxicity when injected into the WT mice providing a broader-than-anticipated window of therapeutic MeCP2 expression in the treatment of Rett syndrome.

Chapter 6

Self-complementary AAV9-mediated delivery of exogenous *MECP2* into neonatal male *Mecp2* knockout mice

6.1 Introduction

In light of the ability of a single-stranded AAV9/CBA-*MECP2* vector to enhance survival and reduce phenotype severity of *Mecp2* knockout mice injected at P0-2 (chapter 5), I would suggest that greater therapeutic gain could be achieved by utilising a vector with increased transduction efficiency. This is supported by a previous report that showed that the degree of phenotype rescue achieved in delayed activation studies is directly correlated with the level of newly-activated endogenous *Mecp2* (Robinson et al., 2012). A recent advance in AAV vector technology has been the development of self-complementary (sc) vectors, whose genome is comprised of complementary copies of the DNA insert linked in *cis* through a mutated AAV inverted terminal repeat (McCarty et al., 2001). Therefore unlike ssAAV, scAAV vectors are not limited by the ability of the host cell to convert single-stranded genome to duplex that is a rate limiting step in the vector transduction (Fu et al., 2003). These scAAV vectors have been reported to have 10-100 fold higher transduction efficiency than traditional ssAAV9 vectors (McCarty et al., 2003). In addition, delivery of scAAV9 through intravenous (IV) injection in neonates has been reported to produce widespread transgene expression in the brain (Foust et al., 2009) and has been shown to rescue the phenotype in the animal model of Spinal Muscular Atrophy (Valori et al., 2010).

The reduced cloning capacity of scAAV vector precludes the cloning of *MECP2* minigene under the control CBA promoter as used in chapter 5. An alternative promoter would be the *Mecp2* endogenous promoter (~677bp) that has been reported to recapitulate the expression pattern of endogenous *Mecp2* in neurons (Adachi et al., 2005). However, this segment is still too large to fit into the reduced capacity scAAV9 along with the *MECP2* minigene. Recently a more

defined short segment (229bp) of *Mecp2* endogenous promoter was proven to drive neuronal specific expression in the brain (Gray et al., 2011b). This short *Mecp2* promoter segment allows concomitant cloning with *MECP2* minigene in the scAAV9 vector which represents a potential tool to drive exogenous MeCP2 expression in post mitotic neurons with high transduction efficiency following peripheral administration.

6.2 Aims

The main aim of the work described in this chapter was to examine the potential of delivering exogenous *MECP2* using the more efficient scAAV9 vector and *Mecp2* endogenous core promoter (MeP). I aimed to establish the effect of this vector on RTT-like phenotypes in *Mecp2*^{stop/y} mice. The specific objectives of this study are:

- ❖ To test the efficiency of scAAV9/MeP-*MECP2* vector to deliver exogenous *MECP2* *in vivo* by intravenous and direct brain injection in neonatal mice.
- ❖ To evaluate the transduction efficiency in the brain and to quantify cellular levels of exogenous MeCP2 after both methods of injection.
- ❖ To investigate the effect of IV and IC injections of scAAV9/MeP-*MECP2* on the trajectory of RTT-like phenotype in *Mecp2* knockout mice.
- ❖ To test for potential overexpression-related toxicity after introducing exogenous MeCP2 to WT neonatal mice.

6.3 Methods

To test the ability of scAAV2 vector with capsid 9 (AAV2/9, from now I will refer to this vector as scAAV9) to globally deliver exogenous *MECP2* with high transduction efficiency, human or mouse *MECP2_e1* isoform coding sequences carrying a C-terminal Myc-tag fusion was cloned into a AAV9 vector-backbone under the control of murine *Mecp2* endogenous core promoter (MeP, 229bp, this construct, scAAV9/MeP-h*MECP2*, henceforth referred to as scAAV9/*MECP2*; figure 6-1a). To compare the effect of global MeCP2 expression versus brain-specific MeCP2 expression on the trajectory of RTT-like phenotypes, two delivery methods were adopted (figure 6-1b); the first was IV (for global expression) injection of 30 μ l of 3.1×10^{11} vector genome (vg) / ml (9.3×10^9 vg / mouse) through the facial vein and the second was direct brain injection (for

brain-specific expression) of 6 μ l of the same titre (1.8×10^9 vg / mouse). A scAAV9 / MeP-*GFP* vector was used as a control vector in all experiments. Male neonatal (P0-2) WT and *Mecp2*^{stop/y} mice were included in this study. Monitoring of RTT-like phenotype trajectory (described in chapter 2 and 5) was carried out weekly to evaluate the therapeutic benefits of the transgene.

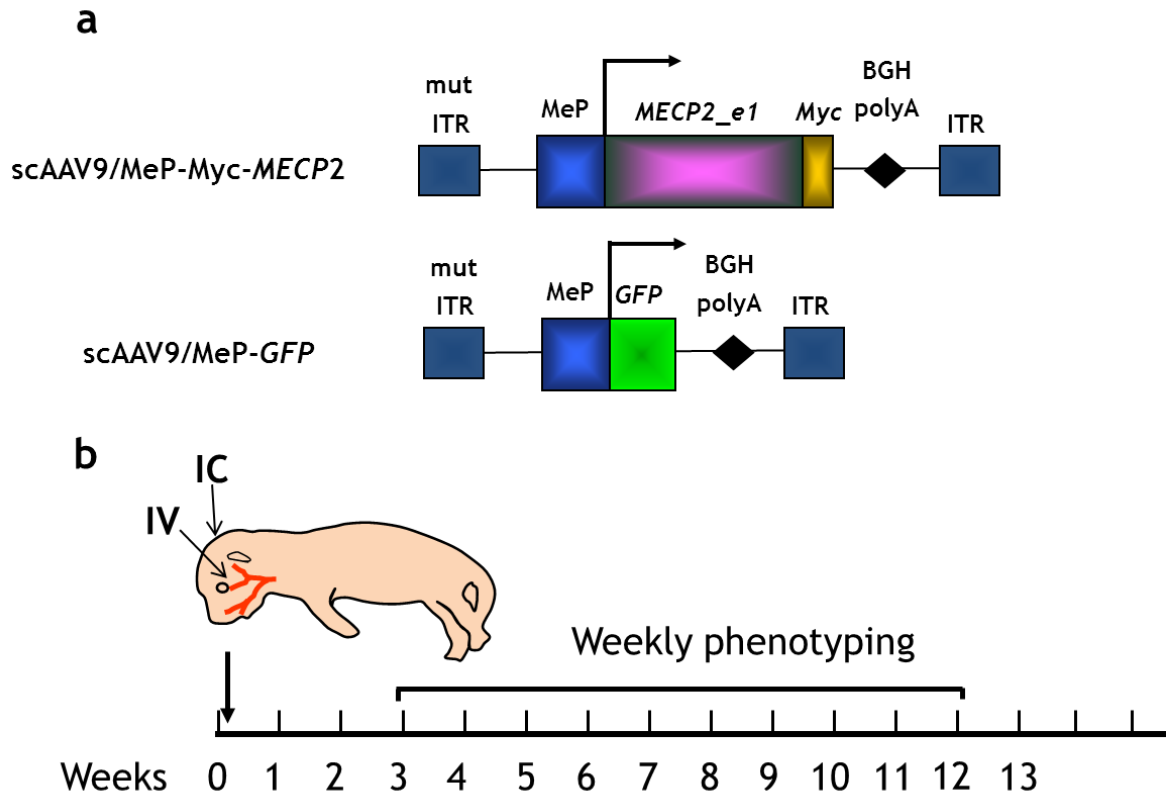


Figure 6-1 scAAV9 vector-constructs and the experimental plan.

(a) *MECP2_e1/Myc* fusion and *GFP* (control) constructs were cloned into AAV2/9 backbones under the control of *Mecp2* endogenous core promoter. (b) Experimental plan in which male WT and *Mecp2*^{stop/y} mice were injected either intravenously or intracranially with scAAV9/*MECP2* at P0-2 and scored for signs of RTT-like phenotypes from 3 weeks onwards. sc; self-complementary, MeP; Murine *Mecp2* endogenous core promoter, ITR; inverted terminal repeat.

6.4 Results

6.4.1 Intravenous injection of scAAV9/*MECP2* in neonatal mice resulted in widespread expression of exogenous MeCP2

To test for exogenous MeCP2 expression in the peripheral organs as well as in the CNS, WT mouse was transcardially perfused with 4% PFA 8 weeks after injection and sections were taken from different organs for immunohistochemical detection of the transgene. Immunolabelling of frozen sections taken from liver, kidney and heart with anti-Myc antibody showed that exogenous MeCP2

expression was targeted to the nucleus as indicated by co-localization with DAPI nuclear stain and recapitulated the characteristic heterochromatin localization with no detectable ectopic expression (figure 6-2).

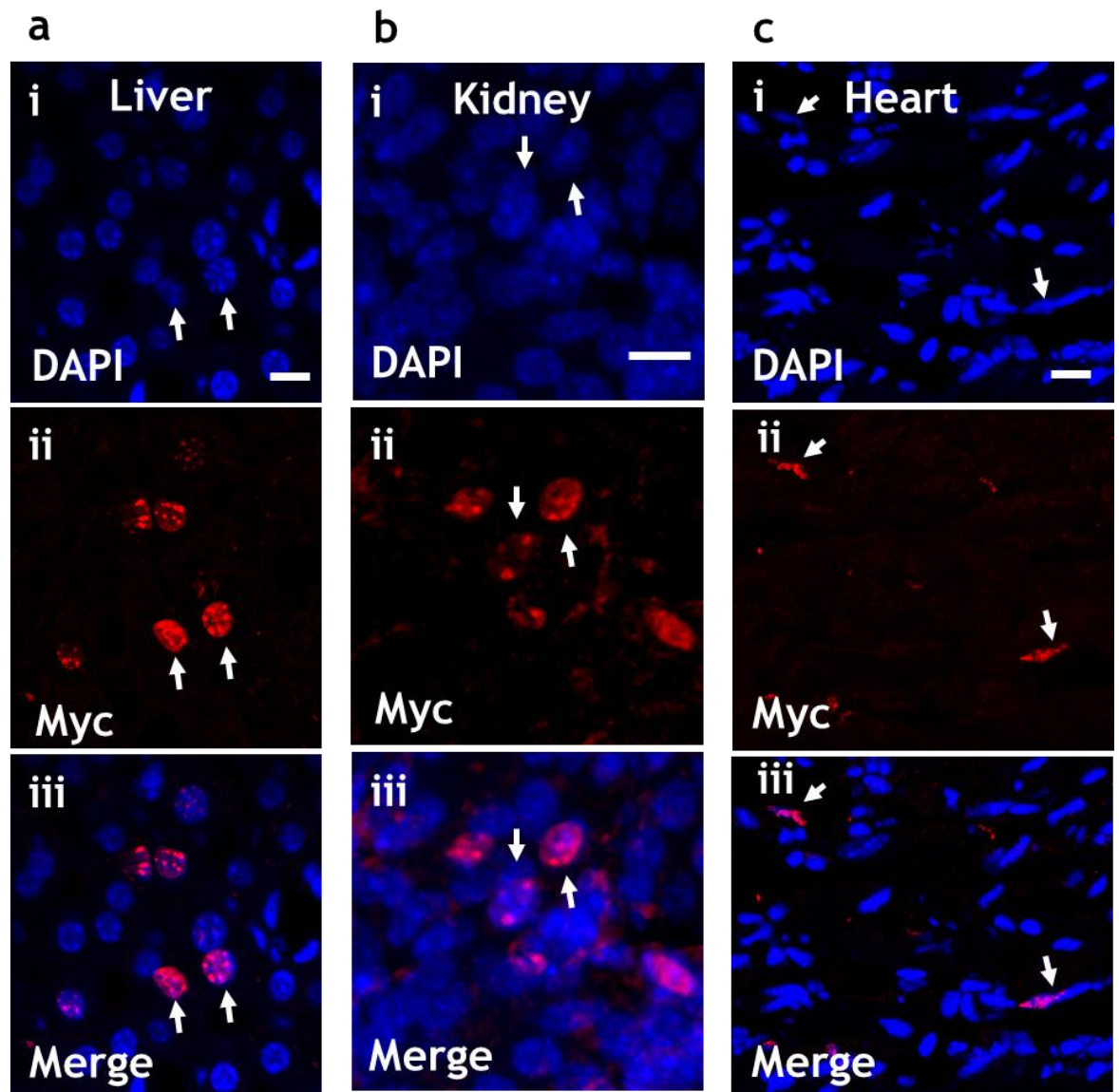


Figure 6-2 IV injection of *scAAV9/MECP2* in neonatal mice produced widespread expression of exogenous MeCP2 in the peripheral tissues. Micrographs showing IV injection of *scAAV9/MECP2* in mice neonates. (a-c); sections were prepared from the liver, kidney and the heart then; (i) stained with DAPI and (ii) immunolabeled with anti-Myc antibody. (iii) Co-localization between anti-Myc immunofluorescence and DAPI fluorescence indicates nuclear targeting of exogenous MeCP2 and confirms peripheral expression of the transgene. Scale bar = 10 μ m.

To confirm transgene expression in the brain after IV injection of *scAAV9/MECP2* in neonatal mice, brain coronal sections were immunolabelled with anti-Myc and anti-NeuN antibodies and stained with DAPI. The results showed that the transgene has been delivered to all brain regions and the exogenous *Mecp2* was allocated to the nucleus with pattern of expression resemble that of the

endogenous protein (heterochromatin targeting) with no obvious ectopic (cytoplasmic) expression. The results also show that exogenous *Mecp2* expressing cells (Myc-immunopositive) are putatively neurons as indicated by co-localization between anti-Myc and anti-NeuN immunofluorescences. However, exogenous *Mecp2* expression was observed in NeuN-immunonegative nuclei indicating that the non-neuronal population of cells (presumed to be glia) were also transduced (figure 6-3).

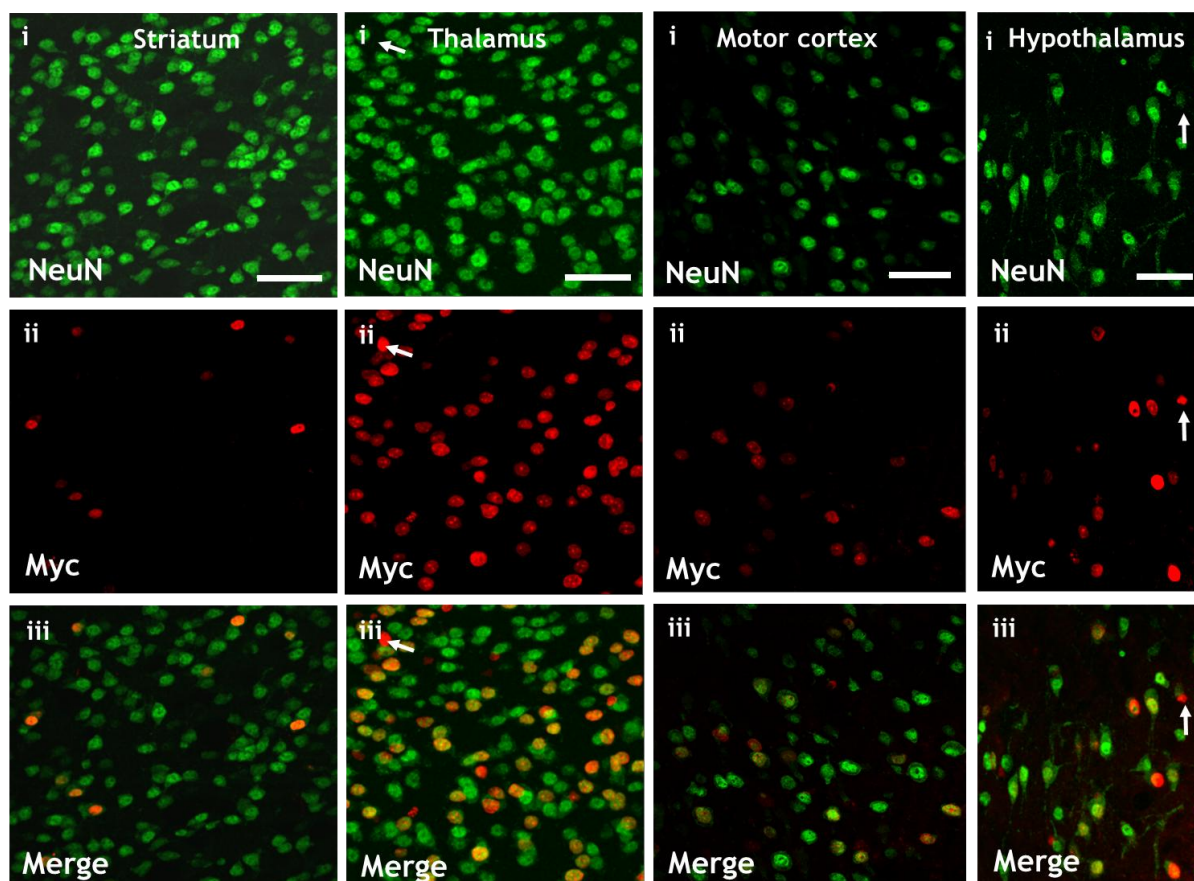


Figure 6-3 IV injection of *scAAV9/MECP2* into neonatal mice resulted in high neuronal transduction in the brain. Micrographs showing sections from striatum, thalamus, motor cortex and hypothalamus that were immunolabelled with (i) anti-NeuN and (ii) anti-Myc antibodies. The transduction efficiency varied across different brain regions with high neuronal transduction. Arrows label Myc-positive, NeuN-negative nuclei (proposed to be glia). Scale bar = 50 μ m.

The transduction efficiency of IV injected *scAAV9/MECP2* varied across brain regions. To measure the transduction efficiency, brain coronal sections prepared from injected mice (11 weeks post-injection) were immunolabelled with anti-Myc antibody and stained with DAPI. The transduction efficiency was calculated by dividing numbers of Myc-immunopositive nuclei by numbers of DAPI stained nuclei in 12 optical sections (N = 3 mice). The results showed that the transduction efficiency in the hippocampus was 12.2 ± 1.6 %, mean \pm SEM, of all

counted cells (N = 140 Myc- immunopositive nuclei of 1160 DAPI-stained nuclei, figure 6-4) whereas the transduction efficiency in the motor cortex was 8.2 ± 0.8 % of all counted cells (N = 146 Myc-immunopositive nuclei of 1811 DAPI-stained nuclei).

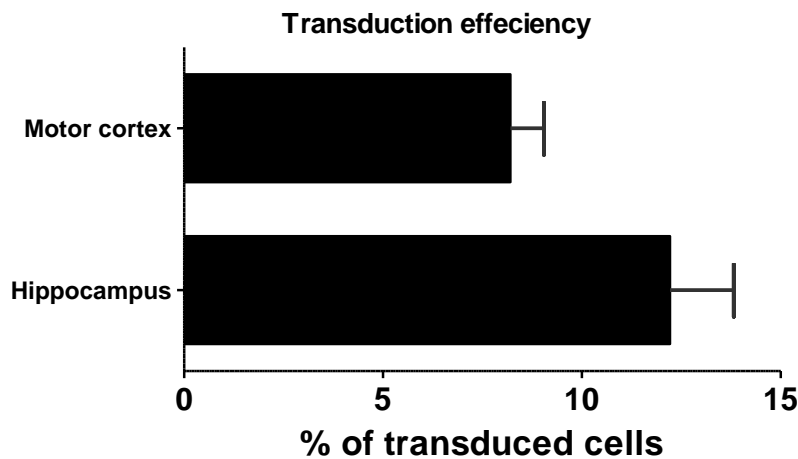


Figure 6-4 Transduction efficiency of scAAV9/*MECP2* in the brain after IV injection in neonatal mice.

Plot showing the transduction efficiency of scAAV9/*MECP2* in the motor cortex and hippocampus. Data is presented as mean \pm SEM, N = 3 mice).

In order to test the extent of transgene expression in the CNS after IV injection of scAAV9/*MECP2*, transverse sections were prepared from the lumbar segment of the spinal cord and immunolabelled with anti-Myc and anti-ChAT (choline acetyltransferase, lower motor neuron-specific marker) antibodies. Exogenous MeCP2 expression (Myc-immunopositive) was widely expressed through the lumbar sections especially in the gray matter (figure 6-5a). There was a co-localization between anti-Myc and anti-ChAT immunofluorescences indicating transgene expression in the lower motor neurons. However, Myc-immunopositive nuclei were also observed in ChAT-immunonegative cells suggesting transgene expression in other cell populations (neurons or glia). High power images further confirm transgene expression in lower motor neurons (figure 6-5b).

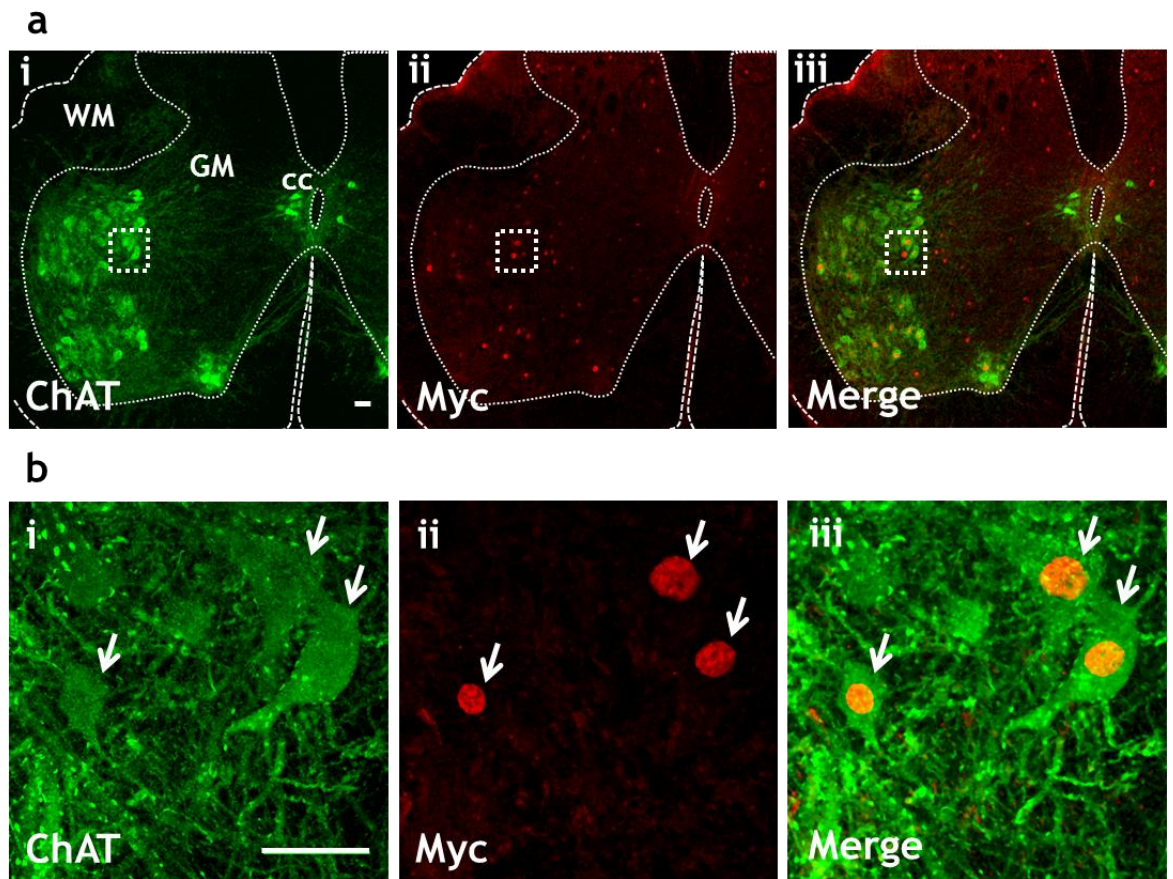


Figure 6-5 IV injection of scAAV9/*MECP2* into neonatal mice produces widespread transgene expression in the spinal cord. Micrograph showing sections from the lumbar segment of the spinal cord that were immunolabelled with; (i) anti-ChAT (lower motor neuron specific marker) and (ii) anti-Myc antibodies. (a) Low power images showing widespread expression of the transgene throughout the spinal cord section. Dotted boxes in (ai-iii) indicate high power images in (bi-iii). (b) High power images showing transgene expression in the lower motor neurons. Arrows indicate the ChAT-positive, Myc-positive lower motor neurons. Scale bar = 50 μ m. ChAT; choline acetyltransferase, cc; central canal, GM; gray matter, WM; white matter.

6.4.2 IV injection of scAAV9/*MECP2* in neonatal mice resulted in *MeCP2* expression at near-physiological cellular levels

Maintaining cellular levels of *MeCP2* within a narrow physiological window is crucial for normal function and to avoid overexpression-related toxicity (Luikenhuis et al., 2004, Na et al., 2012). To quantify the cellular levels of the transgene product and relate this to endogenous *Mecp2* levels, WT neonatal mice were injected intravenously (N = 3) with scAAV9/*MECP2*. Injected mice were perfused 11 weeks post-injection and their coronal brain sections were immunolabelled with anti-Myc and anti-*MeCP2* antibodies. Myc-immunofluorescence used to discriminate transduced cells (figure 6-6a) whereas the intensity of *MeCP2*-immunofluorescence used to quantify the cellular levels of *MeCP2* in transduced and non-transduced cells (discussed in chapter 2).

Transduced cells showed cellular levels of exogenous MeCP2 equal to 1.5 ± 0.1 , mean \pm SEM, times the endogenous levels in the CA3 region of the hippocampus and 1.1 ± 0.1 times the endogenous levels in layer V of the primary motor cortex (figure 6-6b). Analysis of MeCP2 expression levels (measured as immunofluorescence intensity) in transduced and non-transduced cells (N = 3 brains) showed endogenous MeCP2 levels to be tightly regulated (narrow peak SD = 0.1 AU, figure 6-6c), while levels in transduced cells showed increase and varied expression levels (SD = 0.6 AU).

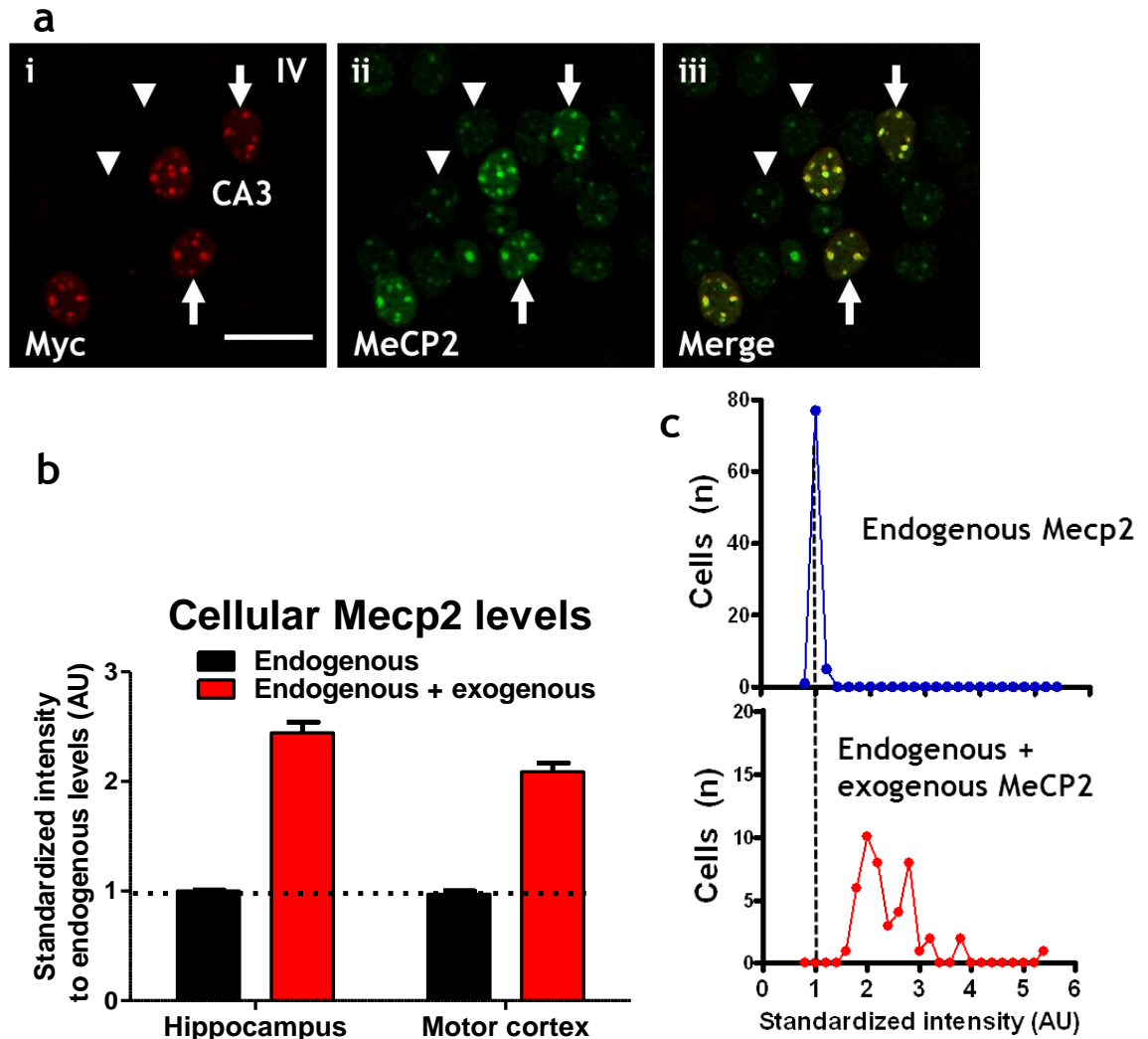


Figure 6-6 IV injection of scAAV9/MECP2 produced near-normal cellular levels of MeCP2. (a) Micrographs showing sections prepared from WT mouse brain 11 weeks after neonatal IV injection. Sections were immunolabelled with (i) anti-Myc and (ii) anti-Mecp2 antibodies. Arrows indicate transduced cells whereas arrowheads indicate non-transduced cells in the CA3 pyramidal cells layer of the hippocampus. Myc immunofluorescence used to discriminate transduced and non-transduced cells (iii). (b) Plot showing the cellular levels of MeCP2 in non-transduced cells (endogenous) and in transduced cells (endogenous + exogenous MeCP2) in the CA3 region of the hippocampus of WT (N = 3). (c) Distribution of MeCP2 levels in transduced and non-transduced CA3 pyramidal cells of the hippocampus (N = 3 brains) after IV injection of scAAV9/MECP2. Immunofluorescence intensity of the endogenous + exogenous MeCP2 showed wide range of expression (N = 46 cells). All data are standardized to the average of endogenous values. Results presented as mean \pm SEM. Scale bar = 20 μ m. AU; arbitrary units.

6.4.3 CNS injection of scAAV9/*MECP2* in neonatal mice produced high transduction efficiency of exogenous MeCP2 throughout the brain

In the previous experiment, IV injection of scAAV9/*MECP2* produced global expression of exogenous MeCP2, but the transduction efficiency in the brain was relatively low. The limited brain transduction after IV injection is probably due to viral spread into the peripheral organs. In order to avoid/minimize peripheral spread of the transgene and to augment transduction efficiency in the brain, scAAV9/*MECP2* was injected directly into the brain of neonatal mice. To test brain transduction after direct intracranial injection, WT and *Mecp2*^{stop/y} neonatal mice (P0-2) were injected directly to the brain with scAAV9/*MECP2* (6 μ l of 3.1×10^{11} vg / ml, 1.8×10^9 vg / mouse). A cohort of neonatal mice were injected with equal dose scAAV9/*GFP* and used as a control. Brain coronal sections were prepared from IC injected mice (N = 3) and immunolabelled with anti-Myc antibody and stained with DAPI. The results showed that exogenous MeCP2 was broadly expressed throughout the brain (figure 6-7) and recapitulated the same nuclear distribution pattern of endogenous *Mecp2*.

To test the extent of exogenous MeCP2 expression in the spinal cord and peripheral organs, sections from the lumbar segment of the spinal cord and from the liver were immunolabelled with anti-Myc antibody and stained with DAPI. Myc-immunopositive cells were observed in the spinal cord, especially in the lower motor neurons, as indicated by co-localization with anti-ChAT antibody. Anti-Myc immunopositive cells were also observed in the liver indicating broad transduction efficiency in the peripheral organ after direct brain injection of scAAV9/*MECP2* (data not shown).

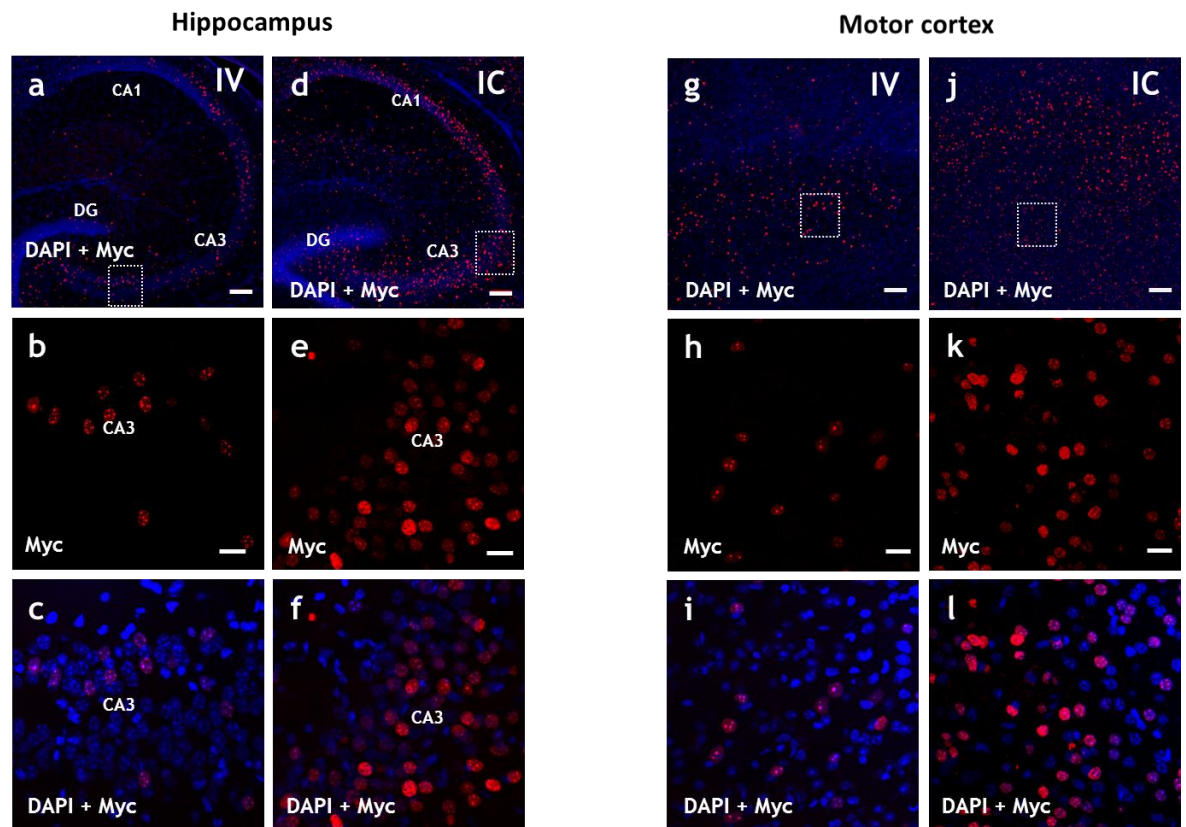


Figure 6-7 IC injection of scAAV9/MECP2 produced higher brain transduction than IV injection in neonatal mice.

Micrograph showing sections prepared from the hippocampus and motor cortex and immunolabelled with anti-Myc antibody and stained with DAPI. (a&d) Low power images showing transgene expression in the hippocampus after IV and IC injection of scAAV9/MECP2. Dotted boxes in (a&d) indicate high power images in (b-f). (b-c) and (e-f) High power images showing transgene expression in the CA3 area of the hippocampus. (g&j) low power images showing exogenous MeCP2 expression in the motor cortex after IV and IC injection of scAAV9/MECP2. Dotted boxes in (g&j) indicate high power images in (h-l). (h-l) and (k-l) High power images showing transgene expression in the deep cortical layer of the motor cortex. Note the increased number of cells expressing exogenous MeCP2 in the hippocampus and the motor cortex after IC injection compared to that after IV injection. Scale bar in a, d, g and j = 100 μ m and in b, e, h and k = 20 μ m.

To confirm the expression of GFP in the control group, brain coronal sections prepared from mice injected IC with scAAV9/GFP were immunolabelled with anti-GFP and anti-NeuN antibodies. Co-localization between GFP and NeuN immunofluorescence indicated that the transgene is putatively expressed in neurons (figure 6-8).

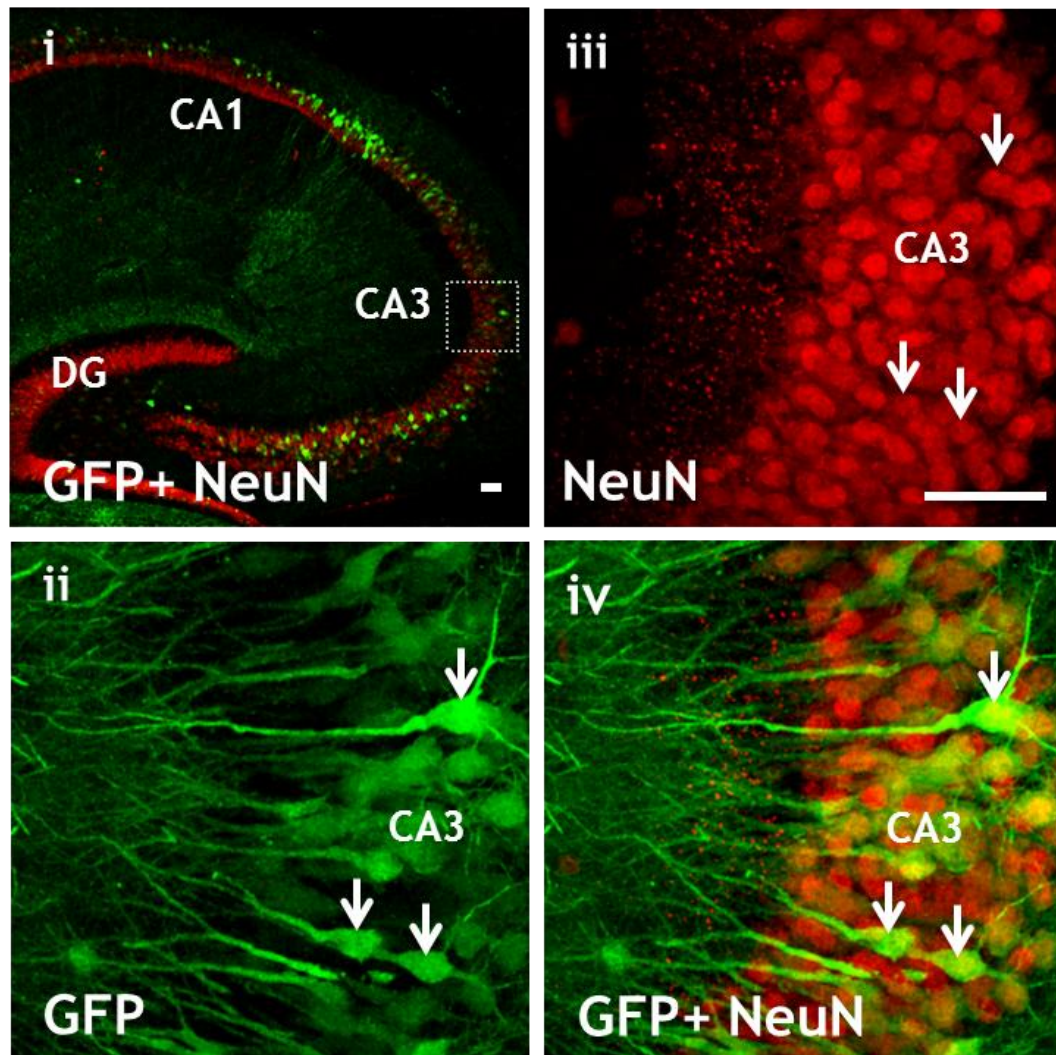


Figure 6-8 IC injection of scAAV9/GFP in neonatal mice produced a broad GFP expression in the brain.

Micrograph showing section prepared from the hippocampus 8 weeks after IC injection and immunolabelled with anti-GFP and anti-NeuN antibodies. (i) Low power image showing co-labelling between GFP (green) and NeuN (red) immunofluorescence in the hippocampal regions. Note the widespread expression of the GFP across the hippocampus. Dotted box in (i) refers to high power images in (ii-iv). (ii-iv) High power micrographs of the CA3 region of the hippocampus showing; (ii) anti-GFP, (iii) anti-NeuN immunofluorescence and (iv) merge of (ii & iii). Arrows refer to cells co-labelled with GFP and NeuN immunofluorescence indicating neuronal transduction. Scale bar = 50 μ m.

To measure the transduction efficiency, the number of Myc-immunopositive nuclei were counted in 18 optical sections (N = 3 mice) and divided by the number of DAPI stained nuclei in the same field. The results showed that the transduction efficiency in the hippocampus was $68 \pm 3.5 \%$, mean \pm SEM, of all counted cells (N = 854 Myc-immunopositive nuclei of 1245 DAPI stained nuclei, figure 6-9) whereas in the motor cortex, the transduction efficiency was $49.5 \pm 4.5 \%$ of all cells (N = 820 Myc-immunopositive cells of 1675 DAPI stained nuclei).

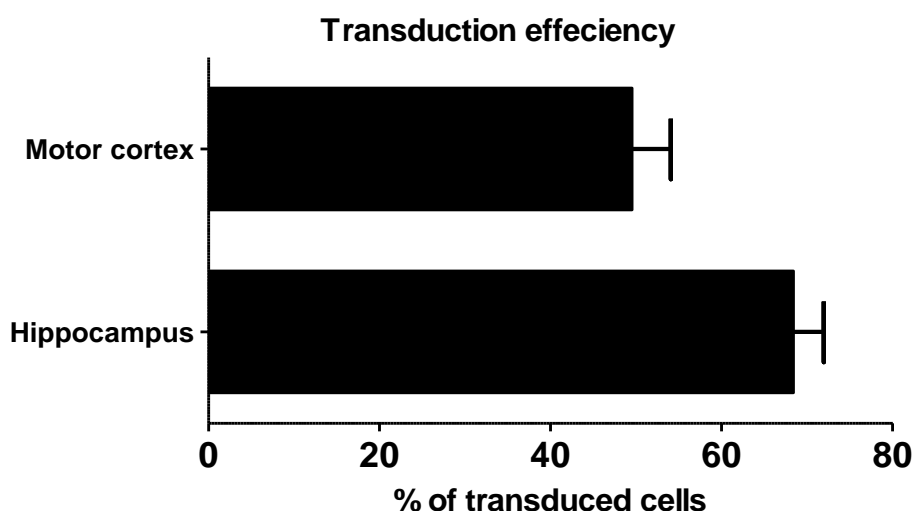


Figure 6-9 IC injection of scAAV9/*MECP2* produced high transduction efficiency in neonatal mice.

Plot showing the transduction efficiency in the motor cortex and hippocampus of 11 week old mouse after IC injection of scAAV9/*MECP2* (N = 3 mice). Data presented as mean ± SEM.

6.4.4 IC injection of scAAV9/*MECP2* in neonatal mice resulted in high cellular levels of MeCP2 expression

To test whether the high brain transduction efficiency obtained after IC injection of scAAV9/*MECP2* is coupled with an increase in *Mecp2* expression levels, brain coronal section from WT neonatal mice (N = 3) injected with scAAV9/*MECP2* were immunolabelled with anti-Myc and anti-MeCP2 antibodies. Myc-immunofluorescence used to distinguish transduced cells (figure 6-10a) whereas the intensity of MeCP2-immunofluorescence used to quantify cellular levels of MeCP2 in transduced and non-transduced cells. The results show that cellular levels of MeCP2 in transduced cells were 1.8 ± 0.1 AU and 1.5 ± 0.1 AU times the endogenous level in the CA3 and layer V of the motor cortex respectively (figure 6-10b). These results suggest that the exogenous MeCP2 was being expressed in *Mecp2*^{stop/y} mice at approximately 1.5 - 1.8 times the endogenous levels after IC injection. Analysis of MeCP2 expression levels (measured as immunofluorescence intensity) in transduced and non-transduced cells after IC (N = 3 brains) injection showed endogenous MeCP2 levels to be tightly regulated (narrow peak SD = 0.1 AU), while levels in transduced cells showed a wide variability in the expression levels (SD = 0.9 AU, figure 6-10c).

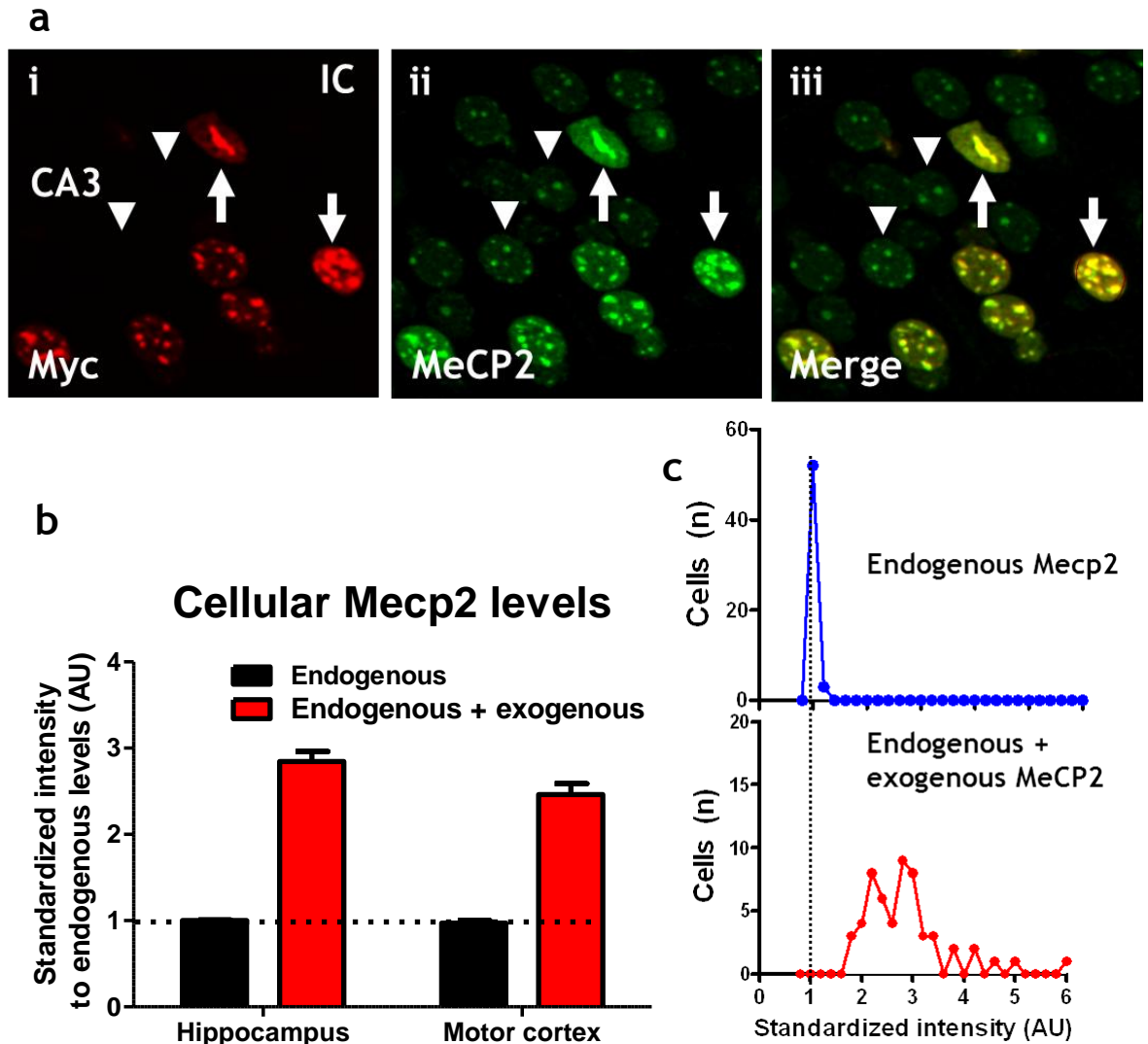


Figure 6-10 *scAAV9/MECP2* expressed high cellular levels of exogenous MeCP2 after IC injection in neonatal mice.

(a) Micrographs showing sections prepared from WT mice brain after IV injection. Sections were immunolabelled with (i) anti-Myc and (ii) anti-Mecp2 antibodies. Arrows indicate transduced cells whereas arrowheads indicate non-transduced cells in the CA3 pyramidal cells layer of the hippocampus. Myc-immunofluorescence used to discriminate transduced and non-transduced cells (iii). (b) Plot showing the cellular levels of MeCP2 in non-transduced cells (endogenous) and in transduced cells (endogenous + exogenous MeCP2) in the CA3 region of the hippocampus of WT (N = 3) mice. (c) Distribution of MeCP2 levels in transduced and non-transduced CA3 pyramidal cells of the hippocampus (N = 3 brains) after IC injection and of *scAAV9/MECP2*. Immunofluorescence intensity of the endogenous + exogenous MeCP2 showed wide range of expression (N = 52 cells). All data are standardized to the average of endogenous values. Results presented as mean \pm SEM. Scale bar = 20 μ m. AU; arbitrary units

6.4.5 scAAV9/*MECP2* injection in neonatal mice resulted in hindlimb motor dysfunction.

To establish whether scAAV9-mediated gene delivery of *MECP2* can improve and/or prevent development of the RTT-like phenotype, *Mecp2*^{stop/y} and corresponding WT littermate mice were injected intravenously (9.3×10^9 vg) or intracerebrally (1.86×10^9 vg) at an early postnatal time point (P1/P2) with either scAAV9/*MECP2* or scAAV9/*GFP* (as a non-therapeutic control). Weekly blind monitoring of these mice for overt RTT-like features using the established observational scoring system (Guy et al., 2007, Liroy et al., 2011, Weng et al., 2011) was carried out. scAAV9/*GFP* control-injected *Mecp2*^{stop/y} mice (N = 5) showed widespread GFP expression across the brain (figure 6-8) and displayed the expected phenotype severity score that started at 4 weeks with a steep increase in the severity score over subsequent weeks. *Mecp2*^{stop/y} mice injected with scAAV9/*MECP2* (N = 7) developed severe hindlimb motor dysfunction as early as 3 weeks post-injection. The phenotype consists of widely separated hindlimb while standing or moving (figure 6-11a) with frequent twitching uncoordinated paddling movements of the hindlimbs. The affected mice were capable of locomotion by dragging their bodies using their forelimbs. The wide separation of the hindlimbs led to very low Pelvic girdle that partially participate in development/ progression of a severe tail lesion in scAAV9/*MECP2* injected mice (figure 6-11b). Tail lesion is not uncommon feature in *Mecp2* knockout mice and it usually starts as small ulcer at the base of the tail then progresses to involve the entire tail. Unfortunately this tail lesion eventually resulted in complete tail necrosis and an anal infection (figure 6-11b) that necessitated culling these mice as early as 6 weeks after injection. Six of nine WT mice injected intravenously with scAAV9/*MECP2* displayed similar hindlimb motor dysfunction and claspings, whereas scAAV9/*GFP* injected WT mice (N = 5) showed no obvious motor deficits.

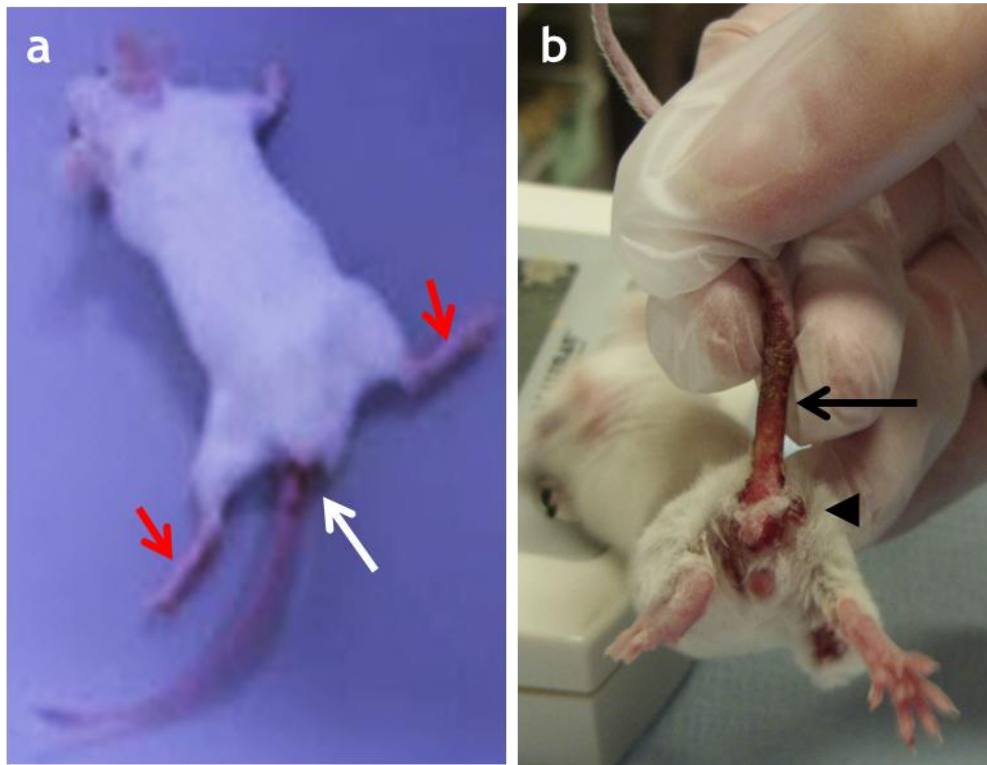


Figure 6-11 scAAV9/MECP2 injection in neonatal mice resulted in Hindlimb motor dysfunction.

(a) A still image of $MECP2^{stop/y}$ mouse 5 month after IV injection with scAAV9/MECP2, red arrows indicate abnormal hindlimb dysfunction whereas white arrow indicates an early stage of the tail lesion. (b) A micrograph of $Mecp2^{stop/y}$ mouse 6 weeks after IV injection of scAAV9/MECP2, arrow indicates advanced tail lesion whereas arrowhead indicates the development of infection at the perianal area that necessitate culling the mouse once reached this stage.

weekly assessment of injected mice using RTT-like phenotype severity score showed that $Mecp2^{stop/y}$ mice injected with scAAV9/MECP2 displayed a significantly ($p < 0.01$, repeated measures ANOVA, tukey`s posthoc pairwise comparison between weeks 3-6) higher phenotype severity score than $Mecp2^{stop/y}$ and WT ($p < 0.01$) mice injected with scAAV9/GFP (figure 6-12a). The aggregate severity score of the WT mice-injected with scAAV9/MECP2 was higher than that of the WT mice-injected with AAV9/GFP, but not significant so. The bodyweight of scAAV9/MECP2 treated $Mecp2^{stop/y}$ mice was significantly lower than scAAV9/GFP-treated $Mecp2^{stop/y}$ mice ($p < 0.01$, repeated measures ANOVA, tukey`s posthoc pairwise comparison) and scAAV9/GFP-treated WT mice ($p < 0.001$). No significant difference was observed in the WT groups treated either with scAAV9/MECP2 or scAAV9/GFP.

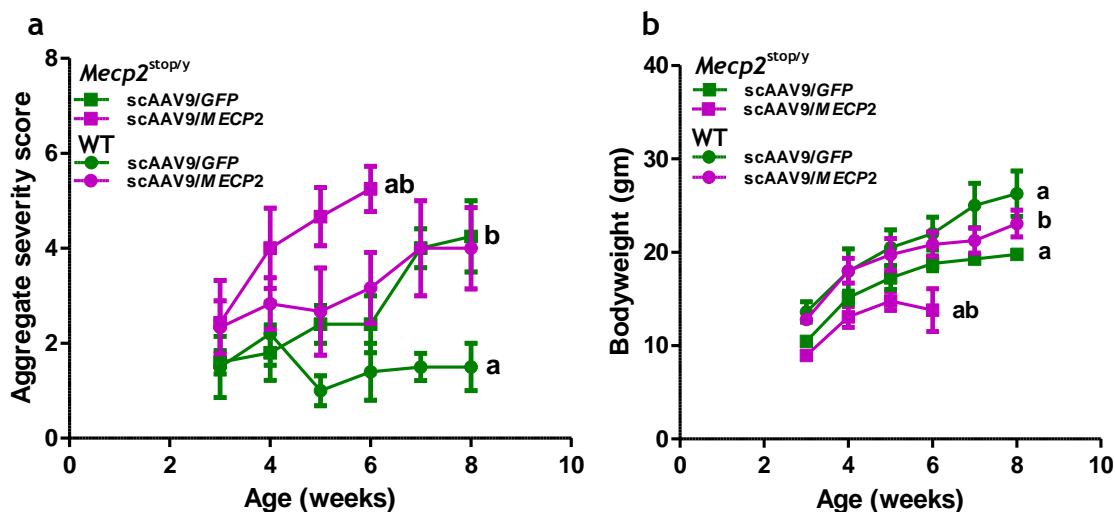


Figure 6-12 Phenotype severity and bodyweight measures after IV injection of scAAV9/MECP2 in neonatal mice. (a) Plot showing the trajectory of the RTT-like phenotype severity score after IV injection of scAAV9/MECP2 or scAAV9/GFP in neonatal mice. (b) Plot showing the bodyweight of scAAV9/MECP2 and scAAV9/GFP treated mice. Groups that share the same letter are significantly different. Values presented as means \pm SEM. Statistical analysis was carried out with (repeated measure ANOVA with tukey's posthoc pairwise comparison between weeks 3-6).

Mecp2^{stop/y} mice injected with scAAV9/MECP2 intracranially displayed similar, though later onset, hindlimb motor dysfunction with onset at ~5 weeks post-treatment). A number of these mice also displayed stunted growth, eye problems (opacity, figure 6-13a,b) and hindlimb clasping (figure 6-13d). WT mice treated with IC injection of scAAV9/MECP2 (N = 4) showed a significantly ($p < 0.01$, repeated measures ANOVA, tukey's posthoc pairwise comparison between weeks 3-8) higher phenotype severity score than WT mice treated with scAAV9/GFP (N = 5) (figure 6-14a). *Mecp2*^{stop/y} showed significantly ($p < 0.05$) higher phenotype severity score than WT mice injected with scAAV9/GFP

Bodyweight measurements showed that WT mice treated with scAAV9/GFP was significantly ($p < 0.001$, repeated measures ANOVA, tukey's posthoc pairwise comparison between weeks 3-8) higher than that of both *Mecp2*^{stop/y} mice-treated either with scAAV9/GFP or scAAV9/MECP2 and WT mice treated with scAAV9/MECP2 (figure 6-14b). The bodyweight of WT and *Mecp2*^{stop/y} mice treated with scAAV9/MECP2 was significantly ($p < 0.01$) lower than the bodyweight of *Mecp2*^{stop/y} mice treated with scAAV9/GFP.

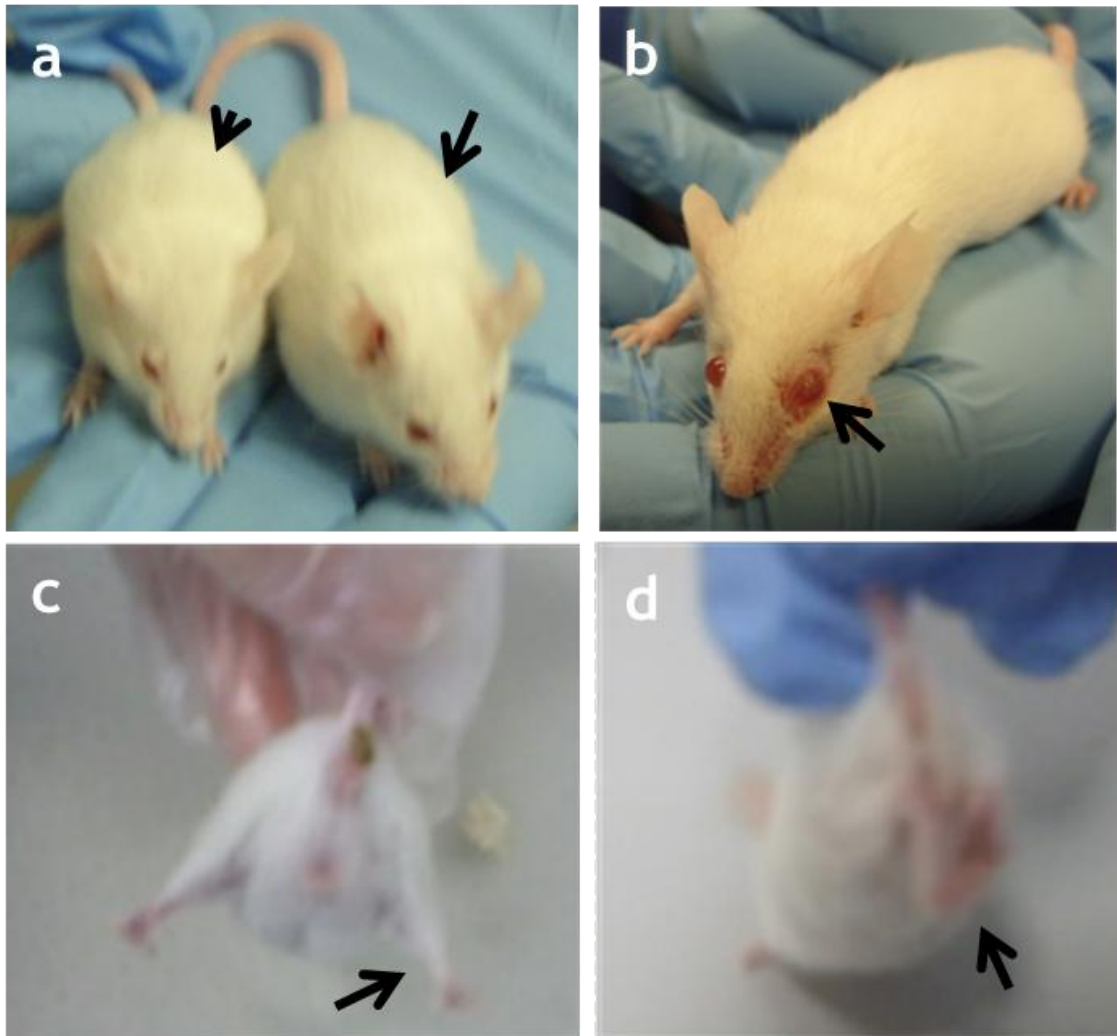


Figure 6-13 IC injection of scAAV9/MECP2 results in abnormal phenotypes in WT mice (a) A micrograph showing stunted growth of a WT mouse (arrow head) treated with IC AAV9/hMECP2 compared to the WT littermate injected by the same virus (arrow) indicating mouse to mouse variability. (b) A micrograph showing eye abnormality (corneal opacity, (arrow) that developed in few WT mice after IC injection with scAAV9/MECP2. (c) A still image showing normal hindlimb reflex (arrow) in WT mouse treated with AAV9/GFP. (d) A still image showing development of hindlimb clasping (arrow) in WT mouse after IC injection of AAV9/MECP2.

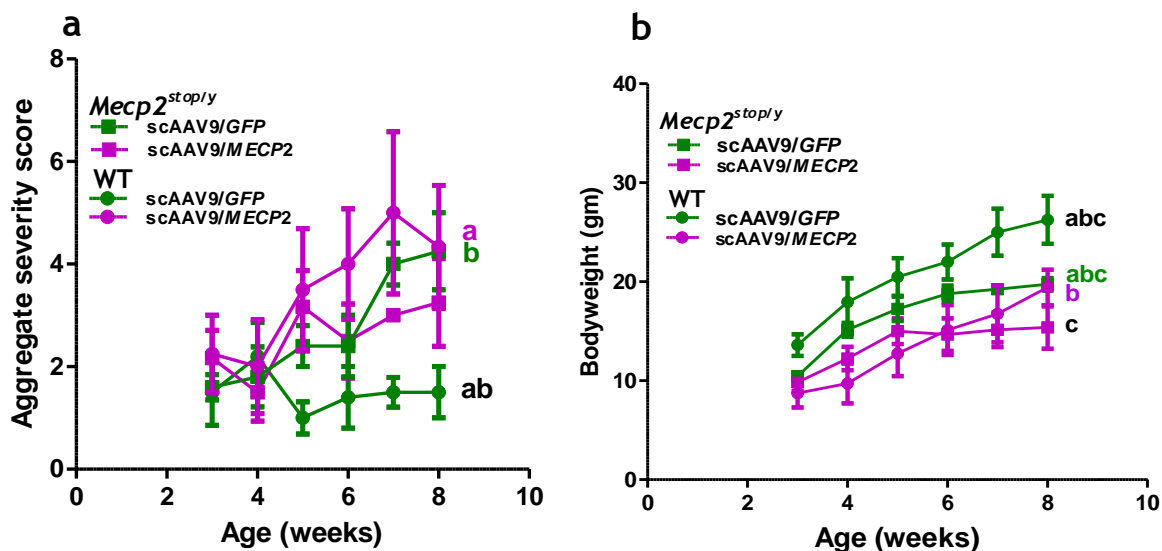


Figure 6-14 Phenotype severity score and bodyweight analysis after IC injection of scAAV9/MECP2 in neonatal mice.

(a) Plot showing the aggregate phenotype severity score of WT mice injected with scAAV9/GFP (N = 5) and scAAV9/MECP2 (n = 4) and *Mecp2*^{stop/y} mice injected with scAAV9/GFP (N = 5) and scAAV9/MECP2 (N = 6). (b) Plot showing the bodyweight of scAAV9/MECP2 and scAAV9/GFP treated mice. Groups that share the same letter are significantly different. Values are presented as mean \pm SEM. Statistical analysis was carried out with repeated measure ANOVA (between weeks 3-8) with tukey's post-hoc pairwise comparison.

6.4.5.1 Hindlimb motor dysfunction is associated with axonal degeneration of the dorsal column of the lumbar spine in scAAV9/MECP2-injected mice.

To investigate the potential underlying causes of the hindlimb motor dysfunction observed in *Mecp2*^{stop/y} and WT mice after neonatal injection of scAAV9/MECP2, four mice (with or without the hindlimb problem) were transcardially perfused using hard fixative (2% glutaldehyde and 4% PFA in 0.1 M cacodylate buffer). Semi-thin (0.5 μ m) sections were made from different regions of the spinal cord (cervical, thoracic and lumbar regions) and stained with toluidine blue dye to show the structure of the axons and their myelin sheath (this experiment was kindly carried out blindly by Dr. Julia Edgar, Institute of Infection, Immunity and Inflammation, University of Glasgow). Light microscopic analysis of these sections showed evidence of axonal degeneration in the dorsal columns of the lumbar region of the spinal cord as indicated by the presence of myelin sheath devoid of axons (figure 6-15). There were no detectable anatomical abnormalities in other regions of the spinal cord in the tested mice (N = 3).

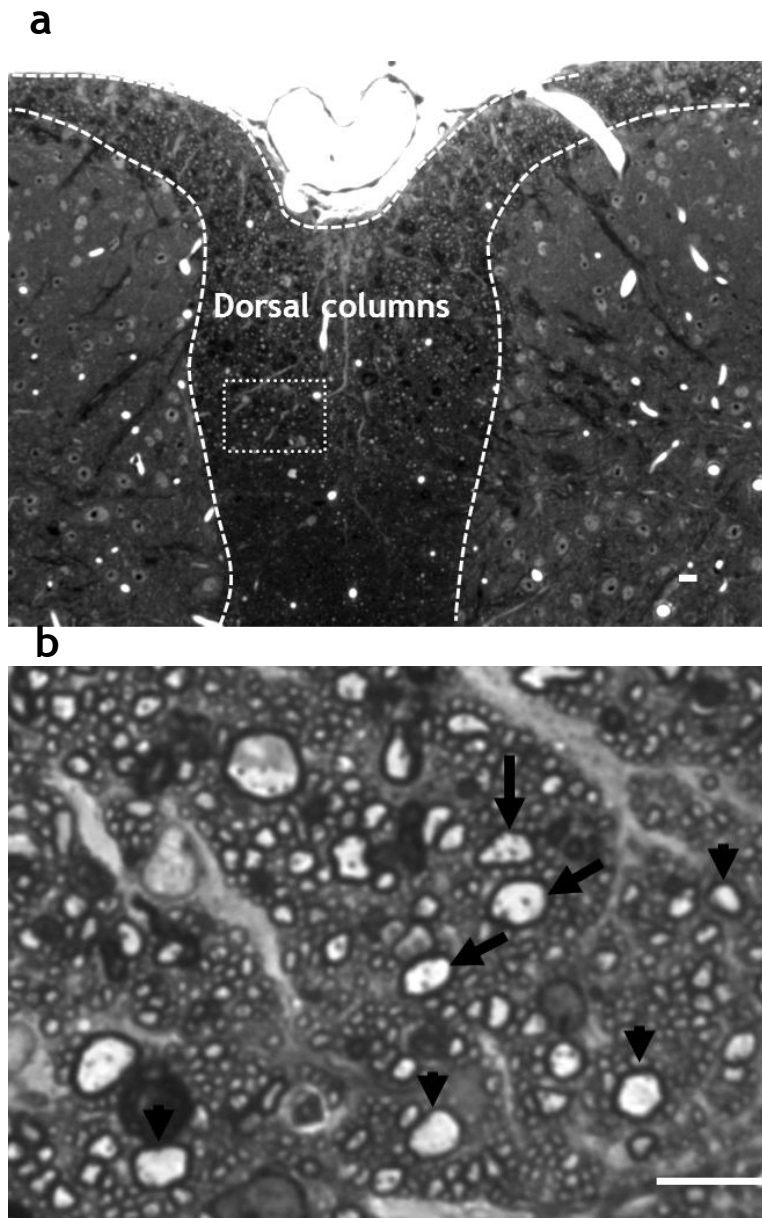


Figure 6-15 Axonal degeneration of the dorsal columns of the lumbar spine
 (a) Low power magnification of the lumbar region of the spinal cord showing the dorsal columns (dashed line). Dotted box indicates high power image. (b) High power image of the dorsal columns showing white myelin sheath with black axon inside (arrows) and empty myelin sheath (arrowheads) denoting axonal degeneration. Scale bar = 10 μ m.

6.4.5.2 CD3 immuno-reactivity in the spinal cord of scAAV9/*MECP2* injected mice

Adeno-associated viruses are currently used in several clinical trials because of their ability to transduce a wide variety of tissues with sustained long term expression (Mingozzi and High, 2007). No immune reactivity was reported in animal studies; however, minimal immune stimulation was reported after AAV injection in clinical trials (Manno et al., 2006, Mingozzi et al., 2007). To exclude the possibility of immune system involvement in the pathogenesis of axonal

degeneration of the dorsal columns, 10 μ m frozen section from the lumbar spine of scAAV9/*MECP2* injected-*Mecp2*^{stop/y} mice which displayed hindlimb motor dysfunction and from control non-injected mice, were stained with mouse anti-CD3 antibodies (CD3 is expressed in natural killer T cells), anti-Myc and anti-NeuN antibodies (figure 6-16). A section from the spleen was included as a positive control for the anti-CD3 antibody. Spleen sections showed the usual pattern of anti-CD3 antibody staining with no evidence of anti-NeuN or anti-Myc positive cells. However in the spinal cord of scAAV9/*MECP2*- injected and non-injected mice, there was co-localization at the cellular level between anti-CD3 and anti-NeuN antibodies (both label neurons with anti NeuN predominantly nuclear and anti-CD3 predominantly cytosolic. In light of this unexpected finding, a second batch of anti-CD3 antibody was tested. However, this produced the same immunolabelling pattern in spinal cord sections which made interpretation of this data difficult.

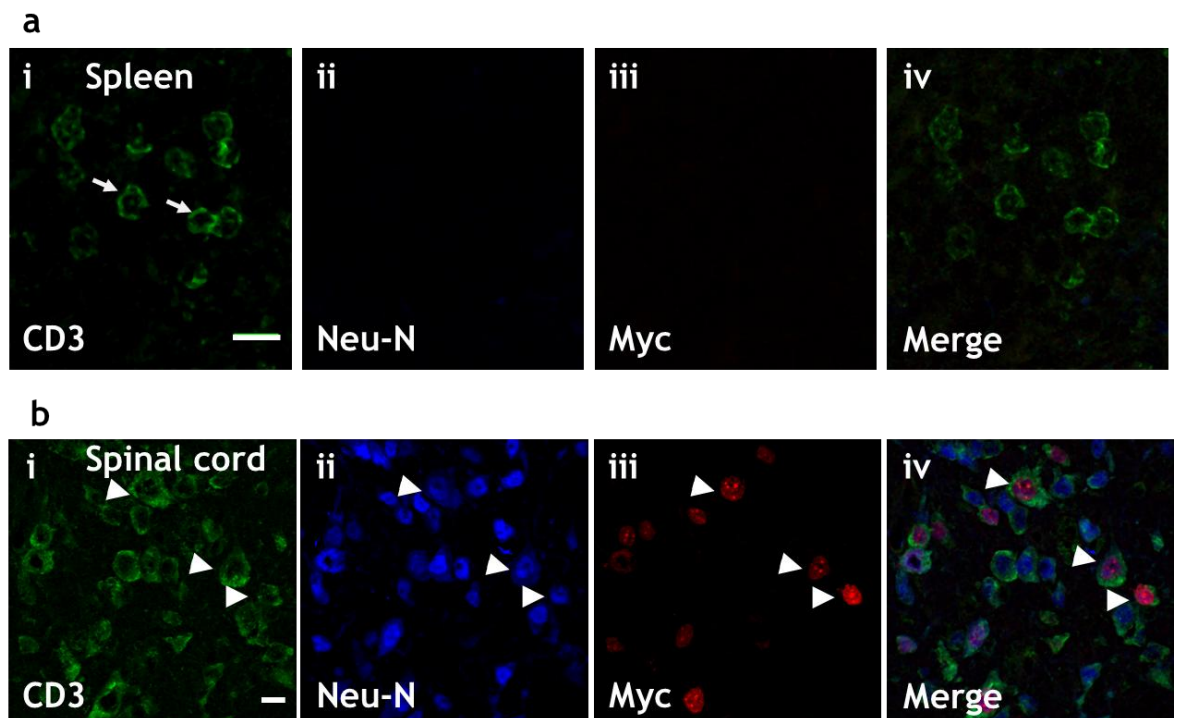


Figure 6-16 Anti-CD3 antibody immunolabelling in the lumbar spine.
(a) Micrograph showing section from the spleen (as a positive control) immunolabelled with (i) anti-CD3, (ii) anti-NeuN and (iii) anti-Myc antibodies. Arrows indicate CD3 expressing T cells in the spleen. **(b)** Micrograph showing section from the lumbar region of the spinal cord immunolabelled with (i) anti-CD3, (ii) anti-NeuN and (iii) anti-Myc antibodies. Arrowheads indicate exogenous MeCP2 expression in CD3-immunopositive, NeuN-immunopositive cells. Scale bar = 10 μ m.

6.4.5.3 Neonatal IV injection of scAAV9/*MECP2* produced hindlimb motor dysfunction in RAG knockout mice.

I showed in the previous experiment that anti-CD3 immunolabelling of the spinal cord was not conclusive due to the fact that anti-CD3 antibody additionally labelled NeuN immunopositive cells (putative neurons). To further investigate the involvement of the immune system in the development of the hindlimb motor dysfunction, three RAG^{-/-} (Recombination Activation Gene) knockout mice were injected IV at P0-2 with scAAV9/*MECP2* at a dose of 30 μ l of 3.1×10^{11} vg / ml (9.3×10^9 vg). These mice lack mature B and T lymphocytes (Mombaerts et al., 1992) (generous gift from DR. Alison Michie, Institute of Cancer Sciences, University of Glasgow). Two of these mice were found dead one week after injection and thus could not be investigated further. Weekly monitoring of the remaining mouse showed that it developed hindlimb motor dysfunction at 5 weeks post-injection similar to previous animals injected with scAAV9/*MECP2*. Sections from the brain of this mouse showed transduction efficiency comparable to that of *Mecp2*^{stop/y} mice injected with the same virus (figure 6-17). These results suggest that a T and B cell-mediated immune response is not likely to be responsible for the hindlimb motor dysfunction seen in scAAV9/*MECP2*-treated mice, however the possible role of the innate immune response remains to be investigated.

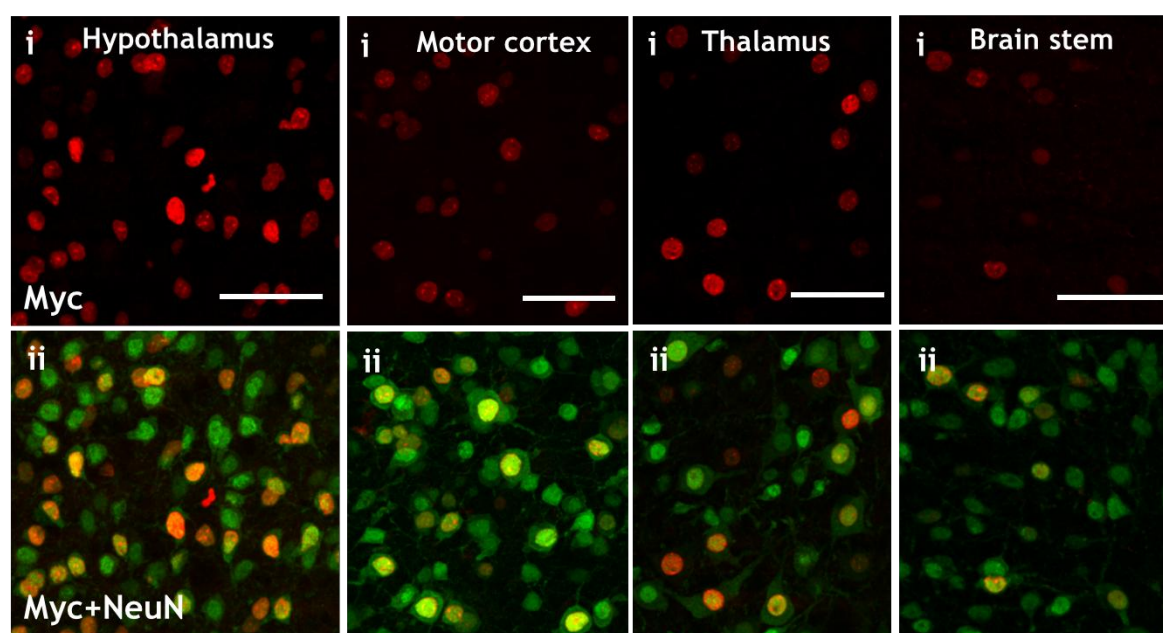


Figure 6-17 Exogenous MeCP2 expression in RAG^{-/-} knockout mouse brain
Micrographs showing exogenous MeCP2 expression in the brain of RAG^{-/-} mouse 8 weeks after neonatal IV injection of scAAV9/*MECP2*. Different brain regions were immunolabelled with (i) anti-Myc and (ii) anti-NeuN. Scale bar = 50 μ m.

6.4.5.4 Neonatal IV injection of scAAV9/*mMecp2* led to a similar motor deficit in *Mecp2*-null mice.

Human and mouse MeCP2 are 96% identical with just 19 amino acids different. Genetic studies have shown human MeCP2 to replace the function of the mouse protein and prevent the onset of RTT-like phenotypes in transgenic mice without overt drawbacks (Collins et al., 2004). However, to further exclude the possibility that using human MeCP2 in a murine model was a potential cause of the motor deficits, a mouse *Mecp2* minigene was cloned in AAV2/9 backbone to generate scAAV9/*mMecp2* virus particles. In addition, I decided to exclude the possibility that the mouse strain was a contributing factor by using *Mecp2*-null mice on a C57BL/6 background. ScAAV9/*mMecp2* (9.3×10^9 vg) was intravenously injected into the facial vein of *Mecp2*^{-/-} (N = 1) and WT (N = 3) mice at P0-2. Hindlimb motor deficit was observed in the WT and *Mecp2*^{-/-} mice 3-4 weeks post-injection (figure 6-18) indicating consistent adverse effect when either the human or mouse *MECP2_e1* encoding sequences are delivered by scAAV9 vector in mice neonates.

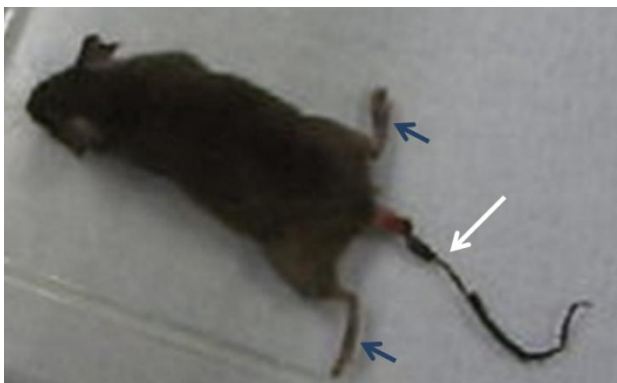


Figure 6-18 IV injection of scAAV9/*mMecp2* into neonatal *Mecp2*^{-/-} mice resulted in hindlimb motor dysfunction.

A still image showing *Mecp2*^{-/-} mice 7 weeks after IV injection of scAAV9/*mMecp2*. Blue arrows indicate abnormal paddling movements characteristic of the hindlimb motor dysfunction whereas white arrow indicates tail lesion that has progressed to tail necrosis.

6.4.5.5 IC injection of scAAV9/MeP-*MECP2* produced higher transduction efficiency and cellular protein levels than the ssAAV9/CBA-*MECP2* in neonatal mice

Due to the discrepancy in the results obtained after IV and IC injection of scAAV9/MeP-*MECP2* construct compared to that obtained after IC injection of ssAAV9/CBA-*MECP2* in neonatal mice I therefore decided to compare the transduction efficiency and cellular levels of *Mecp2* expressed by these vectors

in the hippocampus and motor cortex of the injected mice. The transduction efficiency after IC injection of self-complementary AAV9/MeP-*MECP2* was significantly ($p < 0.001$, one way ANOVA with tukey`s posthoc pairwise comparison) higher than both IV injection of the same vector (scAAV9/MeP-*MECP2*) and IC injection of single-stranded AAV9/CBA-*MECP2* (figure 6-19a). Whereas IC injection of ssAAV9/CBA-*MECP2* showed significantly ($p < 0.01$) higher transduction efficiency than IV injection of scAAV9/MeP-*MECP2* in the motor cortex. IC injection of scAAV9/MeP-*MECP2* produced significantly higher cellular levels of exogenous MeCP2 than that produced by ssAAV9/CBA-*MECP2* in the hippocampus ($p < 0.01$) and motor cortex ($p < 0.001$, figure 6-19b). There was no significant difference in MeCP2 expression levels between IV scAAV9/MeP-*MECP2* injected mice and IC ssAAV9/CBA-*MECP2* injected mice.

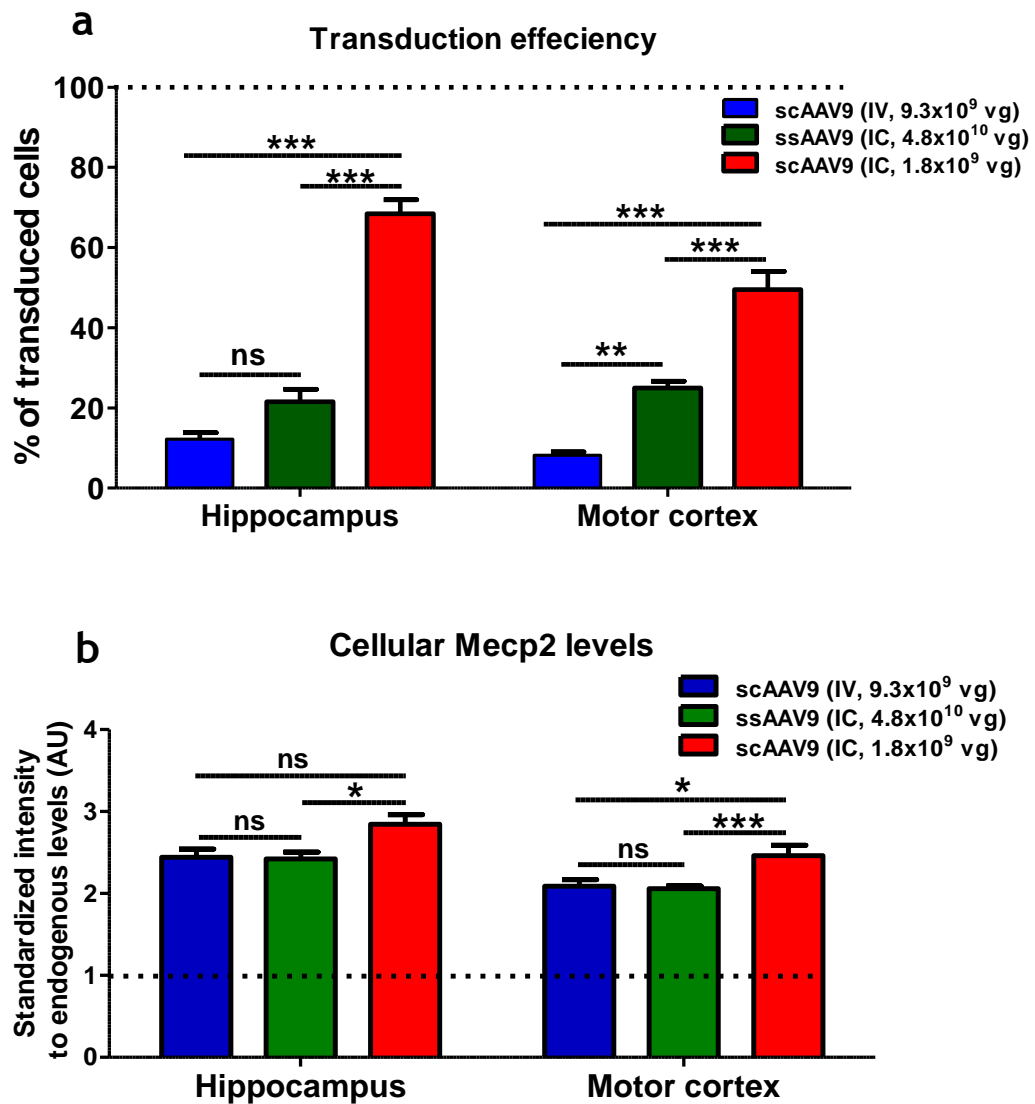


Figure 6-19 scAAV9 mediated higher transduction efficiency and transgene expression after IC injection in neonatal mice.

(a) Plot showing comparison between the transduction efficiency of scAAV9/MeP-*MECP2* after IC and IV injection and that after IC injection of ssAAV9/CBA-*MECP2* in neonatal mice.

(b) Plot showing comparison between cellular levels of exogenous MeCP2 expressed by scAAV9/MeP-*MECP2* after IC and IV injection and that expressed by ssAAV9/CBA-*MECP2* after IC injection in neonatal mice. ns; non-significant, * = $p < 0.05$; ** = $p < 0.05$, *** = $p < 0.001$, one way ANOVA with tukey's posthoc pairwise comparison.

6.5 Discussion

As described in chapter 5, direct neonatal brain injection of ssAAV9/CBA-*MECP2* virus was able to achieve significant, but modest, improvement in the phenotype trajectory and survival of *Mecp2*-null mice despite relatively modest transduction efficiency in the brain. Previous reactivation studies have shown a direct correlation between the degree of phenotype rescue and the percentage of cells expressing *Mecp2* (after delayed activation, Robinson et al., 2012). Therefore we hypothesized that increasing the transduction efficiency by using a

newly developed highly efficient scAAV9 vector (Foust et al., 2009) might produce greater therapeutic benefits in *Mecp2* knockout mice. To test this hypothesis, scAAV9/MeP-*MECP2* virus particles were injected either intravenously (more clinically relevant) or directly into the brain (to achieve high transduction efficiency) into *Mecp2*^{stop/y} mice and their WT littermates. The results showed that scAAV9/MeP-*MECP2* virus particles resulted in mean MeCP2 cellular levels between 100-150 % and 140-184 % of the endogenous *Mecp2* levels after IV and IC neonatal injection respectively with ~5 fold greater transduction efficiency after IC injection. Distribution analysis of *Mecp2* cellular levels revealed that endogenous *Mecp2* levels are very tightly regulated whereas the exogenous MeCP2 showed broader distribution particularly after IC injection which could be explained by increased multiplicity of infection. A finding of major significance was the revelation that *Mecp2*^{stop/y} mice treated with either IV or IC injection of scAAV9/MeP-*MECP2* developed profound hindlimb motor dysfunction as early as 3 weeks of age after IV injection with a more delayed onset (~5 weeks) after IC injection. WT mice injected with this construct displayed variable results with about 67% of the injected mice displaying hindlimb dysfunction. This unexpected toxicity has not been seen in WT and *Mecp2*^{stop/y} mice treated with scAAV9/MeP-*GFP* viruses. The very early high phenotype severity score observed in the IV and IC treated *Mecp2*^{stop/y} mice [normally these mice develop RTT-like phenotype at 5 weeks (Guy et al., 2007, Lioy et al., 2011)] was mainly due to this unusual early hindlimb dysfunction which, though not considered a part of the RTT-like phenotype, impacts on several of the features measured in the scoring system (including gait, hindlimb clasping and mobility). The development of severe tail lesions and anal infection, which was aggravated by the hindlimb dysfunction, and the early termination of the experiment at around 6 weeks of age prohibited tracking the effect of exogenous MeCP2 on the other RTT-like phenotype (e.g. breathing, tremor, general condition and early mortality) the cause of these adverse reactions to the self-complementary AAV/MeP-*MECP2* are not clear. MeCP2 duplication has been reported to produce serious complications in human patients (Meins et al., 2005, Van Esch et al., 2005, Friez et al., 2006). In a mouse model, a two- to three-fold increase in the level of *Mecp2* in post-mitotic neurons produced tremors, gait ataxia, and side-to side swaying (Luikenhuis et al., 2004) whereas modest overexpression (0.6-1 fold of the endogenous *Mecp2*

level) resulted in cognitive impairment, motor coordination deficits and an anxiety-like phenotype (Collins et al., 2004, Na et al., 2012). Interestingly we observed this severe motor dysfunction despite achieving levels of exogenous MeCP2 expression that is comparable to endogenous *Mecp2* levels (after IV injection) and in a relatively low number of cells compared to the duplication studies where the overexpression is global.

Previous study has shown that rapid activation of a conditionally silenced *Mecp2* in mice resulted in severe lethality. However, gradual activation avoided toxicity and achieved phenotype rescue (Guy et al., 2007). Thus, a possible explanation of the overt hind limb phenotype observed after expressing exogenous MeCP2 using scAAV9 vector may be the rapid onset of transgene expression that is associated with self-complementary vectors (Ren et al., 2005). It also explains the absence of this toxicity after using ssAAV9 (more delayed onset of expression) vector to express the same *MECP2* transgene. Previous study has shown that 2-3 fold increase in the expression level of *Mecp2* resulted in motor disability, stunted growth and cataract in mice (Luikenhuis et al., 2004). These phenotypes were observed in mice injected intracranially with scAAV9/*MECP2* vector which indicates that these phenotypes are likely to be due to transgene-related overexpression toxicity.

The overt motor dysfunction was consistently observed only in the hindlimb with apparently normal forelimb function suggesting that the pathology is likely to be in the spinal cord, peripheral nerves of the hindlimb, hindlimb musculature or preferentially affects long fibres. Microscopic examination of the distal spinal cord region was carried out with particular focus on the lumbar regions. The demonstrated axonal degeneration in the dorsal columns of the lumbar spine indicates that the uncoordinated hindlimb movement observed is probably due to lack of sensory perception and not likely to be due to a genuine motor deficit. The occurrence of axonal degeneration only in the lumbar region of the spinal cord suggests that the degeneration process is potentially affecting long axons only. Other parts responsible for sensory perception such as dorsal root ganglia and peripheral nerves, which could be potentially involved in the pathogenesis of this problem, have yet to be investigated.

The presence of activated T-lymphocytes in the spinal cord of patients and animal models of motor neuron disease (e.g. ALS) suggests a potential involvement of immune inflammatory factors in the motor neuron disease process (Alexianu et al., 2001). Taken together with the modest immune response stimulation observed in patient treated with AAV viruses in clinical trials (Manno et al., 2003, Mingozzi and High, 2007, Mingozzi et al., 2007), I hypothesised that axonal degeneration of the dorsal column could be a consequence of AAV9- and/or exogenous MeCP2- inducing an immunological response. The broadly-distributed expression of CD3 receptors in the spinal cord sections prepared from AAV9/*MECP2*-treated and non-treated mice were however shown to be predominantly neuronal as indicated by co-localization with NeuN-immunolabelling. This result suggests that CD3 receptors are expressed in the spinal cord neurons and do not make a reliable assay for lymphocytic infiltration. Indeed, previous reports showed CD3 receptor expression in brain neurons (Garson et al., 1982, Schuller-Petrovic et al., 1983, Syken and Shatz, 2003) with a well-established role in neuronal morphogenesis and dendritic growth (Baudouin et al., 2008). Development of hindlimb motor dysfunction in *RAG*^{-/-} knockout mouse [lack mature T and B cells (Mombaerts et al., 1992)] after neonatal IV injection with AAV9/*MECP2* together with its absence in AAV9/*GFP* injected mice suggest that this hindlimb phenotype is not likely to be due to an adaptive immune response reaction to AAV9 virus particles. Moreover the absence of this hindlimb phenotype in the mice that were injected IC with ssAAV9/*CBA-MECP2* (chapter 5) excludes exogenous MeCP2 *per se* as a trigger to the immune response. Further experiments to investigate the role of the innate immune response need to be done.

The rapid onset of the hindlimb motor dysfunction after IV injection (~3 weeks post-injection) compared to the more delayed onset after IC injection (~5 weeks), despite the fact that IV injection produced lower levels of MeCP2 expression in the brain and 5 fold less brain transduction compared to the IC injection suggests an important role for the peripheral organs in the pathogenesis of this phenotype. An interesting experiment will be to drive peripheral expression of exogenous MeCP2 from an AAV2 vector that cannot pass the BB barrier (Fu et al., 2003) to elucidate the role of peripherally-expressed exogenous MeCP2 in the development of the motor dysfunction phenotype.

The fact that early hindlimb motor dysfunction was seen in all *Mecp2*-null (N = 10) mice treated with scAAV9/*MECP2*, regardless of the method of delivery, whereas only 67 % of the WT mice (N = 9) were affected indicates a putative genotype effect and suggests that the lack of endogenous *Mecp2* is a contributing factor for the occurrence of this phenotype or conversely, that the healthy WT mice are more resilient and resistant to the toxicity.

Human MeCP2 has previously been used for rescue of transgenic *Mecp2*-null mice without producing any detectable adverse effects (Collins et al., 2004). My previous data also showed that human *MECP2*, delivered by a ssAAV9/CBA-*hMECP2* vector, was tolerable in WT animals and produced modest improvement in *Mecp2*-null mice. To further exclude the possible role of human *MECP2* in the development of the hindlimb phenotype, mice were injected with scAAV9/MeP-*mMecp2* that drives expression of mouse form of *Mecp2*. Nevertheless these injected mice displayed a similar motor dysfunction to those injected with human *MECP2* in this study. Together these findings suggest that expression of human MeCP2 in a mice model is probably not a contributing factor in the development of the hindlimb abnormal phenotype.

Interestingly Intravenous injection of scAAV9/MeP-*MECP2* (5×10^{11} vg) in juvenile *Mecp2*-null mice was without apparent toxicity and achieved prolonged survival (this work has been done by Dr. Steven Gray UNC Gene Therapy Centre, University of North Carolina, USA. Gadalla et al 2012 submitted) which indicates that the time of delivery is crucial at least with the construct we used in this experiment. The importance of treatment onset point has yet to be studied systematically however.

Two possible factors haven't been tested in this experiment; the first is the effect of the promoter used in the construct (*Mecp2* endogenous core promoter or chicken beta actin promoter) and the ssAAV9 versus scAAV9 virus construct. Due to the limited cloning capacity of scAAV9, it is not possible to generate scAAV9/CBA-*MECP2*. However a possible experiment would be to generate ssAAV9/MeP-*MECP2* to investigate the possible role of the driving promoter in producing this phenotype.

Concluding remarks

I showed in this chapter that, however, scAAV9/*MECP2* was capable of efficiently delivering *MECP2* into the brain of *Mecp2* knockout mice after peripheral and direct brain injection, this vector resulted in an unexpected and severe overt hindlimb motor dysfunction in *Mecp2* knockout as well as in WT mice. The hindlimb dysfunction may be due to axonal degeneration of posterior columns of the lumbar spine, however other important elements of the sensory and motor control of the hindlimb cannot be ruled out. The exact cause of the axonal degeneration is unclear but it is not likely to be mediated through an adaptive immune response to the viral capsid or to the transgene. I showed previously that IC injection of ssAAV9/CBA-*MECP2* in neonatal mice displayed amelioration in RTT-like phenotype without obvious toxicity in WT mice which indicates that the hindlimb phenotype is likely to be related to the difference in the vector design; transduction efficiency, onset of expression and levels of protein expression rather than the insert *per se*. This data highlights the extreme importance of choosing the right vector, method and age of delivery in any future attempts for RTT gene therapy application to avoid undesirable adverse effects and to achieve maximum therapeutic benefits.

Chapter 7

General discussion

The principal aim of this thesis was to investigate the therapeutic potential of delivering *MECP2* minigene exogenously, through viral vectors, to a mouse model of Rett syndrome. It was anticipated that such a study would provide fundamental information about the pattern and levels of exogenous MeCP2 expression and give an insight into the vector and promoter combinations most capable of delivering therapeutic benefits. Initially I tried focal delivery of *Mecp2* to a specific brain region using a Lentiviral vector to enable region-specific rescue of the RTT-like phenotypes. However with the rapid advances in vector design this study was further extended to investigate the effect of both global and brain-specific delivery of *MECP2*, via an AAV2/9-based vector system, on the prevention/improvement of the RTT-like phenotype in a mouse model of Rett syndrome. This chapter will integrate the major findings and significant discoveries of this thesis and will evaluate the importance of these findings in relation to gene therapy and neuroscience research, and in particular to the evolving field of recent gene therapy in RTT. Further, I will discuss the technical difficulties experienced during this work, in particular the limitations of the methodology, and suggest possible ways to overcome these limitations. Finally, I will discuss possible future experiments to extend this work and derive the maximum benefits from the results I obtained in this study.

7.1 Major findings

The major findings/discoveries reported in this thesis are;

1. Exogenous *Mecp2* expression was achievable *in vitro* and *in vivo* by viral-mediated delivery approaches. The expression pattern of the exogenous *Mecp2* was similar to that of the endogenous *Mecp2* in different species.
2. Achieving near normal cellular levels of exogenous *Mecp2* *in vivo* was possible using appropriate vector and promoter design.

3. Lentivirus-mediated delivery of exogenous *Mecp2* demonstrated that:
 - I. Lentivirus-based vector displayed a high neuronal transduction of *Mecp2* *in vivo* and *in vitro*.
 - II. Direct brain injection achieved high transduction efficiency around the injection sites, however with very limited spread making global delivery an unrealistic prospect.
 - III. Synapsin1 promoter produced levels of *Mecp2* expression close to the WT values (80% of the WT level) whereas PGK promoter produced relatively high (200% of the WT level) expression levels.
 - IV. Reintroduction of *Mecp2* resulted in normalization of nuclear volume measures in *Mecp2* knockout mice.
 - V. Exogenous *Mecp2* maintained the characteristic site-specific phosphorylation at serine 421 seen in WT *Mecp2*. However the high transgenic delivery of *Mecp2* was associated with higher levels of phosphorylation than seen at the basal conditions in WT.
 - VI. *Mecp2*-overexpression in WT neurons led to decreased levels of histone 4 and acetylated H4 suggesting a potential role of *Mecp2* in chromatin remodelling.
4. AAV9-mediated brain delivery of exogenous *MECP2* under the CBA promoter in neonatal mice demonstrated:
 - I. Widespread expression of exogenous MeCP2 throughout the brain with near physiological cellular levels. Transgene spread to peripheral organs was also observed.
 - II. Significant arrest/improvement in the RTT-like phenotype in *Mecp2*-null mice including:
 - a. Cellular phenotype improvement in the form of rescue of neuronal nuclear volume deficits to WT-comparable values.

- b. Improvement/arrest of the RTT-like phenotype particularly in locomotion and exploratory activity.
 - c. Notable impact on survival as *Mecp2*-null mice treated with ssAAV9/CBA-*MECP2* exhibited a significantly higher median survival compared to the control group (GFP-treated).
- III. Overexpressing MeCP2 from the same vector in WT mice was without overt overexpression-related toxicity.
5. Neonatal peripheral (IV) and direct brain (IC) injection of scAAV9/MeP-*MECP2* in *Mecp2* knockout mice demonstrated:
- I. Global brain delivery of *MECP2* was achieved by both delivery routes (IV and IC), however with higher transduction efficiency and cellular levels of MeCP2 after direct brain injection.
 - II. Overt hindlimb motor abnormalities were observed in *Mecp2*^{stop/y} and WT mice after both delivery methods but *Mecp2*^{stop/y} mice displayed a more rapid onset and more severe phenotype.
 - III. This overt hindlimb dysfunction was observed in immunologically compromised mice (*RAG*^{-/-} knockout mouse) after IV injection of the equivalent viruses suggesting that this phenotype is more likely to be due to a transgene-related toxicity.
 - IV. Axonal degeneration in the dorsal columns of the lumbar spine was observed in mice that suffered the hindlimb phenotype.

7.1.1 Lenti-mediated *Mecp2* delivery to *Mecp2* knockout mice

Lentivirus-based vectors are a well-established and widely used tool for gene delivery (Blomer et al., 1996, Azzouz et al., 2004a) because of their ability to transduce terminally differentiated neurons and provide enduring transgene expression with minimal stimulation to the immune response (Kay et al., 2001, Li et al., 2010). In this study I showed that Lentivirus-based vectors are capable of delivering exogenous *Mecp2* to neurons and glia *in vivo* and *in vitro* with a

pattern of expression similar to that of the endogenous *Mecp2* (Lewis et al., 1992, Nan et al., 1996) in mouse- and rat-derived neurons. Exogenous *Mecp2* was mainly expressed in neurons *in vitro* and *in vivo* regardless of the cell-type specificity of the expression-driving promoter (*syn1* or PGK) which could be explained by the high tropism towards neurons particularly when lentiviruses are pseudo-typed with VSV-G envelope (Ho et al., 2008). The cellular level of exogenous *Mecp2* expression was higher in neurons than in glia which could partially be explained by the difference in multiplicity of infection (Wanisch and Yanez-Munoz, 2009), and may be explained also by the difference in cellular machinery (*Mecp2* is very abundant in neurons compared to glia (Nan et al., 1997). These findings (increased exogenous *Mecp2* expression in neurons compared to glia) recapitulate the expression levels of endogenous *Mecp2* in the brain whereby *Mecp2* is approximately 10 times more abundant in neurons than glia (Skene et al., 2010).

The levels of exogenous *Mecp2* varied according to the promoter used; a weak *syn1* promoter produced near physiological levels of exogenous *Mecp2* (80% of the WT levels) whereas a stronger promoter, such as PGK promoter (Owens et al., 2002) produced relatively high cellular levels (200% of the WT levels). This is particularly important when considering the danger of *Mecp2* overexpression-induced toxicity in humans because patients with *MECP2* duplication showed overt neurological deficits (Meins et al., 2005, Friez et al., 2006). In addition, *Mecp2* overexpression models showed that the phenotype severity increases as *Mecp2* increases behind normal levels (Chao and Zoghbi, 2012) with the worst phenotype observed with 2-3 fold increase of *Mecp2* levels (Luikenhuis et al., 2004). Unfortunately the functional consequences of exogenous *Mecp2* could not be evaluated at the organismal level due to the early mortality of the injected mice. However, cellular morphology was investigated instead and this showed that the deficit in nuclear volume in *Mecp2* knockout mice, a constant finding in neurons lacking *Mecp2* (Giacometti et al., 2007, Johnson et al., 2011), was restored to WT comparable values. This data agrees with the previous study that showed improvement in the dendritic arborization and spine density after lentivirus-mediated delivery of *Mecp2* in cultured neurons (Rastegar et al., 2009). This data indicates the possible reversibility/rescue of a well-established cellular phenotype in *Mecp2* knockout mice by exogenous delivery of *Mecp2*.

Nuclear volume rescue could be primarily due to reintroducing a missed highly expressed nuclear protein (*Mecp2*) or is secondary to the effect of downstream genes whose activity is altered by exogenous *Mecp2* expression; however, the functional consequences of this neuronal nuclear volume rescue such as restoration of normal cellular homeostasis are still to be investigated.

A more detailed study of exogenous *Mecp2* at the molecular level revealed that it retains the site-specific phosphorylation at serine 421, an activity-dependent regulator of *Mecp2* function (Zhou et al., 2006, Cohen et al., 2011). The cellular levels of phosphorylation of exogenous *Mecp2* were several folds higher than that of the endogenous protein under basal conditions. This difference could be explained by; (1) an overall increase of *Mecp2* levels in transduced cells however, exogenous *Mecp2* resulted in 2 fold increase in cellular levels of *Mecp2* and approximately 5 fold increase in the phosphorylated *Mecp2* in transduced cells suggesting that the exogenously provided *Mecp2* was disproportionately phosphorylated at this site; (2) overexpression of *Mecp2* could probably produce abnormal distribution / binding of *Mecp2* across the nucleus in a way that results in increased phosphorylation; (3) it could reflect a difference in response to basal neuronal activity; (4) *Mecp2* binds to methylated CpGs mainly within the promoter area of genes to prevent their downstream expression. Once phosphorylated, *Mecp2* was reported to be detached from its binding site and allows gene expression (Chen et al., 2003a, Martinowich et al., 2003). Thus phosphorylated *Mecp2* is not probably active and the high phosphorylation observed in this study could potentially represent an attempt from transduced cells to compensate for excess *Mecp2* expression. The functional consequences of the increased phosphorylation in the transduced cells and whether it could have a role in the overexpression-induced toxicity needs more investigations, particularly in the animal model of *Mecp2* overexpression.

Exogenous *Mecp2*, delivered by a lentivirus-based vector in WT neurons, is a simple and effective way of investigating the effects of overexpressing *Mecp2* on cell structure and function and the possible effect of *Mecp2* on other nuclear proteins (e.g. Histone proteins). Previous studies have shown that *Mecp2* absence is associated with alterations in either the total level of histone proteins or in the acetylated state of some histone proteins (Shahbazian et al., 2002a, Ghosh et al., 2010). In human, it has been reported that the level of ACh4 was

increased in RTT patients (Wan et al., 2001), however in mice models of RTT, it was ACh3 that reported to be increased with no significant alteration in ACh4 (Urduingio et al., 2007, Adachi et al., 2009). In this study I showed that the level of ACh4 decreased in cells overexpressing *Mecp2* (transduced), however this reduction in the acetylation state was accompanied by a parallel reduction in the total cellular H4 levels suggesting that the reduction in the acetylated form of H4 is not likely to be genuine and it occurs as a consequence of reduced total H4. This data indicates potential competition between *Mecp2* and H4 protein similar to that previously reported between *Mecp2* and H1 (Nan et al., 1997, Ghosh et al., 2010, Skene et al., 2010) with potential role of *Mecp2* in chromatin remodelling. My data also suggest that the previous reports of ACh3 hyperacetylation in the *Mecp2* knockout mice might reflect an overall increase in the total cellular level of H3. Analysis of the cellular levels of H4 and ACh4 in the cells expression and cells lacking *Mecp2* in the heterozygous female mice, *Mecp2*^{-/+}, would be a good experiment to further confirm the interaction between H4 and its acetylated state ACh4 and *Mecp2*.

The global expression of *Mecp2* together with the limited spread of the transgene delivery by lentivirus-based vector hinder the use of this vector for global *Mecp2* delivery in RTT mice. Previous reports have shown different methods to enhance lentivirus-mediated gene delivery to the CNS after peripheral administration (Ikeda et al., 2002, Federici et al., 2009). I therefore attempted several methods to enhance *Mecp2* delivery to the CNS using lentivirus-based vectors. Firstly I tried peripheral delivery of lenti-syn1-*ME1FlagRFP* by intravenous injection in the tail vein of adult mice after disturbing the BBB by mannitol injection (Ikeda et al., 2002, McCarty et al., 2009). Analysis of the brain tissue after 4 weeks of injection showed a complete absence of RFP or anti-Flag immunofluorescence across brain regions suggesting that even after putative mannitol disruption of the BBB, lentivirus is not capable of achieving reliable brain transduction. Secondly I pseudo-typed lentivirus particles with rabies virus glycoprotein coat to enable retrograde transport to the CNS after peripheral intramuscular delivery (Mentis et al., 2006, Federici et al., 2009). The virus was able to deliver *Mecp2* to cultured neurons, however several attempts to deliver *Mecp2* under either syn1 or PGK promoter to the CNS via IM injection of rabies-pseudo-typed lentivirus particles, were not successful

as no Flag or RFP immunopositive cells were detected in the spinal cord or in the brain of injected mice. Young animals have a larger extracellular space, that permits better spread of viral particles in the brain parenchyma (Cetin et al., 2006), therefore I finally injected neonatal mice intracranially with lentivirus particles in an attempt to achieve widespread expression in the brain. The RFP signal was detected in the brain after 4 weeks of injection but the transgene was restricted mainly to the inner wall of the ventricles with very limited spread to the brain parenchyma. The relatively large lentivirus, 100-120nm (Fleury et al., 2003) compared to limited extracellular spaces in the brain, 40-60nm (Thorne and Nicholson, 2006), is probably the main cause behind this limited spread. The difficulties in achieving effective brain transduction with lentivirus-based vectors motivated the move to the small-size AAV, 20-30 nm (Chen, 2007), virus to deliver widespread gene-expression in the brain.

7.1.2 Phenotype rescue and prolonged survival after ssAAV9/CBA-*MECP2* brain injection in *Mecp2*-null mice

In chapter 5, I show for the first time 'proof-of-concept' evidence that AAV9-mediated exogenous *MECP2* gene delivery to the brain of *Mecp2*-null mice is capable of achieving therapeutic benefits. I showed that modest brain transduction efficiencies coupled with cellular levels of exogenous MeCP2 approximately equivalent to WT levels resulted in a reduction in several phenotype measures and a significant extension of lifespan. The longest-lived mice survived for 36 week with a relatively stable RTT-like severity score before they were perfused for immuno-histochemical analysis. Analysis of individual parameters of the phenotype severity score revealed that the greatest impact of the treatment was observed in motor behaviour. This was further supported by the improved performance on the open field and treadmill tests. Data from these tests revealed that the motor deficits observed in control *Mecp2*-null mice (GFP-treated) was genuine and unlikely to be due to lack of motivation or anxiety as these mice were partially capable of performing at low speed and failed to perform at the more challenging higher speed tests. This motor impairment was ameliorated by AAV9/*MECP2* injection and was persistently improved in the long-lived mice throughout the experimental period (36 week). Furthermore it indicates that motor related deficits observed in RTT patients (Neul et al., 2010) could be potentially reversible. Another improvement was

observed in exploratory-related behaviours (rearing frequency), which indicates an improvement in the hippocampus-dependent tasks and also reflects an overall improvement in both the general condition of the animal and locomotor activities.

Mecp2-null mice in this study showed a respiratory phenotype that mirrors the clinical picture in humans where apnoeas and rhythm irregularities are prominent features of RTT (Neul et al., 2010). Analysis of breathing in *Mecp2*-null mice treated with ssAAV9-*MECP2* showed no impact on the respiratory phenotype. However this breathing phenotype has previously been shown to be corrected after postnatal activation of *Mecp2* globally (Robinson et al., 2012) or in glial cells (Lioy et al., 2011) which indicates that the respiratory phenotype is treatable at the gene level. The absence of any impact of AAV9/*MECP2*-treatment on breathing phenotype in the mutant mice in this study could be explained by lack or insufficient expression of exogenous MeCP2 in the cells responsible for breathing rhythmogenesis or otherwise contributing to breathing. Brainstem-specific *Mecp2* delivery through AAV9 or lentivirus in *Mecp2*-null mice could help elucidate the role of the breathing centre on rescue the breathing phenotype in RTT mice.

At the cellular level, exogenous MeCP2 expression rescued the nuclear volume of previously *Mecp2* deficient cells in *Mecp2*-null mice (Giacometti et al., 2007, Johnson et al., 2011) to WT comparable values. This effect is mostly cell autonomous as evidenced by comparing transduced and non-transduced cells from the same brain area and also mirrors the difference in nuclear volume and soma size in neurons expressing *Mecp2* and those lacking *Mecp2* in the mosaic heterozygous brain (Ho et al., 2008).

The failure of AAV9/*MECP2*-treated null mice to show substantial improvement in bodyweight indicates that the increased neuronal nuclear volume observed in these mice was unlikely to be related and paralleling overall growth gain in bodyweight. This data provides evidence for structural remodelling of AAV9/*MECP2*-transduced neurons but whether this reflects a broader change in dendritic complexity previously reported after Lentivirus-mediated delivery of *Mecp2 in vitro* (Rastegar et al., 2009) and in the delayed *Mecp2* activation study (Robinson et al., 2012) has not yet been investigated.

In this study I provide the first evidence that *MECP2* delivery by viral mediated approaches in mice, with this vector design and the delivery efficiency, is without detectable overexpression-related toxicity which was reported before in transgenic mice overexpressing *Mecp2* (Collins et al., 2004, Luikenhuis et al., 2004, Na et al., 2012) as indicated by an absence of overt phenotype in the WT-injected mice, despite expressing approximately double the normal level of MeCP2. However a long-term study is required to investigate any potential delayed-onset toxicity (Collins et al., 2004). This data argues against concerns that any attempt to deliver *Mecp2* to null cells in the heterozygous mosaic brain will invariably be accompanied by an overexpression-induced toxicity in the cells expressing WT endogenous *Mecp2*. Here I show that appropriate vector and promoter design is capable of achieving therapeutic benefits without obvious-overexpression toxicity.

In this study I showed at ‘proof-of-concept’ level that delivery of exogenous *MECP2* at a tolerable level to the brain of *Mecp2*-null mice was achievable by neonatal injection of ssAAV9/CBA-*MECP2* vector and produced a partial improvement of the RTT-like phenotype and extended the survival of these mice. Moreover I showed that this level of exogenous MeCP2 expression was without obvious deleterious effect in the WT mice, suggesting a wider than expected window for gene therapy application in the treatment of Rett syndrome.

7.1.3 Global and brain-specific delivery of exogenous *MECP2* using scAAV9/MeP-*MECP2* vector in neonatal mice.

A recent *Mecp2* delayed-activation study has shown the direct correlation between number of cells in which endogenous *Mecp2* is activated and improvement in RTT-like phenotypes (Robinson et al., 2012). This would suggest that the modest phenotype improvement and prolonged survival after exogenous *MECP2* delivery by ssAAV9/CBA-*MECP2* could be augmented by achieving higher transduction efficiencies. McCarty and colleagues have created a new version of AAV in which the single stranded DNA is replaced by double stranded DNA (self-complementary). This vector is ready to express the transgene once inside the cell as, unlike the single stranded AAV, it does not require the host cell to generate the complementary strand (McCarty et al., 2003). As a result, this

vector confers high transduction efficiency compared to the single stranded AAV especially when injected into neonatal mice (Foust et al., 2009). The reduced cloning capacity of scAAV vector prohibited the use of CBA promoter to drive expression of endogenous MeCP2, therefore a small segment of the endogenous *Mecp2* promoter (Adachi et al., 2005) was used instead. This 229bp promoter (MeP) segment of the *Mecp2* endogenous promoter was recently reported to recapitulate the same cellular pattern of endogenous *Mecp2* expression (Gray et al., 2011b). Two parallel experiments were conducted to investigate the therapeutic benefits of scAAV9/MeP-*MECP2* vector in *Mecp2*^{stop/y} mice, the first was to deliver these virus particles peripherally through facial vein injection as it is more relevant approach to human translation and it will help investigate the effect of global delivery of exogenous *MECP2*. The second was to achieve brain-specific delivery of exogenous *MECP2* with high transduction efficiency based on direct brain injection of the vector into neonatal mice.

Direct brain injection of scAAV/Mep-*MECP2* was ~ 5 fold more efficient in transducing brain cells compared to IV injection and it also produced a relatively higher cellular level of exogenous MeCP2 expression. The low brain transduction efficiency observed after IV injection (relative to IC injection) is likely to be due to loss of a large proportion of injected viruses in the peripheral organs (e.g. liver, heart and kidney) which is indicated by the widespread expression of exogenous MeCP2 in peripheral organs. Follow up observational analysis of *Mecp2*^{stop/y} and WT mice showed that these mice injected with scAAV9/MeP-*MECP2* displayed overt hindlimb motor dysfunction as early as 3 weeks in the IV cohort and after 5 weeks in the IC injected cohort. The phenotype trajectory of *Mecp2*^{stop/y} mice regularly starts at around 5 weeks and progressively worsens over the following weeks with early mortality around the age of 10-12 weeks. However, this hindlimb problem worsened 3 of the 6 phenotype criteria (gait, hindlimb clasping and mobility) and led to early scoring of a severe, but atypical RTT-like phenotype. *MECP2* duplication has been reported to produce serious neurological complications in human patients (Meins et al., 2005, Van Esch et al., 2005, Friez et al., 2006). In a mouse model, a two to three fold increase in the level of *Mecp2* in post-mitotic neurons produced tremors, gait ataxia, and side-to side swaying (Luikenhuis et al., 2004) whereas modest overexpression (160-200 % of the endogenous *Mecp2* level) resulted in cognitive impairments,

motor coordination deficits and an anxiety-like phenotype (Collins et al., 2004, Na et al., 2012). In mice model of *Mecp2* overexpression, *Mecp2* was expressed at high levels in all cells/ neurons, however none of these studies has reported this overt motor dysfunction that was observed in the current study in which equivalent levels of exogenous MeCP2 was achieved in a relatively low number of cells. It is possible that the neurons have a threshold of *Mecp2* tolerance behind which toxic effect takes place. It is also possible that the exogenous *MECP2* was delivered to a sub-population of cells with altered/oversensitivity response to any changes in the *Mecp2* levels. Further analysis of the type of cells transduced could help investigate this hypothesis.

Histological examination of the spinal cord was carried out to investigate possible causes of this hindlimb phenotype, with particular attention paid to the lumbar section as dysfunction was mainly confined to the hindlimbs. This examination revealed evidence of axonal degeneration in the dorsal columns of the lumbar spine indicating that the observed hindlimb problem is possibly due to the lack of sensory perception and not probably due to a genuine motor deficit. The occurrence of axonal degeneration only in the lumbar region of the spinal cord suggests that the degeneration process is potentially affecting long axons as observed in some neurological disorders (Fischer and Glass, 2007). Other regions responsible for sensory perception such as the dorsal root ganglia and peripheral nerves were not investigated but may nevertheless be an important locus for the transgene-related hindlimb toxicity.

Early development of the hindlimb motor dysfunction after IV injection, compared to the relatively delayed onset after IC injection, in spite of achieving low transduction efficiency and a relatively more physiological level of exogenous MeCP2 expression, compared to the high transduction efficiency and higher level of exogenous MeCP2 expression after IC injection of the same vector, suggests a potential role for the peripherally expressed MeCP2 in this phenotype. Peripheral delivery of exogenous *MECP2* by an AAV vector that cannot pass the BB barrier (Fu et al., 2003) could help clarify the role of peripherally expressed exogenous MeCP2 in the pathogenesis of this motor dysfunction phenotype.

The rapid onset of exogenous MeCP2 expression achieved by scAAV9 mediated delivery in *Mecp2*-null cells may partially explain the severity and consistency of motor dysfunction in the *Mecp2* knockout mice as compared to the phenotype variability observed in the WT mice (100% of *Mecp2*-null mice and 67% of WT developed motor dysfunction), This hypothesis agrees with a previous reversal study in which rapid activation of endogenous *Mecp2* resulted in sudden death of the *Mecp2*^{stop-cre/y} mice whereas gradual activation was able to rescue RTT-like phenotypes (Guy et al., 2007). This is also in agreement with my previous work (chapter 5) in which delivery of *MECP2* by ssAAV9, which produces a relatively delayed onset of expression (McCarty et al., 2003, Gray et al., 2011a), was without obvious toxicity/ lethality.

Many factors could be involved in the pathogenesis of the hindlimb motor dysfunction. One possibility is stimulating the immune response against either the AAV capsid (Manno et al., 2003, Mingozzi and High, 2007, Mingozzi et al., 2007) or against the exogenous MeCP2 protein. An Initial attempt to investigate this hypothesis was carried out by estimating the level of CD3 protein expression, used as an indicator of lymphocytic infiltration in patient and animal models of motor neuron disorders (Alexianu et al., 2001). Previous reports have shown neuronal CD3 expression in the brain, but not in the spinal cord (Garson et al., 1982, Schuller-Petrovic et al., 1983, Syken and Shatz, 2003, Baudouin et al., 2008). Interestingly, CD3 expression in the lumbar section of the spinal cord of scAAV9/*MECP2*-treated and control untreated mice was observed and this co-localized with NeuN immunofluorescence at the cellular level suggesting that these receptors are normally expressed on the surface of spinal cord neurons and not likely to be due to lymphocytic infiltration. The development of hindlimb phenotype in an immunocompromised (*RAG*^{-/-} knockout mouse) after neonatal IV injection with scAAV9/*MECP2* together with the absence of the hindlimb phenotype in the scAAV9/*GFP*-injected mice suggest that the most parsimonious explanation is that the abnormal phenotype is not likely to be due to the acquired immune response reaction to AAV9 virus particles but to some other transgene-specific toxicity. However, it remains possible that innate immunity system may play a role. The non-toxic and beneficial effects, in WT and null-mice respectively, of ssAAV9/*CBA-MECP2* after IC injection (chapter 5)

in neonatal mice without producing observable motor problems suggest that the exogenous MeCP2 is unlikely to be a potential trigger of the immune system.

Other possibilities investigated were the possible effect of expressing human protein in a murine model and potential mouse strain-specific responses to the injected construct. To investigate both hypotheses at the same time, a comparable virus construct delivering mouse *Mecp2*-e1 minigene was injected IV to *Mecp2*-null mice with C57BL/6 background (the *Mecp2*^{stop/y} mice have a BALB/C background). The hindlimb problem was observed in all injected mice (WT and *Mecp2*-null mice) indicating absence of a strain-specific response to the viral construct. My results also agree with a previous report showing genetic rescue of RTT-like phenotypes by expressing human MeCP2 in transgenic mice without producing detectable deficits (Collins et al., 2004) and also agree with my previous data (chapter 5) that showed therapeutic benefits of human *MECP2* when delivered by ssAAV9 under the CBA promoter in *Mecp2*-null mice.

This data shows for the first time a potential toxic effect of exogenous MeCP2 delivered by scAAV9 under the control of the *Mecp2* endogenous core promoter (229bp) in mice neonates and highlights the importance of vector and promoter design in any future attempts at RTT gene therapy. Further investigations are required to identify the underlying cause of the hindlimb Motor dysfunction and to fully evaluate the therapeutic effects of scAAV9/MeP-*MECP2* vector that was prohibited by the development of the hindlimb phenotype. My results, despite being negative, highlights the importance of the delivery system in achieving therapeutic outcome as indicated by the controversial results obtained after IC injection of ssAAV9/CBA-*MECP2* and scAAV9/MeP-*MECP2* in spite of delivering the same transgene. Minimal differences between the delivery vectors, such as the percentage and type of transduced/expressing cells or the level of exogenous MeCP2 expression, could potentially be the reasons for the different outcomes. Achieving therapeutic benefits with ssAAV9/CBA-*MECP2* delivery provides preliminary, however encouraging, evidence for the potential benefits of gene therapy application in RTT and prerequisite further comprehensive studies in the *Mecp2*^{-/+} heterozygous females (the accurate model of RTT in human) to further investigate these therapeutic benefits.

7.2 Significance of this study

Rett syndrome was for decades considered as a neurodevelopmental disorder that was thought to be incurable. However the reversal studies have shown the potential reversibility of RTT-like phenotypes in mice models. In this study I show the first evidence that RTT-like phenotype can be prevented / improved by delivering *MECP2* to *Mecp2* knockout model using viral vectors and I also highlight the potential neurological adverse effect of this approach. These data however at the proof of concept level should have an impact on the future therapeutic approaches not only for RTT but also for other related neurological disorders. The importance of this study is listed in the following key points;

1. In this thesis I provide a comprehensive study investigating the efficiency of different viral vectors with a range of promoters to drive expression of exogenous *Mecp2* *in vivo* and *in vitro*. This was further extended to evaluate the transfection efficiency and the levels of *Mecp2* expressed under each promoter. These considerations are essential for the field of RTT gene therapy in order to properly design a therapeutic vector.
2. In this thesis I showed that lentivirus-mediated *Mecp2* delivery is a useful tool for highly localized delivery of *Mecp2* in a particular brain area. This may be a valuable tool for studying *Mecp2* function in discrete brain areas. It may also be a useful delivery tool for generating an easy model of *Mecp2* overexpression and potential cell-type specific overexpression-induced toxicity.
3. My thesis provides the first proof of concept evidence for the possibility of achieving phenotypic and survival improvements in a mouse model of RTT by ssAAV9/CBA- mediated *MECP2* delivery in neonates. This data, along with the observed lack of overt adverse effects of this vector in WT mice is positive for extending this work into heterozygous females, a more accurate model of human disease, before considering human translation.
4. My thesis shows that virus-mediated exogenous *MECP2* delivery has an impact on the cellular morphology of the *Mecp2*-null and WT neurons either at an early stage of the development (neonatal injection of ssAAV9)

or after the establishment of RTT-like phenotypes (adult injection of lentivirus). This indicates that RTT-associated morphological deficits are reversible regardless of the time of intervention.

5. My thesis provides evidence of provoked overt neurological/motor phenotype after scAAV9/MeP-mediated MeCP2 expression in neonatal mice. This data shows the crucial importance of choosing the right vector design in any future attempts for RTT gene therapy application to minimize the drawbacks and achieve maximum therapeutic benefits.

7.3 Technical considerations

Most of the technical problems in this study were related to the *Mecp2* knockout model. *Mecp2*-null males are infertile therefore *Mecp2*^{-/+} female must be mated with WT males to generate *Mecp2*^{-/y} male mice (the genotype I was interested in). This breeding scheme means that the segregation ratio of *Mecp2*^{-/y} is 25%. This low percentage is further complicated by the small litter-size (3-5 pups) in *Mecp2*-null lines which further reduces the chances of getting the desired genotype. Moreover the numbers of pups that reach weaning age is also limited, either because of failure to compete with the WT or due to the increased incidence of infanticide (Jugloff et al., 2006). Many steps were taken to improve the breeding such as, doubling the number of heterozygous females in each age group, minimizing cage disturbance and decreasing environmental noise, especially around the delivery time, and avoiding unnecessary handling of the pups to prevent infanticide. Sunflower seeds were also added to the cage which has been previously reported to increase breeding efficiency (Jugloff et al., 2006).

Another problem encountered was that *Mecp2* knockout mice displayed tail lesions around the age of 7-8 weeks. This problem usually starts as small lesions around the tail-base which then progress to skin ulcers and eventually complete necrosis and loss of the tail. This condition is usually accompanied by perianal infection which necessitates culling the affected mice. Attempts were made to try and alleviate this condition by the application of topical antibiotics but this showed very limited benefit. Development of this phenotype in the virus-treated mice interfered with a full investigation of the therapeutic outcome e.g.

lentivirus injection (chapter 4) and scAAV9 injection (chapter 6). One possibility was that this lesion was due to animals fighting with each other, however caging mice individually did not prevent or improve this phenotype. Interestingly, this tail problem has been not observed in the cohort of mice injected with ssAAV9/CBA-*MECP2* (chapter 5) except in 3 mice, however all of them have recovered without treatment. Further investigations are required to identify the underlying cause of this problem.

7.4 Future studies

The nature of this project has been to test various gene delivery processes and then to refine vector design, delivery strategies moving to proof of concept studies in RTT-mice. This represents a logical trajectory in reaching the ultimate goal of developing translational strategies in treating RTT in patients. The results shown in my thesis suggest important future experiments in various directions.

1. Following the success of ssAAV9/CBA-*MECP2* in producing therapeutic benefits after IC injection in neonates, I would recommend several more experiments to further investigate the potential for future human translation;
 - I. The vast majority of RTT patients are females with a mosaic network of cells either expressing normal MeCP2 or lacking functional MeCP2. Therefore the next experiment should be to consider injecting adult pre-symptomatic or symptomatic heterozygous female mice with scAAV9/MeP-*MECP2* through the tail vein to investigate the potential for phenotype prevention / rescue. Comprehensive behavioural analysis before and after the treatment is essential for complete evaluation of the therapeutic outcomes.
 - II. The role of glia in the pathogenesis of RTT has become evident in the last few years (Ballas et al., 2009, Liroy et al., 2011) therefore it would be interesting to investigate the effect of scAAV9-mediated exogenous expression of *Mecp2* in glia on the phenotype trajectory of *Mecp2* knockout mice. This may be achieved by using a glial-specific promoter

such as GFAP promoter or by using AAV capsid mutants showing high glial tropism.

- III. The peripheral delivery of exogenous *MECP2* is the most clinically relevant method for gene delivery; however with the expected low transduction efficiency after peripheral injection in adult, direct brain injection of AAV9 could be an option, therefore an interesting experiment would be to investigate the effect of region-specific delivery of *MECP2* on the reversal of a particular phenotype (breathing, motor behaviours) in heterozygous female mice. This would also address basic neurobiological questions by mapping aspects of RTT-phenotype/reversal to discrete brain regions.
- IV. Optimizing viral delivery methods to increase transduction efficiency in adult mice brain such as; intrathecal, intra-arterial or IV injection after disturbing the BBB with mannitol (Fu et al., 2003).
- V. Optimizing the vector construct to enable targeting of exogenous *Mecp2* to null cells in heterozygous mosaic brain to avoid overexpression in the cells that express normal endogenous *Mecp2* through:
 - a. Designing a vector with a *Mecp2* minigene and siRNA that can knockdown endogenous *Mecp2* in the cells expressing the normal *Mecp2* allele.
 - b. Designing a vector that drives expression of exogenous *Mecp2* under the control of *Mecp2* target promoter (e.g. mouse *BDNF* exon 4 promoter)(Chen et al., 2003a, Martinowich et al., 2003). This promoter could theoretically be silenced in cells that are already expressing normal *Mecp2* which binds and represses the promoter but would not be in cells which contain no endogenous *Mecp2* (Gadalla et al., 2011).
 - c. Screening a library of AAV capsid mutants for selective tropism to the *Mecp2*-null cells.

2. Since injection of scAAV9/MeP-*MECP2* in mice neonates was accompanied by overt hindlimb motor dysfunction in contrast to the therapeutic benefits of ssAAV9/CBA-*MECP2*, the following experiments could help determine the reasons for this problem;
 - I. Delivery of exogenous *MECP2* under *Mecp2* endogenous promoter by ssAAV9 (ssAAV9/MeP-*MECP2*) vector through direct brain injection in mice neonates. This experiment should help investigate the role of the MeP promoter in the development of the hindlimb phenotype, as the same vector with CBA promoter showed no apparent toxicities.
 - II. Neonatal delivery of exogenous *MECP2* under CBA promoter by scAAV9 (scAAV9/CBA-*MECP2*) vector. This experiment could test the possible role of AAV9 vector-structure (sc versus ss) in the hindlimb pathology. However this experiment is difficult to carry out due to the limited cloning capacity of scAAV9. Nevertheless it may be possible to further truncate the CBA promoter to enable packaging.
 - III. Peripheral delivery of exogenous *MECP2* by pseudotyping scAAV/MeP using capsids 2 or 1 which are unable to cross the BBB. This experiment would help define the role of peripherally expressed MeCP2 in the abnormal phenotype.
 - IV. Measurement of the innate immune response (e.g. cytokines) in the affected mice to identify the role of immune response stimulation in this phenotype (as RAG^{-/-} knockout mice experiment already excluded mature T and B cells as a cause of this problem).

7.5 Summary

The investigation of viral-mediated exogenous *MECP2* delivery to the *Mecp2* knockout mice has been extremely productive in several respects. First it shows that Lentivirus-based vectors, despite producing enduring expression in neurons, are not suitable for global brain expression of *Mecp2* due to limited spread of the virus. Nevertheless Lentivirus-based vectors are still potentially useful if localized brain injection is required. Second, this study shows the first proof of

therapeutic benefits (improved motor behaviours and prolonged survival) of exogenous *MECP2* delivered in *Mecp2*-null mice by ssAAV9/CBA-*MECP2* vector in neonatal mice. Finally, my study is the first to report overt neurological/motor deficits in *Mecp2* knockout mice after systemic and local delivery of exogenous *MECP2* by scAAV9/MeP-*MECP2* vector to neonates. I believe that this study provides the groundwork for further studies to identify the potential of achieving therapeutic benefits in *Mecp2*^{-/+} female mice, a more accurate model of human RTT, and also for studies to investigate the underlying pathology of the hindlimb motor deficit to enable avoiding this problem in the future clinical translation.

References

- Abdala AP, Dutschmann M, Bissonnette JM, Paton JF (2010) Correction of respiratory disorders in a mouse model of Rett syndrome. *Proc Natl Acad Sci U S A* 107:18208-18213.
- Abordo-Adesida E, Follenzi A, Barcia C, Sciascia S, Castro MG, Naldini L, Lowenstein PR (2005) Stability of lentiviral vector-mediated transgene expression in the brain in the presence of systemic antivector immune responses. *Hum Gene Ther* 16:741-751.
- Adachi M, Autry AE, Covington HE, 3rd, Monteggia LM (2009) MeCP2-mediated transcription repression in the basolateral amygdala may underlie heightened anxiety in a mouse model of Rett syndrome. *J Neurosci* 29:4218-4227.
- Adachi M, Keefer EW, Jones FS (2005) A segment of the *Mecp2* promoter is sufficient to drive expression in neurons. *Hum Mol Genet* 14:3709-3722.
- Aiken C (1997) Pseudotyping human immunodeficiency virus type 1 (HIV-1) by the glycoprotein of vesicular stomatitis virus targets HIV-1 entry to an endocytic pathway and suppresses both the requirement for Nef and the sensitivity to cyclosporin A. *J Virol* 71:5871-5877.
- Akkina RK, Walton RM, Chen ML, Li QX, Planelles V, Chen IS (1996) High-efficiency gene transfer into CD34+ cells with a human immunodeficiency virus type 1-based retroviral vector pseudotyped with vesicular stomatitis virus envelope glycoprotein G. *J Virol* 70:2581-2585.
- Alexianu ME, Kozovska M, Appel SH (2001) Immune reactivity in a mouse model of familial ALS correlates with disease progression. *Neurology* 57:1282-1289.
- Alvarez-Saavedra M, Saez MA, Kang D, Zoghbi HY, Young JI (2007) Cell-specific expression of wild-type MeCP2 in mouse models of Rett syndrome yields insight about pathogenesis. *Hum Mol Genet* 16:2315-2325.
- Amir RE, Van den Veyver IB, Wan M, Tran CQ, Francke U, Zoghbi HY (1999) Rett syndrome is caused by mutations in X-linked MECP2, encoding methyl-CpG-binding protein 2. *Nat Genet* 23:185-188.
- Archer H, Evans J, Leonard H, Colvin L, Ravine D, Christodoulou J, Williamson S, Charman T, Bailey ME, Sampson J, de Klerk N, Clarke A (2007) Correlation between clinical severity in patients with Rett syndrome with a p.R168X or p.T158M MECP2 mutation, and the direction and degree of skewing of X-chromosome inactivation. *Journal of medical genetics* 44:148-152.
- Armstrong D, Dunn JK, Antalffy B, Trivedi R (1995) Selective dendritic alterations in the cortex of Rett syndrome. *J Neuropathol Exp Neurol* 54:195-201.
- Arruda VR, Stedman HH, Nichols TC, Haskins ME, Nicholson M, Herzog RW, Couto LB, High KA (2005) Regional intravascular delivery of AAV-2-F.IX to skeletal muscle achieves long-term correction of hemophilia B in a large animal model. *Blood* 105:3458-3464.

- Asaka Y, Jugloff DG, Zhang L, Eubanks JH, Fitzsimonds RM (2006) Hippocampal synaptic plasticity is impaired in the Mecp2-null mouse model of Rett syndrome. *Neurobiol Dis* 21:217-227.
- Azzouz M, Hottinger A, Paterna JC, Zurn AD, Aebischer P, Bueler H (2000) Increased motoneuron survival and improved neuromuscular function in transgenic ALS mice after intraspinal injection of an adeno-associated virus encoding Bcl-2. *Hum Mol Genet* 9:803-811.
- Azzouz M, Kingsman SM, Mazarakis ND (2004a) Lentiviral vectors for treating and modeling human CNS disorders. *J Gene Med* 6:951-962.
- Azzouz M, Le T, Ralph GS, Walmsley L, Monani UR, Lee DC, Wilkes F, Mitrophanous KA, Kingsman SM, Burghes AH, Mazarakis ND (2004b) Lentivector-mediated SMN replacement in a mouse model of spinal muscular atrophy. *J Clin Invest* 114:1726-1731.
- Ballas N, Lioy DT, Grunseich C, Mandel G (2009) Non-cell autonomous influence of MeCP2-deficient glia on neuronal dendritic morphology. *Nat Neurosci* 12:311-317.
- Baudouin SJ, Angibaud J, Loussouarn G, Bonnamain V, Matsuura A, Kinebuchi M, Naveilhan P, Boudin H (2008) The signaling adaptor protein CD3zeta is a negative regulator of dendrite development in young neurons. *Mol Biol Cell* 19:2444-2456.
- Bauman ML, Kemper TL, Arin DM (1995) Pervasive neuroanatomic abnormalities of the brain in three cases of Rett's syndrome. *Neurology* 45:1581-1586.
- Bedwell DM, Kaenjak A, Benos DJ, Bebok Z, Bubien JK, Hong J, Tousson A, Clancy JP, Sorscher EJ (1997) Suppression of a CFTR premature stop mutation in a bronchial epithelial cell line. *Nat Med* 3:1280-1284.
- Berns KI (1990) Parvovirus replication. *Microbiol Rev* 54:316-329.
- Bibikova M, Carroll D, Segal DJ, Trautman JK, Smith J, Kim YG, Chandrasegaran S (2001) Stimulation of homologous recombination through targeted cleavage by chimeric nucleases. *Mol Cell Biol* 21:289-297.
- Bienemann AS, Martin-Rendon E, Cosgrave AS, Glover CP, Wong LF, Kingsman SM, Mitrophanous KA, Mazarakis ND, Uney JB (2003) Long-term replacement of a mutated nonfunctional CNS gene: reversal of hypothalamic diabetes insipidus using an EIAV-based lentiviral vector expressing arginine vasopressin. *Mol Ther* 7:588-596.
- Bienvenu T, Chelly J (2006) Molecular genetics of Rett syndrome: when DNA methylation goes unrecognized. *Nat Rev Genet* 7:415-426.
- Blomer U, Naldini L, Kafri T, Trono D, Verma IM, Gage FH (1997) Highly efficient and sustained gene transfer in adult neurons with a lentivirus vector. *J Virol* 71:6641-6649.
- Blomer U, Naldini L, Verma IM, Trono D, Gage FH (1996) Applications of gene therapy to the CNS. *Hum Mol Genet* 5 Spec No:1397-1404.

- Bondy CA, Cheng CM (2004) Signaling by insulin-like growth factor 1 in brain. *Eur J Pharmacol* 490:25-31.
- Boulos S, Meloni BP, Arthur PG, Bojarski C, Knuckey NW (2006) Assessment of CMV, RSV and SYN1 promoters and the woodchuck post-transcriptional regulatory element in adenovirus vectors for transgene expression in cortical neuronal cultures. *Brain Res* 1102:27-38.
- Braun KSaT (1995) Monoclonal anti-flag antibodies react with a new isoform of rat Mg²⁺ dependent protein phosphatase B. *Biochemical and biophysical Research Communications* 207:708-714.
- Brendel C, Klahold E, Gartner J, Huppke P (2009) Suppression of nonsense mutations in Rett syndrome by aminoglycoside antibiotics. *Pediatr Res* 65:520-523.
- Brolund L, Kuster A, Korr S, Vogt M, Muller-Newen G (2011) A receptor fusion protein for the inhibition of murine oncostatin M. *BMC Biotechnol* 11:3.
- Brooks AI, Stein CS, Hughes SM, Heth J, McCray PM, Jr., Sauter SL, Johnston JC, Cory-Slechta DA, Federoff HJ, Davidson BL (2002) Functional correction of established central nervous system deficits in an animal model of lysosomal storage disease with feline immunodeficiency virus-based vectors. *Proc Natl Acad Sci U S A* 99:6216-6221.
- Brucke T, Sofic E, Killian W, Rett A, Riederer P (1987) Reduced concentrations and increased metabolism of biogenic amines in a single case of Rett-syndrome: a postmortem brain study. *J Neural Transm* 68:315-324.
- Bukovsky AA, Song JP, Naldini L (1999) Interaction of human immunodeficiency virus-derived vectors with wild-type virus in transduced cells. *J Virol* 73:7087-7092.
- Carter BJ, Khoury G, Rose JA (1972) Adenovirus-associated virus multiplication. IX. Extent of transcription of the viral genome in vivo. *J Virol* 10:1118-1125.
- Cetin A, Komai S, Eliava M, Seeburg PH, Osten P (2006) Stereotaxic gene delivery in the rodent brain. *Nat Protoc* 1:3166-3173.
- Chahrour M, Jung SY, Shaw C, Zhou X, Wong ST, Qin J, Zoghbi HY (2008) MeCP2, a key contributor to neurological disease, activates and represses transcription. *Science* 320:1224-1229.
- Chahrour M, Zoghbi HY (2007) The story of Rett syndrome: from clinic to neurobiology. *Neuron* 56:422-437.
- Chandler SP, Guschin D, Landsberger N, Wolffe AP (1999) The methyl-CpG binding transcriptional repressor MeCP2 stably associates with nucleosomal DNA. *Biochemistry* 38:7008-7018.
- Chang Q, Khare G, Dani V, Nelson S, Jaenisch R (2006) The disease progression of Mecp2 mutant mice is affected by the level of BDNF expression. *Neuron* 49:341-348.

- Chao HT, Chen H, Samaco RC, Xue M, Chahrour M, Yoo J, Neul JL, Gong S, Lu HC, Heintz N, Ekker M, Rubenstein JL, Noebels JL, Rosenmund C, Zoghbi HY (2010) Dysfunction in GABA signalling mediates autism-like stereotypies and Rett syndrome phenotypes. *Nature* 468:263-269.
- Chao HT, Zoghbi HY (2012) MeCP2: only 100% will do. *Nat Neurosci* 15:176-177.
- Chao HT, Zoghbi HY, Rosenmund C (2007) MeCP2 controls excitatory synaptic strength by regulating glutamatergic synapse number. *Neuron* 56:58-65.
- Chen H (2007) Comparative observation of the recombinant adeno-associated virus 2 using transmission electron microscopy and atomic force microscopy. *Microsc Microanal* 13:384-389.
- Chen RZ, Akbarian S, Tudor M, Jaenisch R (2001) Deficiency of methyl-CpG binding protein-2 in CNS neurons results in a Rett-like phenotype in mice. *Nat Genet* 27:327-331.
- Chen WG, Chang Q, Lin Y, Meissner A, West AE, Griffith EC, Jaenisch R, Greenberg ME (2003a) Derepression of BDNF transcription involves calcium-dependent phosphorylation of MeCP2. *Science* 302:885-889.
- Chen WG, West AE, Tao X, Corfas G, Szentirmay MN, Sawadogo M, Vinson C, Greenberg ME (2003b) Upstream stimulatory factors are mediators of Ca²⁺-responsive transcription in neurons. *J Neurosci* 23:2572-2581.
- Choleris E, Thomas AW, Kavaliers M, Prato FS (2001) A detailed ethological analysis of the mouse open field test: effects of diazepam, chlordiazepoxide and an extremely low frequency pulsed magnetic field. *Neurosci Biobehav Rev* 25:235-260.
- Cobb S, Guy J, Bird A (2010) Reversibility of functional deficits in experimental models of Rett syndrome. *Biochem Soc Trans* 38:498-506.
- Cohen S, Gabel HW, Hemberg M, Hutchinson AN, Sadacca LA, Ebert DH, Harmin DA, Greenberg RS, Verdine VK, Zhou Z, Wetsel WC, West AE, Greenberg ME (2011) Genome-wide activity-dependent MeCP2 phosphorylation regulates nervous system development and function. *Neuron* 72:72-85.
- Collins AL, Levenson JM, Vilaythong AP, Richman R, Armstrong DL, Noebels JL, David Sweatt J, Zoghbi HY (2004) Mild overexpression of MeCP2 causes a progressive neurological disorder in mice. *Hum Mol Genet* 13:2679-2689.
- D'Cruz JA, Wu C, Zahid T, El-Hayek Y, Zhang L, Eubanks JH (2010) Alterations of cortical and hippocampal EEG activity in MeCP2-deficient mice. *Neurobiol Dis* 38:8-16.
- Dani VS, Chang Q, Maffei A, Turrigiano GG, Jaenisch R, Nelson SB (2005) Reduced cortical activity due to a shift in the balance between excitation and inhibition in a mouse model of Rett syndrome. *Proc Natl Acad Sci U S A* 102:12560-12565.
- Dastidar SG, Bardai FH, Ma C, Price V, Rawat V, Verma P, Narayanan V, D'Mello SR (2012) Isoform-Specific Toxicity of Mecp2 in Postmitotic Neurons: Suppression of Neurotoxicity by FoxG1. *J Neurosci* 32:2846-2855.

- Daya S, Berns KI (2008) Gene therapy using adeno-associated virus vectors. *Clin Microbiol Rev* 21:583-593.
- de Almeida LP, Zala D, Aebischer P, Deglon N (2001) Neuroprotective effect of a CNTF-expressing lentiviral vector in the quinolinic acid rat model of Huntington's disease. *Neurobiol Dis* 8:433-446.
- Degano AL, Pasterkamp RJ, Ronnett GV (2009) MeCP2 deficiency disrupts axonal guidance, fasciculation, and targeting by altering Semaphorin 3F function. *Mol Cell Neurosci* 42:243-254.
- Denning W, Das S, Guo S, Xu J, Kappes JC, Hel Z (2012) Optimization of the Transductional Efficiency of Lentiviral Vectors: Effect of Sera and Polycations. *Mol Biotechnol*.
- DePolo NJ, Reed JD, Sheridan PL, Townsend K, Sauter SL, Jolly DJ, Dubensky TW, Jr. (2000) VSV-G pseudotyped lentiviral vector particles produced in human cells are inactivated by human serum. *Mol Ther* 2:218-222.
- Derecki NC, Cronk JC, Lu Z, Xu E, Abbott SB, Guyenet PG, Kipnis J (2012) Wild-type microglia arrest pathology in a mouse model of Rett syndrome. *Nature* 484:105-109.
- Dittgen T, Nimmerjahn A, Komai S, Licznarski P, Waters J, Margrie TW, Helmchen F, Denk W, Brecht M, Osten P (2004) Lentivirus-based genetic manipulations of cortical neurons and their optical and electrophysiological monitoring in vivo. *Proc Natl Acad Sci U S A* 101:18206-18211.
- Dolen G, Osterweil E, Rao BS, Smith GB, Auerbach BD, Chattarji S, Bear MF (2007) Correction of fragile X syndrome in mice. *Neuron* 56:955-962.
- Dragatsis I, Zeitlin S (2001) A method for the generation of conditional gene repair mutations in mice. *Nucleic Acids Res* 29:E10.
- Dragich JM, Kim YH, Arnold AP, Schanen NC (2007) Differential distribution of the MeCP2 splice variants in the postnatal mouse brain. *J Comp Neurol* 501:526-542.
- Duan D, Li Q, Kao AW, Yue Y, Pessin JE, Engelhardt JF (1999) Dynamin is required for recombinant adeno-associated virus type 2 infection. *J Virol* 73:10371-10376.
- Duan D, Sharma P, Yang J, Yue Y, Dudus L, Zhang Y, Fisher KJ, Engelhardt JF (1998) Circular intermediates of recombinant adeno-associated virus have defined structural characteristics responsible for long-term episomal persistence in muscle tissue. *J Virol* 72:8568-8577.
- Dull T, Zufferey R, Kelly M, Mandel RJ, Nguyen M, Trono D, Naldini L (1998) A third-generation lentivirus vector with a conditional packaging system. *J Virol* 72:8463-8471.
- Duque S, Joussemet B, Riviere C, Marais T, Dubreil L, Douar AM, Fyfe J, Moullier P, Colle MA, Barkats M (2009) Intravenous administration of self-complementary AAV9 enables transgene delivery to adult motor neurons. *Mol Ther* 17:1187-1196.

- Ehninger D, Li W, Fox K, Stryker MP, Silva AJ (2008) Reversing neurodevelopmental disorders in adults. *Neuron* 60:950-960.
- Engerstrom IW (1992) Rett syndrome: the late infantile regression period--a retrospective analysis of 91 cases. *Acta Paediatr* 81:167-172.
- Eslamboli A, Georgievska B, Ridley RM, Baker HF, Muzyczka N, Burger C, Mandel RJ, Annett L, Kirik D (2005) Continuous low-level glial cell line-derived neurotrophic factor delivery using recombinant adeno-associated viral vectors provides neuroprotection and induces behavioral recovery in a primate model of Parkinson's disease. *J Neurosci* 25:769-777.
- Federici T, Kutner R, Zhang XY, Kuroda H, Tordo N, Boulis NM, Reiser J (2009) Comparative analysis of HIV-1-based lentiviral vectors bearing lyssavirus glycoproteins for neuronal gene transfer. *Genet Vaccines Ther* 7:1.
- Feigin A, Kaplitt MG, Tang C, Lin T, Mattis P, Dhawan V, During MJ, Eidelberg D (2007) Modulation of metabolic brain networks after subthalamic gene therapy for Parkinson's disease. *Proc Natl Acad Sci U S A* 104:19559-19564.
- Felgner PL, Gadek TR, Holm M, Roman R, Chan HW, Wenz M, Northrop JP, Ringold GM, Danielsen M (1987) Lipofection: a highly efficient, lipid-mediated DNA-transfection procedure. *Proc Natl Acad Sci U S A* 84:7413-7417.
- Fernandez F, Morishita W, Zuniga E, Nguyen J, Blank M, Malenka RC, Garner CC (2007) Pharmacotherapy for cognitive impairment in a mouse model of Down syndrome. *Nat Neurosci* 10:411-413.
- Ferrari FK, Samulski T, Shenk T, Samulski RJ (1996) Second-strand synthesis is a rate-limiting step for efficient transduction by recombinant adeno-associated virus vectors. *J Virol* 70:3227-3234.
- Fischer LR, Glass JD (2007) Axonal degeneration in motor neuron disease. *Neurodegener Dis* 4:431-442.
- Fleury S, Simeoni E, Zuppinger C, Deglon N, von Segesser LK, Kappenberger L, Vassalli G (2003) Multiply attenuated, self-inactivating lentiviral vectors efficiently deliver and express genes for extended periods of time in adult rat cardiomyocytes in vivo. *Circulation* 107:2375-2382.
- Foust KD, Nurre E, Montgomery CL, Hernandez A, Chan CM, Kaspar BK (2009) Intravascular AAV9 preferentially targets neonatal neurons and adult astrocytes. *Nat Biotechnol* 27:59-65.
- Frankiewicz T, Parsons CG (1999) Memantine restores long term potentiation impaired by tonic N-methyl-D-aspartate (NMDA) receptor activation following reduction of Mg²⁺ in hippocampal slices. *Neuropharmacology* 38:1253-1259.
- Friez MJ, Jones JR, Clarkson K, Lubs H, Abuelo D, Bier JA, Pai S, Simensen R, Williams C, Giampietro PF, Schwartz CE, Stevenson RE (2006) Recurrent infections, hypotonia, and mental retardation caused by duplication of MECP2 and adjacent region in Xq28. *Pediatrics* 118:e1687-1695.

- Fu H, Muenzer J, Samulski RJ, Breese G, Sifford J, Zeng X, McCarty DM (2003) Self-complementary adeno-associated virus serotype 2 vector: global distribution and broad dispersion of AAV-mediated transgene expression in mouse brain. *Mol Ther* 8:911-917.
- Gadalla KK, Bailey ME, Cobb SR (2011) MeCP2 and Rett syndrome: reversibility and potential avenues for therapy. *The Biochemical journal* 439:1-14.
- Garson JA, Beverley PC, Coakham HB, Harper EI (1982) Monoclonal antibodies against human T lymphocytes label Purkinje neurones of many species. *Nature* 298:375-377.
- Ghosh RP, Horowitz-Scherer RA, Nikitina T, Shlyakhtenko LS, Woodcock CL (2010) MeCP2 binds cooperatively to its substrate and competes with histone H1 for chromatin binding sites. *Mol Cell Biol* 30:4656-4670.
- Giacometti E, Luikenhuis S, Beard C, Jaenisch R (2007) Partial rescue of MeCP2 deficiency by postnatal activation of MeCP2. *Proc Natl Acad Sci U S A* 104:1931-1936.
- Gigout L, Rebollo P, Clement N, Warrington KH, Jr., Muzyczka N, Linden RM, Weber T (2005) Altering AAV tropism with mosaic viral capsids. *Mol Ther* 11:856-865.
- Girard M, Couvert P, Carrie A, Tardieu M, Chelly J, Beldjord C, Bienvenu T (2001) Parental origin of de novo MECP2 mutations in Rett syndrome. *Eur J Hum Genet* 9:231-236.
- Glover CP, Bienemann AS, Heywood DJ, Cosgrave AS, Uney JB (2002) Adenoviral-mediated, high-level, cell-specific transgene expression: a SYN1-WPRE cassette mediates increased transgene expression with no loss of neuron specificity. *Mol Ther* 5:509-516.
- Goetze B, Grunewald B, Baldassa S, Kiebler M (2004) Chemically controlled formation of a DNA/calcium phosphate coprecipitate: application for transfection of mature hippocampal neurons. *J Neurobiol* 60:517-525.
- Goffin D, Allen M, Zhang L, Amorim M, Wang IT, Reyes AR, Mercado-Berton A, Ong C, Cohen S, Hu L, Blendy JA, Carlson GC, Siegel SJ, Greenberg ME, Zhou Z (2012) Rett syndrome mutation MeCP2 T158A disrupts DNA binding, protein stability and ERP responses. *Nat Neurosci* 15:274-283.
- Gray SJ, Choi VW, Asokan A, Haberman RA, McCown TJ, Samulski RJ (2011a) Production of recombinant adeno-associated viral vectors and use in in vitro and in vivo administration. *Curr Protoc Neurosci* Chapter 4:Unit 4 17.
- Gray SJ, Foti SB, Schwartz JW, Bachaboina L, Taylor-Blake B, Coleman J, Ehlers MD, Zylka MJ, McCown TJ, Samulski RJ (2011b) Optimizing promoters for recombinant adeno-associated virus-mediated gene expression in the peripheral and central nervous system using self-complementary vectors. *Hum Gene Ther* 22:1143-1153.

- Gray SJ, Matagne V, Bachaboina L, Yadav S, Ojeda SR, Samulski RJ (2011c) Preclinical differences of intravascular AAV9 delivery to neurons and glia: a comparative study of adult mice and nonhuman primates. *Mol Ther* 19:1058-1069.
- Greenwood SM, Mizielińska SM, Frenguelli BG, Harvey J, Connolly CN (2007) Mitochondrial dysfunction and dendritic beading during neuronal toxicity. *J Biol Chem* 282:26235-26244.
- Grieger JC, Choi VW, Samulski RJ (2006) Production and characterization of adeno-associated viral vectors. *Nat Protoc* 1:1412-1428.
- Grieger JC, Samulski RJ (2005a) Adeno-associated virus as a gene therapy vector: vector development, production and clinical applications. *Adv Biochem Eng Biotechnol* 99:119-145.
- Grieger JC, Samulski RJ (2005b) Packaging capacity of adeno-associated virus serotypes: impact of larger genomes on infectivity and postentry steps. *J Virol* 79:9933-9944.
- Guy J, Gan J, Selfridge J, Cobb S, Bird A (2007) Reversal of neurological defects in a mouse model of Rett syndrome. *Science* 315:1143-1147.
- Guy J, Hendrich B, Holmes M, Martin JE, Bird A (2001) A mouse *Mecp2*-null mutation causes neurological symptoms that mimic Rett syndrome. *Nat Genet* 27:322-326.
- Hagberg B (2002) Clinical manifestations and stages of Rett syndrome. *Ment Retard Dev Disabil Res Rev* 8:61-65.
- Hagberg B, Aicardi J, Dias K, Ramos O (1983) A progressive syndrome of autism, dementia, ataxia, and loss of purposeful hand use in girls: Rett's syndrome: report of 35 cases. *Ann Neurol* 14:471-479.
- Hannan GN, Lehnert SA, MacAvoy ES, Jennings PA, Molloy PL (1993) An engineered PGK promoter and lac operator-repressor system for the regulation of gene expression in mammalian cells. *Gene* 130:233-239.
- Hansen J, Qing K, Srivastava A (2001) Infection of purified nuclei by adeno-associated virus 2. *Mol Ther* 4:289-296.
- Hermens WT, Verhaagen J (1998) Viral vectors, tools for gene transfer in the nervous system. *Prog Neurobiol* 55:399-432.
- Herzog RW, Hagstrom JN, Kung SH, Tai SJ, Wilson JM, Fisher KJ, High KA (1997) Stable gene transfer and expression of human blood coagulation factor IX after intramuscular injection of recombinant adeno-associated virus. *Proc Natl Acad Sci U S A* 94:5804-5809.
- Hioki H, Kameda H, Nakamura H, Okunomiya T, Ohira K, Nakamura K, Kuroda M, Furuta T, Kaneko T (2007) Efficient gene transduction of neurons by lentivirus with enhanced neuron-specific promoters. *Gene Ther* 14:872-882.
- Ho KL, McNae IW, Schmiedeberg L, Klose RJ, Bird AP, Walkinshaw MD (2008) MeCP2 binding to DNA depends upon hydration at methyl-CpG. *Mol Cell* 29:525-531.

- Hockly E, Cordery PM, Woodman B, Mahal A, van Dellen A, Blakemore C, Lewis CM, Hannan AJ, Bates GP (2002) Environmental enrichment slows disease progression in R6/2 Huntington's disease mice. *Ann Neurol* 51:235-242.
- Howard M, Frizzell RA, Bedwell DM (1996) Aminoglycoside antibiotics restore CFTR function by overcoming premature stop mutations. *Nat Med* 2:467-469.
- Huppke P, Held M, Laccone F, Hanefeld F (2003) The spectrum of phenotypes in females with Rett Syndrome. *Brain Dev* 25:346-351.
- Ikeda M, Bhattacharjee AK, Kondoh T, Nagashima T, Tamaki N (2002) Synergistic effect of cold mannitol and Na(+)/Ca(2+) exchange blocker on blood-brain barrier opening. *Biochem Biophys Res Commun* 291:669-674.
- Inagaki K, Fuess S, Storm TA, Gibson GA, McTiernan CF, Kay MA, Nakai H (2006) Robust systemic transduction with AAV9 vectors in mice: efficient global cardiac gene transfer superior to that of AAV8. *Mol Ther* 14:45-53.
- Isaacs JS, Murdock M, Lane J, Percy AK (2003) Eating difficulties in girls with Rett syndrome compared with other developmental disabilities. *J Am Diet Assoc* 103:224-230.
- Itoh M, Ide S, Takashima S, Kudo S, Nomura Y, Segawa M, Kubota T, Mori H, Tanaka S, Horie H, Tanabe Y, Goto Y (2007) Methyl CpG-binding protein 2 (a mutation of which causes Rett syndrome) directly regulates insulin-like growth factor binding protein 3 in mouse and human brains. *J Neuropathol Exp Neurol* 66:117-123.
- Jankowsky JL, Melnikova T, Fadale DJ, Xu GM, Slunt HH, Gonzales V, Younkin LH, Younkin SG, Borchelt DR, Savonenko AV (2005) Environmental enrichment mitigates cognitive deficits in a mouse model of Alzheimer's disease. *J Neurosci* 25:5217-5224.
- Jarraya B, Boulet S, Ralph GS, Jan C, Bonvento G, Azzouz M, Miskin JE, Shin M, Delzescaux T, Drouot X, Herard AS, Day DM, Brouillet E, Kingsman SM, Hantraye P, Mitrophanous KA, Mazarakis ND, Palfi S (2009) Dopamine gene therapy for Parkinson's disease in a nonhuman primate without associated dyskinesia. *Sci Transl Med* 1:2ra4.
- Jensen TW, Chen Y, Miller WM (2003) Small increases in pH enhance retroviral vector transduction efficiency of NIH-3T3 cells. *Biotechnol Prog* 19:216-223.
- Jiang H, Lillicrap D, Patarroyo-White S, Liu T, Qian X, Scallan CD, Powell S, Keller T, McMurray M, Labelle A, Nagy D, Vargas JA, Zhou S, Couto LB, Pierce GF (2006) Multiyear therapeutic benefit of AAV serotypes 2, 6, and 8 delivering factor VIII to hemophilia A mice and dogs. *Blood* 108:107-115.
- Jiang M, Deng L, Chen G (2004) High Ca(2+)-phosphate transfection efficiency enables single neuron gene analysis. *Gene Ther* 11:1303-1311.
- Johnson RA, Lam M, Punzo AM, Li H, Lin BR, Ye K, Mitchell GS, Chang Q (2011) 7,8-dihydroxyflavone (7,8-DHF) exhibits therapeutic efficacy in a mouse model of Rett syndrome. *J Appl Physiol*.

- Jones PL, Veenstra GJ, Wade PA, Vermaak D, Kass SU, Landsberger N, Strouboulis J, Wolffe AP (1998) Methylated DNA and MeCP2 recruit histone deacetylase to repress transcription. *Nat Genet* 19:187-191.
- Jugloff DG, Logan R, Eubanks JH (2006) Breeding and maintenance of an *Mecp2*-deficient mouse model of Rett syndrome. *J Neurosci Methods* 154:89-95.
- Jugloff DG, Vandamme K, Logan R, Visanji NP, Brotchie JM, Eubanks JH (2008) Targeted delivery of an *Mecp2* transgene to forebrain neurons improves the behavior of female *Mecp2*-deficient mice. *Hum Mol Genet* 17:1386-1396.
- Julu PO, Kerr AM, Apartopoulos F, Al-Rawas S, Engerstrom IW, Engerstrom L, Jamal GA, Hansen S (2001) Characterisation of breathing and associated central autonomic dysfunction in the Rett disorder. *Arch Dis Child* 85:29-37.
- Julu PO, Kerr AM, Hansen S, Apartopoulos F, Jamal GA (1997) Functional evidence of brain stem immaturity in Rett syndrome. *Eur Child Adolesc Psychiatry* 6 Suppl 1:47-54.
- Jung BP, Jugloff DG, Zhang G, Logan R, Brown S, Eubanks JH (2003) The expression of methyl CpG binding factor MeCP2 correlates with cellular differentiation in the developing rat brain and in cultured cells. *J Neurobiol* 55:86-96.
- Kale A, Amende I, Meyer GP, Crabbe JC, Hampton TG (2004) Ethanol's effects on gait dynamics in mice investigated by ventral plane videography. *Alcohol Clin Exp Res* 28:1839-1848.
- Karlsson S (1991) Treatment of genetic defects in hematopoietic cell function by gene transfer. *Blood* 78:2481-2492.
- Karra D, Dahm R (2010) Transfection techniques for neuronal cells. *J Neurosci* 30:6171-6177.
- Kaspar BK, Frost LM, Christian L, Umaphathi P, Gage FH (2005) Synergy of insulin-like growth factor-1 and exercise in amyotrophic lateral sclerosis. *Ann Neurol* 57:649-655.
- Kay MA, Glorioso JC, Naldini L (2001) Viral vectors for gene therapy: the art of turning infectious agents into vehicles of therapeutics. *Nat Med* 7:33-40.
- Kay MA, Manno CS, Ragni MV, Larson PJ, Couto LB, McClelland A, Glader B, Chew AJ, Tai SJ, Herzog RW, Arruda V, Johnson F, Scallan C, Skarsgard E, Flake AW, High KA (2000) Evidence for gene transfer and expression of factor IX in haemophilia B patients treated with an AAV vector. *Nat Genet* 24:257-261.
- Kells AP, Fong DM, Dragunow M, During MJ, Young D, Connor B (2004) AAV-mediated gene delivery of BDNF or GDNF is neuroprotective in a model of Huntington disease. *Mol Ther* 9:682-688.
- Kerr AM, Armstrong DD, Prescott RJ, Doyle D, Kearney DL (1997) Rett syndrome: analysis of deaths in the British survey. *Eur Child Adolesc Psychiatry* 6 Suppl 1:71-74.

- Kishi N, Macklis JD (2004) MECP2 is progressively expressed in post-migratory neurons and is involved in neuronal maturation rather than cell fate decisions. *Mol Cell Neurosci* 27:306-321.
- Kishi N, Macklis JD (2010) MeCP2 functions largely cell-autonomously, but also non-cell-autonomously, in neuronal maturation and dendritic arborization of cortical pyramidal neurons. *Exp Neurol* 222:51-58.
- Kline DD, Ogier M, Kunze DL, Katz DM Exogenous brain-derived neurotrophic factor rescues synaptic dysfunction in *Mecp2*-null mice. *J Neurosci* 30:5303-5310.
- Klose RJ, Bird AP (2006) Genomic DNA methylation: the mark and its mediators. *Trends Biochem Sci* 31:89-97.
- Klugmann M, Leichtlein CB, Symes CW, Serikawa T, Young D, During MJ (2005) Restoration of aspartoacylase activity in CNS neurons does not ameliorate motor deficits and demyelination in a model of Canavan disease. *Mol Ther* 11:745-753.
- Knudsen GP, Neilson TC, Pedersen J, Kerr A, Schwartz M, Hulten M, Bailey ME, Orstavik KH (2006) Increased skewing of X chromosome inactivation in Rett syndrome patients and their mothers. *European journal of human genetics : EJHG* 14:1189-1194.
- Kondo M, Gray LJ, Pelka GJ, Christodoulou J, Tam PP, Hannan AJ (2008) Environmental enrichment ameliorates a motor coordination deficit in a mouse model of Rett syndrome--*Mecp2* gene dosage effects and BDNF expression. *Eur J Neurosci* 27:3342-3350.
- Kosai K, Kusaga, A., Isagai, T., Hirata, K., Nagano, S., Murofushi, Y., Takahashi, T., Takashima, S., Matsuishi, T (2005) Rett syndrome is reversible and treatable by MeCP2 gene therapy into the striatum in mice. *Molecular Therapy* 11 Supplement 1.
- Kotin RM, Linden RM, Berns KI (1992) Characterization of a preferred site on human chromosome 19q for integration of adeno-associated virus DNA by non-homologous recombination. *EMBO J* 11:5071-5078.
- Kriaucionis S, Bird A (2004) The major form of MeCP2 has a novel N-terminus generated by alternative splicing. *Nucleic Acids Res* 32:1818-1823.
- Kuroda H, Kutner RH, Bazan NG, Reiser J (2009) Simplified lentivirus vector production in protein-free media using polyethylenimine-mediated transfection. *J Virol Methods* 157:113-121.
- Lai Z, Brady RO (2002) Gene transfer into the central nervous system in vivo using a recombinant lentivirus vector. *J Neurosci Res* 67:363-371.
- LaSalle JM, Goldstine J, Balmer D, Greco CM (2001) Quantitative localization of heterogeneous methyl-CpG-binding protein 2 (MeCP2) expression phenotypes in normal and Rett syndrome brain by laser scanning cytometry. *Hum Mol Genet* 10:1729-1740.

- Lauterborn JC, Lynch G, Vanderklisch P, Arai A, Gall CM (2000) Positive modulation of AMPA receptors increases neurotrophin expression by hippocampal and cortical neurons. *J Neurosci* 20:8-21.
- Le Roith D (1997) Seminars in medicine of the Beth Israel Deaconess Medical Center. Insulin-like growth factors. *N Engl J Med* 336:633-640.
- Ledda M, Barni L, Altieri L, Pannese E (2000) Decrease in the nucleo-cytoplasmic volume ratio of rabbit spinal ganglion neurons with age. *Neurosci Lett* 286:171-174.
- Leggio MG, Mandolesi L, Federico F, Spirito F, Ricci B, Gelfo F, Petrosini L (2005) Environmental enrichment promotes improved spatial abilities and enhanced dendritic growth in the rat. *Behav Brain Res* 163:78-90.
- Lekman A, Witt-Engerstrom I, Gottfries J, Hagberg BA, Percy AK, Svennerholm L (1989) Rett syndrome: biogenic amines and metabolites in postmortem brain. *Pediatr Neurol* 5:357-362.
- Leonard H, Bower C (1998) Is the girl with Rett syndrome normal at birth? *Dev Med Child Neurol* 40:115-121.
- Lewis JD, Meehan RR, Henzel WJ, Maurer-Fogy I, Jeppesen P, Klein F, Bird A (1992) Purification, sequence, and cellular localization of a novel chromosomal protein that binds to methylated DNA. *Cell* 69:905-914.
- Li M, Husic N, Lin Y, Christensen H, Malik I, McIver S, Daniels CM, Harris DA, Kotzbauer PT, Goldberg MP, Snider BJ (2010) Optimal promoter usage for lentiviral vector-mediated transduction of cultured central nervous system cells. *J Neurosci Methods* 189:56-64.
- Li S, Huang L (2000) Nonviral gene therapy: promises and challenges. *Gene Ther* 7:31-34.
- Lioy DT, Garg SK, Monaghan CE, Raber J, Foust KD, Kaspar BK, Hirrlinger PG, Kirchhoff F, Bissonnette JM, Ballas N, Mandel G (2011) A role for glia in the progression of Rett's syndrome. *Nature* 475:497-500.
- Lois C, Hong EJ, Pease S, Brown EJ, Baltimore D (2002) Germline transmission and tissue-specific expression of transgenes delivered by lentiviral vectors. *Science* 295:868-872.
- Lonetti G, Angelucci A, Morando L, Boggio EM, Giustetto M, Pizzorusso T Early environmental enrichment moderates the behavioral and synaptic phenotype of MeCP2 null mice. *Biol Psychiatry* 67:657-665.
- Long SW, Ooi JY, Yau PM, Jones PL A brain-derived mecp2 complex supports a role for MeCP2 in RNA processing. *Biosci Rep*.
- Lotan M, Shapiro M (2005) Management of young children with Rett disorder in the controlled multi-sensory (Snoezelen) environment. *Brain Dev* 27 Suppl 1:S88-S94.
- Luikenhuis S, Giacometti E, Beard CF, Jaenisch R (2004) Expression of MeCP2 in postmitotic neurons rescues Rett syndrome in mice. *Proc Natl Acad Sci U S A* 101:6033-6038.

- Maddon PJ, McDougal JS, Clapham PR, Dalglish AG, Jamal S, Weiss RA, Axel R (1988) HIV infection does not require endocytosis of its receptor, CD4. *Cell* 54:865-874.
- Maezawa I, Jin LW (2010) Rett syndrome microglia damage dendrites and synapses by the elevated release of glutamate. *J Neurosci* 30:5346-5356.
- Maezawa I, Swanberg S, Harvey D, LaSalle JM, Jin LW (2009) Rett syndrome astrocytes are abnormal and spread MeCP2 deficiency through gap junctions. *J Neurosci* 29:5051-5061.
- Malik V, Rodino-Klapac LR, Viollet L, Wall C, King W, Al-Dahhak R, Lewis S, Shilling CJ, Kota J, Serrano-Munuera C, Hayes J, Mahan JD, Campbell KJ, Banwell B, Dasouki M, Watts V, Sivakumar K, Bien-Willner R, Flanigan KM, Sahenk Z, Barohn RJ, Walker CM, Mendell JR Gentamicin-induced readthrough of stop codons in Duchenne muscular dystrophy. *Ann Neurol* 67:771-780.
- Maliszewska-Cyna E, Bawa D, Eubanks JH (2010) Diminished prevalence but preserved synaptic distribution of N-methyl-d-aspartate receptor subunits in the methyl CpG binding protein 2(MeCP2)-null mouse brain. *Neuroscience* 168:624-632.
- Manno CS, Chew AJ, Hutchison S, Larson PJ, Herzog RW, Arruda VR, Tai SJ, Ragni MV, Thompson A, Ozelo M, Couto LB, Leonard DG, Johnson FA, McClelland A, Scallan C, Skarsgard E, Flake AW, Kay MA, High KA, Glader B (2003) AAV-mediated factor IX gene transfer to skeletal muscle in patients with severe hemophilia B. *Blood* 101:2963-2972.
- Manno CS, Pierce GF, Arruda VR, Glader B, Ragni M, Rasko JJ, Ozelo MC, Hoots K, Blatt P, Konkle B, Dake M, Kaye R, Razavi M, Zajko A, Zehnder J, Rustagi PK, Nakai H, Chew A, Leonard D, Wright JF, Lessard RR, Sommer JM, Tigges M, Sabatino D, Luk A, Jiang H, Mingozzi F, Couto L, Ertl HC, High KA, Kay MA (2006) Successful transduction of liver in hemophilia by AAV-Factor IX and limitations imposed by the host immune response. *Nat Med* 12:342-347.
- Manuvakhova M, Keeling K, Bedwell DM (2000) Aminoglycoside antibiotics mediate context-dependent suppression of termination codons in a mammalian translation system. *Rna* 6:1044-1055.
- Marchetto MC, Carromeu C, Acab A, Yu D, Yeo GW, Mu Y, Chen G, Gage FH, Muotri AR A model for neural development and treatment of Rett syndrome using human induced pluripotent stem cells. *Cell* 143:527-539.
- Martin R, Mogg AE, Heywood LA, Nitschke L, Burke JF (1989) Aminoglycoside suppression at UAG, UAA and UGA codons in *Escherichia coli* and human tissue culture cells. *Mol Gen Genet* 217:411-418.
- Martinowich K, Hattori D, Wu H, Fouse S, He F, Hu Y, Fan G, Sun YE (2003) DNA methylation-related chromatin remodeling in activity-dependent BDNF gene regulation. *Science* 302:890-893.
- Matarazzo V, Cohen D, Palmer AM, Simpson PJ, Khokhar B, Pan SJ, Ronnett GV (2004) The transcriptional repressor *Mecp2* regulates terminal neuronal differentiation. *Mol Cell Neurosci* 27:44-58.

- Mazarakis ND, Azzouz M, Rohll JB, Ellard FM, Wilkes FJ, Olsen AL, Carter EE, Barber RD, Baban DF, Kingsman SM, Kingsman AJ, O'Malley K, Mitrophanous KA (2001) Rabies virus glycoprotein pseudotyping of lentiviral vectors enables retrograde axonal transport and access to the nervous system after peripheral delivery. *Hum Mol Genet* 10:2109-2121.
- McBride JL, During MJ, Wu J, Chen EY, Leurgans SE, Kordower JH (2003) Structural and functional neuroprotection in a rat model of Huntington's disease by viral gene transfer of GDNF. *Exp Neurol* 181:213-223.
- McBride SM, Choi CH, Wang Y, Liebelt D, Braunstein E, Ferreiro D, Sehgal A, Siwicki KK, Dockendorff TC, Nguyen HT, McDonald TV, Jongens TA (2005) Pharmacological rescue of synaptic plasticity, courtship behavior, and mushroom body defects in a *Drosophila* model of fragile X syndrome. *Neuron* 45:753-764.
- McCarty DM, DiRosario J, Gulaid K, Muenzer J, Fu H (2009) Mannitol-facilitated CNS entry of rAAV2 vector significantly delayed the neurological disease progression in MPS IIIB mice. *Gene Ther* 16:1340-1352.
- McCarty DM, Fu H, Monahan PE, Toulson CE, Naik P, Samulski RJ (2003) Adeno-associated virus terminal repeat (TR) mutant generates self-complementary vectors to overcome the rate-limiting step to transduction in vivo. *Gene Ther* 10:2112-2118.
- McCarty DM, Monahan PE, Samulski RJ (2001) Self-complementary recombinant adeno-associated virus (scAAV) vectors promote efficient transduction independently of DNA synthesis. *Gene Ther* 8:1248-1254.
- McCarty DM, Young SM, Jr., Samulski RJ (2004) Integration of adeno-associated virus (AAV) and recombinant AAV vectors. *Annu Rev Genet* 38:819-845.
- McGraw CM, Samaco RC, Zoghbi HY (2011) Adult neural function requires MeCP2. *Science* 333:186.
- McNair K, Broad J, Riedel G, Davies CH, Cobb SR (2007) Global changes in the hippocampal proteome following exposure to an enriched environment. *Neuroscience* 145:413-422.
- Medrihan L, Tantalaki E, Aramuni G, Sargsyan V, Dudanova I, Missler M, Zhang W (2008) Early defects of GABAergic synapses in the brain stem of a MeCP2 mouse model of Rett syndrome. *J Neurophysiol* 99:112-121.
- Meins M, Lehmann J, Gerresheim F, Herchenbach J, Hagedorn M, Hameister K, Epplen JT (2005) Submicroscopic duplication in Xq28 causes increased expression of the MECP2 gene in a boy with severe mental retardation and features of Rett syndrome. *J Med Genet* 42:e12.
- Mentis GZ, Gravell M, Hamilton R, Shneider NA, O'Donovan MJ, Schubert M (2006) Transduction of motor neurons and muscle fibers by intramuscular injection of HIV-1-based vectors pseudotyped with select rabies virus glycoproteins. *J Neurosci Methods* 157:208-217.

- Miao CH, Nakai H, Thompson AR, Storm TA, Chiu W, Snyder RO, Kay MA (2000) Nonrandom transduction of recombinant adeno-associated virus vectors in mouse hepatocytes in vivo: cell cycling does not influence hepatocyte transduction. *J Virol* 74:3793-3803.
- Mingozzi F, High KA (2007) Immune responses to AAV in clinical trials. *Curr Gene Ther* 7:316-324.
- Mingozzi F, Maus MV, Hui DJ, Sabatino DE, Murphy SL, Rasko JE, Ragni MV, Manno CS, Sommer J, Jiang H, Pierce GF, Ertl HC, High KA (2007) CD8(+) T-cell responses to adeno-associated virus capsid in humans. *Nat Med* 13:419-422.
- Mnatzakanian GN, Lohi H, Munteanu I, Alfred SE, Yamada T, MacLeod PJ, Jones JR, Scherer SW, Schanen NC, Friez MJ, Vincent JB, Minassian BA (2004) A previously unidentified MECP2 open reading frame defines a new protein isoform relevant to Rett syndrome. *Nat Genet* 36:339-341.
- Mohandas T, Sparkes RS, Shapiro LJ (1981) Reactivation of an inactive human X chromosome: evidence for X inactivation by DNA methylation. *Science* 211:393-396.
- Mombaerts P, Iacomini J, Johnson RS, Herrup K, Tonegawa S, Papaioannou VE (1992) RAG-1-deficient mice have no mature B and T lymphocytes. *Cell* 68:869-877.
- Moretti P, Levenson JM, Battaglia F, Atkinson R, Teague R, Antalffy B, Armstrong D, Arancio O, Sweatt JD, Zoghbi HY (2006) Learning and memory and synaptic plasticity are impaired in a mouse model of Rett syndrome. *J Neurosci* 26:319-327.
- Moretti P, Zoghbi HY (2006) MeCP2 dysfunction in Rett syndrome and related disorders. *Curr Opin Genet Dev* 16:276-281.
- Moss RB, Rodman D, Spencer LT, Aitken ML, Zeitlin PL, Waltz D, Milla C, Brody AS, Clancy JP, Ramsey B, Hamblett N, Heald AE (2004) Repeated adeno-associated virus serotype 2 aerosol-mediated cystic fibrosis transmembrane regulator gene transfer to the lungs of patients with cystic fibrosis: a multicenter, double-blind, placebo-controlled trial. *Chest* 125:509-521.
- Na ES, Nelson ED, Adachi M, Autry AE, Mahgoub MA, Kavalali ET, Monteggia LM (2012) A Mouse Model for MeCP2 Duplication Syndrome: MeCP2 Overexpression Impairs Learning and Memory and Synaptic Transmission. *J Neurosci* 32:3109-3117.
- Nag N, Moriuchi JM, Peitzman CG, Ward BC, Kolodny NH, Berger-Sweeney JE (2009) Environmental enrichment alters locomotor behaviour and ventricular volume in Mecp2 1lox mice. *Behav Brain Res* 196:44-48.
- Nakai H, Storm TA, Kay MA (2000) Recruitment of single-stranded recombinant adeno-associated virus vector genomes and intermolecular recombination are responsible for stable transduction of liver in vivo. *J Virol* 74:9451-9463.
- Nakai H, Yant SR, Storm TA, Fuess S, Meuse L, Kay MA (2001) Extrachromosomal recombinant adeno-associated virus vector genomes are primarily responsible for stable liver transduction in vivo. *J Virol* 75:6969-6976.

- Naldini L, Blomer U, Gage FH, Trono D, Verma IM (1996a) Efficient transfer, integration, and sustained long-term expression of the transgene in adult rat brains injected with a lentiviral vector. *Proc Natl Acad Sci U S A* 93:11382-11388.
- Naldini L, Blomer U, Gallay P, Ory D, Mulligan R, Gage FH, Verma IM, Trono D (1996b) In vivo gene delivery and stable transduction of nondividing cells by a lentiviral vector. *Science* 272:263-267.
- Namihira M, Nakashima K, Taga T (2004) Developmental stage dependent regulation of DNA methylation and chromatin modification in a immature astrocyte specific gene promoter. *FEBS Lett* 572:184-188.
- Nan X, Campoy FJ, Bird A (1997) MeCP2 is a transcriptional repressor with abundant binding sites in genomic chromatin. *Cell* 88:471-481.
- Nan X, Ng HH, Johnson CA, Laherty CD, Turner BM, Eisenman RN, Bird A (1998) Transcriptional repression by the methyl-CpG-binding protein MeCP2 involves a histone deacetylase complex. *Nature* 393:386-389.
- Nan X, Tate P, Li E, Bird A (1996) DNA methylation specifies chromosomal localization of MeCP2. *Mol Cell Biol* 16:414-421.
- Nash KL, Lever AM (2004) Green fluorescent protein: green cells do not always indicate gene expression. *Gene Ther* 11:882-883.
- Nathwani AC, Benjamin R, Nienhuis AW, Davidoff AM (2004) Current status and prospects for gene therapy. *Vox Sang* 87:73-81.
- Nelson ED, Kavalali ET, Monteggia LM (2006) MeCP2-dependent transcriptional repression regulates excitatory neurotransmission. *Curr Biol* 16:710-716.
- Neul JL, Kaufmann WE, Glaze DG, Christodoulou J, Clarke AJ, Bahi-Buisson N, Leonard H, Bailey ME, Schanen NC, Zappella M, Renieri A, Huppke P, Percy AK (2010) Rett syndrome: revised diagnostic criteria and nomenclature. *Ann Neurol* 68:944-950.
- Neul JL, Zoghbi HY (2004) Rett syndrome: a prototypical neurodevelopmental disorder. *Neuroscientist* 10:118-128.
- Nikitina T, Shi X, Ghosh RP, Horowitz-Scherer RA, Hansen JC, Woodcock CL (2007) Multiple modes of interaction between the methylated DNA binding protein MeCP2 and chromatin. *Mol Cell Biol* 27:864-877.
- Nithianantharajah J, Hannan AJ (2006) Enriched environments, experience-dependent plasticity and disorders of the nervous system. *Nat Rev Neurosci* 7:697-709.
- Nomura Y (2005) Early behavior characteristics and sleep disturbance in Rett syndrome. *Brain Dev* 27 Suppl 1:S35-S42.
- Nudelman I, Rebibo-Sabbah A, Cherniavsky M, Belakhov V, Hainrichson M, Chen F, Schacht J, Pilch DS, Ben-Yosef T, Baasov T (2009) Development of novel aminoglycoside (NB54) with reduced toxicity and enhanced suppression of disease-causing premature stop mutations. *J Med Chem* 52:2836-2845.

- Ogier M, Wang H, Hong E, Wang Q, Greenberg ME, Katz DM (2007) Brain-derived neurotrophic factor expression and respiratory function improve after amphetamine treatment in a mouse model of Rett syndrome. *J Neurosci* 27:10912-10917.
- Owens GC, Mistry S, Edelman GM, Crossin KL (2002) Efficient marking of neural stem cell-derived neurons with a modified murine embryonic stem cell virus, MESV2. *Gene Ther* 9:1044-1048.
- Palmer A, Qayumi J, Ronnett G (2008) MeCP2 mutation causes distinguishable phases of acute and chronic defects in synaptogenesis and maintenance, respectively. *Mol Cell Neurosci* 37:794-807.
- Park JY, Hwang EM, Park N, Kim E, Kim DG, Kang D, Han J, Choi WS, Ryu PD, Hong SG (2007) Gateway RFP-fusion vectors for high throughput functional analysis of genes. *Mol Cells* 23:357-362.
- Pelka GJ, Watson CM, Radziewicz T, Hayward M, Lahooti H, Christodoulou J, Tam PP (2006) Mecp2 deficiency is associated with learning and cognitive deficits and altered gene activity in the hippocampal region of mice. *Brain* 129:887-898.
- Pereira DJ, McCarty DM, Muzyczka N (1997) The adeno-associated virus (AAV) Rep protein acts as both a repressor and an activator to regulate AAV transcription during a productive infection. *J Virol* 71:1079-1088.
- Philippe C, Villard L, De Roux N, Raynaud M, Bonnefond JP, Pasquier L, Lesca G, Mancini J, Jonveaux P, Moncla A, Chelly J, Bienvenu T (2006) Spectrum and distribution of MECP2 mutations in 424 Rett syndrome patients: a molecular update. *Eur J Med Genet* 49:9-18.
- Pintaudi M, Calevo MG, Vignoli A, Parodi E, Aiello F, Baglietto MG, Hayek Y, Buoni S, Renieri A, Russo S, Cogliati F, Giordano L, Canevini M, Veneselli E Epilepsy in Rett syndrome: clinical and genetic features. *Epilepsy Behav* 19:296-300.
- Popescu AC, Sidorova E, Zhang G, Eubanks JH Aminoglycoside-mediated partial suppression of MECP2 nonsense mutations responsible for Rett syndrome in vitro. *J Neurosci Res* 88:2316-2324.
- Rahim AA, Wong AM, Hofer K, Buckley SM, Mattar CN, Cheng SH, Chan JK, Cooper JD, Waddington SN (2011) Intravenous administration of AAV2/9 to the fetal and neonatal mouse leads to differential targeting of CNS cell types and extensive transduction of the nervous system. *FASEB J* 25:3505-3518.
- Rahim AA, Wong AM, Howe SJ, Buckley SM, Acosta-Saltos AD, Elston KE, Ward NJ, Philpott NJ, Cooper JD, Anderson PN, Waddington SN, Thrasher AJ, Raivich G (2009) Efficient gene delivery to the adult and fetal CNS using pseudotyped non-integrating lentiviral vectors. *Gene Ther* 16:509-520.
- Rampon C, Jiang CH, Dong H, Tang YP, Lockhart DJ, Schultz PG, Tsien JZ, Hu Y (2000) Effects of environmental enrichment on gene expression in the brain. *Proc Natl Acad Sci U S A* 97:12880-12884.

- Rastegar M, Hotta A, Pasceri P, Makarem M, Cheung AY, Elliott S, Park KJ, Adachi M, Jones FS, Clarke ID, Dirks P, Ellis J (2009) MECP2 isoform-specific vectors with regulated expression for Rett syndrome gene therapy. *PLoS One* 4:e6810.
- Ren C, Kumar S, Shaw DR, Ponnazhagan S (2005) Genomic stability of self-complementary adeno-associated virus 2 during early stages of transduction in mouse muscle in vivo. *Hum Gene Ther* 16:1047-1057.
- Rett A (1966) [On a unusual brain atrophy syndrome in hyperammonemia in childhood]. *Wien Med Wochenschr* 116:723-726.
- Rizzo MA, Davidson MW, Piston DW (2009) Fluorescent protein tracking and detection: fluorescent protein structure and color variants. *Cold Spring Harb Protoc* 2009:pdb top63.
- Robinson L, Guy J, McKay L, Brockett E, Spike R, Selfridge J, De Sousa D, Merusi C, Riedel G, Bird A, Cobb SR (2012) Morphological and functional reversal of phenotypes in a mouse model of Rett syndrome. *Brain* In press.
- Rols MP, Delteil C, Golzio M, Dumond P, Cros S, Teissie J (1998) In vivo electrically mediated protein and gene transfer in murine melanoma. *Nat Biotechnol* 16:168-171.
- Roux JC, Dura E, Villard L (2008) Tyrosine hydroxylase deficit in the chemoafferent and the sympathoadrenergic pathways of the *Mecp2* deficient mouse. *Neurosci Lett* 447:82-86.
- Roux JC, Panayotis N, Dura E, Villard L (2010) Progressive noradrenergic deficits in the locus coeruleus of *Mecp2* deficient mice. *J Neurosci Res* 88:1500-1509.
- Roux JC, Villard L (2007) [Pharmacological treatment of Rett syndrome improves breathing and survival in a mouse model]. *Med Sci (Paris)* 23:805-807.
- Rueda N, Florez J, Martinez-Cue C (2008) Chronic pentylentetrazole but not donepezil treatment rescues spatial cognition in Ts65Dn mice, a model for Down syndrome. *Neurosci Lett* 433:22-27.
- Sakai H, Kawamura M, Sakuragi J, Sakuragi S, Shibata R, Ishimoto A, Ono N, Ueda S, Adachi A (1993) Integration is essential for efficient gene expression of human immunodeficiency virus type 1. *J Virol* 67:1169-1174.
- Samaco RC, Mandel-Brehm C, Chao HT, Ward CS, Fyffe-Maricich SL, Ren J, Hyland K, Thaller C, Maricich SM, Humphreys P, Greer JJ, Percy A, Glaze DG, Zoghbi HY, Neul JL (2009) Loss of MeCP2 in aminergic neurons causes cell-autonomous defects in neurotransmitter synthesis and specific behavioral abnormalities. *Proc Natl Acad Sci U S A* 106:21966-21971.
- Samulski RJ, Berns KI, Tan M, Muzyczka N (1982) Cloning of adeno-associated virus into pBR322: rescue of intact virus from the recombinant plasmid in human cells. *Proc Natl Acad Sci U S A* 79:2077-2081.

- Sanlioglu S, Benson PK, Yang J, Atkinson EM, Reynolds T, Engelhardt JF (2000) Endocytosis and nuclear trafficking of adeno-associated virus type 2 are controlled by rac1 and phosphatidylinositol-3 kinase activation. *J Virol* 74:9184-9196.
- Saunders NR, Joakim Ek C, Dziegielewska KM (2009) The neonatal blood-brain barrier is functionally effective, and immaturity does not explain differential targeting of AAV9. *Nat Biotechnol* 27:804-805; author reply 805.
- Saxena A, de Lagarde D, Leonard H, Williamson SL, Vasudevan V, Christodoulou J, Thompson E, MacLeod P, Ravine D (2006) Lost in translation: translational interference from a recurrent mutation in exon 1 of MECP2. *J Med Genet* 43:470-477.
- Schanen NC, Dahle EJ, Capozzoli F, Holm VA, Zoghbi HY, Francke U (1997) A new Rett syndrome family consistent with X-linked inheritance expands the X chromosome exclusion map. *American journal of human genetics* 61:634-641.
- Schmid RS, Tsujimoto N, Qu Q, Lei H, Li E, Chen T, Blaustein CS (2008) A methyl-CpG-binding protein 2-enhanced green fluorescent protein reporter mouse model provides a new tool for studying the neuronal basis of Rett syndrome. *Neuroreport* 19:393-398.
- Schnepf BC, Jensen RL, Chen CL, Johnson PR, Clark KR (2005) Characterization of adeno-associated virus genomes isolated from human tissues. *J Virol* 79:14793-14803.
- Schuller-Petrovic S, Gebhart W, Lassmann H, Rumpold H, Kraft D (1983) A shared antigenic determinant between natural killer cells and nervous tissue. *Nature* 306:179-181.
- Sferra TJ, Backstrom K, Wang C, Rennard R, Miller M, Hu Y (2004) Widespread correction of lysosomal storage following intrahepatic injection of a recombinant adeno-associated virus in the adult MPS VII mouse. *Mol Ther* 10:478-491.
- Shahbazian M, Young J, Yuva-Paylor L, Spencer C, Antalffy B, Noebels J, Armstrong D, Paylor R, Zoghbi H (2002a) Mice with truncated MeCP2 recapitulate many Rett syndrome features and display hyperacetylation of histone H3. *Neuron* 35:243-254.
- Shahbazian MD, Antalffy B, Armstrong DL, Zoghbi HY (2002b) Insight into Rett syndrome: MeCP2 levels display tissue- and cell-specific differences and correlate with neuronal maturation. *Hum Mol Genet* 11:115-124.
- Simmons DA, Rex CS, Palmer L, Pandeyarajan V, Fedulov V, Gall CM, Lynch G (2009) Up-regulating BDNF with an ampakine rescues synaptic plasticity and memory in Huntington's disease knockin mice. *Proc Natl Acad Sci U S A* 106:4906-4911.
- Skene PJ, Illingworth RS, Webb S, Kerr AR, James KD, Turner DJ, Andrews R, Bird AP (2010) Neuronal MeCP2 is expressed at near histone-octamer levels and globally alters the chromatin state. *Mol Cell* 37:457-468.
- Smrt RD, Eaves-Egenes J, Barkho BZ, Santistevan NJ, Zhao C, Aimone JB, Gage FH, Zhao X (2007) Mecp2 deficiency leads to delayed maturation and altered gene expression in hippocampal neurons. *Neurobiol Dis* 27:77-89.

- Smrt RD, Pfeiffer RL, Zhao X (2011) Age-dependent expression of MeCP2 in a heterozygous mosaic mouse model. *Human molecular genetics* 20:1834-1843.
- Srivastava A, Lusby EW, Berns KI (1983) Nucleotide sequence and organization of the adeno-associated virus 2 genome. *J Virol* 45:555-564.
- Stancheva I, Collins AL, Van den Veyver IB, Zoghbi H, Meehan RR (2003) A mutant form of MeCP2 protein associated with human Rett syndrome cannot be displaced from methylated DNA by notch in *Xenopus* embryos. *Mol Cell* 12:425-435.
- Stearns NA, Schaevitz LR, Bowling H, Nag N, Berger UV, Berger-Sweeney J (2007) Behavioral and anatomical abnormalities in *Mecp2* mutant mice: a model for Rett syndrome. *Neuroscience* 146:907-921.
- Steffenburg U, Hagberg G, Hagberg B (2001) Epilepsy in a representative series of Rett syndrome. *Acta Paediatr* 90:34-39.
- Summerford C, Samulski RJ (1998) Membrane-associated heparan sulfate proteoglycan is a receptor for adeno-associated virus type 2 virions. *J Virol* 72:1438-1445.
- Swaney WP, Sorgi FL, Bahnson AB, Barranger JA (1997) The effect of cationic liposome pretreatment and centrifugation on retrovirus-mediated gene transfer. *Gene Ther* 4:1379-1386.
- Syken J, Shatz CJ (2003) Expression of T cell receptor beta locus in central nervous system neurons. *Proc Natl Acad Sci U S A* 100:13048-13053.
- Thorne RG, Nicholson C (2006) In vivo diffusion analysis with quantum dots and dextrans predicts the width of brain extracellular space. *Proc Natl Acad Sci U S A* 103:5567-5572.
- Toyama R, Bende SM, Dhar R (1992) Transcriptional activity of the human immunodeficiency virus-1 LTR promoter in fission yeast *Schizosaccharomyces pombe*. *Nucleic Acids Res* 20:2591-2596.
- Tropea D, Giacometti E, Wilson NR, Beard C, McCurry C, Fu DD, Flannery R, Jaenisch R, Sur M (2009) Partial reversal of Rett Syndrome-like symptoms in MeCP2 mutant mice. *Proc Natl Acad Sci U S A* 106:2029-2034.
- Trowbridge RS, Lehmann J, Torchio C, Brophy P (1980) Visna virus synthesized in absence of host-cell division and DNA synthesis. *Microbios* 29:71-80.
- Urduinguio RG, Pino I, Roperio S, Fraga MF, Esteller M (2007) Histone H3 and H4 modification profiles in a Rett syndrome mouse model. *Epigenetics* 2:11-14.
- Valori CF, Ning K, Wyles M, Mead RJ, Grierson AJ, Shaw PJ, Azzouz M (2010) Systemic delivery of scAAV9 expressing SMN prolongs survival in a model of spinal muscular atrophy. *Sci Transl Med* 2:35ra42.
- Van Esch H, Bauters M, Ignatius J, Jansen M, Raynaud M, Hollanders K, Lugtenberg D, Bienvenu T, Jensen LR, Gecz J, Moraine C, Marynen P, Fryns JP, Froyen G (2005) Duplication of the MECP2 region is a frequent cause of severe mental retardation and progressive neurological symptoms in males. *Am J Hum Genet* 77:442-453.

- van Woerden GM, Harris KD, Hojjati MR, Gustin RM, Qiu S, de Avila Freire R, Jiang YH, Elgersma Y, Weeber EJ (2007) Rescue of neurological deficits in a mouse model for Angelman syndrome by reduction of alphaCaMKII inhibitory phosphorylation. *Nat Neurosci* 10:280-282.
- Viemari JC, Roux JC, Tryba AK, Saywell V, Burnet H, Pena F, Zanella S, Bevingut M, Barthelemy-Requin M, Herzing LB, Moncla A, Mancini J, Ramirez JM, Villard L, Hilaire G (2005) *Mecp2* deficiency disrupts norepinephrine and respiratory systems in mice. *J Neurosci* 25:11521-11530.
- Villard L, Levy N, Xiang F, Kpebe A, Labelle V, Chevillard C, Zhang Z, Schwartz CE, Tardieu M, Chelly J, Anvret M, Fontes M (2001) Segregation of a totally skewed pattern of X chromosome inactivation in four familial cases of Rett syndrome without MECP2 mutation: implications for the disease. *Journal of medical genetics* 38:435-442.
- Voituron N, Hilaire G The benzodiazepine Midazolam mitigates the breathing defects of *Mecp2*-deficient mice. *Respir Physiol Neurobiol*.
- Voituron N, Zanella S, Menuet C, Dutschmann M, Hilaire G (2009) Early breathing defects after moderate hypoxia or hypercapnia in a mouse model of Rett syndrome. *Respir Physiol Neurobiol* 168:109-118.
- Voituron N, Zanella S, Menuet C, Lajard AM, Dutschmann M, Hilaire G Early abnormalities of post-sigh breathing in a mouse model of Rett syndrome. *Respir Physiol Neurobiol* 170:173-182.
- Wachter RM, Watkins JL, Kim H (2010) Mechanistic diversity of red fluorescence acquisition by GFP-like proteins. *Biochemistry* 49:7417-7427.
- Wagner JA, Reynolds T, Moran ML, Moss RB, Wine JJ, Flotte TR, Gardner P (1998) Efficient and persistent gene transfer of AAV-CFTR in maxillary sinus. *Lancet* 351:1702-1703.
- Walther W, Stein U (2000) Viral vectors for gene transfer: a review of their use in the treatment of human diseases. *Drugs* 60:249-271.
- Wan M, Zhao K, Lee SS, Francke U (2001) MECP2 truncating mutations cause histone H4 hyperacetylation in Rett syndrome. *Hum Mol Genet* 10:1085-1092.
- Wang J, Xie J, Lu H, Chen L, Hauck B, Samulski RJ, Xiao W (2007) Existence of transient functional double-stranded DNA intermediates during recombinant AAV transduction. *Proc Natl Acad Sci U S A* 104:13104-13109.
- Wang R, Liang J, Jiang H, Qin LJ, Yang HT (2008) Promoter-dependent EGFP expression during embryonic stem cell propagation and differentiation. *Stem Cells Dev* 17:279-289.
- Wang W, Qu Q, Smith FI, Kilpatrick DL (2005) Self-inactivating lentiviruses: versatile vectors for quantitative transduction of cerebellar granule neurons and their progenitors. *J Neurosci Methods* 149:144-153.

- Wanisch K, Yanez-Munoz RJ (2009) Integration-deficient lentiviral vectors: a slow coming of age. *Mol Ther* 17:1316-1332.
- Warrington KH, Jr., Herzog RW (2006) Treatment of human disease by adeno-associated viral gene transfer. *Hum Genet* 119:571-603.
- Welch EM, Barton ER, Zhuo J, Tomizawa Y, Friesen WJ, Trifillis P, Paushkin S, Patel M, Trotta CR, Hwang S, Wilde RG, Karp G, Takasugi J, Chen G, Jones S, Ren H, Moon YC, Corson D, Turpoff AA, Campbell JA, Conn MM, Khan A, Almstead NG, Hedrick J, Mollin A, Risher N, Weetall M, Yeh S, Branstrom AA, Colacino JM, Babiak J, Ju WD, Hirawat S, Northcutt VJ, Miller LL, Spatrack P, He F, Kawana M, Feng H, Jacobson A, Peltz SW, Sweeney HL (2007) PTC124 targets genetic disorders caused by nonsense mutations. *Nature* 447:87-91.
- Weng SM, McLeod F, Bailey ME, Cobb SR (2011) Synaptic plasticity deficits in an experimental model of rett syndrome: long-term potentiation saturation and its pharmacological reversal. *Neuroscience*.
- Wu Z, Sun J, Zhang T, Yin C, Yin F, Van Dyke T, Samulski RJ, Monahan PE (2008) Optimization of self-complementary AAV vectors for liver-directed expression results in sustained correction of hemophilia B at low vector dose. *Mol Ther* 16:280-289.
- Xiao X, Li J, Samulski RJ (1998) Production of high-titer recombinant adeno-associated virus vectors in the absence of helper adenovirus. *J Virol* 72:2224-2232.
- Yang C, van der Woerd MJ, Muthurajan UM, Hansen JC, Luger K (2011) Biophysical analysis and small-angle X-ray scattering-derived structures of MeCP2-nucleosome complexes. *Nucleic Acids Res* 39:4122-4135.
- Yang NS, Burkholder J, Roberts B, Martinell B, McCabe D (1990) In vivo and in vitro gene transfer to mammalian somatic cells by particle bombardment. *Proc Natl Acad Sci U S A* 87:9568-9572.
- Young JI, Hong EP, Castle JC, Crespo-Barreto J, Bowman AB, Rose MF, Kang D, Richman R, Johnson JM, Berget S, Zoghbi HY (2005) Regulation of RNA splicing by the methylation-dependent transcriptional repressor methyl-CpG binding protein 2. *Proc Natl Acad Sci U S A* 102:17551-17558.
- Young JI, Zoghbi HY (2004) X-chromosome inactivation patterns are unbalanced and affect the phenotypic outcome in a mouse model of rett syndrome. *American journal of human genetics* 74:511-520.
- Zanella S, Mebarek S, Lajard AM, Picard N, Dutschmann M, Hilaire G (2008) Oral treatment with desipramine improves breathing and life span in Rett syndrome mouse model. *Respir Physiol Neurobiol* 160:116-121.
- Zhang L, He J, Jugloff DG, Eubanks JH (2008) The MeCP2-null mouse hippocampus displays altered basal inhibitory rhythms and is prone to hyperexcitability. *Hippocampus* 18:294-309.
- Zhang ZW, Zak JD, Liu H MeCP2 is required for normal development of GABAergic circuits in the thalamus. *J Neurophysiol* 103:2470-2481.

- Zhong L, Zhou X, Li Y, Qing K, Xiao X, Samulski RJ, Srivastava A (2008) Single-polarity recombinant adeno-associated virus 2 vector-mediated transgene expression in vitro and in vivo: mechanism of transduction. *Mol Ther* 16:290-295.
- Zhou Z, Hong EJ, Cohen S, Zhao WN, Ho HY, Schmidt L, Chen WG, Lin Y, Savner E, Griffith EC, Hu L, Steen JA, Weitz CJ, Greenberg ME (2006) Brain-specific phosphorylation of MeCP2 regulates activity-dependent Bdnf transcription, dendritic growth, and spine maturation. *Neuron* 52:255-269.
- Zincarelli C, Soltys S, Rengo G, Rabinowitz JE (2008) Analysis of AAV serotypes 1-9 mediated gene expression and tropism in mice after systemic injection. *Mol Ther* 16:1073-1080.
- Zufferey R, Dull T, Mandel RJ, Bukovsky A, Quiroz D, Naldini L, Trono D (1998) Self-inactivating lentivirus vector for safe and efficient in vivo gene delivery. *J Virol* 72:9873-9880.
- Zufferey R, Nagy D, Mandel RJ, Naldini L, Trono D (1997) Multiply attenuated lentiviral vector achieves efficient gene delivery in vivo. *Nat Biotechnol* 15:871-875.